

AMERICAN UNIVERSITY OF BEIRUT

MODELING OF SAND COLUMNS IN SOFT CLAYS
UNDER DRAINED LOADING CONDITIONS

by
AYOUB SAMIR KASEM RIMAN

A thesis
submitted in partial fulfillment of the requirements
for the degree of Master of Engineering
to the Department of Civil and Environmental Engineering
of the Faculty of Engineering and Architecture
at the American University of Beirut

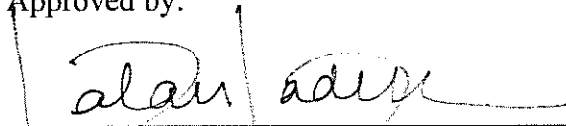
Beirut, Lebanon
May 2013

AMERICAN UNIVERSITY OF BEIRUT

MODELING OF SAND COLUMNS IN SOFT CLAYS
UNDER DRAINED LOADING CONDITIONS

by
AYOUB SAMIR KASEM RIMAN

Approved by:



Dr. Salah Sadek, Professor
Civil and Environmental Engineering

Advisor



Dr. Shadi Najjar, Assistant Professor
Civil and Environmental Engineering

Co-Advisor



Dr. Ghassan Chehab, Assistant Professor
Civil and Environmental Engineering

Member of Committee

Date of thesis defense: May 16, 2013

AMERICAN UNIVERSITY OF BEIRUT

THESIS RELEASE FORM

I, Ayoub Samir Kasem Riman

authorize the American University of Beirut to supply copies of my thesis to libraries or individuals upon request.

do not authorize the American University of Beirut to supply copies of my thesis to libraries or individuals for a period of two years starting with the date of the thesis deposit.

Signature

Date

ACKNOWLEDGMENTS

Special thanks are directed to my advisors, Dr. Salah Sadek and Dr. Shadi Najjar, for their continuous support and guidance through all the stages of this research study. Many thanks go to Mr. Samer Hassan, Mr. Hani Bou Lattouf, and Mrs. Zakeya Deeb.

My appreciations go to Mr. Issam Ghalayini, Dr. Sherif Wissa and Mr. Nadim Haddad for their continuous encouragement and support;

Last but not least, a special thank you goes to my family... and to HER, for being supportive.

AN ABSTRACT OF THE THESIS OF

Ayoub Samir Kasem Riman for Master of Engineering
Major: Civil Engineering

Title: Modeling of Sand Columns in Soft Clays Under Drained Loading Conditions

Sand columns are used as a ground improvement method to enhance the mechanical properties and speed up the consolidation of weak cohesive strata. Some of the research studies on sand columns have used the finite element method (FEM) in analyzing the behavior of reinforced clays, where the sand was modeled using conventional constitutive models which do not account for the post peak strain softening that generally occurs in compacted sands. Most of the studies to date adopted the elastic perfectly-plastic Mohr coulomb model, with a few using hyperbolic constitutive models. The recently developed hypoplastic model provides the ability to account for the post peak strain softening in sands. To our knowledge, the hypoplastic model for soils has never been used in the analysis of problems involving sand columns in soft clays. The objective of this thesis is to investigate and predict the drained load response of clay specimens that are reinforced with sand columns of different diameters, heights, and confinement conditions using the FEM. The Hypoplastic soil model will be the primary model to be used in the FEM, where the Mohr Coulomb and Hardening soil models will be used in some parts for comparison purposes. The first stage of the study is comprised of modeling in Plaxis 2D a series of triaxial tests that were previously performed on normally consolidated Kaolin clay specimens reinforced with Ottawa sand columns, where the area replacement ratio, the column penetration ratio, and the confining pressure were varied. This will be the first research study to use the hypoplastic model in modeling sand columns using the FEM software Plaxis2D and to compare the FE-predicted load response to that measured in the laboratory. In the second stage of the study, a comprehensive 2D FEM analysis will be conducted to predict the load-response of a wider range of area replacement ratios and sand column penetration ratios. The main goal of the 2D FEM analysis is to generate representative soil models that can predict the behavior of clay-sand column systems to be used in further similar research studies. Also two field scale applications were simulated using Plaxis 3D and compared to the literature and the analytical methods, highlighting important issues to be considered in the design of sand columns.

CONTENTS

ACKNOWLEDGMENTS	v
ABSTRACT	vii
LIST OF ILLUSTRATIONS	xi
LIST OF TABLES	xx

Chapter

1. INTRODUCTION AND SCOPE.....	1
1.1. Introduction.....	1
1.2. Background.....	3
1.3. Selected Soil Model.....	5
1.4. Scope of Work	5
2. LITERATURE REVIEW	7
2.1. Introduction.....	7
2.2. FEM to Study the Effects of Column Installation	8
2.3. FEM to Study the Effect of Column Encasement.....	12
2.4. FEM to Study the Group versus Single column behavior	18
2.5. FEM to Verify Related Theories in Literature.....	20
2.6. FEM to Model Laboratory Tests	22
2.7. Limitations of Published Studies	27

3. HYPOPLASTIC MODEL.....	29
3.1. Introduction.....	29
3.2. Hypoplasticity	29
3.3. Materials Properties	31
3.3.1. Kaolin Clay	31
3.3.2. Ottawa Sand	34
3.4. Hypoplastic model – Ottawa Sand.....	37
3.4.1. e_{d0} , e_{c0} and e_{i0}	38
3.4.2. The critical state friction angle φ_c	41
3.4.3. Parameters h_s and n	41
3.4.4. Parameters α and β	41
3.4.5. Intergranular parameters	42
3.4.6. Single Element Analyses and Soil Model Verification	43
3.5. Hypoplastic model – Kaolin Clay.....	45
3.5.1. Material Parameters	45
3.5.2. Single Element Analyses and Soil Model Verification	46
3.6. Summary.....	49
4. MODELING THE TRIAXIAL TESTS	51
4.1. Introduction.....	51
4.2. The Triaxial Test preparation and setup - Lab.....	51
4.2.1. Normally Consolidated Kaolin Clay Samples	51
4.2.2. Ottawa Sand Columns.....	58
4.3. Modeling the triaxial tests – Plaxis 2D.....	62
4.4. FEM Results	68
4.4.1. Deformations and Modes of Failure	68

4.4.2.	Stress-Strain Behavior.....	75
4.4.3.	Stress Distribution.....	77
4.5.	Comparing Hypoplasticity with Other Soil Models	92
4.6.	Comparison of FEM and Experimental results.....	95
5.	COLUMN PENETRATION RATIO.....	99
5.1.	Introduction.....	99
5.2.	Modeling Various Penetration Ratios.....	99
5.2.1.	Test Results	104
5.2.2.	Stress-Strain Behavior.....	105
5.3.	FEM vs Experimental	113
6.	MODELING A FIELD-SCALE APPLICATION	117
6.1.	Introduction.....	117
6.2.	The Field-Scale Application – No 1	118
6.2.1.	The Soil Models	120
6.2.2.	The 3D Model	124
6.2.2.1.	Geometry and Mesh	124
6.2.2.2.	Construction Stages and Phases	128
6.2.3.	FEM Results - Plaxis 3D.....	129
6.2.3.1.	Vertical Deformations and Modes of Failure.....	129
6.2.3.2.	Load-Settlement Behavior	131
6.2.4.	Comparison with the Single column Triaxial Lab tests.....	136
6.2.5.	Comparison of FEM and Theory / literature.....	137
6.3.	The Field-Scale Application – No 2	145
6.3.1.	Load-Settlement Behavior	147

7. CONCLUSIONS	151
7.1. Introduction.....	151
7.2. Comments and recommendations.....	153
7.2.1. Hypoplasticity, Mohr Coulomb and Hardening Soil	153
7.2.2. Comparison of Deformations - FEM vs. Experimental	154
7.2.3. Comparison of Stress Strain Behavior - FEM vs. Experimental .	155
7.2.4. Effect on Stress Strain Behavior – Column Penetration Ratios...	162
7.2.5. FEM vs Experimental results – Column Penetration Ratios.....	162
7.2.6. FEM under prediction for the Full penetration Columns.....	163
7.2.7. Modeling a field-scale application.....	164
7.3. Significance of this Research.....	165
 BIBLIOGRAPHY	 166

ILLUSTRATIONS

Figure	Page
2.1. Elshazly et al. (2007), idealized axisymmetric conditions (a) stone columns grid with respect to the reference central column; and (b) the corresponding idealized concentric ring.....	9
2.2. Elshazly et al. (2007), the geometry and mesh that were adopted to model the group of stone columns in axisymmetric conditions using the idealized concentric circles concept.	10
2.3. Chen et al. (2009), comparison of measured and calculated stress–strain curves for the clay model.....	11
2.4. Chen et al. (2009), the Pier and Cap as modeled in FLAC (a) plan view (b) 3D view.....	11
2.5. Chen et al. (2009), comparison between the computed and measured load.settlement curves.....	12
2.6. Raithel and Kempfert (2000), the assumptions and boundary conditions used in the analytical model.....	13
2.7. Raithel and Kempfert (2000), comparative calculation a) Load-settlement curve b) Load-strain curve.....	13
2.8. Murugesan and Rajagopal (2006), typical finite element mesh used in the analyses.....	15
2.9. Lo et al. (2010), the idealized unit cell concept used in the FEM.....	16
2.10. Castro and Sagaseta (2011), the idealized unit cell concept used in the analyses.....	17
2.11. Castro and Sagaseta (2011), comparison between the analytical and numerical analyses.....	18
2.12. Elshazly et al. (2008), the unit cell model.....	19
2.13. Elshazly et al. (2008), the idealized concept used in the analyses of the grid system.....	19
2.14. Elshazly et al. (2008), typical 2D axisymmetric modeling for a foundation resting on improved layered soil.....	20

2.15.	Elshazly et al. (2008), deformed mesh of a foundation over a group of sand columns	20
2.16.	Zahmatkesh and Choobbasti (2010)	21
2.17.	Zahmatkesh and Choobbasti (2010), comparison of SRR with existing theories.....	21
2.18.	Ambily and Gandhi (2007), single column test arrangement (a) column area loading (b) entire area loading	23
2.19.	Ambily and Gandhi (2007), group test arrangement (a) plan view (b) section of test tank (c) details of pressure cell.....	23
2.20.	Ambily and Gandhi (2007), finite element discretization for single column (unit cell).....	24
2.21.	Ambily and Gandhi (2007), Finite element discretization for group test.....	24
2.22.	Ambily and Gandhi (2007), comparing the FEM to experimental results for the single column model	24
2.23.	Ambily and Gandhi (2007), comparing the FEM to experimental results for the single and the group of columns models.....	24
2.24.	Shahu and Reddy (2011), the adopted FE model	26
2.25.	Shahu and Reddy (2011), comparison between the FEM and experimental results	27
2.26.	Shahu and Reddy (2011), response contours of group foundation at failure.....	27
3.1.	e-log P for normally consolidated Kaolin clay	33
3.2.	Variation of C_v with consolidation pressure for Kaolin clay.....	34
3.3.	Sieve analysis curve for Ottawa sand	35
3.4.	Deviatoric stress versus axial strain for Ottawa sand.	36
3.5.	Mohr Coulomb effective stress failure envelop for Ottawa sand	37
3.6.	Limiting Void Ratios by Gudehus (1996)	39
3.7.	The Function of α and β , α controls the dependency of peak friction angle and β influences the size of the response envelope (Masin 2005).....	42

3.8.	Single element analysis on Ottawa sand under a confining pressure of 100 kPa	43
3.9.	Single element analysis on Ottawa sand under a confining pressure of 150 kPa	44
3.10.	Single element analysis on Ottawa sand under a confining pressure of 200 kPa	44
3.11.	Single element analysis vs experimental triaxial tests on Ottawa sand.....	45
3.12.	Parameters of the clay Hypoplastic model from different sources, Masin (2005).....	46
3.13.	Single element analysis on Kaolin clay under a confining pressure (σ_3) of 100 kPa	47
3.14.	Single element analysis on Kaolin clay under a confining pressure (σ_3) of 150 kPa	48
3.15.	Single element analysis on Kaolin clay under a confining pressure (σ_3) of 200 kPa	48
3.16.	Single element analysis vs experimental triaxial tests on Kaolin clay	49
4.1.	Picture for custom fabricated 1 dimensional consolidometers	52
4.2.	Photo for a Split PVC pipe and Wrapped PVC pipe with duct tape	53
4.3.	Custom fabricated 1 dimensional consolidometer.....	54
4.4.	Water content and void ratio along the height of the sample after consolidation.....	56
4.5.	Kaolin specimen (a) after removal from custom fabricated consolidometer, (b) dismantling and (c) after removal from PVC pipe	57
4.6.	Kaolin specimen (a) after trimming, (b) Installation of porous stones, (c) installation of filter paper around.	57
4.7.	Cell chamber (a) Brass tube with the rubber membrane. (b) Installation of Kaolin specimen on the cell chamber, (c) Insertion of glass cover around cell chamber.....	58
4.8.	Wrapping the Kaolin specimen with PVC tubes prior to auguring.....	59

4.9.	Custom fabricated auguring machine (a) 2cm diameter auger (b) auguring of specimen by 2cm diameter augur, (c) Removal of Kaolin material by 3 cm diameter augur	60
4.10.	Freezing the sand columns	61
4.11.	Sand column installation (a) Predrilled 3.cm diameter hole, (b) Insertion of frozen sand column in clay, and (c) Reinforced Kaolin specimen with frozen sand column.....	62
4.12.	Vertical cross section of Kaolin specimen with ordinary sand column of diameter 2cm and height 10.65cm after column insertion.	62
4.13.	The suggested model showing the adopted triangular mesh and boundary condition.	63
4.14.	A generic sample of the partially penetrating sand column model showing the three calculation phases.....	67
4.15.	Plaxis 2D calculations setup showing the 7 phases in each Model	68
4.16.	Horizontal displacements for Model 1 at 100, 150 and 200 kPa (from left to right)	70
4.17.	Deformed mesh for Model 1 at 100, 150 and 200 kPa (from left to right)	70
4.18.	Horizontal displacements for Model 2 at 100, 150 and 200 kPa (from left to right)	71
4.19.	Deformed mesh for Model 2 at 100, 150 and 200 kPa (from left to right)	71
4.20.	Horizontal displacements for Model 3 at 100, 150 and 200 kPa (from left to right)	72
4.21.	Deformed mesh for Model 3 at 100, 150 and 200 kPa (from left to right)	72
4.22.	Horizontal displacements for Model 4 at 100, 150 and 200 kPa (from left to right)	73
4.23.	Deformed mesh for Model 4 at 100, 150 and 200 kPa (from left to right)	73
4.24.	Horizontal displacements for Model 5 at 100, 150 and 200 kPa (from left to right)	74
4.25.	Deformed mesh for Model 5 at 100, 150 and 200 kPa (from left to right)	74
4.26.	Stress Strain curves for partial penetration models (M1 and M2).....	75

4.27.	Stress Strain curves for full penetration models (M3 and M4)	76
4.28.	Stress Strain curve for the additional partial penetration model (M5)	76
4.29.	Stress distribution in Model M2 (3cm Sand Column, Partial Penetration) at a confining pressure σ_3 of 100 kPa (Global View)	78
4.30.	Stress distribution in Model M2 (3cm Sand Column, Partial Penetration) at a confining pressure σ_3 of 100 kPa (Zoomed View).....	78
4.31.	Stress distribution along a horizontal axis 3cm below the sample top, in Model M2 (3cm Sand Column, Partial Penetration) at a confining pressure σ_3 of 100 kPa	79
4.32.	Stress distribution in Model M2 (3cm Sand Column, Partial Penetration) at a confining pressure σ_3 of 150 kPa (Global View)	79
4.33.	Stress distribution in Model M2 (3cm Sand Column, Partial Penetration) at a confining pressure σ_3 of 150 kPa (Zoomed View).....	80
4.34.	Stress distribution along a horizontal axis 3cm below the sample top, in Model M2 (3cm Sand Column, Partial Penetration) at a confining pressure σ_3 of 150 kPa	80
4.35.	Stress distribution in Model M2 (3cm Sand Column, Partial Penetration) at a confining pressure σ_3 of 200 kPa (Global View)	81
4.36.	Stress distribution in Model M2 (3cm Sand Column, Partial Penetration) at a confining pressure σ_3 of 200 kPa (Zoomed View).....	81
4.37.	Stress distribution along a horizontal axis 3cm below the sample top, in Model M2 (3cm Sand Column, Partial Penetration) at a confining pressure σ_3 of 200 kPa	82
4.38.	Stress distribution in Model M4 (3cm Sand Column, Full Penetration) at a confining pressure σ_3 of 100 kPa (Global View)	82
4.39.	Stress distribution in Model M4 (3cm Sand Column, Full Penetration) at a confining pressure σ_3 of 100 kPa (Zoomed View).....	83
4.40.	Stress distribution along a horizontal axis 3cm below the sample top, in Model M4 (3cm Sand Column, Full Penetration) at a confining pressure σ_3 of 100 kPa.....	83
4.41.	Stress distribution in Model M4 (3cm Sand Column, Full Penetration) at a confining pressure σ_3 of 150 kPa (Global View)	84

4.42.	Stress distribution in Model M4 (3cm Sand Column, Full Penetration) at a confining pressure σ_3 of 150 kPa (Zoomed View).....	84
4.43.	Stress distribution along a horizontal axis 3cm below the sample top, in Model M4 (3cm Sand Column, Full Penetration) at a confining pressure σ_3 of 150 kPa.....	85
4.44.	Stress distribution in Model M4 (3cm Sand Column, Full Penetration) at a confining pressure σ_3 of 200 kPa (Global View)	85
4.45.	Stress distribution in Model M4 (3cm Sand Column, Full Penetration) at a confining pressure σ_3 of 200 kPa (Zoomed View).....	86
4.46.	Stress distribution along a horizontal axis 3cm below the sample top, in Model M4 (3cm Sand Column, Full Penetration) at a confining pressure σ_3 of 200 kPa.....	86
4.47.	Stress Ratio (SR) plotted vs confining pressures, σ_3 of 100kPa, 150 kPa and 200 kPa	88
4.48.	Deviatoric Stresses were read from the above indicated stress points locations, one located in the sand column and one in the surrounding clay.....	89
4.49.	Stress Ratio (SR) plotted vs axial strain for σ_3 of 100kPa, 150 kPa and 200 kPa, relative to Model 2: 3cm Diameter sand column / Partial Penetration	90
4.50.	Stress Ratio (SR) plotted vs axial strain for σ_3 of 100kPa, 150 kPa and 200 kPa, relative to Model 4: 3cm Diameter sand column / Full Penetration	91
4.51.	Stress Ratio (SR) plotted vs axial strain for σ_3 of 100kPa, 150 kPa and 200 kPa, for both Model 2 and Model 4.....	92
4.52.	Hardening Soil (HS) Model of the Ottawa Sand vs Experimental.....	93
4.53.	Hardening Soil (HS) Model of the Kaolin Clay vs Experimental.....	93
4.54.	Model M2 output of the three soil models	94
4.55.	Model M4 output of the three soil models	95
4.56.	Stress Strain curves of Model vs Experimental results for partial penetration M1 and M2	96
4.57.	Stress Strain curves of Model vs Experimental results for full penetration M3 and M4	96

4.58.	Stress Strain curves of Model vs Experimental results for partial penetration M5 (on the left the lab test curve was smoothened, on the right is unprocessed curve)	97
4.59.	A good match between Lab and FEM in the stress strain curve for 3cm full penetration sand column when increasing the critical angle of friction by 3 degrees	98
5.1.	Deviatoric stress at a 2% vertical strain for the 2cm diameter column	105
5.2.	Deviatoric stress at a 12% vertical strain for the 2cm diameter column	106
5.3.	Deviatoric stress at a 2% vertical strain for the 3cm diameter column	106
5.4.	Deviatoric stress at a 12% vertical strain for the 3cm diameter column	107
5.5.	Deviatoric stress at a 2% vertical strain for the 3.5cm diameter column	107
5.6.	Deviatoric stress at a 12% vertical strain for the 3.5cm diameter column	108
5.7.	Deviatoric stress at a 2% vertical strain for the 4cm diameter column	108
5.8.	Deviatoric stress at a 12% vertical strain for the 4cm diameter column	109
5.9.	Improvement Ratio for the 2cm diameter column.....	110
5.10.	Improvement Ratio for the 3cm diameter column.....	110
5.11.	Improvement Ratio for the 3.5cm diameter column.....	111
5.12.	Improvement Ratio for the 4cm diameter column.....	111
5.13.	Deviatoric stress at 12% vertical strain for all the modeled tests.....	112
5.14.	Deviatoric stress at 2% vertical strain for all the modeled tests.....	113
5.15.	Lab vs FEM, the deviatoric stress at 12% strain for the 3cm sand column....	114
5.16.	A good match between Lab and FEM in the stress strain curve for 3cm full penetration sand column when increasing the critical angle of friction by 3 degrees	116
6.1.	Sand columns 0.5m in dia. placed in 1m c-c square grid	119
6.2.	The Field Application, a Raft Placed over 25 Sand Columns	119
6.3.	The MC Soil Parameters-General.....	121

6.4.	The MC Soil Parameters-Strength and Deformation	121
6.5.	The MC Soil Parameters -Initial Conditions	122
6.6.	Results of the MC single element analysis on the sand under a confining pressure (σ_3) of 100 kPa.....	122
6.7.	Results of the MC-single element analysis on Clay under a confining pressure (σ_3) of 100 kPa.....	123
6.8.	The Linear Elastic Concrete Raft Parameters.....	124
6.9.	The 10 m thick clay layer was divided into 4 sub layers (2.5 m each).....	125
6.10.	The Mesh generated.....	125
6.11.	The mesh view from the surface.....	126
6.12.	The mesh view at 2.5 m below surface	126
6.13.	The mesh view at 5.0 m below surface	127
6.14.	The mesh view at 7.5 m below surface	127
6.15.	The global view of the vertical displacement output.....	130
6.16.	The vertical displacement under and around the raft	130
6.17.	Loading Stress vs Settlement at the center of the raft	132
6.18.	Load settlement response of the 5m x 5m raft footing.....	132
6.19.	Calculated Settlement Reduction Ratio vs loading stress	133
6.20.	Calculated Settlement Improvement Ratio (β) vs loading stress.....	134
6.21.	Calculated Stress Improvement Ratio vs axial strain	136
6.22.	Zahmatkesh and Choobbasti (2010),	137
6.23.	Zahmatkesh and Choobbasti (2010), comparison of SRR with existing theories.....	138
6.24.	The 7.2m wide square footings used for the field tests in Krish (2004), 0.8m diameter stone columns placed in 1.4 m c-c spacing square grid.	139
6.25.	The stone column configuration under the 3m wide square footing used for the field tests in Krish (2004).....	140

6.26.	The field test setup of the 3m wide square footing in Krish (2004).....	141
6.27.	Load settlement response of the 7.2m wide square footing in Krish (2006) (Left), and the Load settlement response of the 5mx5m raft done in this research study (right)	142
6.28.	Improvement factor (β) for the 7.2m wide square footing in Krish (2006) (Left), and the Improvement factor (β) for the 5mx5m raft done in this research study (right).	143
6.29.	Improvement factor (β) vs loadind stress for various column to ground stiffness values, Krish (2004).	143
6.30.	Load settlement response of the 7.2m wide square footing in Krish (2006) (Left), and the Load settlement response of the 5mx5m raft done in this research study (right)	144
6.31.	The field-scale application No 2.....	145
6.32.	Loading Stress vs Settlement at the center of the raft	147
6.33.	Load settlement response of the 5mx5m raft footing, with varied L/D ratios	148
6.34.	Calculated Settlement Improvement Ratio (β) vs Loading Stress.....	149
6.35.	Calculated Settlement Improvement Ratio (β) vs L/D	149
6.36.	Improvement factor (β) vs loadind stress for various column to ground stiffness values, Krish (2004).	150

TABLES

Table	Page
3.1. Index properties of Kaolin clay.....	31
3.2. Initial properties of 1-dimensional consolidation test specimen of Kaolin clay.....	32
3.3. One.Dimensional consolidation pressure test results.....	32
3.4. Coefficient of consolidation obtained from t50 and t90.....	33
3.5. Index properties of Ottawa sand	35
3.6. Sieve analysis results for Ottawa sand.....	35
3.7. Hypoplastic parameters determined for some granular materials, Głębowicz (2006).....	40
4.1. Loading sequence during 1.D consolidation of Kaolin slurry	55
4.2. The five triaxial models (FEM) to be built	66
4.3. Average deviatoric stress distribution and SR	87
5-1. Modeled triaxial tests representing various penetration ratios.....	100
6.1. MODEL 1 and MODEL 2	118
6.2. The MC Soil Models Parameters	120
6.3. Load vs Settlement at the center of the raft and SRR	131
6.4. Improvement Ratio (IR) due to ground reinforcement	135
6.5. The Hardening Soil Models Parameters	146
6.6. MODEL S1 to MODEL S6.....	146
7.1. Hypoplastic parameters for Ottawa sand and Kaolin.....	151

CHAPTER 1

INTRODUCTION AND SCOPE

1.1. Introduction

Sand columns are granular inclusions used to improve the mechanical properties of soft clays by accelerating their rate of consolidation and introducing stiffer elements in the ground. When sand columns are used as vertical drains to accelerate the rate of consolidation of the clay strata, the possible positive reinforcing role that these columns can play with regards to improving the short term and long term bearing capacity of the clay/sand column system is usually neglected in design (Najjar et al., 2010). Some of the research studies on stone/sand columns reinforced soils have included FEM as the major part of the study or as a method to verify and check experimental results. In all of these studies the sand was modeled using conventional constitutive models that do not account for the post-peak strain softening that is expected for compacted sands. Most of the studies used the elastic perfectly-plastic Mohr coulomb model and a few used hyperbolic models. The hypoplastic model which can account for the post-peak strain softening in sands has to our knowledge never been used in modeling sand columns in soft clays.

This research study aims at using numerical models within an FEM context to capture the response of sand columns in soft clays. The intended effort will build on, and complement, the experimental research work that was conducted by Maalouf (2012). In her work, Maalouf (2012) completed an experimental laboratory testing program using “fully drained” triaxial tests (15 consolidated drained tests in total) on

normally consolidated Kaolin specimens, reinforced with partially or fully penetrating single sand columns. The parameters that were varied were the diameter of the sand columns, the depth of penetration of the columns, and the effective confining pressure.

The main objective of this research study is to build a FE model where the sand columns and the surrounding clay are represented by the hypoplastic soil model and to compare the results of the FE predictions (using Plaxis 2D) to the results of the experimental triaxial tests (Maalouf 2012). Based on the results of the comparison between FEM and experimental results, more variations are to be introduced in the FEM analysis to predict the performance of clays that are reinforced with sand columns at different area replacement ratios and sand column penetration depths. Accordingly sand columns of 2cm, 3cm, 3.5cm and 4cm diameters were modeled for a range of column penetration ratios under the three confinement pressures of 100kPa, 150kPa and 200 kPa. As a result of this, 120 triaxial tests were modeled in Plaxis 2D.

The main goal is to build representative soil models that can predict the results of additional experimental tests that could be conducted in the future for the same clay and sand material. This will open the doors to a new coupled, laboratory and FEM, analyses to any similar work at the American university of Beirut (AUB). From the finding of this study, the researchers can use the same obtained models in case the same soils (which are available at AUB) were used.

Also an exercise was carried out to simulate two field-scale applications, where a 5m x 5m raft foundation is placed over 25 sand columns penetrating 7.5m into the natural clayey ground and loaded uniformly. The methodology and results of modeling the field applications were compared with similar previous studies done by others and

theory to assess the reliability of the finite element method in such applications and also to evaluate its usefulness in designing sand columns.

1.2. Background

The use of sand columns as a ground improvement method dates back to the early 1970s. Several experimental studies on the behavior of stone/sand columns were carried out, where single sand columns were tested by direct loading of the columns or both single sand columns and column groups were loaded using either model foundations or top plates of typical triaxial cells.

Some of the investigative works in this area have relied solely or significantly on finite element analyses, others have used the FEM as a method to corroborate the experimental results. Up to our knowledge, in all the works the sand was modeled using constitutive models that do not account for the post-peak strain softening that is characteristics of dense sands. Most of the researchers used the Mohr coulomb model and a few used hyperbolic models to represent the response of the sand inclusions.

The hypoplastic model which accounts for the post-peak strain softening in sands has not to our knowledge been used in modeling sand columns in soft clays and presents a promising avenue and tool to reliably model the full range of the complex response of the composite system.

Hypoplasticity is a particular class of incrementally non-linear constitutive models, developed during the 1990's at the University of Karlsruhe to predict the behavior of soils. Unlike elasto-plasticity, in hypoplasticity the strain rate is not decomposed into elastic and plastic parts and the models do not explicitly use the concepts of the yield surface and plastic potential surface.

The Hypoplasticity models are capable of predicting the important features of the soil performance, such as the critical state, non-linear behavior in the small and large strain ranges, dependency of the peak strength on soil density and the soil stiffness on the loading direction, etc. Some of the important milestones in the development of hypoplasticity are briefly listed below:

- The early hypoplastic models were developed by means of trial and error procedures, as illustrated in Kolymbas (1991).
- Gudehus (1996) implemented the critical state concept by proposing a modification to include the influence of the stress level (barotropy) and the influence of density (pyknotropy).
- The model was later revised by von Wolffersdorff (1996) to incorporate the Matsuoka-Nakai critical state stress condition.
- The Von Wolffersdorff (1996) model is nowadays considered as a standard hypoplastic model for granular materials and is implemented in the FEM software PLAXIS.
- Later developments focused on hypoplasticity for fine grained soils.
- Herle and Kolymbas (2004) modified the model by Von Wolffersdorff (1996) to account for lower friction angles and independent calibration of bulk and shear stiffnesses.
- Based on Herle and Kolymbas (2004) and Niemunis (2002) "generalized hypoplasticity" principle, Masin (2005) developed a hypoplastic model for clays characterized by a simple calibration procedure and capability of correctly predicting the strain behaviour. Masin (2007) then proposed modifications of the model from Masin (2005) to consider the behaviour of clays with meta-stable structure.
- The clay hypoplastic model of Masin (2005 and 2007) is also incorporated in the FEM software PLAXIS.

1.3. Selected Soil Model

The proper selection of constitutive models for the sand columns and surrounding clay in FEM analyses is of great importance. The models need to be representative and capable of simulating the behavior of the material as close as possible to reality. When it comes to sand, the models utilized in published FEM studies generally ignore the strain softening that occurs in sand and assume that the load carrying capacity of the sand column increases with strain (strain hardening models) or remains constant beyond the peak strength. Hypoplasticity is the basis of a relatively recent constitutive model that is capable of modeling the strain softening behavior in sands. Accordingly, this research study will explore this model for the first time in applications involving sand columns in clay. Also this model will be compared to the Mohr Coulomb and Hardening Soil models in such an application.

Beside the inability to model the post peak soil softening, the Mohr Coulomb and Hardening Soil models are incapable of accommodating different void ratios of the same material. For each void ratio a new soil model is needed since the angle of friction and cohesion changes accordingly. This is not the case for Hypoplasticity, where one model accommodates all void ratios. The Hypoplasticity is more global and accommodates any initial void ratio of the material.

1.4. Scope of Work

The scope of work can be briefed as per the following sequence of Chapters:

- Chapter 2
 - ⇒ Carrying out a background/literature review about the research topic
- Chapter 3
 - ⇒ Derivation of the Hypoplastic model parameters for the sand and clay

- Chapter 4
 - ⇒ Modelling the experimental triaxial tests of Maalouf (2012) in Plaxis 2D
 - ⇒ Comparing the FEM and the experimental results
- Chapter 5
 - ⇒ Modelling additional 120 triaxial tests with varying column diameters, column penetration ratios and confinement pressures in Plaxis 2D.
 - ⇒ Comparing the FEM and the experimental results
 - ⇒ Evaluating the reliability and use of the obtained soil models.
- Chapter 6
 - ⇒ Modelling a field scale application in Plaxis 3D
 - ⇒ Comparing the FEM results to previous work and theory
- Chapter 7
 - Concluding the whole research study and Suggesting further researches

CHAPTER 2

LITERATURE REVIEW

2.1. Introduction

The use of sand columns as a ground improvement method dates back to the early 1970s. Some of the experimental studies on the behavior of stone/sand columns include the work done by Hughes and Withers (1974), Juran and Guermaizi (1987), Juran and Riccobono (1991), Narasimha Rao et al. (1992), Muir Wood et al. (2000), Sivakumar et al. (2004), McKelvey et al. (2004), Ayadat and Hanna (2005), Black et al. (2006, 2007), and Najjar et al. (2010) where single sand columns were tested by direct loading of the columns or both single sand columns and column groups were loaded using either model foundations or top plates of typical triaxial cells.

Some of the investigative works in this area have relied solely or significantly on finite element analyses, others have used the FEM as a method to corroborate the experimental results. In all of these papers (Raithel and Kempfert, 2000; Murugesan and Rajagopal, 2006; Ambily and Gandhi, 2007; Elshazly et al. 2007; Elshazly et al. 2008; Tan et al. 2008; Chen et al. 2009; Lo et al. 2010; Zahmatkesh and Choobbasti, 2010; Castro and Sagasetta, 2011; and Shahu and Reddy, 2011) the sand was modeled using constitutive models that do not account for the post-peak strain softening that is characteristics of dense sands. Most of the researchers used the Mohr coulomb model and a few such as Raithel and Kempfert (2000) and Murugesan and Rajagopal (2006) used hyperbolic models to represent the response of the sand inclusions. The hypoplastic model which accounts for the post-peak strain softening in sands has not to

our knowledge been used in modeling sand columns in soft clays and thus exploring this path may reveal some enhancements in modeling the full range of the complex response of the composite system.

The above-referenced papers have used the FEM to study one of the following: (1) The effects of the method of installation of sand columns on the load response, (2) the improved performance of geosynthetic encased sand columns compared to ordinary columns, (3) the relation between group and single column behavior and (4) the performance of sand columns where FEM analyses are verified by theories from literature or (5) coupled with experimental testing. All of the mentioned five categories will be discussed further in the proceeding sections

2.2. FEM to Study the Effects of Column Installation

The effects of the method of installation of sand/stone columns on the load response was studied by Elshazly et al. (2007) and Chen et al. (2009) using the FE method. Elshazly et al. (2007) used results from full-scale field tests and finite element analyses (Plaxis) to study the effect of inter-column spacing on the horizontal state of stress around the stone column after installation. The field tests were conducted using a 2.0m-diameter concrete footing placed over 1.0m diameter stone columns installed in several grid arrangements. The stone columns were constructed with well-graded gravel (wet method) using a vibrator with a diameter of 290mm. The finite element analyses have assumed the hardening soil model, which is originally based on the hyperbolic Duncan-Chang model, for the natural soil and the gravel that forms the installed stone columns. The model was developed using idealized axisymmetric conditions with 15-noded triangular mesh elements in Plaxis 2D to imitate the field tests (See Figure 2.1

and Figure 2.2). The FEM analyses were inversely posed to determine the initial stresses in the soil based on the known settlements from the field test results and the post installation material properties. Thus, the FEM in this paper was used as a back analysis tool that revealed the significant effect of the inter-columnar spacing of the stone columns and indicated the changes in the initial stresses due to the installation of sand columns.

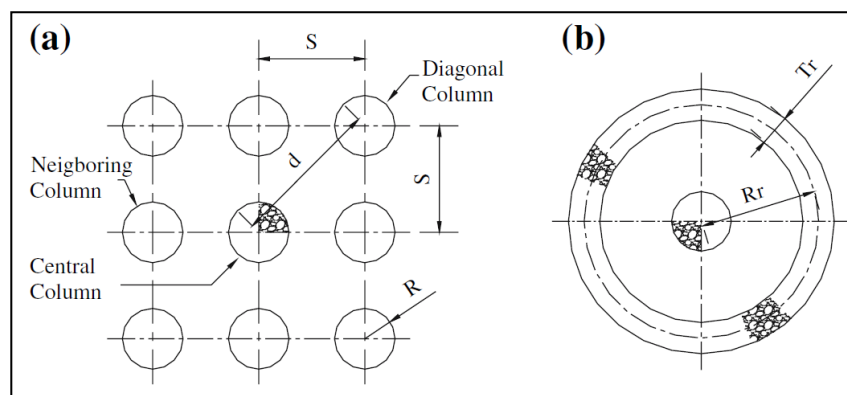


Figure 2.1. Elshazly et al. (2007), idealized axisymmetric conditions (a) stone columns grid with respect to the reference central column; and (b) the corresponding idealized concentric ring.

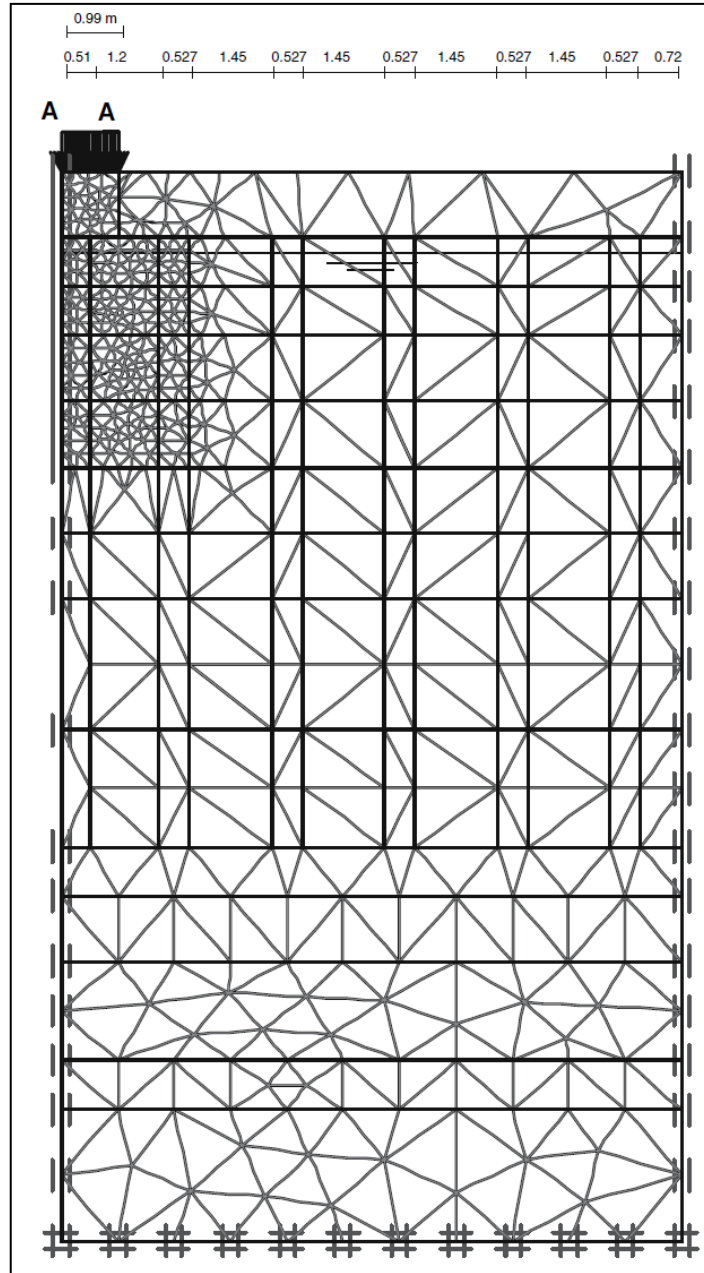


Figure 2.2. Elshazly et al. (2007), the geometry and mesh that were adopted to model the group of stone columns in axisymmetric conditions using the idealized concentric circles concept.

Chen et al. (2009) conducted a 3D finite element analysis using FLAC to quantify the difference in the response of rammed and un-rammed aggregate piers. The pier was tested in the field using stress-controlled loading applied through a footing resting on the pier. The FEM analysis was conducted assuming that the clay could be modeled using the modified Cam-clay model (see Figure 2.3) and the aggregate by the

Mohr-Coulomb model. The 3D finite element model was square in plan view and consists of brick and shell elements as shown in Figure 2.4. Fully drained conditions were assumed during loading and resulted in good comparison between computed and measured load settlement response at the top and tip of the pier (see Figure 2.5).

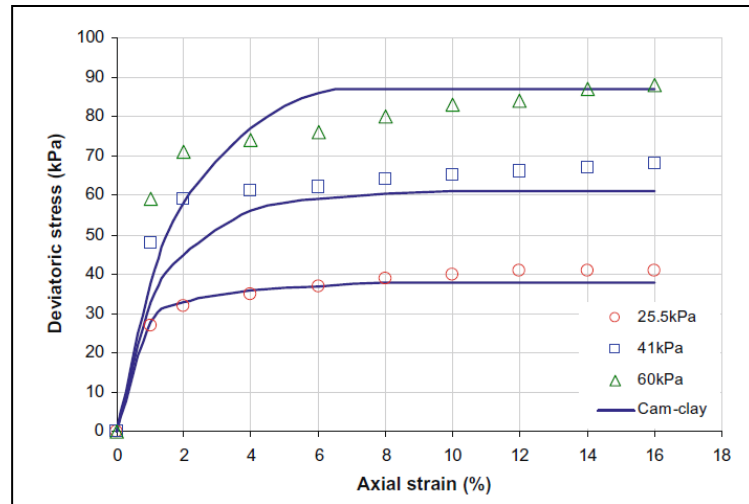


Figure 2.3. Chen et al. (2009), comparison of measured and calculated stress–strain curves for the clay model.

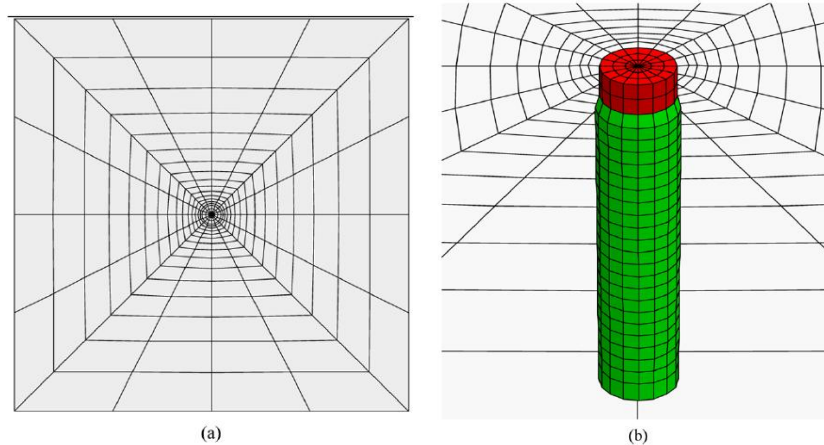


Figure 2.4. Chen et al. (2009), the Pier and Cap as modeled in FLAC (a) plan view (b) 3D view

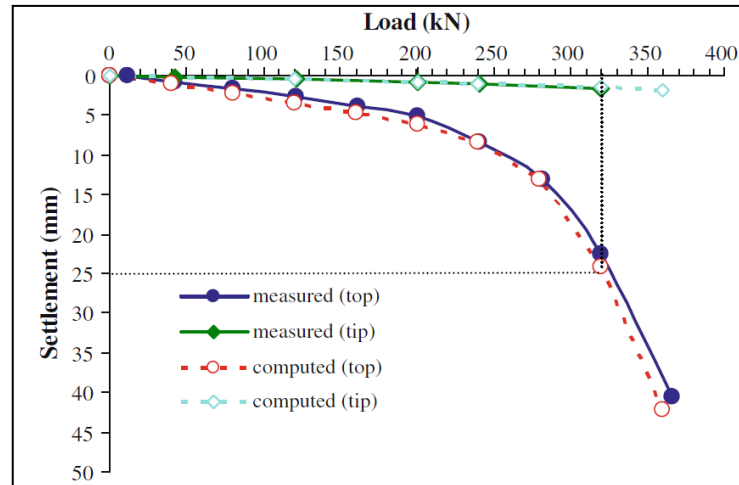


Figure 2.5. Chen et al. (2009), comparison between the computed and measured load-settlement curves

2.3. FEM to Study the Effect of Column Encasement

The improved performance of sand columns encased with geosynthetic fabric was studied by Raithel and Kempfert (2000), Murugesan and Rajagopal (2006), Lo et al. (2010) and Castro and Sagaseta (2011) using the finite element method.

Raithel and Kempfert (2000) presented an analytical model for predicting the pressure-settlement response of an axisymmetric unit cell of clay with a geosynthetic encased sand/stone column. In the model, the settlement in the column and soil was assumed to be equal, with an increased coefficient of lateral pressure adopted for the displacement method compared to the replacement method which was assumed similar to the initial at rest conditions. The model predictions were compared with FEM results using PLAXIS 2D where the Cam-Clay model was used for the clay and a modified Duncan-Chang model (a hyperbolic model) was used for the stone column. The geotextiles were assumed to be linear elastic. The unit cell concept was adopted in the analytical and FEM model, which assumes a single column in axisymmetric conditions (see Figure 2.6). In general, the FEM and the analytical method showed similar behavior and results. The differences in results get closer as the loading increases and

the ring tension in the geotextile coating is activated, which reveals that only small differences will be observed during serviceability state (see Figure 2.7).

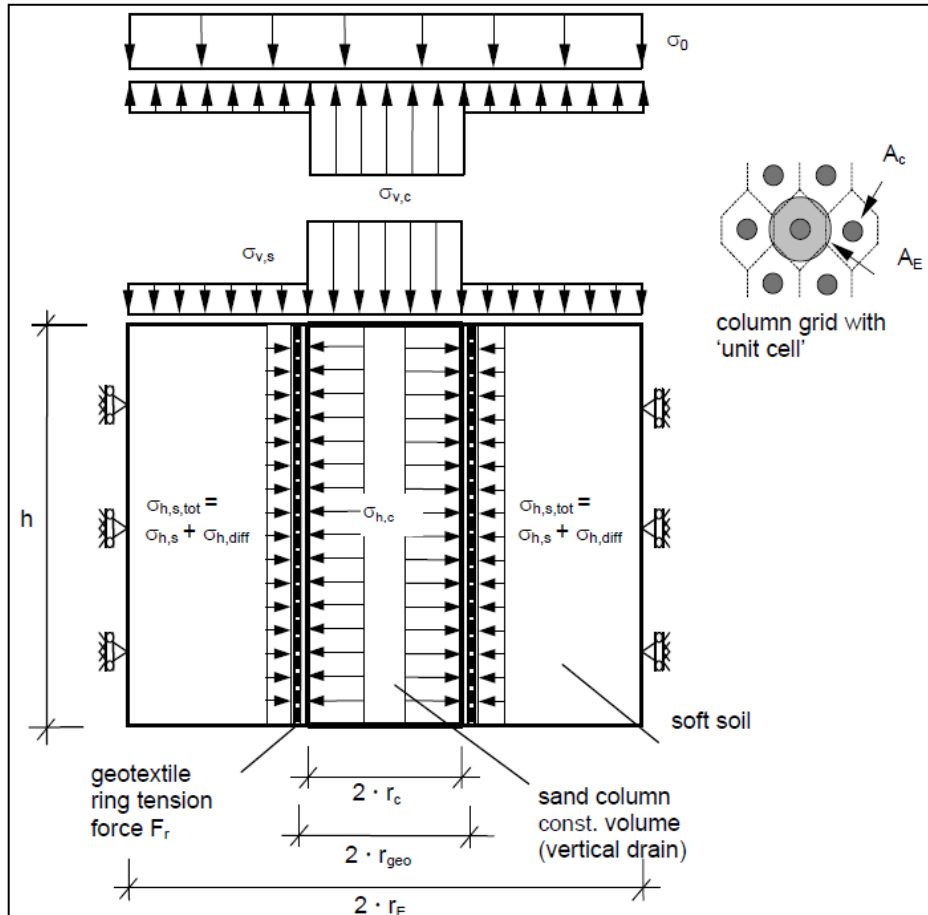


Figure 2.6. Raithel and Kempfert (2000), the assumptions and boundary conditions used in the analytical model

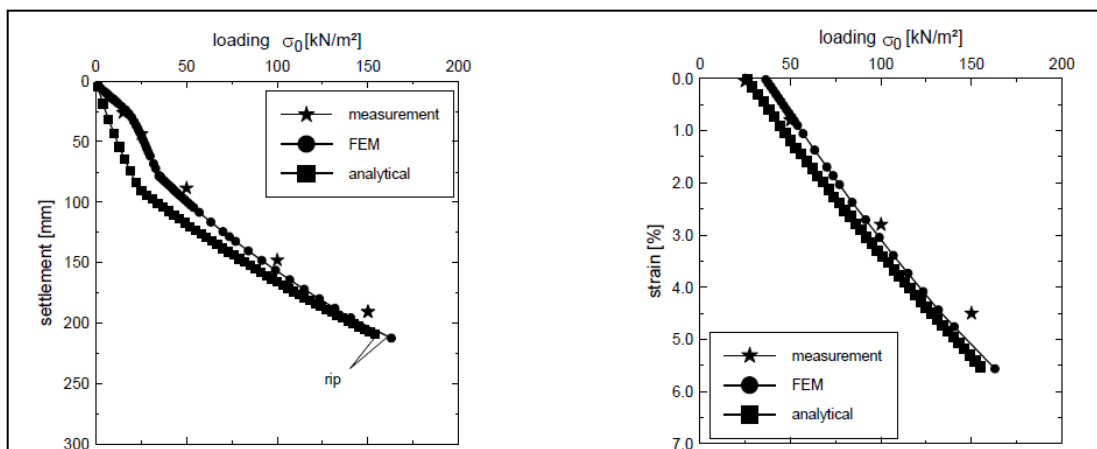


Figure 2.7. Raithel and Kempfert (2000), comparative calculation a) Load-settlement curve b) Load-strain curve

Murugesan and Rajagopal (2006) used the Finite Element Method (FEM) to conduct a parametric study of the effect of encasing stone columns with geosynthetic material on the degree of improvement in their load carrying capacity. In the study, the stone columns and the soft soils were modeled using hyperbolic non-linear elastic Duncan-Chang models, while the geosynthetic encasement around the stone column was modeled as a linear elastic material and discretized with continuum elements around the stone column. The FEM analyses were performed in 'GEOFEM' using the idealized axisymmetric cylindrical unit cell concept with 8-node quadrilateral mesh elements (see Figure 2.8). The results of the parametric study have reflected the effects of the properties of the founding soils, the stone columns and encasements on the improved performance which was quantified by the reduction in settlement and the lateral bulging of the stone column. Some of the interesting conclusions were that the lateral confining stresses are higher with encasement, the encasement at the top portion of the stone column up to twice the diameter is found to be adequate in improving its load carrying capacity, and the load carrying capacity of encased columns as compared to the ordinary stone columns is less dependent on the strength of the surrounding soil.

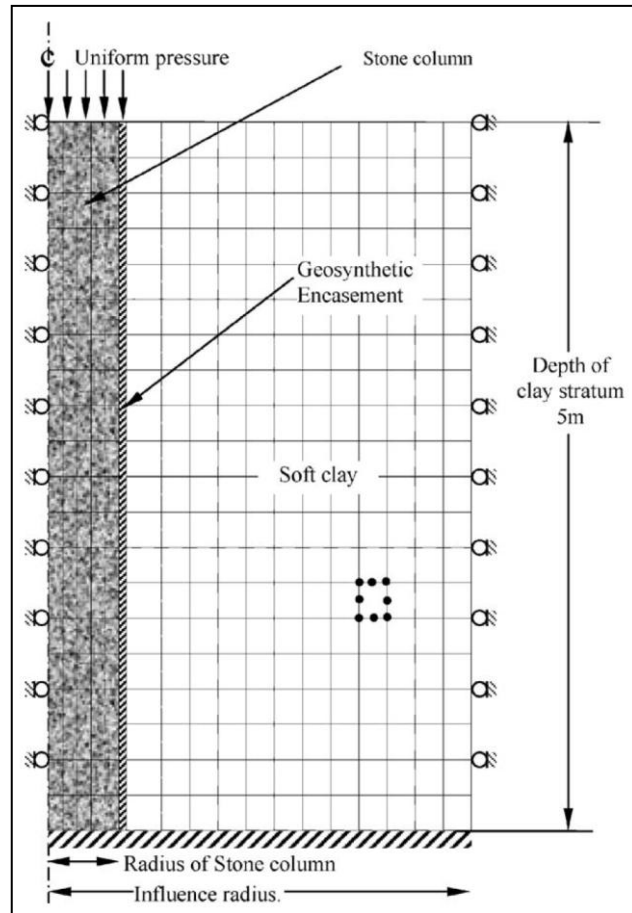


Figure 2.8. Murugesan and Rajagopal (2006), typical finite element mesh used in the analyses.

Lo et al. (2010) presented the results of a time-dependent coupled FE analysis, using AFENA software, which utilized the idealized unit cell concept (see Figure 2.9) to study the bearing and settlement response of a stone column reinforced with geosynthetic encasement under an embankment-type loading. The Cam-clay model was used to model the soft clay and a modified Mohr-Coulomb elastic plastic model similar to Duncan-Chang was used to model the stone column. The results of the FEM were compared to a simplified analyses solution suggested by the authors previously, where the FEM showed higher settlements. The FEM results have reflected the enhanced performance due to the use of encasements in stone columns.

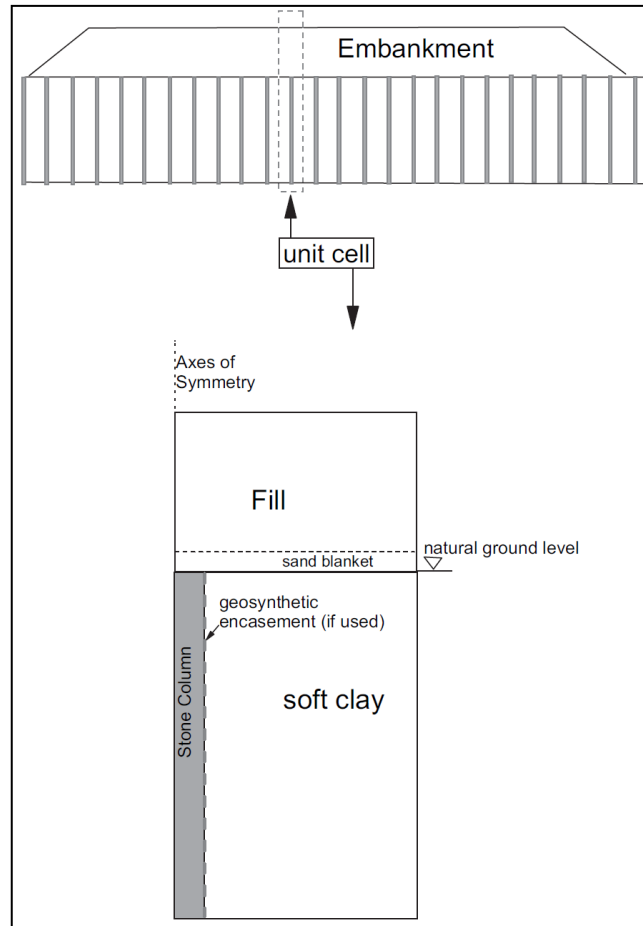


Figure 2.9. Lo et al. (2010), the idealized unit cell concept used in the FEM

Castro and Sagaseta (2011) presented an analytical model for studying the improvement brought by encased stone columns to the settlement and consolidation time of soft clays. The solution is presented at a horizontal slice at a depth z in the unit cell and a solution for the entire unit cell is obtained by integration. The idealized unit cell concept was adopted in the analyses (see Figure 2.10). The solution is presented for undrained loading followed by a consolidation process. The authors argue that for geotextile-encased columns, consolidation may be as fast as the loading pace indicating that a drained assumption may be more applicable. The real behavior is expected to be partially drained depending on the permeability and the rate of loading. The analytical model was checked with FE solutions using Plaxis. The FEM used the elasto-plastic

Mohr Coulomb model for the stone column and encasement, while the soft clay was considered as an elastic material. A simplified formulation of the solution was developed assuming drained conditions, which was in agreement with the numerical analyses (see Figure 2.11).

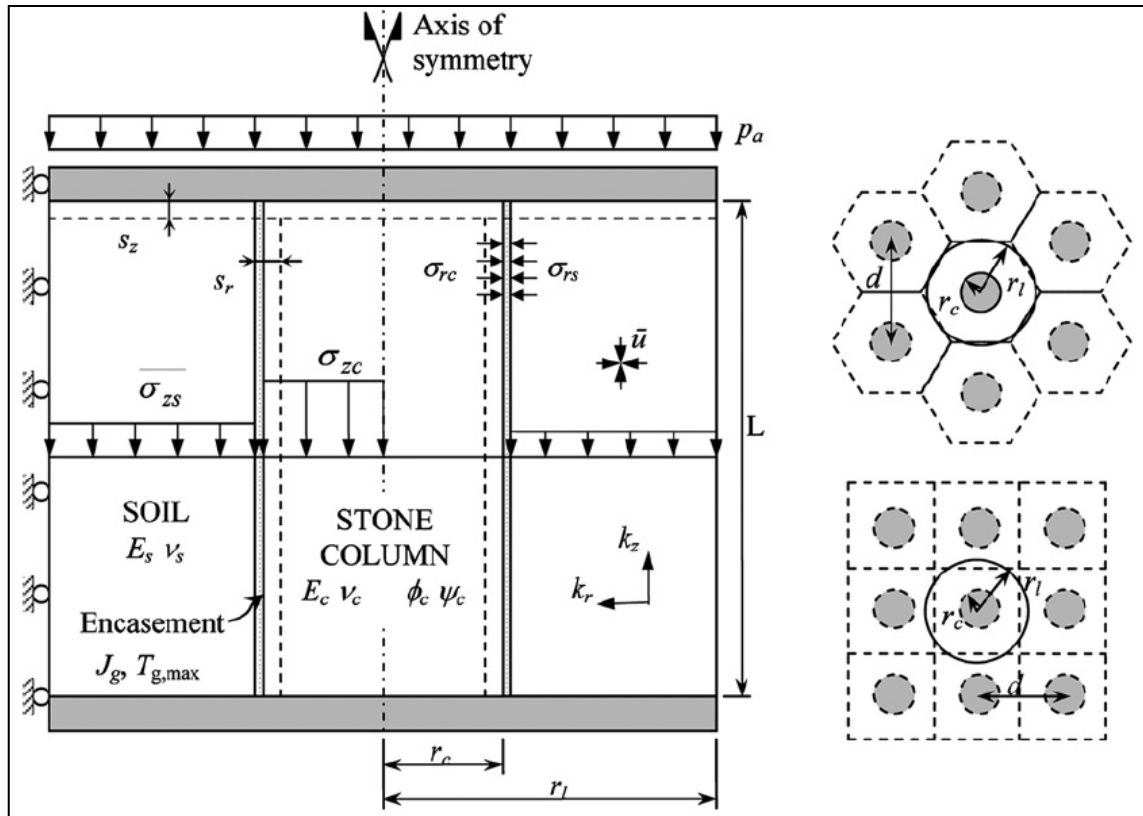


Figure 2.10. Castro and Sagaseta (2011), the idealized unit cell concept used in the analyses.

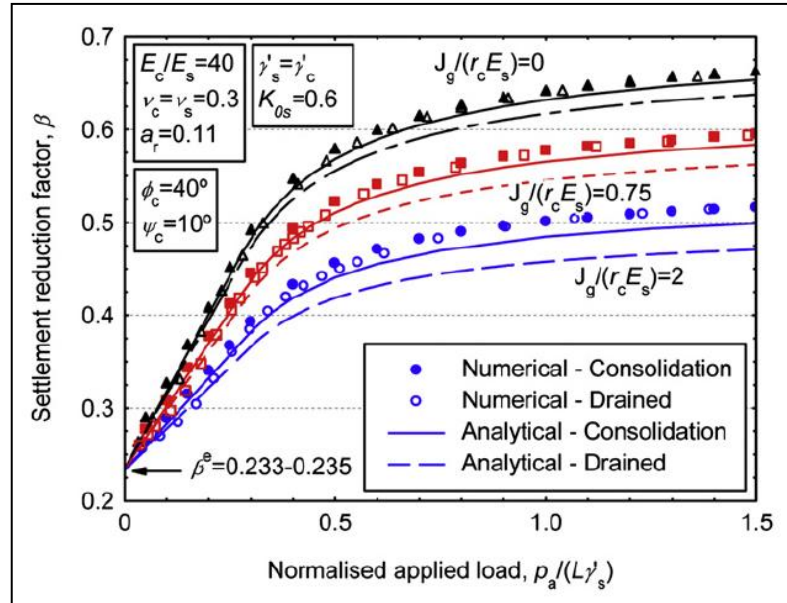


Figure 2.11. Castro and Sagaseta (2011), comparison between the analytical and numerical analyses.

2.4. FEM to Study the Group versus Single column behavior

The relation between group and single column behavior was studied by Elshazly et al. (2008) using the FE method. Elshazly et al. (2008) conducted an FEM analysis using Plaxis 2D to compare between settlements of foundations with limited extents and the unit cell concept. A post-installation horizontal to vertical stress ratio (K^*) of 1.5 was used in the analysis to represent the effect of column installation. Foundations with diameters B ranging from 5 to 50m and size ratios B/L ranging from 0.5 to 4.7 were used in the analysis. Pressures of 30, 90, and 150 kPa were used in the analysis. The finite element analyses have assumed the hardening soil model, which is originally based on the hyperbolic Duncan-Chang model, for the soft clay and the gravel that forms the stone columns. The model was developed using idealized axisymmetric conditions with 15-noded triangular mesh elements in Plaxis 2D (see Figure 2.12 to Figure 2.15). Results indicate that the ratio of the settlement of the group compared to the settlement of an equivalent unit cell increased as the B/L ratio of the foundation

increased. The authors have derived settlement correction factors between the group and unit cell models.

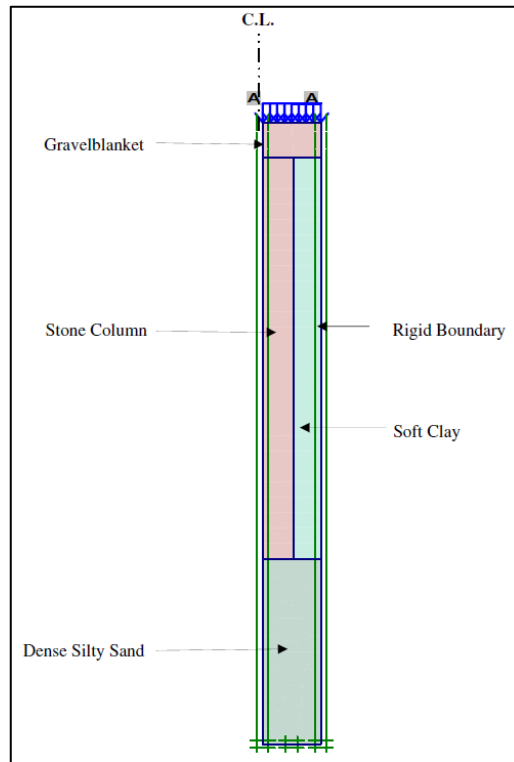


Figure 2.12. Elshazly et al. (2008), the unit cell model.

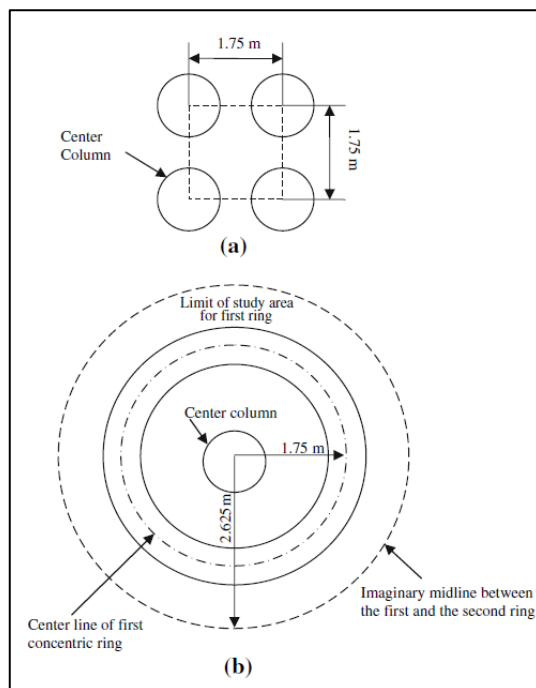


Figure 2.13. Elshazly et al. (2008), the idealized concept used in the analyses of the grid system

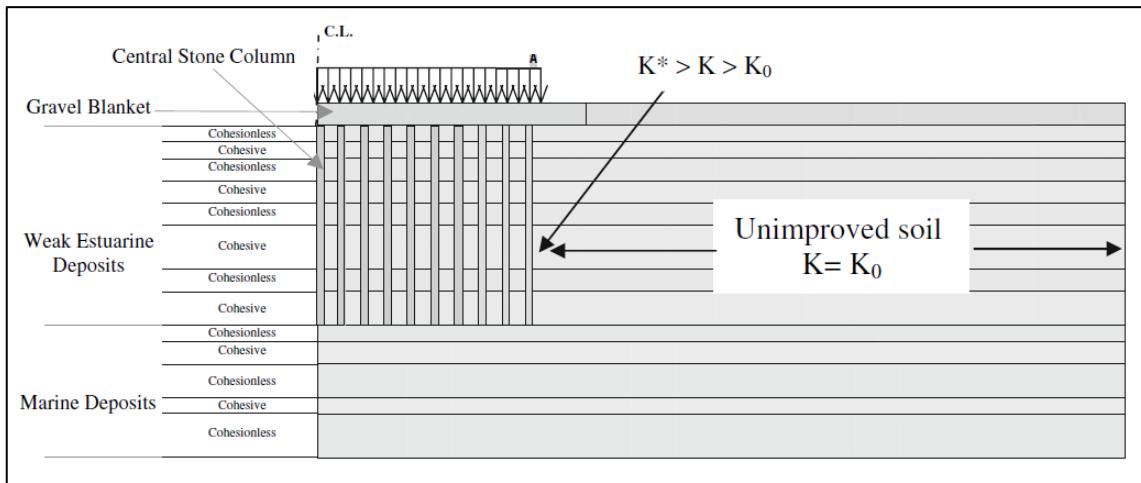


Figure 2.14. Elshazly et al. (2008), typical 2D axisymmetric modeling for a foundation resting on improved layered soil.

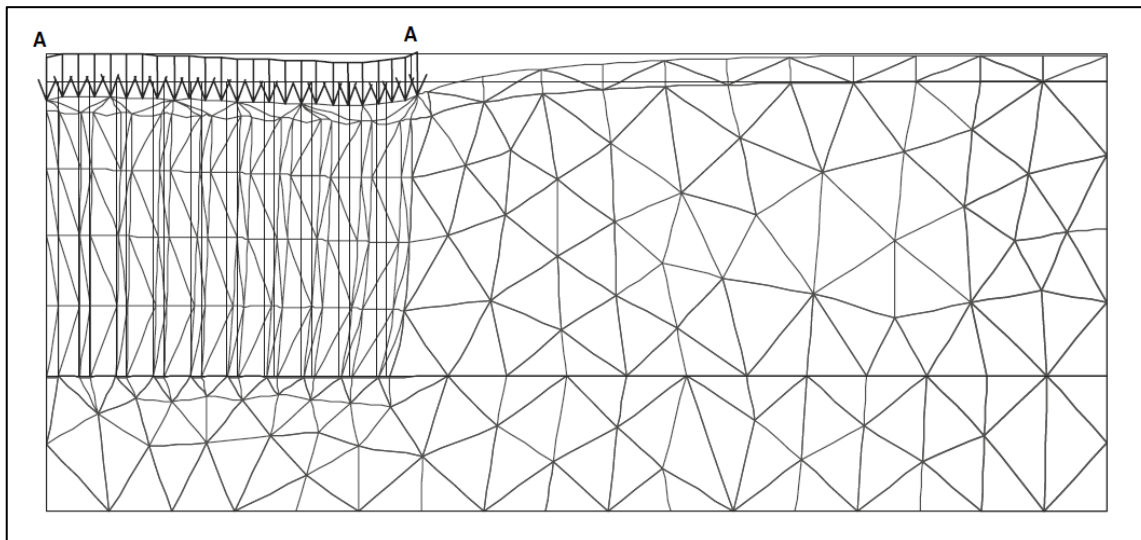


Figure 2.15. Elshazly et al. (2008), deformed mesh of a foundation over a group of sand columns

2.5. FEM to Verify Related Theories in Literature

Studies in which the performance of sand columns was investigated using FEM and compared / verified by the results of relative theories in literature include the work by Zahmatkesh & Choobbasti (2010).

Zahmatkesh and Choobbasti (2010) conducted finite element analyses using Plaxis to investigate the performance of stone columns in soft clay. The FEM was

conducted using the Mohr-Coulomb criterion for the soft clay and the sand/stone columns under drained conditions, where a rigid raft was placed on top of the reinforced ground. The single column models used axisymmetric conditions while the group columns models used an idealized plane strain conditions (See Figure 2.16). The column installation was also simulated to obtain the stresses due to the compaction of the columns. From the FEM analyses the authors estimated the coefficient of lateral pressure (k_0) after the columns installation and the settlement reduction ratio (SRR) of the soil. The results were compared to those obtained from standard analytical design methods (see Figure 2.17).

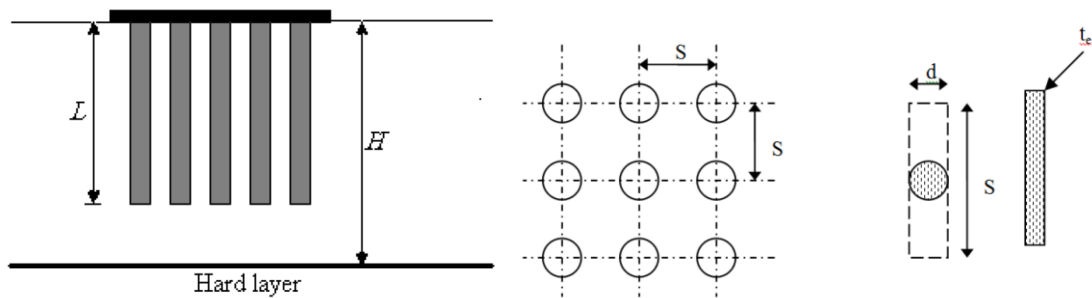


Figure 2.16. Zahmatkesh and Choobbasti (2010)

ρ	Present work			Priebe(1976)	Priebe(1995)	Poorooshasb et al(1996)(H/L=1)
	H/L=1	H/L=1.5	H/L=2	(H/L=1)	H/L=1	
10	0.77	0.83	0.86	0.61	0.62	0.65
15	0.67	0.76	0.83	0.50	0.52	0.52
20	0.60	0.71	0.76	0.42	0.44	0.43
25	0.50	0.63	0.69	0.35	0.38	0.35
30	0.41	0.59	0.68	0.29	0.33	0.28

Figure 2.17. Zahmatkesh and Choobbasti (2010), comparison of SRR with existing theories

2.6. FEM to Model Laboratory Tests

Studies in which the performance of sand columns was investigated using both FEM and experimental testing include the work by Ambily and Gandhi (2007) and Shahu and Reddy (2011).

Ambily and Gandhi (2007) developed a design procedure for stone columns considering the load sharing between the stone and the surrounding soft clay. The authors used the results of an experimental program coupled with FEM numerical analyses to develop the proposed design method. The experimental program involved tests that were conducted on single (see Figure 2.18) and group 10cm-diameter stone columns in a triangular pattern that were installed to full depth in a 450 mm thick soft clay specimen (see Figure 2.19).

The FEM was carried out using Plaxis 2D in axisymmetric conditions with 15-noded triangular mesh elements for both models, the single column (see Figure 2.20) and group of columns (see Figure 2.21) where the seven columns were idealized as a central column surrounded by six columns replaced by a ring having equivalent thickness and material properties. The soft clay, stones, and sand were modeled as Mohr-Coulomb elasto-plastic material. A drained behavior is assumed for all the materials.

The FEM results showed a good match to the experimental results, whether in the single column (see Figure 2.22) or the group of columns (see Figure 2.23) models.

For triangular column groups with spacing to column diameter ratio (s/d) of 3, the behavior of the reinforced samples was found to be similar to the specimens reinforced with a single column, where the entire area is loaded (see Figure 2.23). Accordingly, the authors mention that the unit cell concept can simulate the behavior of

the internal columns for s/d ratios varying from 1.5 to 4 where a large number of columns are loaded simultaneously, and suggest further experimental study to be carried out to verify this concept for closer spacing. As the shear strength of the clay decreases, more load will be taken by the stone column (stress concentration factor between 4 and 6). Finally, the authors proposed a design method for stone columns in soft clays.

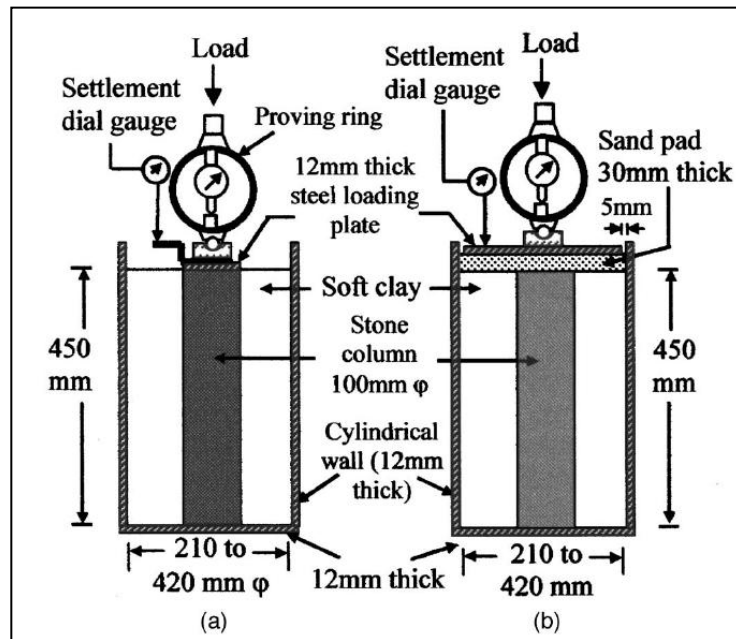


Figure 2.18. Ambily and Gandhi (2007), single column test arrangement (a) column area loading (b) entire area loading

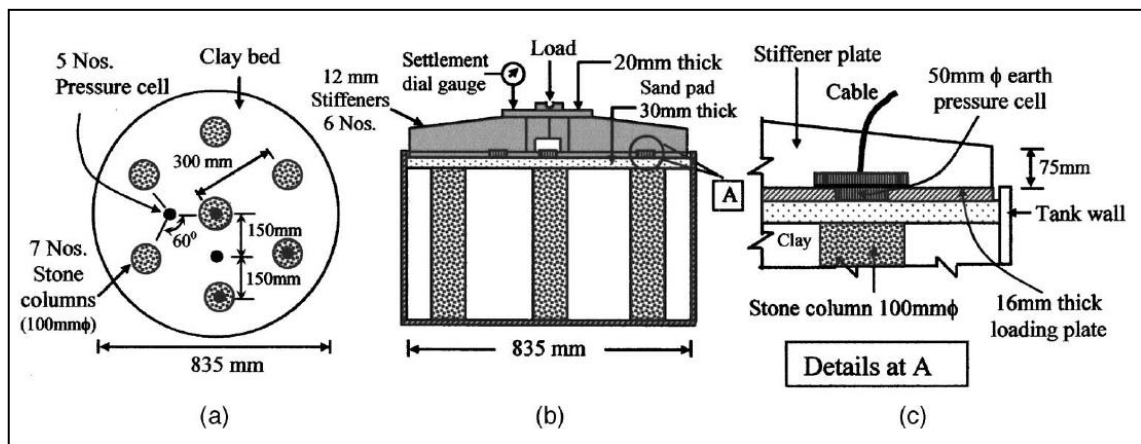


Figure 2.19. Ambily and Gandhi (2007), group test arrangement (a) plan view (b) section of test tank (c) details of pressure cell

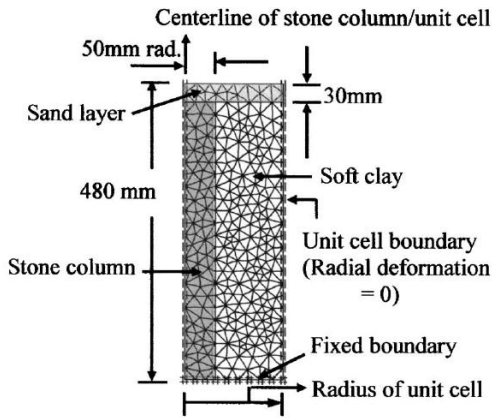


Figure 2.20. Ambily and Gandhi (2007), finite element discretization for single column (unit cell)

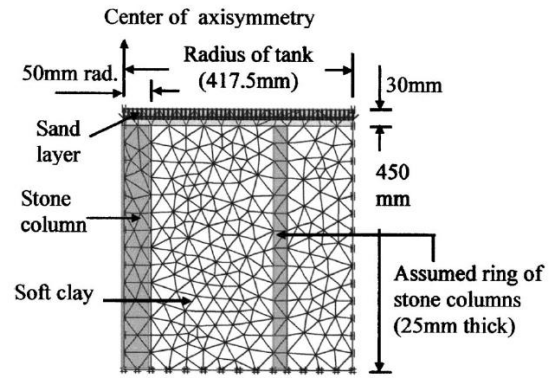


Figure 2.21. Ambily and Gandhi (2007), Finite element discretization for group test.

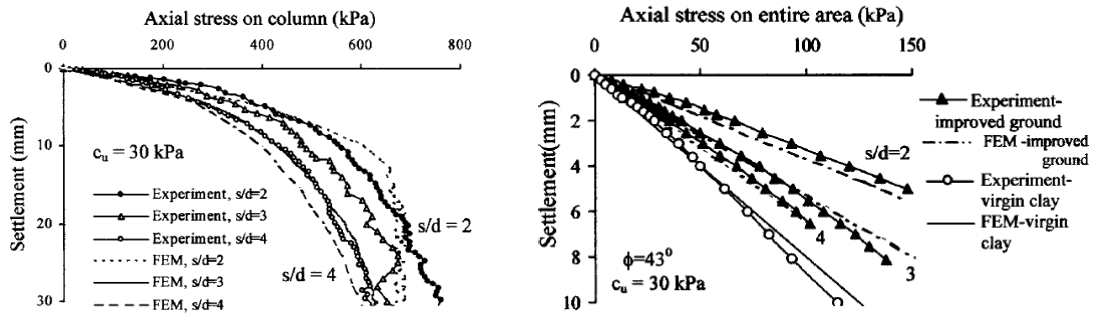


Figure 2.22. Ambily and Gandhi (2007), comparing the FEM to experimental results for the single column model

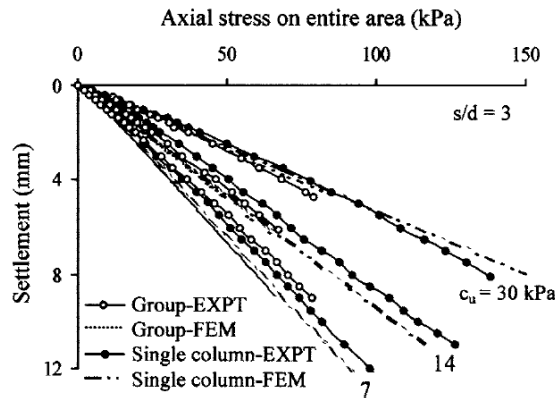


Figure 2.23. Ambily and Gandhi (2007), comparing the FEM to experimental results for the single and the group of columns models

Shahu and Reddy (2011) presented results of fully drained 1-g model tests that were conducted in Perspex cylinder tanks of 30-cm diameter and 60cm depth on groups

of stone columns installed in a bed of kaolin (30cm thick) consolidated from a slurry using a pressure of 30, 60, or 90 kPa. The undrained shear strength of the clay bed was found to be between 7 and 9 kPa. The columns were formed of Barbadur sand at a typical diameter of 1.3cm with some tests conducted with columns of 2.5cm diameter. A footing with a diameter of 10cm was used to load the groups, with the number of columns in the group ranging from 5 to 21, resulting in area ratios of 10%, 20%, and 30%. All columns were installed in a square grid using the replacement method with heights of 10cm or 15cm and were formed either dry or wet at relative densities of 50% and 80%. The load was applied in 10 to 14 equal increments of 15 kPa maintained until the settlement rate became less than 1mm/day. Results of stress versus settlement were presented with the stress normalized by the initial effective geostatic stress and the settlement normalized by the column length. Results indicate a relatively linear behavior up to a given displacement at which non-linear behavior is observed. The authors defined this boundary as failure. Results indicate that the higher the area ratio the higher the failure stress and stiffness of the group. For a given area ratio, increasing the L/D ratio of the columns resulted in an increased in the failure stress and stiffness. Results also indicated that increasing the density of the columns from 50% to 80% decreases the settlement of the group at a given normalized pressure.

A 3-D finite element model was created using ABAQUS to analyze the laboratory test results. The clayey soil was modeled using the Cam-clay model and the sand columns using the Mohr-Coulomb elastic-perfectly plastic model (see Figure 2.24). The FE mesh was calibrated with results of triaxial tests. Interesting 3D images of the failure of the column group are presented and indicate that as one moves away from the center of the column group, outward bending of the columns increase, with central

columns not showing signs of bending (see Figure 2.26). The FEM predictions and the measured-model test results were in close agreement (see Figure 2.25). The predicted values of the ultimate load and the corresponding settlement by the finite-element analysis as compared with the measured results lie within 3 to 21% and 4 to 37%, respectively. The inaccuracy in the finite-element results may occur because of mesh convergence issues, the subjectivity/uncertainties in obtaining the constitutive model parameters, and inappropriateness of the constitutive model employed for the granular material.

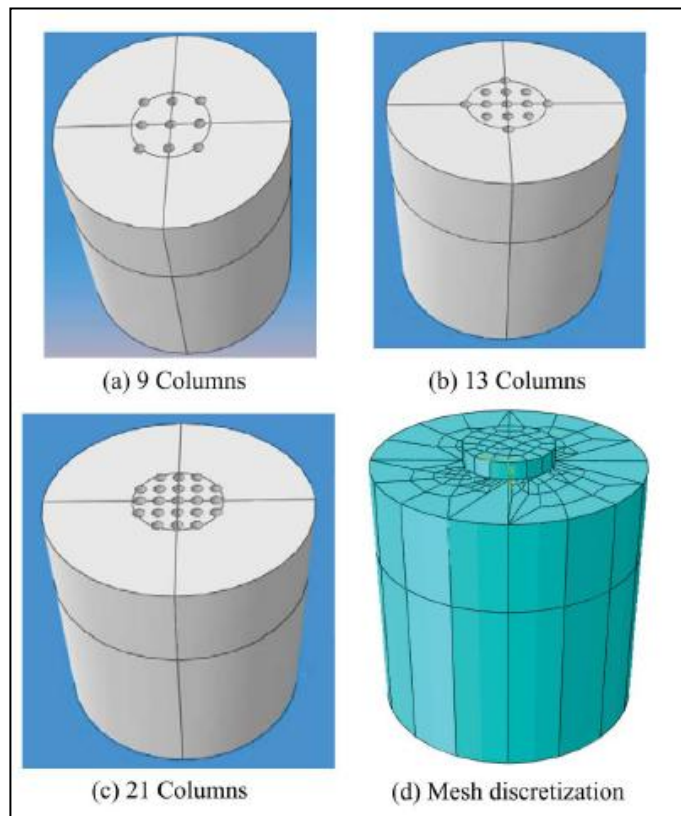


Figure 2.24. Shahu and Reddy (2011), the adopted FE model

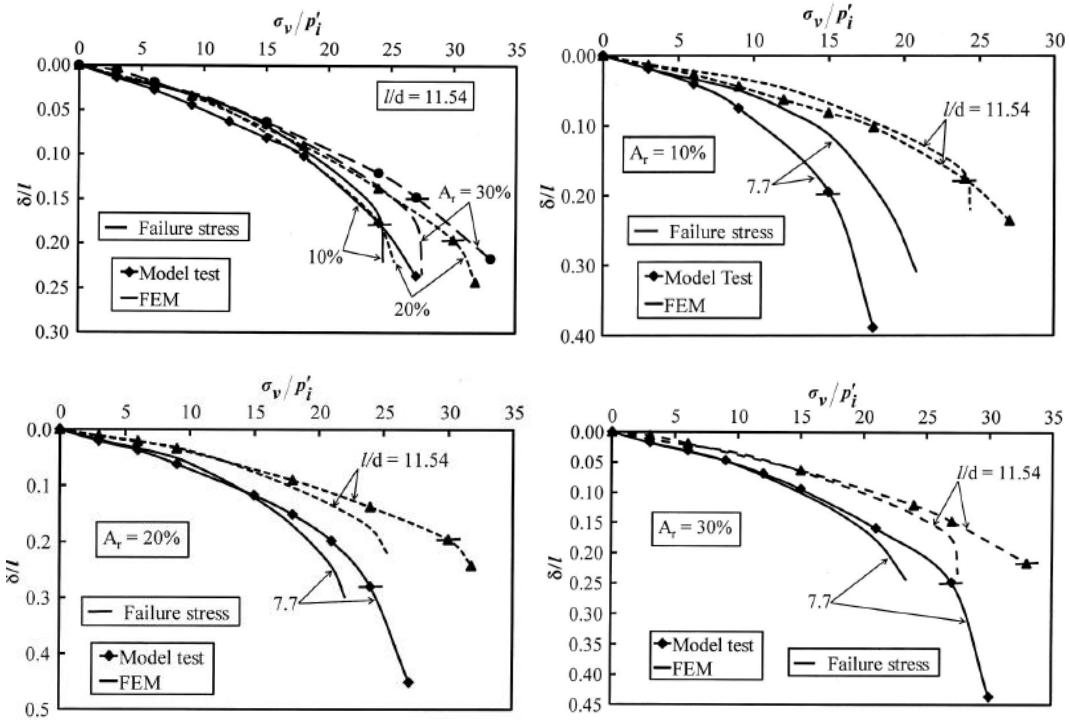


Figure 2.25. Shahu and Reddy (2011), comparison between the FEM and experimental results

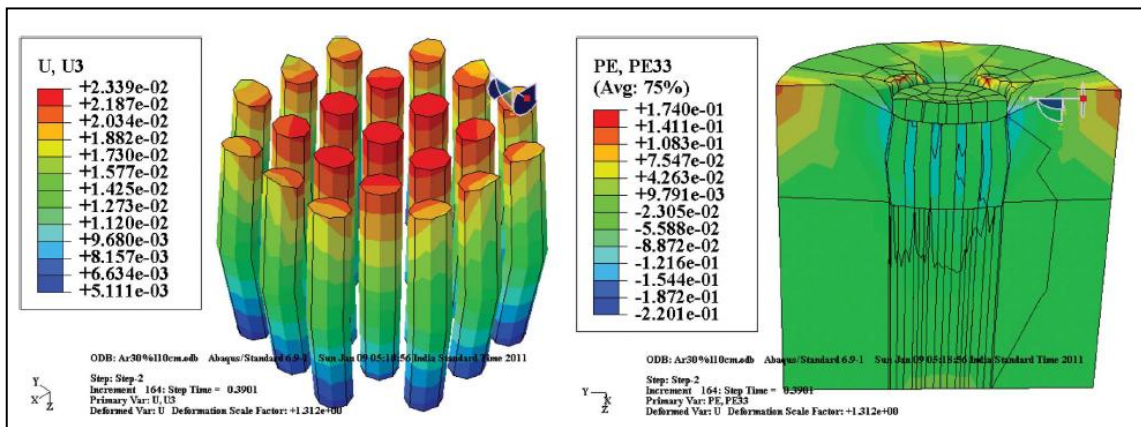


Figure 2.26. Shahu and Reddy (2011), response contours of group foundation at failure

2.7. Limitations of Published Studies

The proper selection of constitutive models for the sand columns and surrounding clay in FEM analyses is of great importance. The models need to be representative and capable of simulating the behavior of the material as close as possible to reality. When it comes to sand, the models utilized in published FEM

studies generally ignore the strain softening that occurs in sand and assume that the load carrying capacity of the sand column increases with strain (strain hardening models) or remains constant beyond the peak strength. It is hypothesized that a model that captures the strain softening behavior that is associated with the typical load response of medium dense to dense sands may result in better predictions of the load response of the clay/sand column composite. Hypoplasticity is the basis of a relatively recent constitutive model that is capable of modeling the strain softening behavior in sands. Accordingly, this research study will explore this model for the first time in applications involving sand columns in clay and will compare it to other soil models to check how beneficial and practical it is. Further details about Hypoplasticity will be presented in Chapter 3.

CHAPTER 3

HYPOPLASTIC MODEL

3.1. Introduction

This Chapter starts by introducing Hypoplasticity, then briefly describes the properties of the materials used in the laboratory testing program of Maalouf (2012). The two materials used in the triaxial tests specimens are Kaolin clay and Ottawa sand. Atterberg limits, specific gravity, hydrometer analysis, and 1-dimensional consolidation tests were performed using Kaolin clay. The results of the consolidation tests were used to determine the coefficient of consolidation of the clay using the log time method and the square root of time method. For Ottawa sand, sieve analysis, triaxial, and relative density tests were performed.

Having the properties of the materials from Maalouf (2012) and referring to some of the published data on Ottawa sands and Kaolin clay, the Hypoplastic model parameters for the sand and clay were derived, calibrated and verified.

3.2. Hypoplasticity

Hypoplasticity is a particular class of incrementally non-linear constitutive models, developed during the 1990's at the University of Karlsruhe to predict the behavior of soils. Unlike elasto-plasticity, in hypoplasticity the strain rate is not decomposed into elastic and plastic parts and the models do not explicitly use the concepts of the yield surface and plastic potential surface.

The Hypoplasticity models are capable of predicting the important features of the soil performance, such as the critical state, non-linear behavior in the small and large strain ranges, dependency of the peak strength on soil density and the soil stiffness on the loading direction, etc. Some of the important milestones in the development of hypoplasticity are briefly listed below:

- The early hypoplastic models were developed by means of trial and error procedures, as illustrated in Kolymbas (1991).
- Gudehus (1996) implemented the critical state concept by proposing a modification to include the influence of the stress level (barotropy) and the influence of density (pyknotropy).
- The model was later revised by von Wolffersdorff (1996) to incorporate the Matsuoka-Nakai critical state stress condition.
- The Von Wolffersdorff (1996) model is nowadays considered as a standard hypoplastic model for granular materials and is implemented in the FEM software PLAXIS.
- Later developments focused on hypoplasticity for fine grained soils.
- Herle and Kolymbas (2004) modified the model by Von Wolffersdorff (1996) to account for lower friction angles and independent calibration of bulk and shear stiffnesses.
- Based on Herle and Kolymbas (2004) and Niemunis (2002) "generalized hypoplasticity" principle, Masin (2005) developed a hypoplastic model for clays characterized by a simple calibration procedure and capability of correctly predicting the strain behaviour. Masin (2007) then proposed modifications of the model from Masin (2005) to consider the behaviour of clays with meta-stable structure.
- The clay hypoplastic model of Masin (2005 and 2007) is also incorporated in the FEM software PLAXIS.

3.3. Materials Properties

3.3.1. Kaolin Clay

The Index properties for the Kaolin clay were determined in the laboratory and are presented in Table 3.1.

Table 3.1. Index properties of Kaolin clay

Liquid limit (%)	Plastic limit (%)	Plasticity index	Specific gravity	Percent finer than 10 μm (%)	Percent finer than 2 μm (%)
55.7	33.3	22.4	2.52	85	53

The consolidation properties of the Kaolin slurry were obtained from a one-dimensional consolidation test that was conducted on a clay sample with a diameter of 5.08cm and a height 1.91cm. The test specimen was trimmed from a larger specimen which was consolidated from a slurry in a 1-dimensional prefabricated consolidometer under a vertical effective stress of 100 kPa. The specific gravity, initial water content, and initial void ratio of the slurry-consolidated specimen are presented in Table 3.2.

The consolidation test was performed in accordance with the requirements of ASTM 2435. The results pertaining to the loading and unloading stages are presented in Table 3.3. Figure 3.1 shows the variation of the void ratio versus the logarithm of the effective vertical stress, where the void ratio is defined at the end of each load increment (24 hours from the onset of loading). Based on the e-Log p curve presented in Figure 3.1, the virgin compression (C_c), reloading (C_r), and swelling (C_s) slopes are computed as 0.413, 0.146, and 0.157, respectively. Based on Casagrande's approach, the pre-consolidation pressure was determined from the e-log p curve as 96 kPa.

Table 3.2. Initial properties of 1-dimensional consolidation test specimen of Kaolin clay

Specific gravity	2.52
Initial water content (%)	61
Initial void ratio	1.53
Initial saturation (%)	100 (assumed)

Table 3.3. One-Dimensional consolidation pressure test results

Cosolidation pressure (kPa)	Final dial reading (cm)	Change in specimen height (cm)	Final specimen height (cm)	Height of void (cm)	Final void ratio	Average height during consolidation (cm)
0	0		1.905	1.153	1.534	
		0.144				1.833
10	0.144		1.761	1.009	1.342	
		0.033				1.7445
20	0.177		1.728	0.976	1.298	
		0.05				1.703
49	0.227		1.678	0.926	1.232	
		0.068				1.644
98	0.295		1.61	0.858	1.141	
		0.08				1.57
196	0.375		1.53	0.778	1.035	
		0.09				1.485
383	0.465		1.44	0.688	0.915	
		0.097				1.3915
775	0.562		1.343	0.591	0.786	
		0.103				1.2915
1550	0.665		1.24	0.488	0.649	
		-0.044				1.262
383	0.621		1.284	0.532	0.708	
		-0.07				1.319
98	0.551		1.354	0.602	0.801	
		-0.062				1.385
20	0.489		1.416	0.664	0.883	

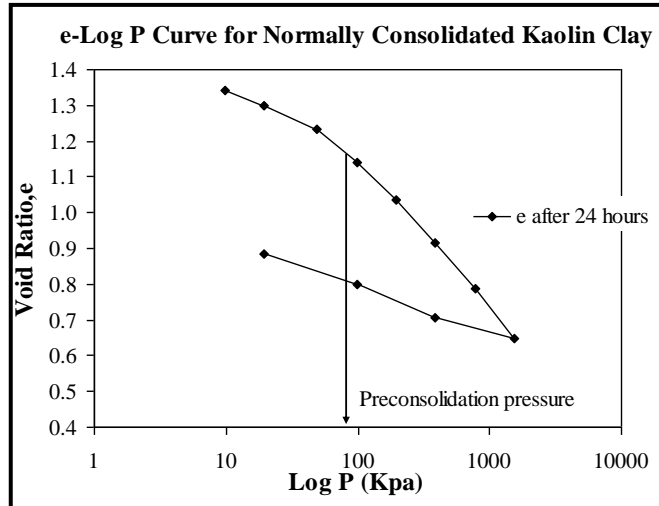


Figure 3.1. e-log P for normally consolidated Kaolin clay

Calculated values for the coefficient of consolidation (C_v) are presented as a function of the vertical effective stress in Table 3.4, and are plotted as a function of the logarithm of the vertical effective stress on Figure 3.2.

Table 3.4. Coefficient of consolidation obtained from t_{50} and t_{90}

Consolidation pressure (kPa)	Coefficient of consolidation, C_v (cm^2/min)	
	From t_{90}	From t_{50}
10	0.055	0.103
20	0.101	0.156
49	0.104	0.156
98	0.112	0.175
196	0.136	0.182
383	0.147	0.231
775	0.152	0.214
1550	0.030	0.013

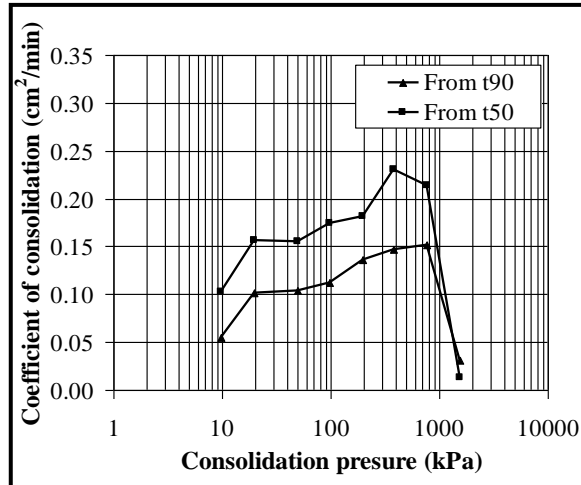


Figure 3.2. Variation of C_v with consolidation pressure for Kaolin clay

3.3.2. Ottawa Sand

The soil used in the reinforced columns was Ottawa sand which is a well-known laboratory tested material. Grain size distribution analyses conducted on Ottawa sand indicate that the particles have a mean diameter, D_{50} of 0.34mm, a uniformity coefficient, U_c of 2.3, and a coefficient of curvature, C_c of 0.82. The sand classifies as poorly graded sand (SP) according to the Unified Soil Classification System (USCS). The index properties for Ottawa sand and the sieve analysis results are shown in Table 3.5 and Table 3.6, respectively, while the particle size distribution curve is shown in Figure 3.3.

Table 3.5. Index properties of Ottawa sand

D ₁₀ (mm)	0.22
D ₃₀ (mm)	0.3
D ₆₀ (mm)	0.5
Coefficient of uniformity (D ₆₀ /D ₁₀)	2.3
Coefficient of curvature (D ₃₀) ² /(D ₆₀ *D ₁₀)	0.82
Soil classification (USCS)	SP
Maximum void ratio (e _{max})	0.49
Minimum void ratio (e _{min})	0.75
Specific gravity	2.65

Table 3.6. Sieve analysis results for Ottawa sand

Sieve No.	Diameter (mm)	Weight of retained soil (gm)	Cumulative percent retained (%)	Cumulative percent finer (%)
20	0.84	0	0.0	100.0
40	0.42	223.8	28.0	72.0
60	0.25	464.4	86.2	13.8
100	0.15	87.2	97.1	2.9
140	0.105	18.5	99.5	0.5
200	0.075	1.5	99.6	0.4
pan		2.8	100.0	0.0

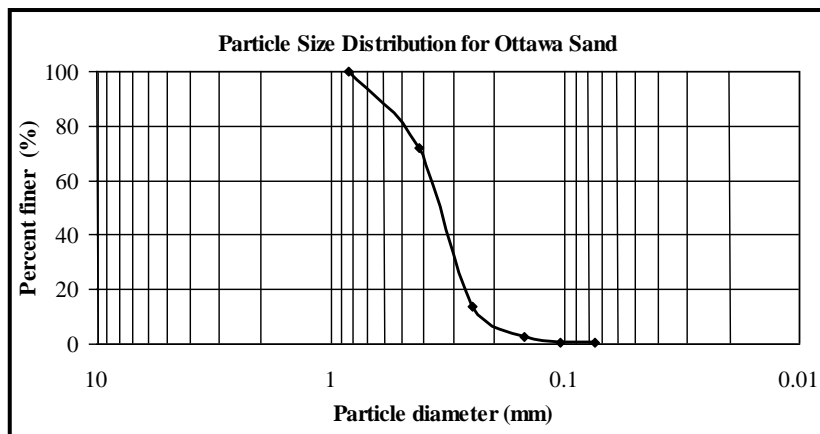


Figure 3.3. Sieve analysis curve for Ottawa sand

Consolidated drained (CD) triaxial tests were conducted on Ottawa sand at confining pressures of 100, 150, and 200 kPa. Ottawa sand triaxial specimens with a height of 14.2cm and a diameter of 7.1cm were prepared at a dry density of 16.2 kN/m³

(corresponding to a relative density of 44%, and a void ratio of 0.604). This density corresponds to the dry density of the sand column that was used to reinforce the Kaolin clay specimens in the testing program. Variation of deviatoric stress with axial strain for the Ottawa sand during CD testing at the different confining pressures is shown on Figure 3.4. As indicated by the Mohr Coulomb effective stress failure envelop for the Ottawa sand (Figure 3.5), the drained angle of friction (ϕ') corresponds to a value of about 35° and a cohesion of zero.

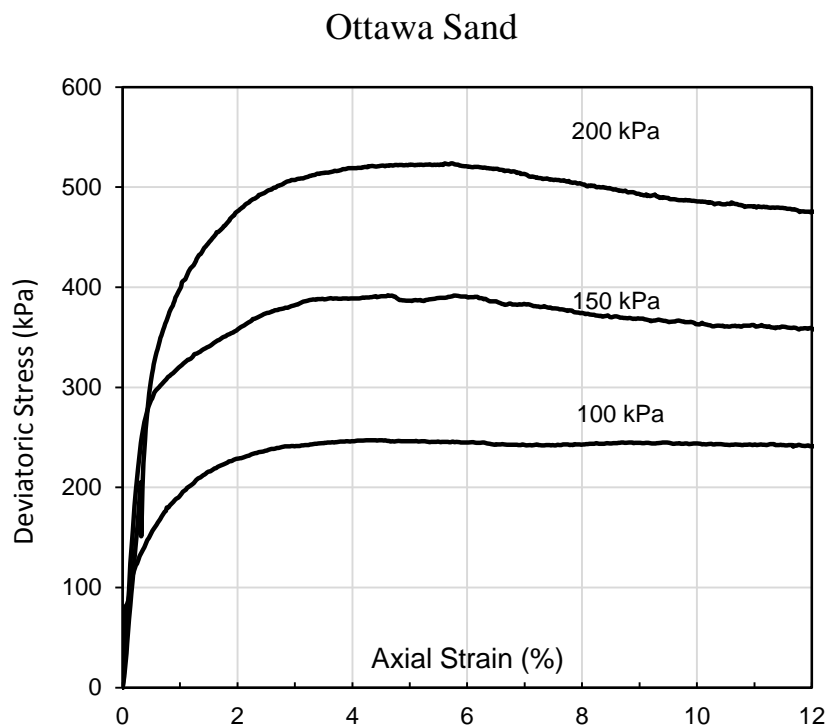


Figure 3.4. Deviatoric stress versus axial strain for Ottawa sand.

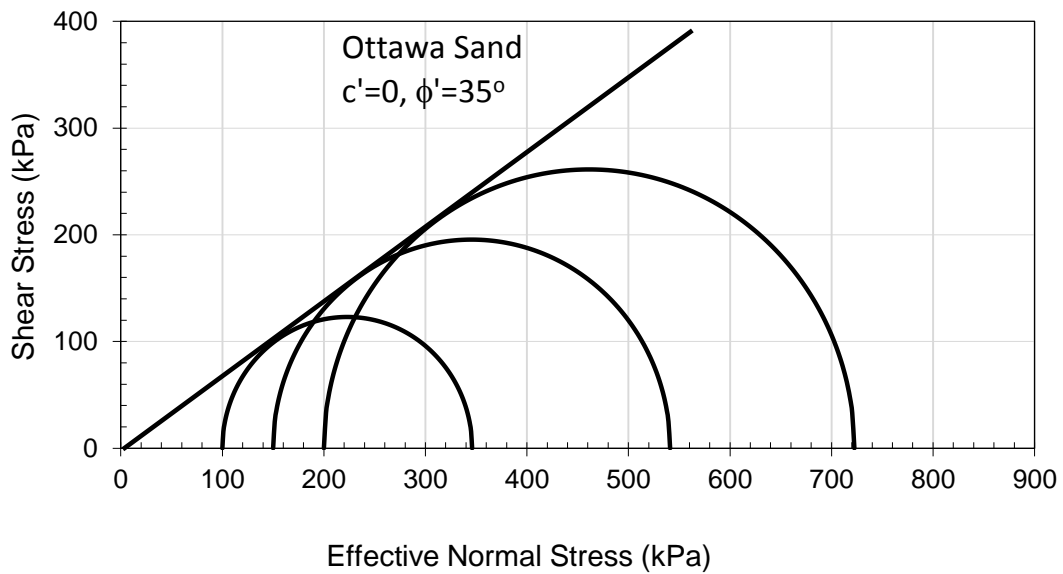


Figure 3.5. Mohr Coulomb effective stress failure envelop for Ottawa sand

3.4. Hypoplastic model – Ottawa Sand

The soil used in the reinforced columns was Ottawa sand which is a well-known laboratory tested material. Since not all the required lab tests were carried in the lab on the Ottawa sands, we went through the literature to obtain some parameters from reliable published data.

As mentioned in the previous chapter, grain size distribution analyses conducted on Ottawa sand indicate that the particles have a mean diameter, D_{50} of 0.34mm, a uniformity coefficient, U_c of 2.3, and a coefficient of curvature, C_c of 0.82. The sand classifies as poorly graded sand (SP) according to the Unified Soil Classification System (USCS). The maximum void ratio (e_{max}) and the minimum void ratio (e_{min}) are 0.75 and 0.49 respectively.

The sand hypoplastic model by von Wolffersdorff (1996) requires 8 material parameters:

- e_{d0} , e_{c0} and e_{i0} are reference void ratios specifying positions of limiting void ratio curves
- ϕ_c is the critical state friction angle
- h_s and n control the shape of limiting void ratio curves (normal compression lines and critical state line)
- α controls the dependency of peak friction angle on relative density
- β controls the dependency of soil stiffness on relative density
- Herle and Gudehus (1999) have detailed the Calibration procedure for the von Wolffersdorff hypoplastic model.

Each of the above listed parameters will be discussed in the preceding sections and the methodology adopted in determining or obtaining these parameters will be illustrated.

3.4.1. e_{d0} , e_{c0} and e_{i0}

The minimal void ratio e_d , maximal void ratio e_i and critical void ratio e_c are parameters that designate particular boundary functions of void ratio (Glebowicz 2006).

Parameter e_i (isotropic normal compression) applies for void ratio for the loosest sand, which can exist under given stress where above this value the skeleton of sand does not exist.

Parameter e_c is the critical state (CSL) void ratio of the soil sample. This void ratio is reached when the soil is subjected to the triaxial compression test and the Coulomb-Mohr envelope is reached.

Parameter e_d is the minimal void ratio at the state of maximum density, which could be reached after cyclic shearing of the soil sample.

In the von Wolffersdorff model the maximal, minimal and critical void ratios decrease, when the mean pressure p increases according to Equation 3.1, where e_{d0} , e_{c0} and e_{i0} are values of these parameters for a mean pressure $p = 0$ (Figure 3.6).

Equation 3.1 The Von Wolffersdorff model's equation

$$\frac{e_d}{e_{d0}} = \frac{e_c}{e_{c0}} = \frac{e_i}{e_{i0}} = \exp \left[- \left(\frac{3p}{h_s} \right)^n \right],$$

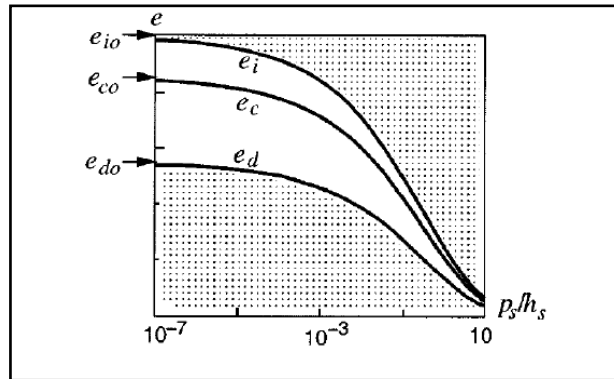


Figure 3.6. Limiting Void Ratios by Gudehus (1996)

Referring to Figure 3.6, it is obvious that e_{d0} , e_{c0} and e_{i0} are theoretical values, determined from extrapolation. This is because non-stress state cannot be achieved in Earth's gravity. Equation 3.1 was experimentally confirmed, in the isotropic case, for a wide range of mean stress.

Parameters e_{d0} , e_{c0} and e_{i0} can be estimated by simple geotechnical tests. According to particular experimental results (Herle, Gudehus 1999), the following relations of e_{\min} and e_{\max} and hypoplastic parameters (e_{d0} , e_{c0} and e_{i0}) were accepted and widely used (Tejchman 2004):

$$e_{d0} \approx e_{\min}$$

$$e_{c0} \approx e_{\max}$$

$$e_{i0} \approx 1.2e_{\max}$$

Accordingly, for the Ottawa sand the following parameter's values can be derived from the above:

$$e_{d0} \approx e_{\min} = 0.49$$

$$e_{c0} \approx e_{\max} = 0.75 \text{ (used 0.76)}$$

$$e_{i0} \approx 1.2e_{\max} = 0.9 \text{ (used 0.88)}$$

Comparing the above results to published data on Ottawa sands, we found that what was published by Głebowicz (2006) is similar to what we have (

Table 3.7). e_{d0} , e_{c0} and e_{i0} in

Table 3.7 for the Ottawa sand are similar to what we got for the sand used in this research study.

Table 3.7. Hypoplastic parameters determined for some granular materials, Głebowicz (2006)

Material	φ [°]	h_s [MPa]	n	e_{d0}	e_{c0}	e_{i0}	α	β
Toyoura sand	30	2600	0.27	0.61	0.98	1.10	0.18	1.00
Hochstetten sand	33	1500	0.28	0.55	0.95	1.05	0.25	1.50
Schlabendorf sand	33	1600	0.19	0.44	0.85	1.00	0.25	1.00
Hostun sand	31	1000	0.29	0.61	0.91	1.09	0.13	2.00
Karlsruhe sand	30	5800	0.28	0.53	0.84	1.00	0.13	1.05
Zbraslav sand	31	5700	0.25	0.52	0.82	0.95	0.23	1.00
Ottawa sand	30	4900	0.29	0.49	0.76	0.88	0.10	1.00
Ticino sand	31	5800	0.31	0.60	0.93	1.05	0.20	1.00
SLB sand	30	8900	0.33	0.49	0.79	0.90	0.14	1.00
Hochstetten gravel	36	32000	0.18	0.26	0.45	0.50	0.10	1.80
plastics	32	110	0.33	0.53	0.73	0.80	0.08	1.00
wheat	39	20	0.37	0.57	0.84	0.95	0.02	1.00
Skarpa sand	31	5000	0.3	0.43	0.68	0.8	0.26	0.97

3.4.2. The critical state friction angle φ_c

A simple estimation of the critical state friction angle (φ_c) can be obtained from the angle of repose of a dry granular material or from directly measuring the angle of friction at the critical state in shear tests.

As mentioned by Salgado et al (2000), the critical-state shear strength develops at axial strains exceeding 25%. Thus the critical-state angle of friction can be determined from triaxial tests at strain ranges between 25% and 40%, which is beyond the recorded data of the triaxial tests carried out on the Ottawa sand used in this research. However, a value of $\varphi_c = 30^\circ$ can be adopted from the published parameters on Ottawa sand (Table 3.1) by Głębowski (2006). This value was verified later on by carrying out a single element analysis and getting a good match with the lab test results.

3.4.3. Parameters h_s and n

The parameter h_s is used as a reference pressure and it denotes the granulate hardness. The exponent n accounts for the pressure sensitivity of a grain skeleton. In the absence of any Oedometric test carried out on a loose Ottawa sand sample, the parameters h_s and n can be assumed from the published parameters by Głębowski (2006). Since the two soils have similar reference void ratios, the parameters $h_s = 4900$ MPa and $n=0.29$ from the relation of Equation 3.1 is expected to be similar. These values were verified later on by carrying out a single element analysis and getting a good match with the lab test results.

3.4.4. Parameters α and β

Parameter α controls the dependency of peak friction angle (φ_p) on relative void ratio (see Figure 3.7). The parameter β influences the size of the response envelope (see

Figure 3.7). Both α and β were calibrated using the single element analysis which resulted in the values of 0.12 and 1.0 respectively.

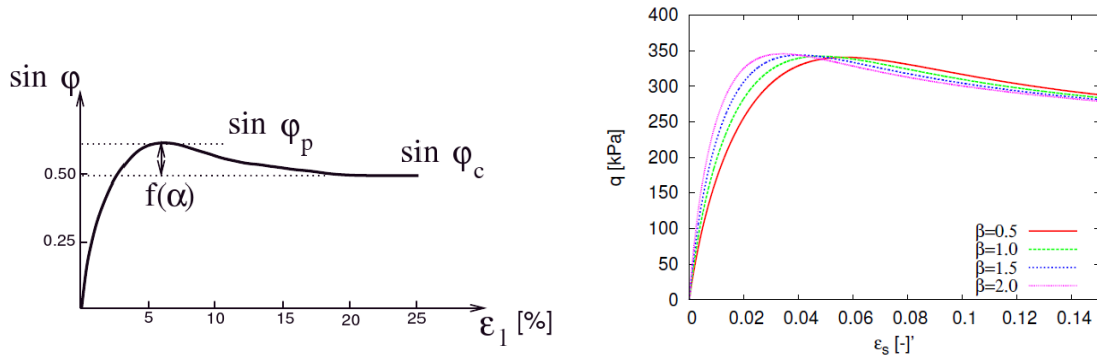


Figure 3.7. The Function of α and β , α controls the dependency of peak friction angle and β influences the size of the response envelope (Masin 2005)

3.4.5. Intergranular parameters

The Intergranular strain concept by Niemunis and Herle (1997) enables to model small-strain-stiffness effects in hypoplasticity. It requires 5 material parameters:

- m_R : parameter controlling the initial (very-small-strain) shear modulus upon 180° strain path reversal and in the initial loading
- m_T : parameter controlling the initial shear modulus upon 90° strain path reversal
- R : The size of the elastic range (in the strain space)
- β_r and X : control the rate of degradation of the stiffness with strain.

To have better match in the triaxial stress strain curves at strains less than 2%, we have used typical intergranular parameters that were suggested by Masin (2005) and carried out minor calibrations / adjustment in the single element analyses. The adopted intergranular parameters are:

- $m_R = 5.0$
- $m_T = 2.0$

- $R = 10^{-4}$
- $\beta_r = 0.12$
- $X = 1.0$

3.4.6. Single Element Analyses and Soil Model Verification

Using the single element analysis application “Soil Test” in Plaxis 2D, all the triaxial tests carried out on the Ottawa sand under confining pressures (σ_3) of 100 kPa, 150 kPa and 200 kPa were simulated with results shown in Figure 3.8, Figure 3.9 and Figure 3.10 respectively. These results were then overlapped on the experimental triaxial tests carried out on the Ottawa sand and reflected a very good match (Figure 3.11).

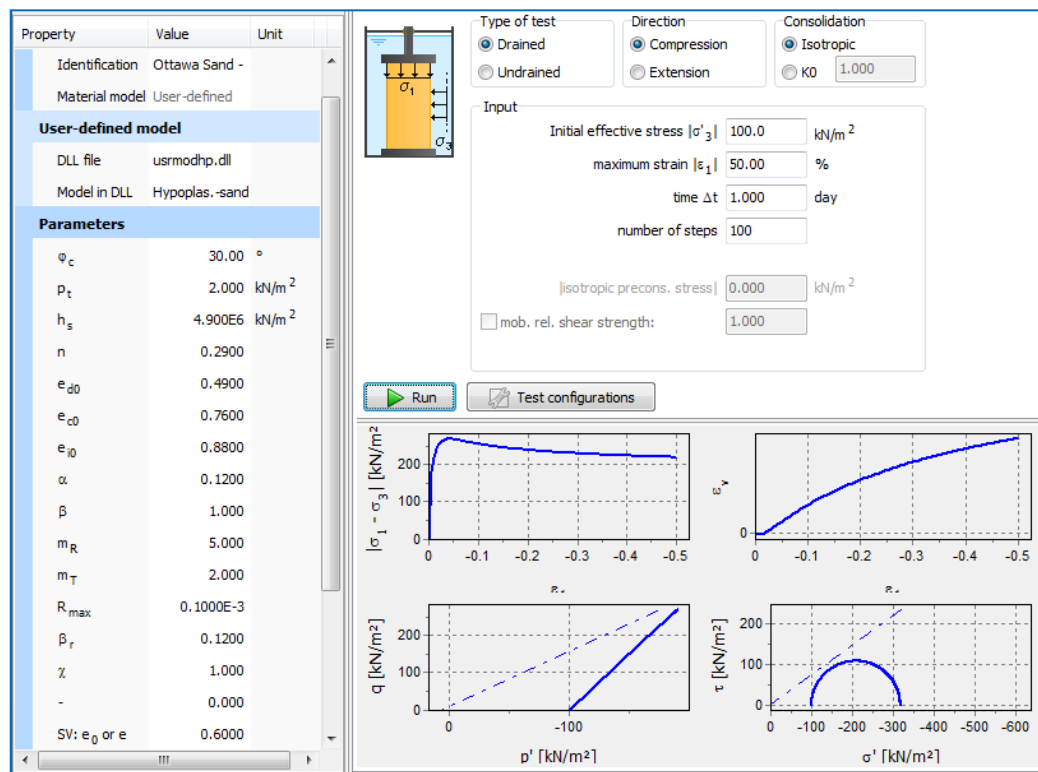


Figure 3.8. Single element analysis on Ottawa sand under a confining pressure of 100 kPa

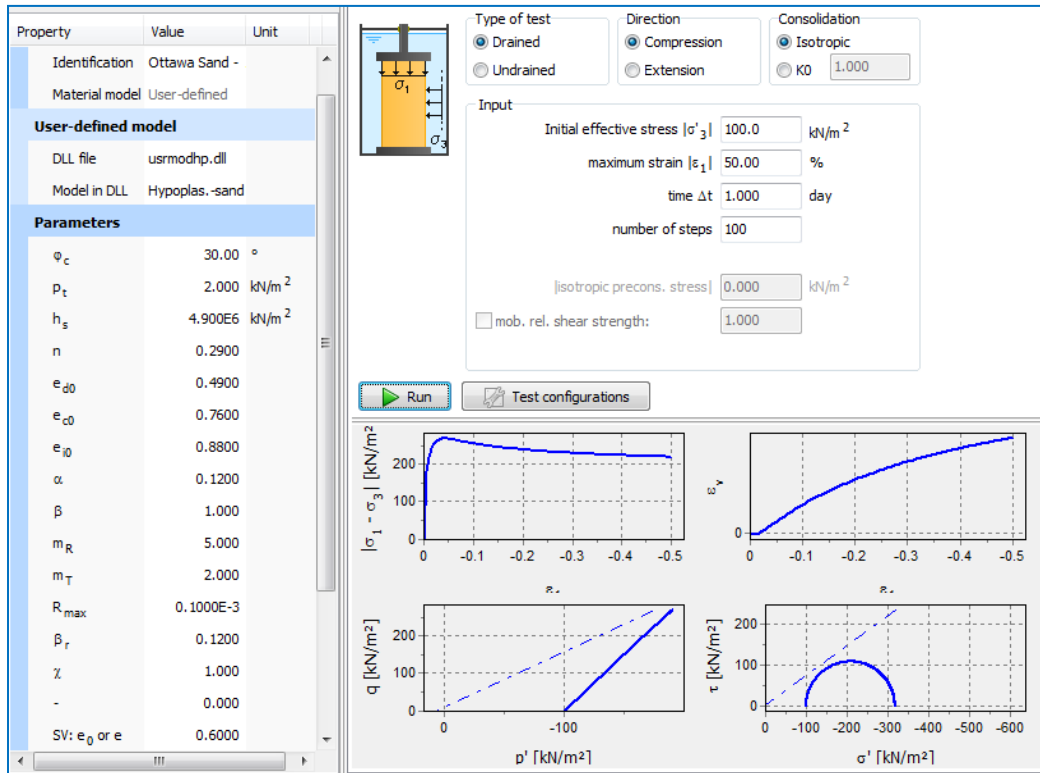


Figure 3.9. Single element analysis on Ottawa sand under a confining pressure of 150 kPa

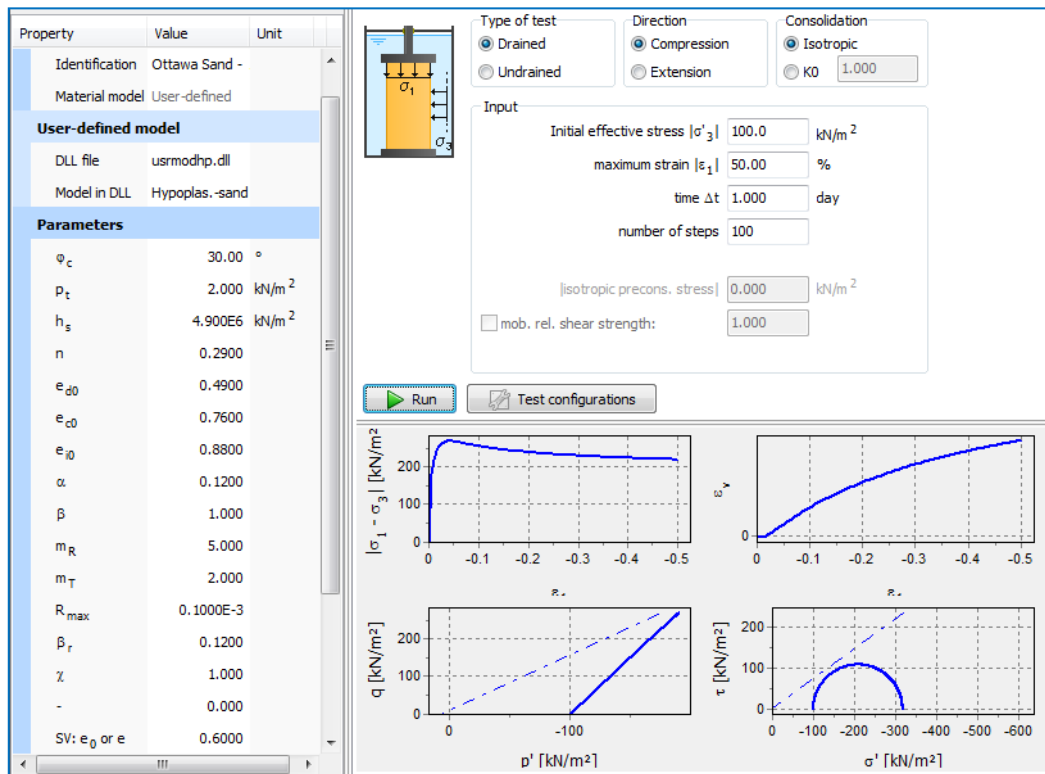


Figure 3.10. Single element analysis on Ottawa sand under a confining pressure of 200 kPa

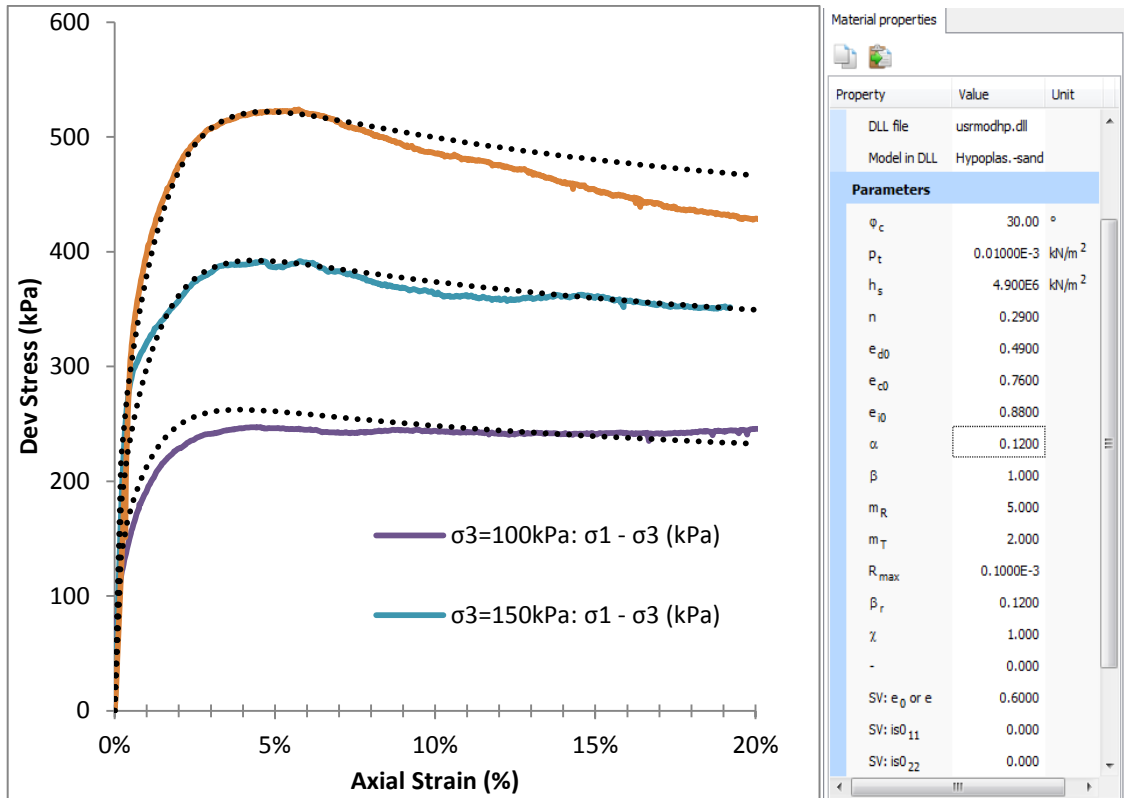


Figure 3.11. Single element analysis vs experimental triaxial tests on Ottawa sand

3.5. Hypoplastic model – Kaolin Clay

The clay hypoplastic model (Masin, 2005) requires altogether five material parameters. The parameters are equivalent to the parameters of the Modified Cam-clay model, but not identical.

- φ_c is the critical state friction angle
- N and λ^* control the position and slope of the isotropic normal compression line
- K^* controls the slope of the isotropic unloading line
- r controls the shear stiffness

3.5.1. Material Parameters

Since the triaxial tests were carried out on the Kaolin clay to strains where the critical state was not reached, the critical state friction angle cannot be determined.

However, we have tried some published hypoplastic parameters for different types of clays in the single element analysis and found what is highlighted in the table below of a good match to our lab test results. Accordingly we have adopted the same φ_c , N , λ^* and K^* and carried out minor calibrations by varying the r value as recommended by Masin (2005).

	φ_c	λ^*	κ^*	N	r
London clay	22.6°	0.11	0.016	1.375	0.4
Brno clay	19.9°	0.13	0.01	1.51	0.45
Fujinomori clay	34°	0.045	0.011	0.887	1.3
Bothkennar clay	35°	0.12	0.01	1.34	0.07
Pisa clay	21.9°	0.14	0.01	1.56	0.3
Beaucaire clay	33°	0.06	0.01	0.85	0.4
Kaolin	27.5°	0.11	0.01	1.32	0.45
London clay (data Gasparre)	21.9°	0.1	0.02	1.26	0.5
Kaolin	27.5°	0.07	0.01	0.92	0.67
Trmice clay	18.7°	0.09	0.01	1.09	0.18
Koper silty clay	33°	0.103	0.015	1.31	0.3
min.	18.7°	0.045	0.01	0.85	0.07
max.	35°	0.14	0.02	1.56	0.67

Figure 3.12. Parameters of the clay Hypoplastic model from different sources, Masin (2005)

The final hypoplastic parameters for our Kaolin clay are listed below:

- $\varphi_c = 27.5^\circ$
- $N = 0.113$
- $\lambda^* = 0.01$
- $K^* = 1.32$
- $R = 0.1$

3.5.2. Single Element Analyses and Soil Model Verification

Using the single element analysis application “Soil Test” in Plaxis 2D, all the triaxial tests carried out on the Kaolin clay under confining pressures (σ_3) of 100 kPa, 150 kPa and 200 kPa were simulated with results shown in Figure 3.13, Figure 3.14 and

Figure 3.15 respectively. These results were then overlapped on the experimental triaxial tests' stress-strain curves that were carried out on the Kaolin clay (Figure 3.16).

Comparing the single element analysis results to that of the experimental triaxial test results we see a very good match for confining pressure of 100 kPa and 150 kPa, while there is an over prediction for the 200 kPa confining pressure. Observing the trend in the three confining pressures' curves, we can conclude that the hypoplastic model represent the Kaolin clay. Further triaxial tests can be carried out in the future to confirm these results.

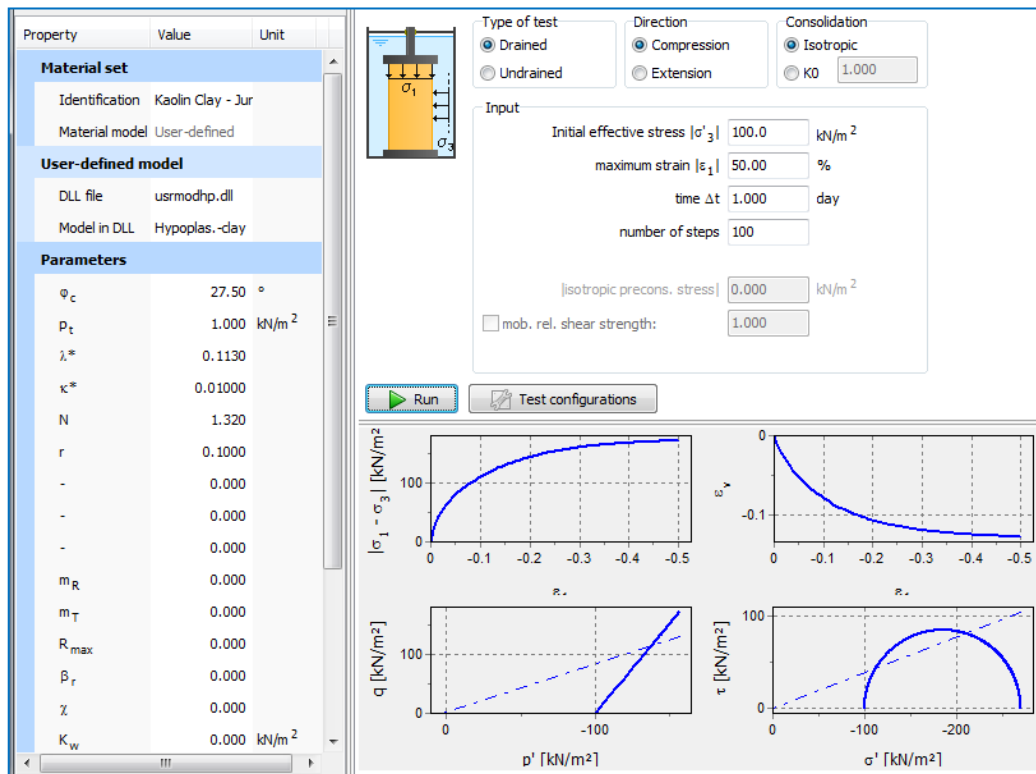


Figure 3.13. Single element analysis on Kaolin clay under a confining pressure (σ_3) of 100 kPa

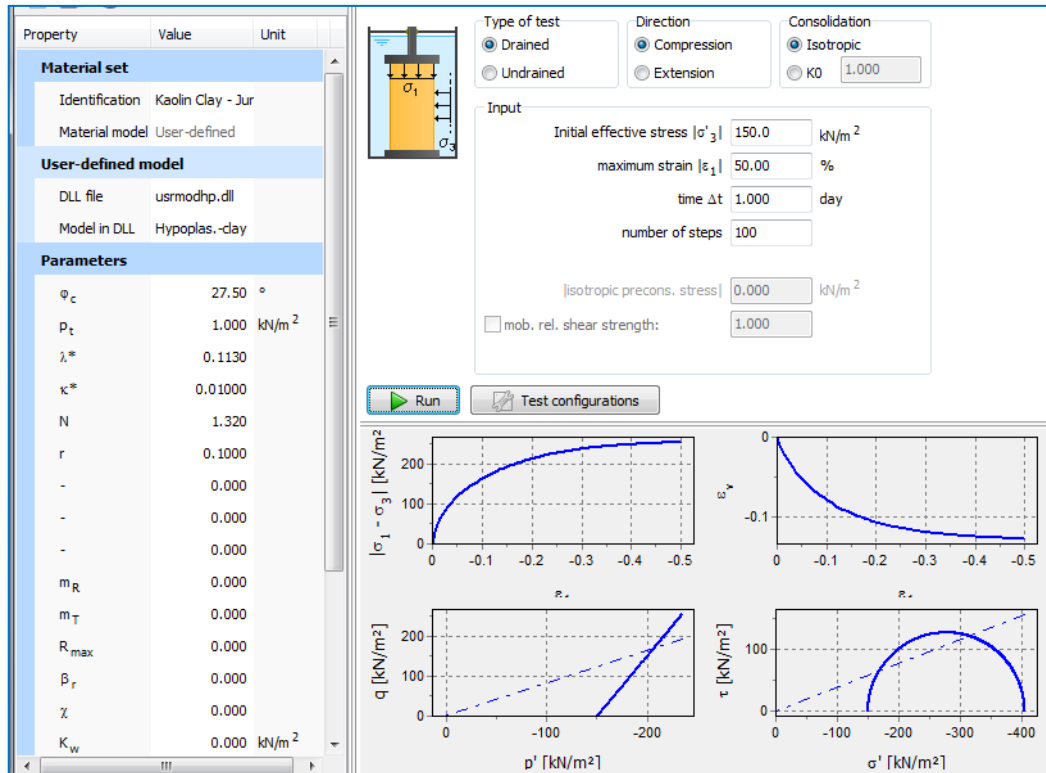


Figure 3.14. Single element analysis on Kaolin clay under a confining pressure (σ_3) of 150 kPa

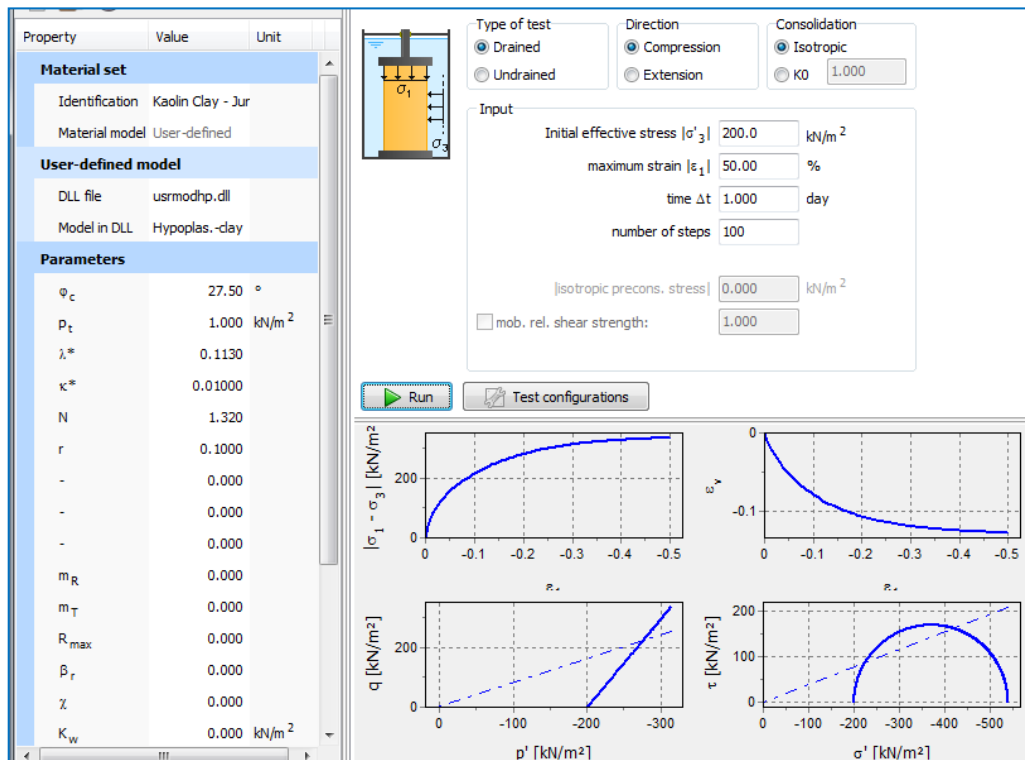


Figure 3.15. Single element analysis on Kaolin clay under a confining pressure (σ_3) of 200 kPa

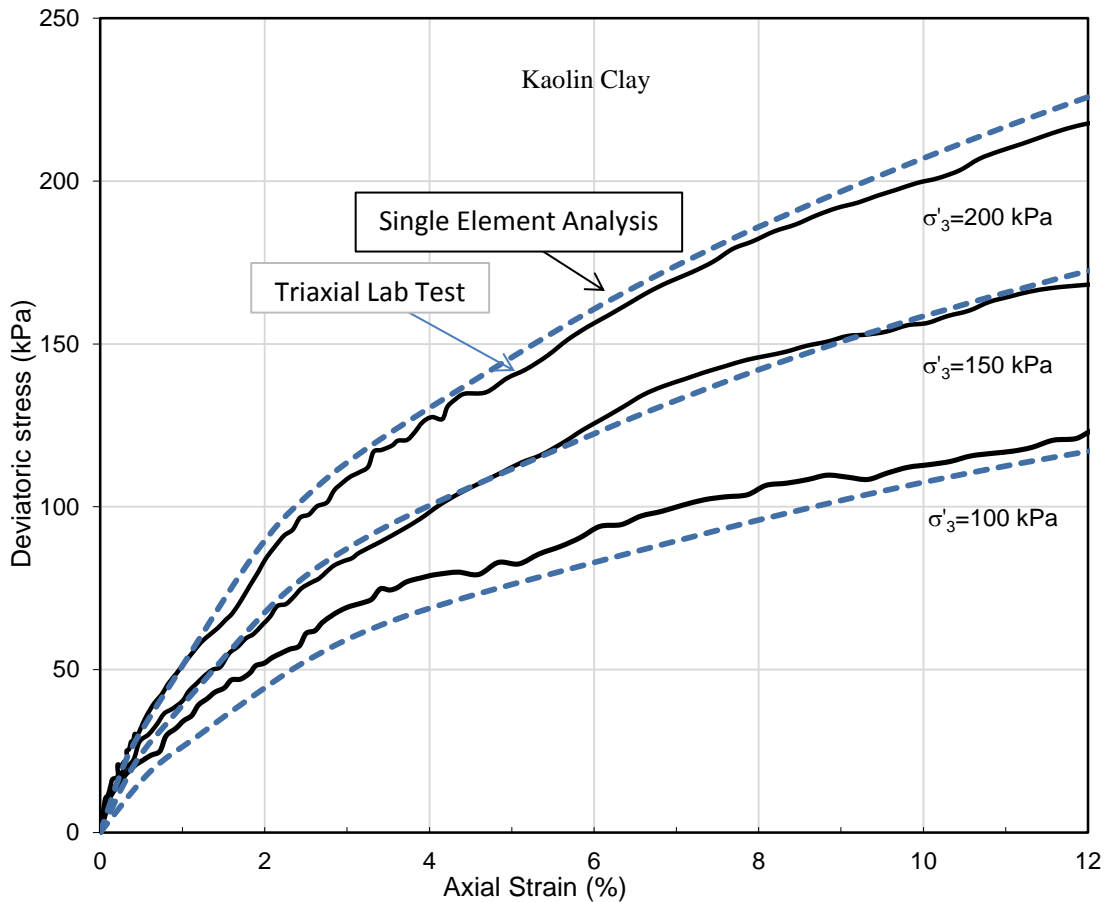


Figure 3.16. Single element analysis vs experimental triaxial tests on Kaolin clay

3.6. Summary

In this chapter, the Hypoplastic model parameters for the Ottawa sand and Kaolin clay that were used in the experimental triaxial tests were derived. The single element analysis was carried out to calibrate and verify the soil models and the results were satisfactory. Accordingly, we have the hypoplastic models for the Ottawa sand and Kaolin clay available for the next steps of this research study where triaxial tests on composite samples will be modeled.

The derived Hypoplastic parameters for the Ottawa sand are:

1. $e_{d0} = 0.49$
2. e_{c0} used 0.76
3. $e_{i0} = 0.88$

4. $\varphi_c = 30^\circ$
5. $h_s = 4900 \text{ MPa}$
6. $n=0.29$
7. $\alpha=0.12$
8. $\beta=1.0$
9. Intergranular parameters:
 - $mR = 5.0, mT = 2.0, R = 10^{-4}, \beta_r = 0.12$ and $X = 1.0$

The derived Hypoplastic parameters for the Kaolin Clay are:

1. $\varphi_c = 27.5^\circ$
2. $N = 0.113$
3. $\lambda^* = 0.01$
4. $K^* = 1.32$
5. $R = 0.1$

CHAPTER 4

MODELING THE TRIAXIAL TESTS

4.1. Introduction

The Finite Element software Plaxis 2D was used to simulate the consolidated drained (CD) tests that were carried out on the reinforced clay specimens in Maalouf (2012), where the samples were isotropically consolidated under confining pressure of 100, 150 and 200 kPa and sheared drained by applying a vertical (axial) displacement of 12% at a slow strain rate of 0.25%/hr. Throughout the tests, the total confining pressure was kept constant as the vertical stress was increased in the compression.

The methodology and results of modeling the consolidated drained tests that were conducted on the Kaolin specimens in Maalouf (2012) using the Hypoplastic soil models are presented in this chapter. The results include the deformation patterns and the stress strain behavior. The hypoplastic model was also cross checked and compared to the Mohr Coulomb model and Hardening Soil Models. Then a comparison between the FEM and Experimental lab test results of Maalouf (2012) was carried out to assess the reliability of the finite element method in such application.

4.2. The Triaxial Test preparation and setup - Lab

4.2.1. Normally Consolidated Kaolin Clay Samples

As mentioned in Maalouf (2012), Kaolin clay powder was mixed with water at a water content of 100% (i.e. 1.8 times its liquid limit). Four 1-D consolidometers were fabricated for the purpose of consolidating the Kaolin slurry (Figure 4.1). Each

consolidometer consisted of a PVC pipe segment with a height of 35cm, an external and internal diameter of 7.3cm and 7.1cm respectively, and a wall thickness of 0.1cm. The PVC pipe segment was cut longitudinally in the vertical direction into two halves to function as a split mold (Figure 4.2), thus eliminating the need for extruding the soil sample after consolidation. The two PVC sections were held in place using high-strength duct tape (Figure 4.2) which was wrapped around the two cylindrical PVC sections to prevent leakage of slurry and to ensure that lateral strains are negligible during 1-D consolidation under the desired axial load. The advantage behind using a split PVC pipe was to ensure that an undisturbed, relatively soft, normally consolidated clay specimen can be obtained and removed with minimal disturbance after consolidation was achieved.



Figure 4.1. Picture for custom fabricated 1-dimensional consolidometers

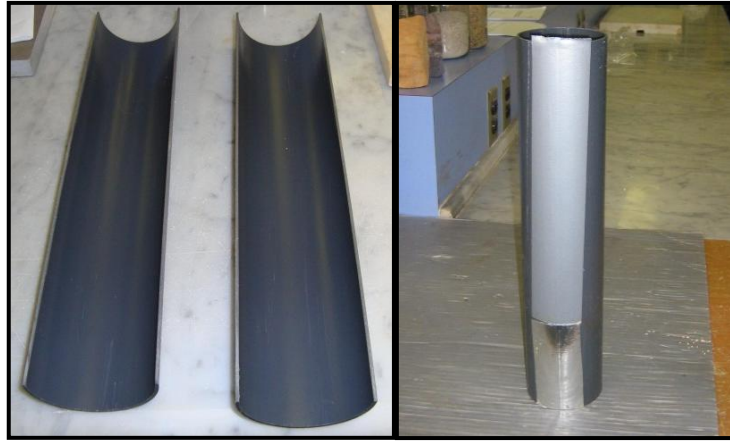


Figure 4.2. Photo for a Split PVC pipe and Wrapped PVC pipe with duct tape

At its lower end, the PVC pipe segment was fixed in place by means of a hollow steel cylinder with a height of 9cm as shown in Figure 4.1 and Figure 4.3. The stiff and heavy cylinder wraps tightly around the bottom of the PVC segment to provide additional lateral confinement and support to the PVC segment during slurry consolidation. The inner walls of the steel cylinder were coated with a thin layer of oil to facilitate the removal of the PVC segment once consolidation was achieved. Moreover, the circumference of the steel rod was coated with a thin layer of grease at the location of the steel rod guide to reduce friction between the steel rod and the guide rod. A porous stone and a filter paper were used to provide a freely draining boundary at the lower end of the soil specimen.

At its upper end, the soil specimen was loaded with a loading system consisting of dead weights similar to those used in 1-D consolidation tests. The dead weights were seated on a circular steel plate that transferred the load to the top of the soil specimen through a circular steel rod having a diameter of 1cm. A perforated circular steel piston with a diameter of 7.1 cm (same as inner diameter of PVC pipe) was fixed to the bottom of the steel rod to act as a loading plate which transmitted the load to the slurry. The soil

was separated from the loading plate with a porous stone and a filter paper to provide a freely draining boundary at the top of the soil specimen. To reduce friction between the perforated loading plate and the PVC segment, the outside periphery of the loading plate was also coated with a thin layer of oil.

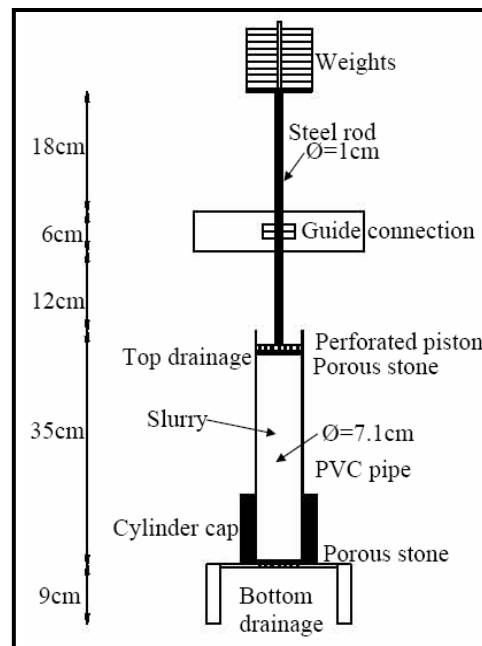


Figure 4.3. Custom fabricated 1-dimensional consolidometer

The slurry was poured into the appropriate consolidometer and consolidated under K_0 conditions using a vertical effective stress of 100 kPa. After pouring the slurry in the appropriate consolidometer (initial specimen height was 35cm), the clay was allowed to consolidate under its own weight for a period of 4 hours. During 1-D consolidation, drainage was allowed from both ends of the sample through the top and bottom porous stones. Dead weights were then added in stages to the top of the sample, with each weight applied for a specified time period according to the loading sequence shown in Table 4.1.

Table 4.1. Loading sequence during 1.D consolidation of Kaolin slurry

Accumulated weights (Kg)	0.5	1	2	4	8	12	20	30	40
Applied pressure (kPa)	1.25	2.5	5	10	20	30	50	75	100
Duration (Hr)	4	4	24	24	24	24	24	24	24

The consolidation time periods that were allocated to each loading increment were estimated based on the results of the 1D consolidation test and were adjusted using trial and error. A typical time duration that is required to fully consolidate a clay sample under an effective normal stress of 100 kPa is approximately 7.5 days.

The water content after consolidation was found to be relatively uniform (about 53%) throughout the depth of the sample. The variations of the water content and the void ratio with depth were determined by slicing a consolidated clay sample into 7 pieces and determining the void ratio and water content for each slice. The variation of the void ratio and water content with depth for a typical sample is shown in Figure 4.4. The variations are relatively small indicating a relatively uniform degree of consolidation in the sample. As expected, the void ratio was found to be the smallest at the upper and lower ends of the sample where the sample is completely drained during consolidation.

Additional measures were taken to further reduce disturbance during sample preparation. These measures included spreading a thin layer of oil over the inner surfaces of the PVC pipes to reduce friction between the kaolin specimen and the inner surface of the pipe. This allowed for dismantling the pipe and removing the soil specimen from the consolidometer with minimal disturbance to the soil specimen.

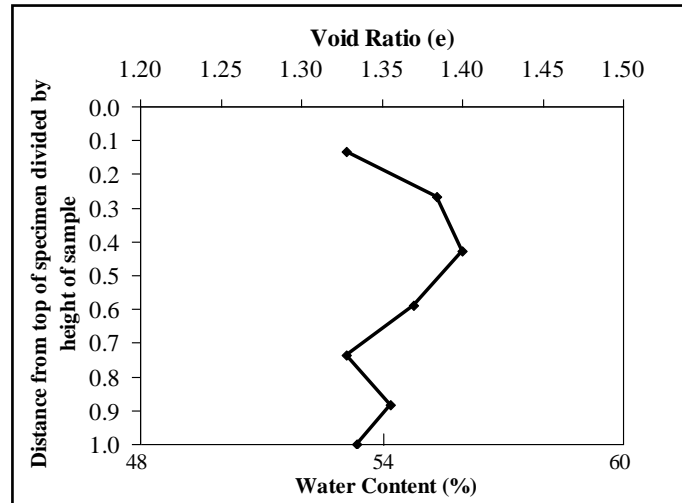


Figure 4.4. Water content and void ratio along the height of the sample after consolidation

At the end of primary consolidation under a pressure of 100 kPa, the dead weights were removed and the PVC cylinder was slowly pulled out from the cylindrical cap of the consolidometer as shown in Figure 4.5 (a). The duct tape surrounding the periphery of the PVC cylinder was unwrapped and the two PVC pieces were dismantled as shown in Figure 4.5 (b). The consolidated Kaolin specimen is shown in Figure 4.5 (c). The clay specimen was then trimmed to a final height of 14.2cm (initial height is about 18 cm) by means of a sharp spatula as shown in Figure 4.6 (a). Two presoaked porous stones were then placed on the top and bottom of the Kaolin specimen and the sample was prepared for triaxial testing as shown in Figure 4.6 (b). Finally, the sample was wrapped with a presoaked filter paper that has longitudinal perforations in order to speed up the process of consolidation in the triaxial cell (Figure 4.6 c).

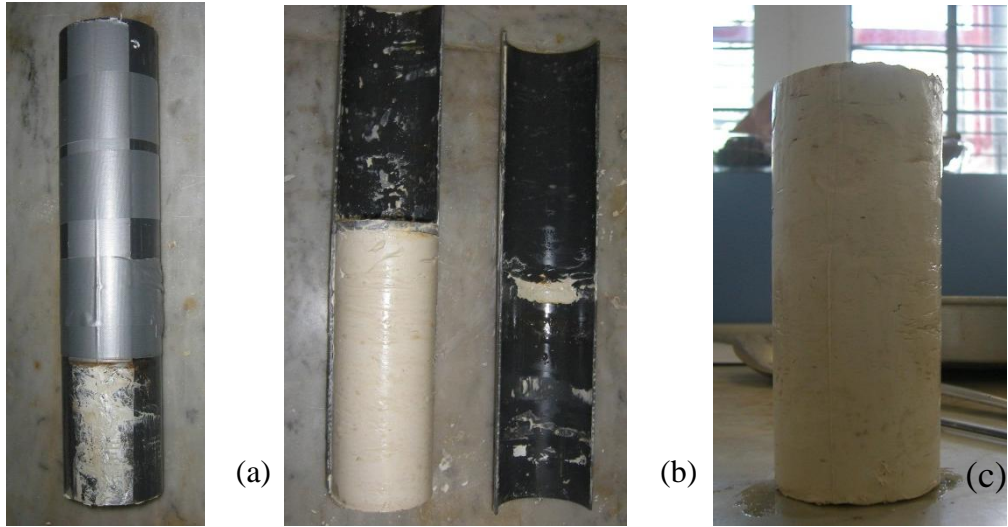


Figure 4.5. Kaolin specimen (a) after removal from custom fabricated consolidometer, (b) dismantling and (c) after removal from PVC pipe.

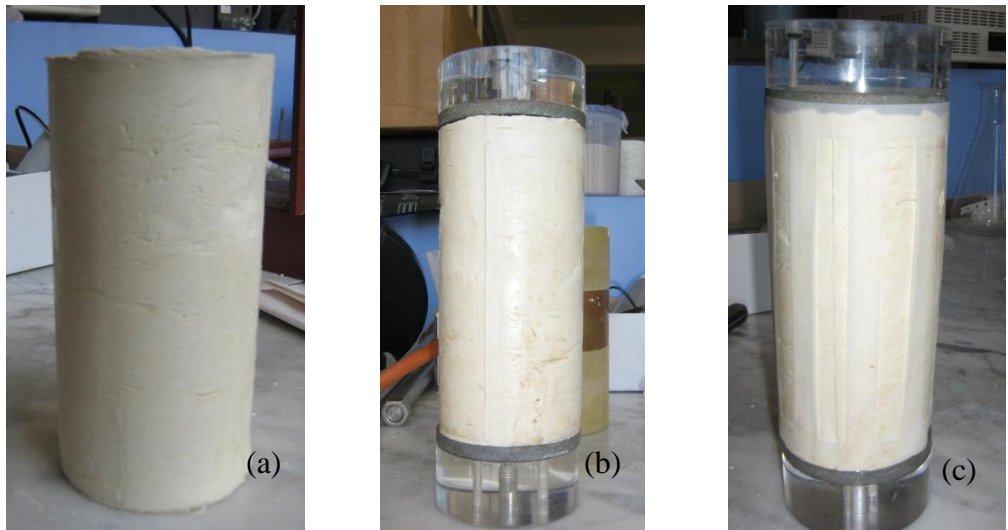


Figure 4.6. Kaolin specimen (a) after trimming, (b) Installation of porous stones, (c) installation of filter paper around.

A thin rubber membrane with a diameter of 7.1cm was then placed on the inside of a cylindrical brass membrane stretcher. To facilitate the placement of the membrane into the stretcher, a thin layer of powder was sprayed over the membrane. Vacuum was then applied to ensure that the membrane adhered well to the inner walls of the stretcher (Figure 4.7 (a)). The stretcher was then positioned around the soil specimen and the vacuum was released. Rubber bands were used to fasten the membrane tightly around

the specimen. The specimen was then attached to the base of the triaxial cell and the top drainage tubes were inserted into the holes of the top cap as shown in Figure 4.7 (b). The triaxial cell was then assembled and the seating piston positioned over the top cap (Figure 4.7 (c)). Finally, the triaxial cell was placed in the system in preparation for saturation, consolidation, and shear.

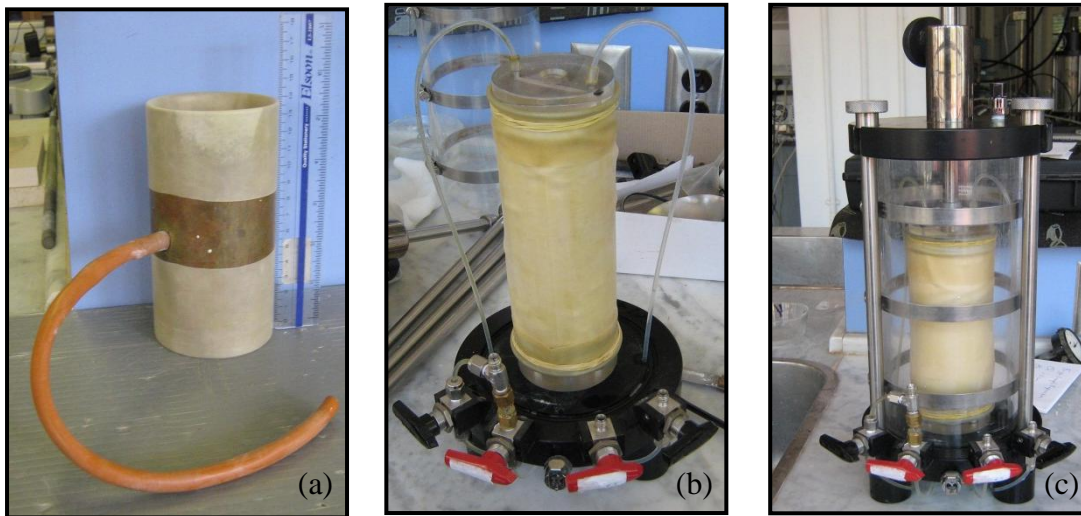


Figure 4.7. Cell chamber (a) Brass tube with the rubber membrane. (b) Installation of Kaolin specimen on the cell chamber, (c) Insertion of glass cover around cell chamber

4.2.2. Ottawa Sand Columns

As mentioned in Maalouf (2012), the first step in the preparation of clay specimens that were reinforced with single sand columns involved the formation of a hole with a diameter of 2cm or 3cm, in the middle of the clay specimen. For this purpose, a custom-fabricated hand auguring apparatus was manufactured in the machine shop. The auguring apparatus was used to drill holes with different penetration depths in the clay specimen. The procedure followed in drilling holes is presented below.

After dismantling the cylindrical Kaolin specimen from the PVC pipe and trimming it to a final height of 14.2cm, the specimen was wrapped with two lubricated

plastic cylindrical PVC tubes which were in turn wrapped with duct tape around their circumference as shown in Figure 4.8. The wrapped specimen was then placed on the auguring apparatus that is shown in Figure 4.9(a). Augurs with diameters of 2cm or 3cm were connected to the auguring machine as shown in Figure 4.9(b) and (c) respectively. During drilling, the vertical alignment of the rotating rod is maintained through the presence of plastic guide plates that are connected to the top and bottom of the steel rod. The penetration of the augur into the specimen is continued in stages till the required penetration length is achieved. The augured clay material was collected on the augur as shown in Figure 4.9 (c).

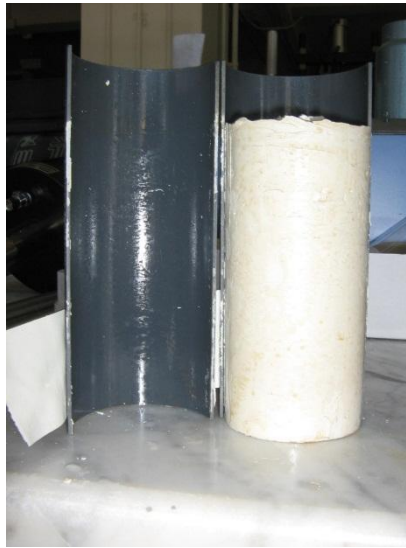


Figure 4.8. Wrapping the Kaolin specimen with PVC tubes prior to auguring

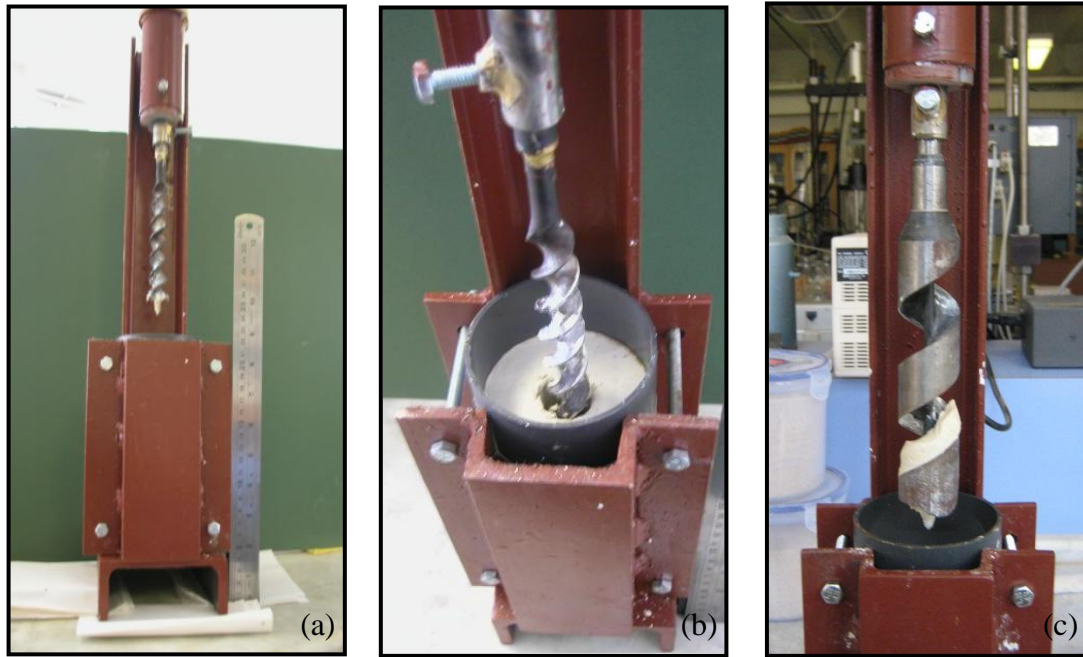


Figure 4.9. Custom fabricated auguring machine (a) 2cm diameter auger (b) auguring of specimen by 2cm diameter auger, (c) Removal of Kaolin material by 3 cm diameter auger

For sand columns with heights of 10.65cm (partially penetrating column), a mark was made on the steel rod to indicate the required penetration distance of the auger. Auguring was continued in stages until the depth of the augured hole reached the marked length. The maximum penetration distance of the auger into the Kaolin specimen in each stage is 3cm for the purpose of reducing the suction pressure that is generated as the auger is retrieved from the Kaolin specimen.

Columns that were encased with geotextile fabrics were used to prepare the sand columns. After saturating the sand column with water, the column was inserted into a flask and placed inside the freezer (Figure 4.10. a). After freezing, the geotextile fabric was detached from the frozen sand column by cutting the geotextile fabric along its vertical stitching using a sharp cutter. To prevent thawing of the sand column while cutting the geotextile fabric, the cutting operation was performed on a tray filled with frozen water (Figure 4.10 b). The unreinforced sand column (Figure 4.10 c) was then

inserted in the predrilled hole (Figure 4.11 a through c) and left to thaw. The uniformity and the vertical alignment of the inserted frozen sand column is revealed in Figure 4.12 where a kaolin specimen was cut vertically along its length directly after inserting the ordinary sand column of diameter 2cm and height of 10.65cm.

Although freezing of sand columns is not usually implemented in the field, the idea behind using frozen sand columns is to be able to construct columns with mechanical properties that are repeatable and uniform across the different samples. The friction angle of Ottawa sand depends on the initial density of the column material, which in turn depends on the column diameter. Thus, any variation in the column diameter from one sample to another will lead to variations in the column density and the friction angle of the column material. By constructing frozen columns in which sand particles are compacted outside the Kaolin specimen, the column diameter and density will be uniform and repeatable.



Figure 4.10. Freezing the sand columns

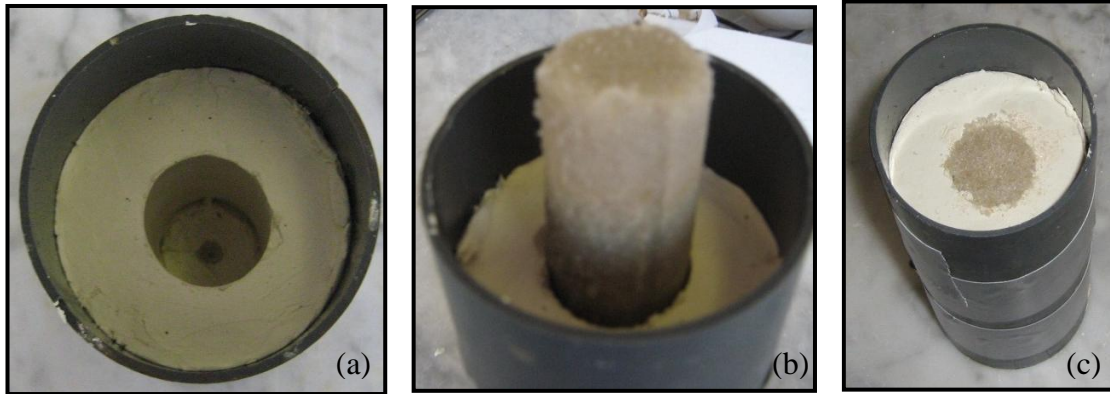


Figure 4.11. Sand column installation (a) Predrilled 3.cm diameter hole, (b) Insertion of frozen sand column in clay, and (c) Reinforced Kaolin specimen with frozen sand column.



Figure 4.12. vertical cross section of Kaolin specimen with ordinary sand column of diameter 2cm and height 10.65cm after column insertion.

4.3. Modeling the triaxial tests – Plaxis 2D

A finite element model (FEM) is required to simulate and represent the laboratory drained triaxial tests that were conducted by Maalouf (2012) on clay samples that were reinforced with partially and fully penetrating sand columns at confining pressures of 100, 150 and 200 kPa. The normally consolidated Kaolin samples were of a diameter of 7.1cm and a length of 14.2cm and reinforced with 2cm or 3cm-diameter sand columns, respectively.

For this purpose, an axisymmetric analysis was conducted in Plaxis 2D with 15-Noded triangular elements and using the hypoplastic soil models that were derived in 3. The boundary conditions (Figure 4.13) will consist of: Full fixity at the base of the sample representing the base porous stone and cap, a horizontal fixity will be placed at the left boundary (the vertical axisymmetric axis), a plate will be placed on the top of the sample to represent the top porous cap where the soil will be fully fixed, and no fixities will be applied to the right boundary.

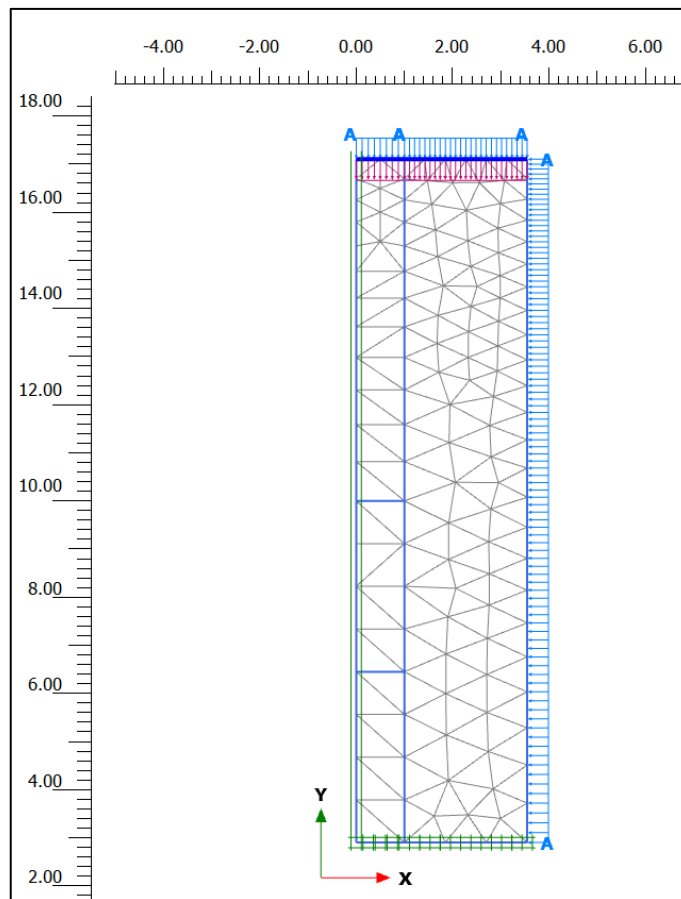


Figure 4.13. The suggested model showing the adopted triangular mesh and boundary condition.

There are five triaxial models to be built to represent the experimental CD triaxial tests that were carried out in Maalouf (2012) and the one additional that was

carried out during the work of this thesis as a confirmatory test. Each model corresponds to the specific geometry of the tested specimens and does simulate the whole triaxial test procedure for the three confining pressures of 100kPa, 150 kPa and 200 kPa by introducing 7 phases as listed below and detailed in Table 4.2:

- Model 1: 2cm Diameter, Partially penetrating (0.75) sand column
 - ⇒ Phase 1: Initial phase
 - ⇒ Phase 2: Isotropic Consolidation, $\sigma_3=100$ kPa
 - ⇒ Phase 3: Axial Displacement of 1.704 cm (12%) is applied
 - ⇒ Phase 4: Isotropic Consolidation , $\sigma_3=150$ kPa (Starts from Phase 2)
 - ⇒ Phase 5: Axial Displacement of 1.704 cm (12%) is applied
 - ⇒ Phase 6: Isotropic Consolidation , $\sigma_3=200$ kPa (Starts from Phase 2)
 - ⇒ Phase 7: Axial Displacement of 1.704 cm(12%) is applied

- Model 2: 3cm Diameter, Partially penetrating (0.75) sand column
 - ⇒ Phase 1: Initial phase
 - ⇒ Phase 2: Isotropic Consolidation, $\sigma_3=100$ kPa
 - ⇒ Phase 3: Axial Displacement of 1.704 cm (12%) is applied
 - ⇒ Phase 4: Isotropic Consolidation , $\sigma_3=150$ kPa (Starts from Phase 2)
 - ⇒ Phase 5: Axial Displacement of 1.704 cm (12%) is applied
 - ⇒ Phase 6: Isotropic Consolidation , $\sigma_3=200$ kPa (Starts from Phase 2)
 - ⇒ Phase 7: Axial Displacement of 1.704 cm(12%) is applied

- Model 3: 2cm Diameter, Fully penetrating (1.0) sand column
 - ⇒ Phase 1: Initial phase
 - ⇒ Phase 2: Isotropic Consolidation, $\sigma_3=100$ kPa
 - ⇒ Phase 3: Axial Displacement of 1.704 cm (12%) is applied
 - ⇒ Phase 4: Isotropic Consolidation , $\sigma_3=150$ kPa (Starts from Phase 2)
 - ⇒ Phase 5: Axial Displacement of 1.704 cm (12%) is applied
 - ⇒ Phase 6: Isotropic Consolidation , $\sigma_3=200$ kPa (Starts from Phase 2)

- ⇒ Phase 7: Axial Displacement of 1.704 cm(12%) is applied
- Model 4: 3cm Diameter, Fully penetrating (1.0) sand column
 - ⇒ Phase 1: Initial phase
 - ⇒ Phase 2: Isotropic Consolidation, $\sigma_3=100$ kPa
 - ⇒ Phase 3: Axial Displacement of 1.704 cm (12%) is applied
 - ⇒ Phase 4: Isotropic Consolidation , $\sigma_3=150$ kPa (Starts from Phase 2)
 - ⇒ Phase 5: Axial Displacement of 1.704 cm (12%) is applied
 - ⇒ Phase 6: Isotropic Consolidation , $\sigma_3=200$ kPa (Starts from Phase 2)
 - ⇒ Phase 7: Axial Displacement of 1.704 cm(12%) is applied
- Model 5: 4cm Diameter, Partially penetrating (0.75) sand column
 - ⇒ Phase 1: Initial phase
 - ⇒ Phase 2: Isotropic Consolidation, $\sigma_3=100$ kPa
 - ⇒ Phase 3: Axial Displacement of 1.704 cm (12%) is applied
 - ⇒ Phase 4: Isotropic Consolidation , $\sigma_3=150$ kPa (Starts from Phase 2)
 - ⇒ Phase 5: Axial Displacement of 1.704 cm (12%) is applied
 - ⇒ Phase 6: Isotropic Consolidation , $\sigma_3=200$ kPa (Starts from Phase 2)
 - ⇒ Phase 7: Axial Displacement of 1.704 cm(12%) is applied

Table 4.2. The five triaxial models (FEM) to be built

Model No.	Test No.	Confining pressure σ_3 , (kPa)	Diameter of sand column (mm)	Area replacement ratio: A_c/A_s (%)	Column Penetration Ratio: H_c/H_s	Height of Sand Column: H_s (cm)
Model 1	M1-100	100	20	7.9	0.75	10.65
	M1-150	150	20	7.9	0.75	10.65
	M1-200	200	20	7.9	0.75	10.65
Model 2	M2-100	100	30	17.8	0.75	10.65
	M2-150	150	30	17.8	0.75	10.65
	M2-200	200	30	17.8	0.75	10.65
Model 3	M3-100	100	20	7.9	1	14.2
	M3-150	150	20	7.9	1	14.2
	M3-200	200	20	7.9	1	14.2
Model 4	M4-100	100	30	17.8	1	14.2
	M4-150	150	30	17.8	1	14.2
	M4-200	200	30	17.8	1	14.2
Model 5*	M5-100	100	40	31.7	0.75	10.65
	M5-150	150	40	31.7	0.75	10.65
	M5-200	200	40	31.7	0.75	10.65

For each Model, the triaxial test will be conducted in three calculation phases (Figure 4.14 and Figure 4.15) which will be repeated for each confinement pressure (100, 150 and 200 kPa):

- Phase 1 – In the initial phase, using the k_0 procedure, zero initial stresses will be generated (the density, $\gamma = 0$). No loading is applied in this phase.
- Phase 2, 4 and 6 – Isotropic consolidation is carried out by applying a pressure equivalent to the confinement pressures (σ_3) of 100kPa, 150 kPa and 200 kPa respectively, on the top and the right boundaries of the model in fully drained conditions.

- Phase 3, 5 and 7 – After the Isotropic consolidation the displacements are reset to zero. A prescribed displacement equivalent to 12% of the sample height (1.704 cm) is applied in fully drained conditions. Plaxis will automatically subdivide the loading into appropriate steps; however we have always insured that it is reflecting a representative output.

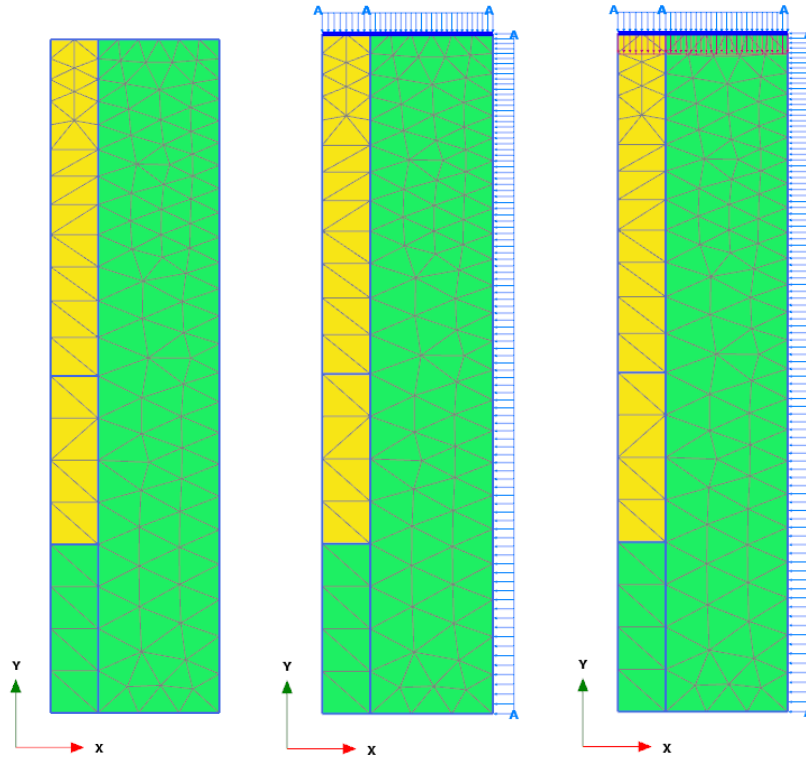


Figure 4.14. A generic sample of the partially penetrating sand column model showing the three calculation phases.

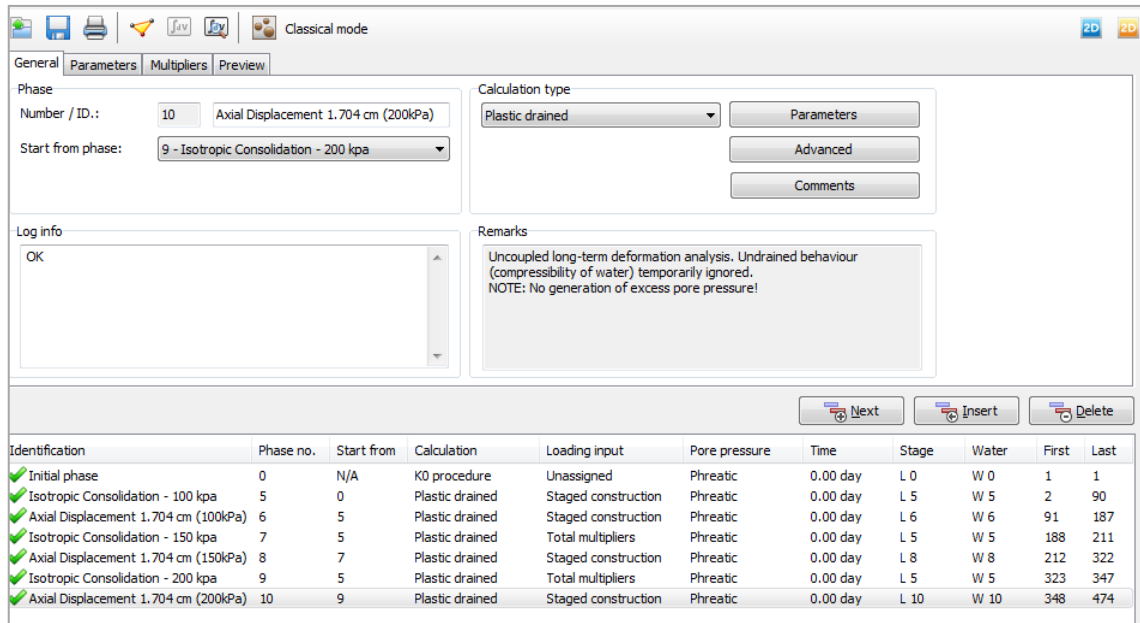


Figure 4.15. Plaxis 2D calculations setup showing the 7 phases in each Model

4.4. FEM Results

The FEM analysis can produce a wide range of results relative to stresses and strains. In this chapter, the results relative to the sample deformation and shear stresses will be present to illustrate the mode of failure and produce the resulting stress strain curves.

4.4.1. Deformations and Modes of Failure

The sample deformation under the axial stress is illustrated in the two types of output: deformed mesh and the horizontal deformation arrows.

For the partially penetrated columns (Model 1, Model 2 and Model 5), bulging was observed at the lower third of the specimen (Figure 4.16, Figure 4.17, Figure 4.18, Figure 4.19, Figure 4.24 and Figure 4.25). These observations agree with Maalouf (2012) and the findings from previous studies (Hughes and Withers 1974, Sivakumar et al. 2004 and Najjar et al. 2010) which indicate that for partially penetrating columns of

short lengths, the stresses at the base of the column generally exceed the bearing capacity of the soil leading to a premature bearing capacity failure in the unreinforced lower portion of the specimen. For the fully penetrating columns (Model 3 and Model 4), bulging was observed at the middle of the specimen (Figure 4.20, Figure 4.21, Figure 4.22 and Figure 4.23). All of the mentioned observations concerning the specimen's deformations agree with Maalouf (2012).

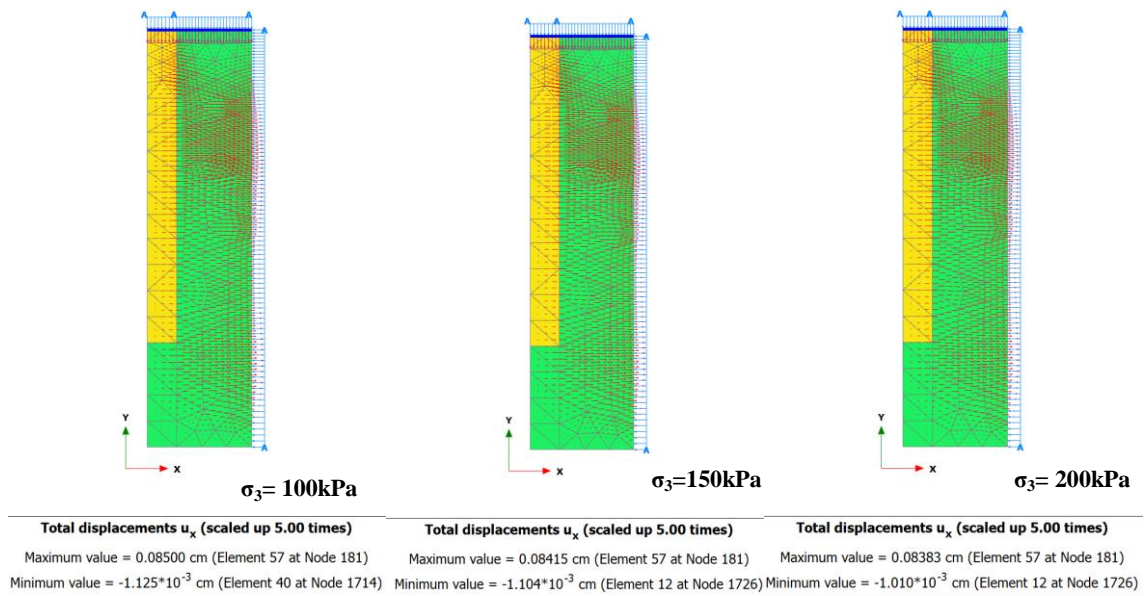


Figure 4.16. Horizontal displacements for Model 1 at 100, 150 and 200 kPa (from left to right)

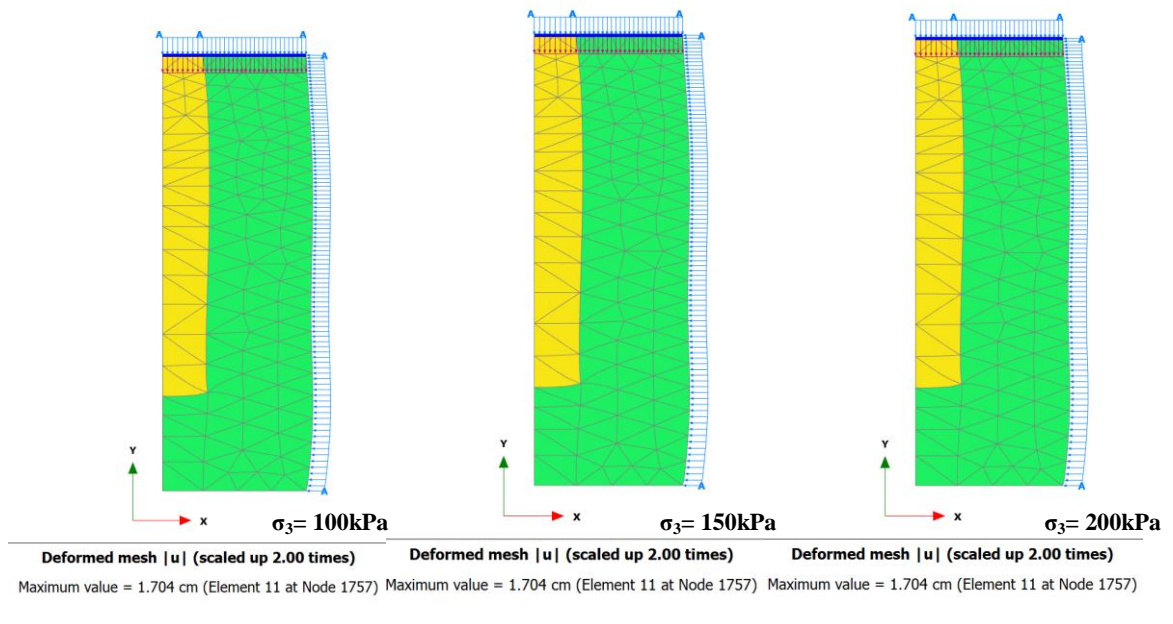


Figure 4.17. Deformed mesh for Model 1 at 100, 150 and 200 kPa (from left to right)

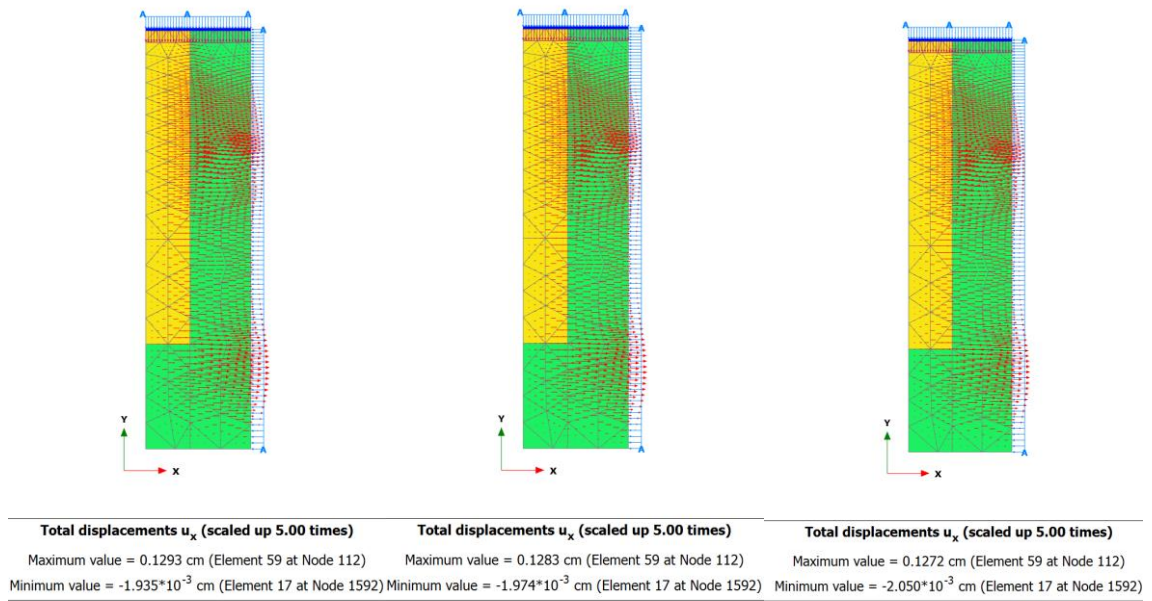


Figure 4.18. Horizontal displacements for Model 2 at 100, 150 and 200 kPa (from left to right)

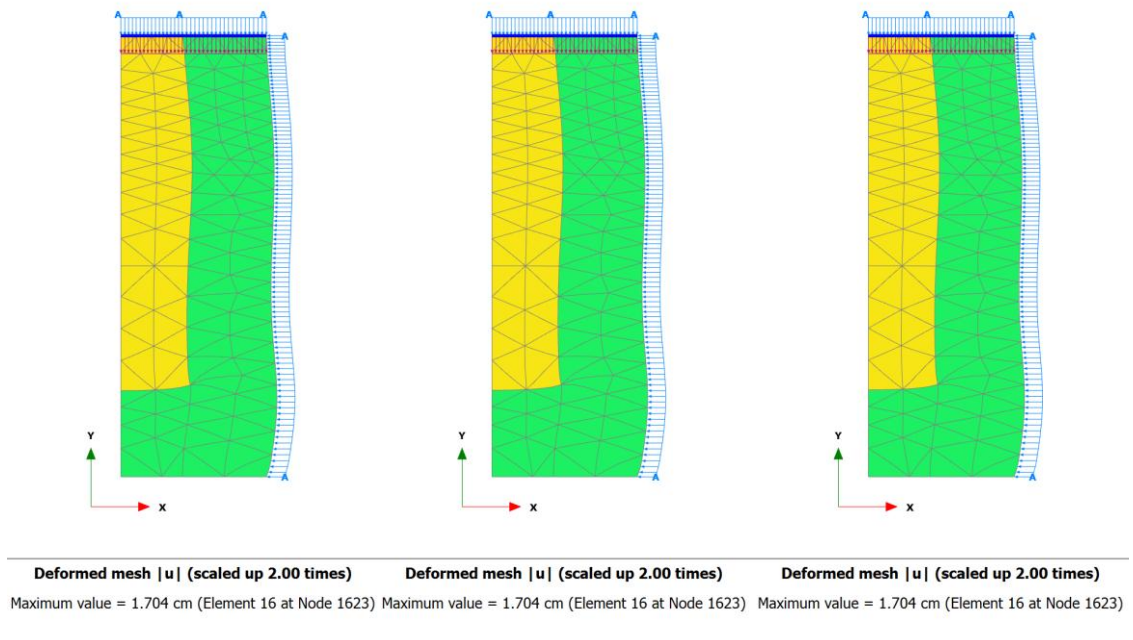


Figure 4.19. Deformed mesh for Model 2 at 100, 150 and 200 kPa (from left to right)

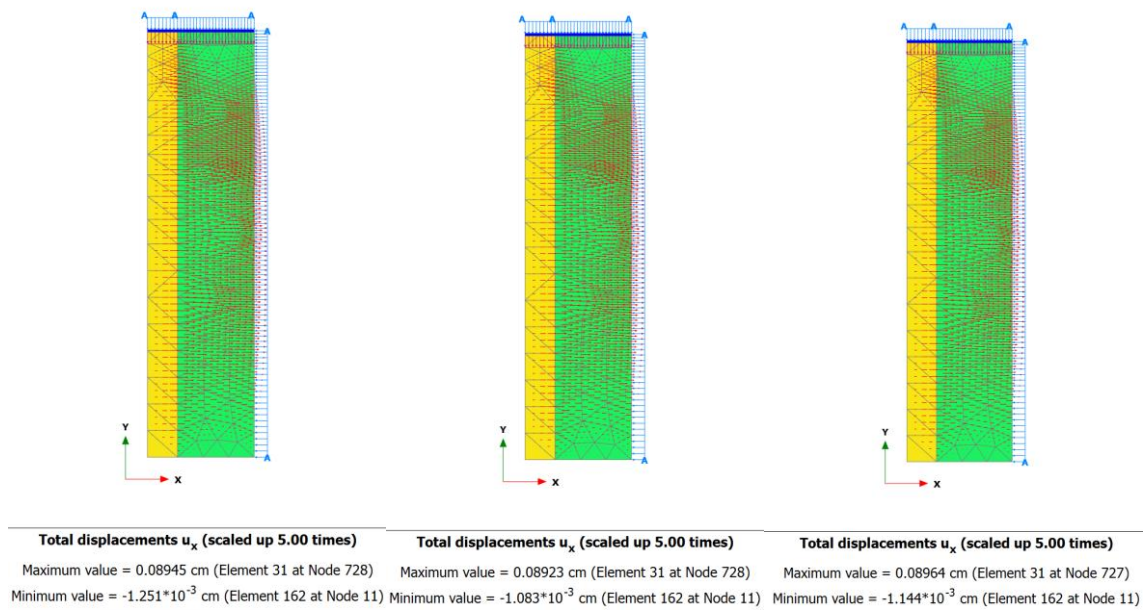


Figure 4.20. Horizontal displacements for Model 3 at 100, 150 and 200 kPa (from left to right)

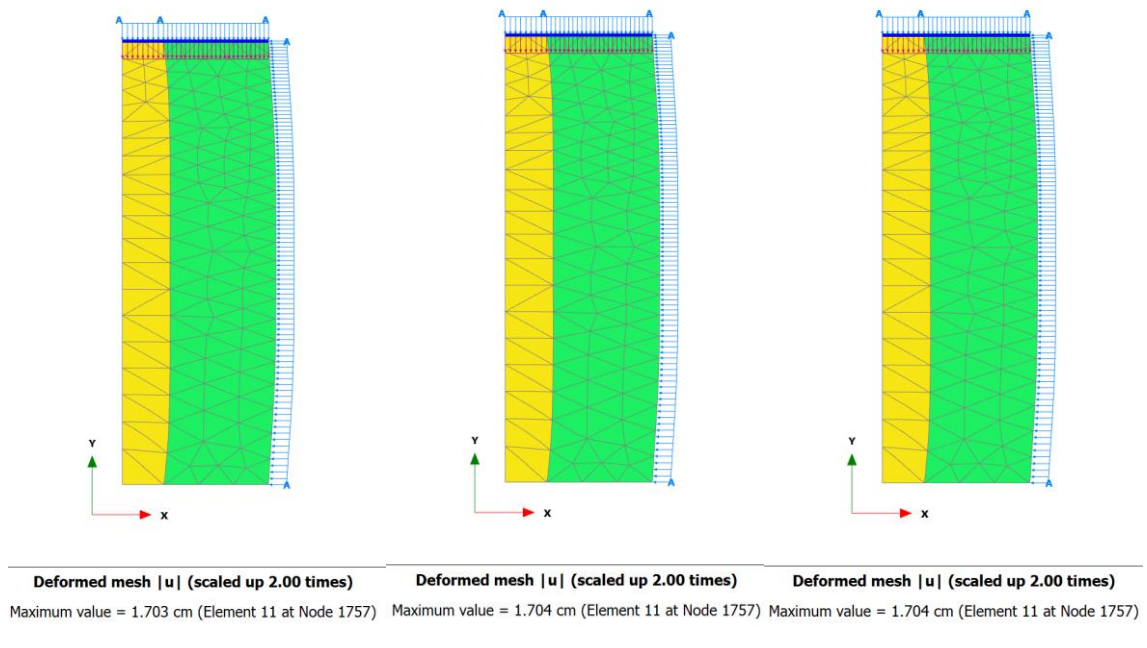


Figure 4.21. Deformed mesh for Model 3 at 100, 150 and 200 kPa (from left to right)

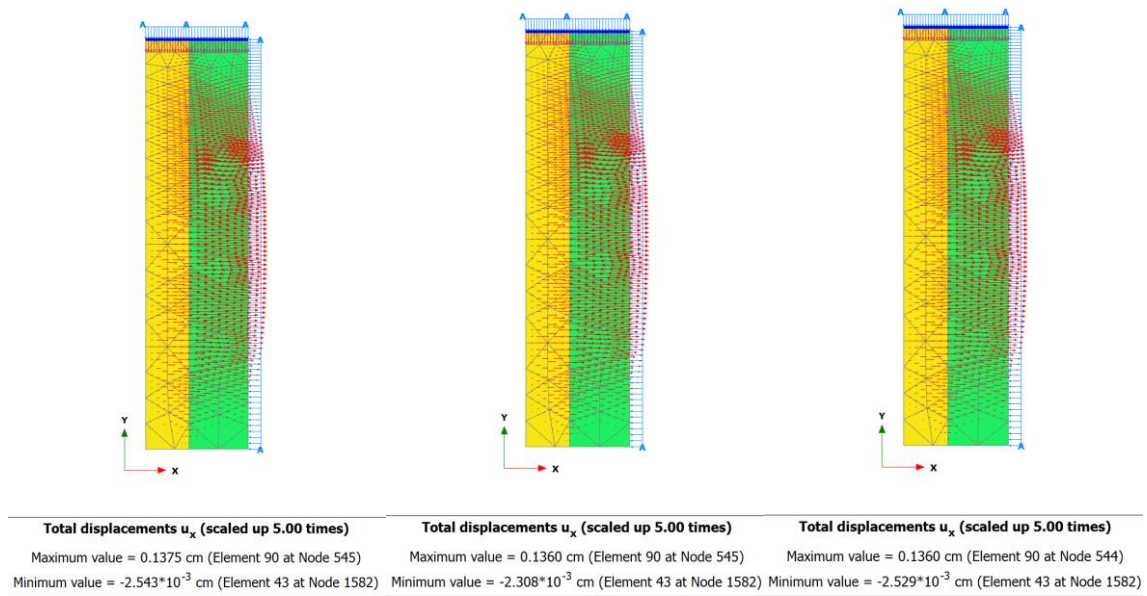


Figure 4.22. Horizontal displacements for Model 4 at 100, 150 and 200 kPa (from left to right)

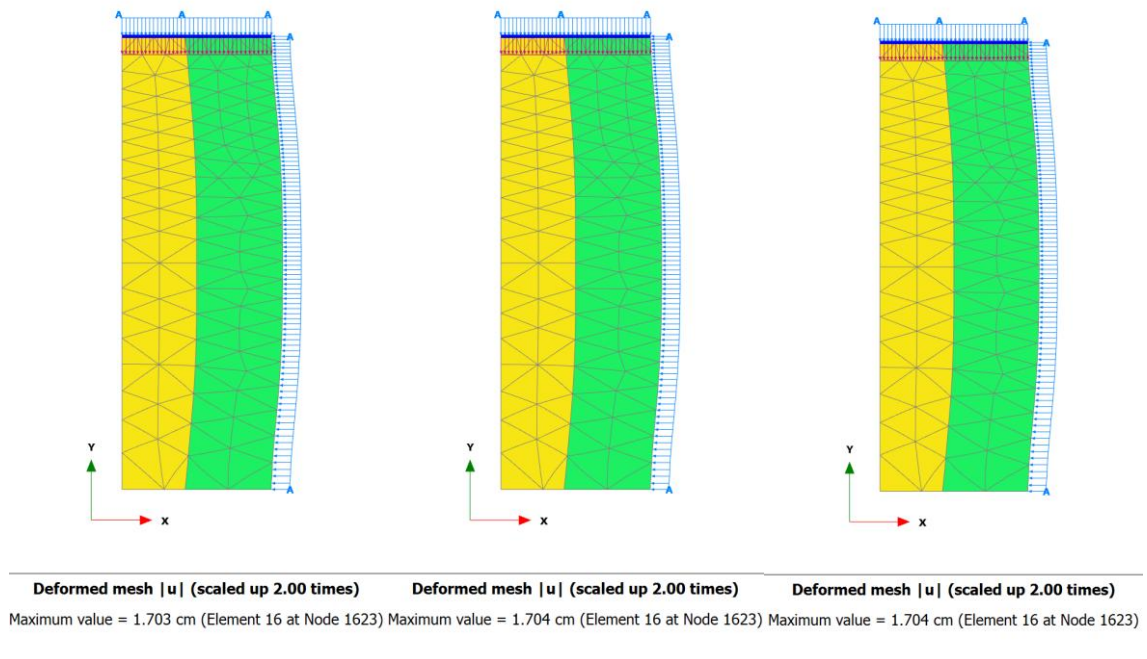


Figure 4.23. Deformed mesh for Model 4 at 100, 150 and 200 kPa (from left to right)

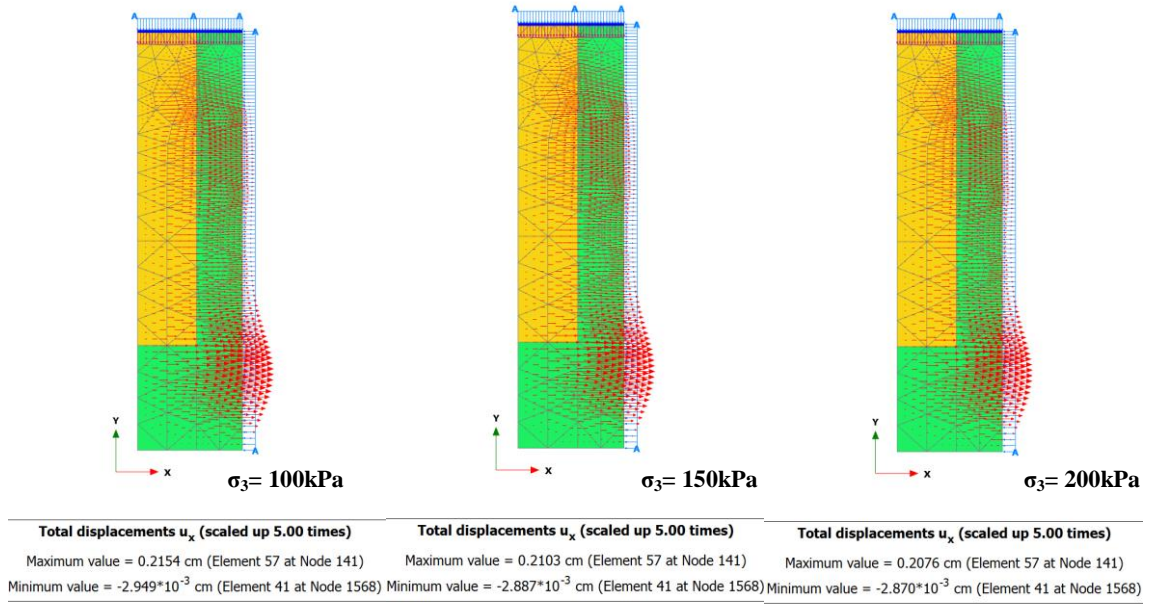


Figure 4.24. Horizontal displacements for Model 5 at 100, 150 and 200 kPa (from left to right)

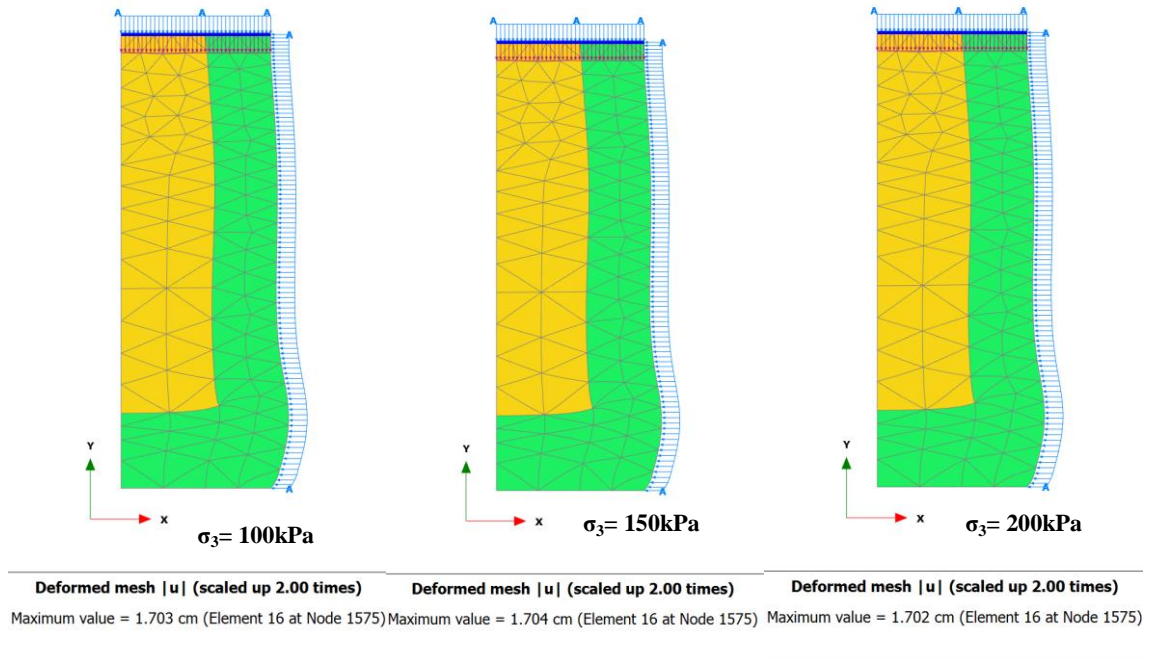


Figure 4.25. Deformed mesh for Model 5 at 100, 150 and 200 kPa (from left to right)

4.4.2. Stress-Strain Behavior

To study the stress-strain behavior in all the models, the deviatoric axial stress was plotted against the axial strain for all the models (Figure 4.26, Figure 4.27 and Figure 4.28). All the curves indicate that for the same sand column diameter, the full penetration columns result in a stiffer composite sample compared to the partial penetration columns. For each penetration category (full or partial), the larger the sand column diameter, the stiffer is the composite specimen. These are in line with what was observed in Maalouf (2012).

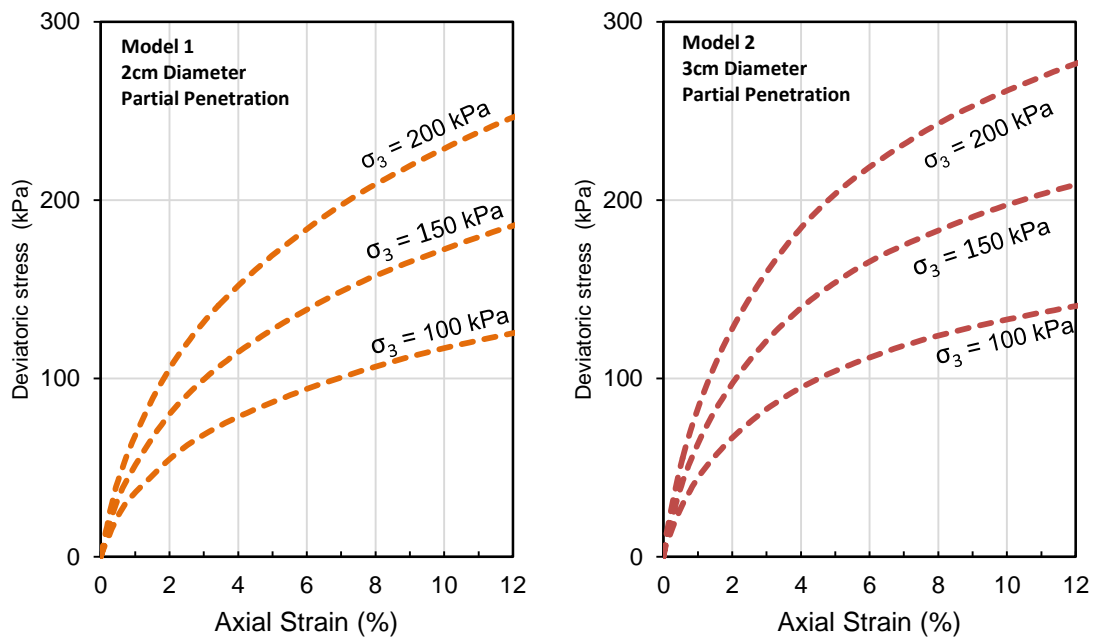


Figure 4.26. Stress Strain curves for partial penetration models (M1 and M2)

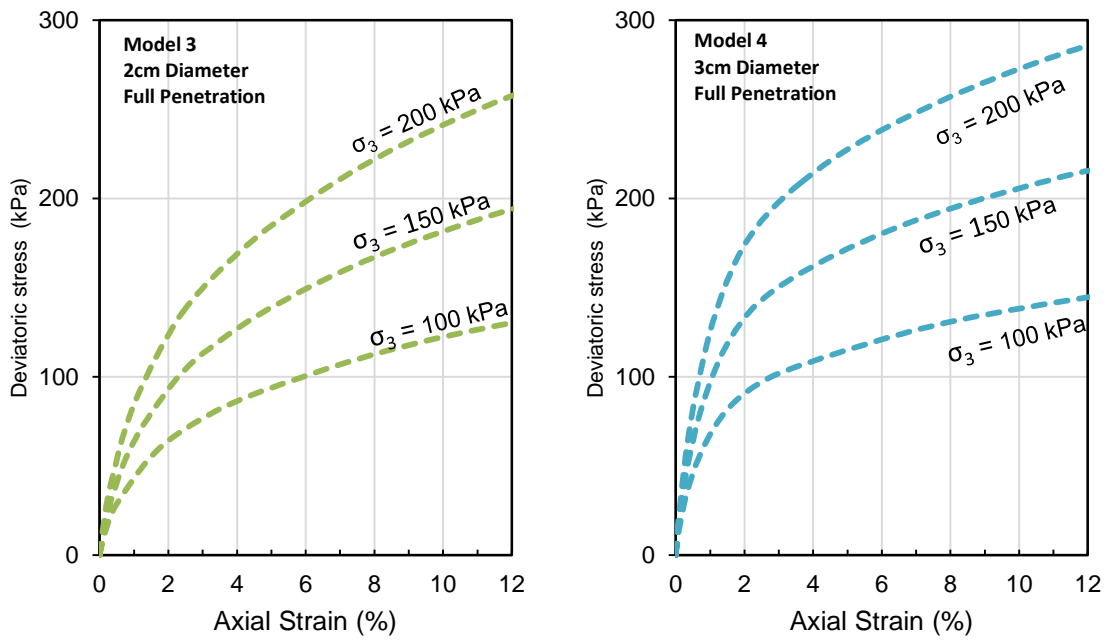


Figure 4.27. Stress Strain curves for full penetration models (M3 and M4)

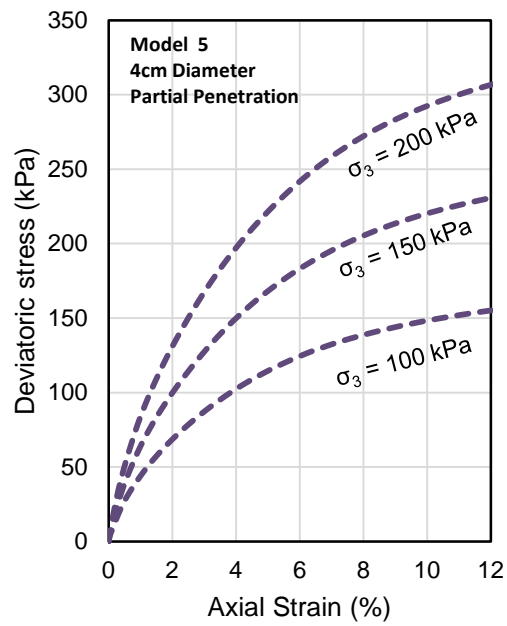


Figure 4.28. Stress Strain curve for the additional partial penetration model (M5)

4.4.3. Stress Distribution

The vertical loading stress concentration in the sand column and in the surrounding clay was reflected in the deviatoric stress distribution across the vertical plain output. The output relative to the 3cm sand column sample (Model 2 Partial Penetration and Model 4 Full Penetration) were displayed in a global and zoomed view stress distribution intensity output across the vertical plain (Figure 4.29, Figure 4.30, Figure 4.32, Figure 4.33, Figure 4.35 and Figure 4.36) and plotted on horizontal cross-section located 3cm below the sample top (Figure 4.31, Figure 4.34 and Figure 4.37).

The average stress distribution for all the Models (2cm and 3cm diameters sand columns) at an axial strain of 10% to 12%, were obtained from Plaxis 2D output and tabulated in Table 4.3. The Stress Ratio (Sand/Clay), denoted as SR, was also calculated for all the models by dividing the average deviatoric stress in the sand column by the average deviatoric stress in the surrounding clay. The SR was ranging between 2.8 and 3.1, with an average of 2.9. In general, the stress sustained by the sand columns was about 3 times the stress sustained by the surrounding clay.

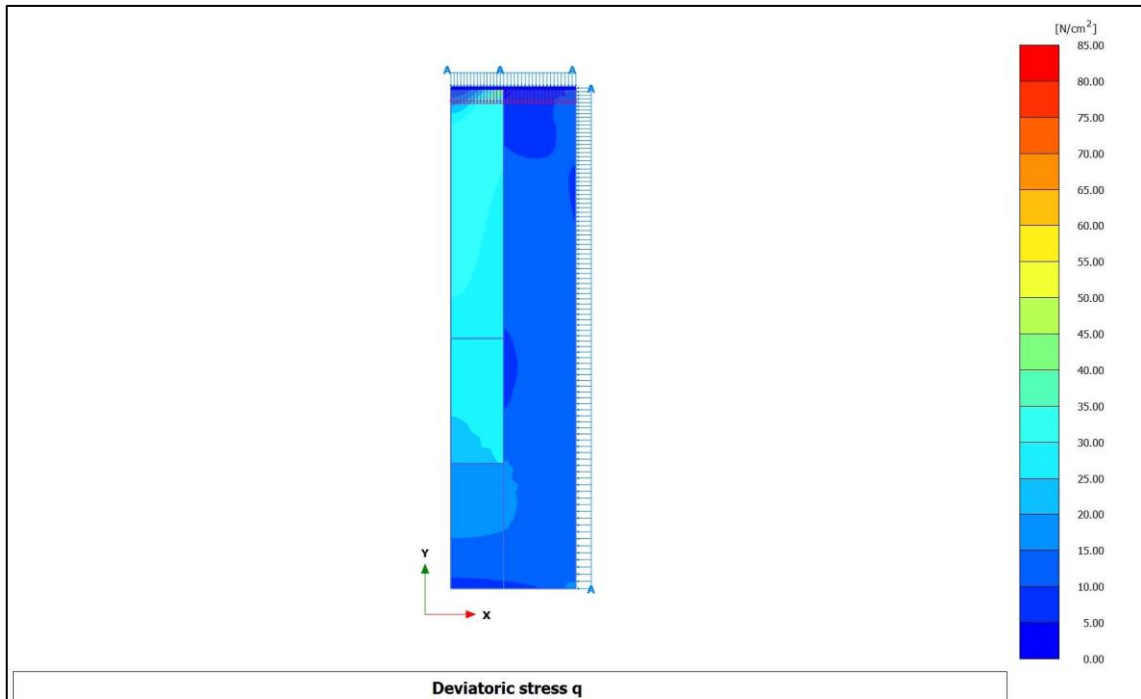


Figure 4.29. Stress distribution in Model M2 (3cm Sand Column, Partial Penetration) at a confining pressure σ_3 of 100 kPa (Global View)

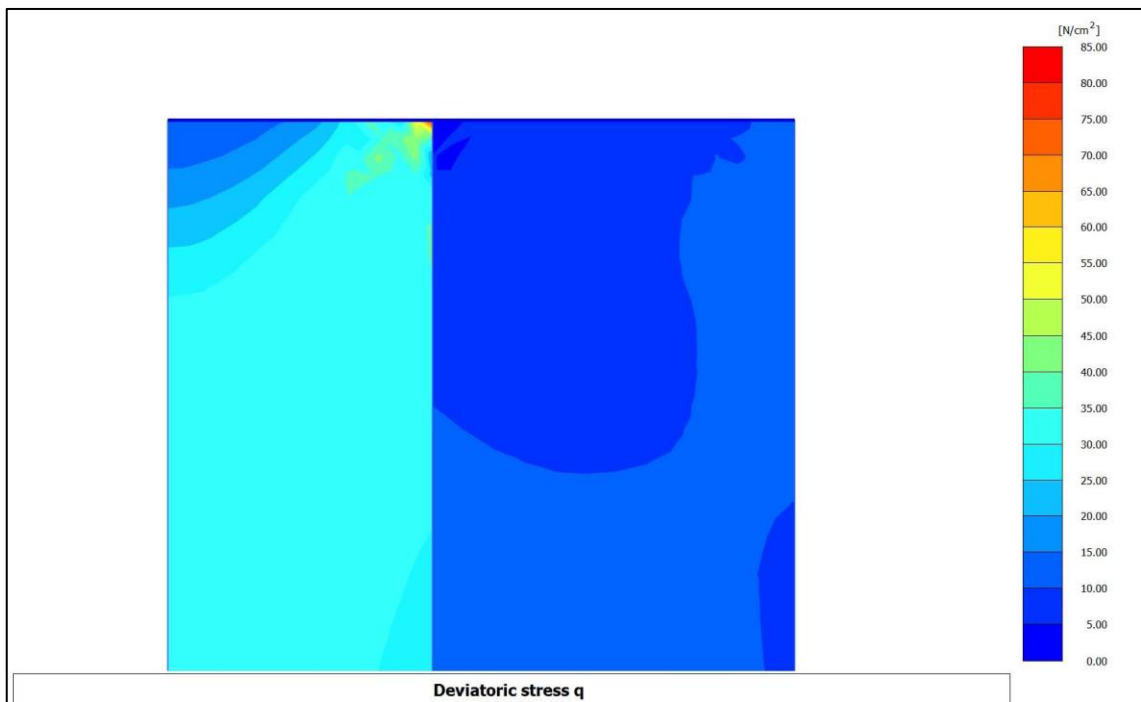


Figure 4.30. Stress distribution in Model M2 (3cm Sand Column, Partial Penetration) at a confining pressure σ_3 of 100 kPa (Zoomed View)

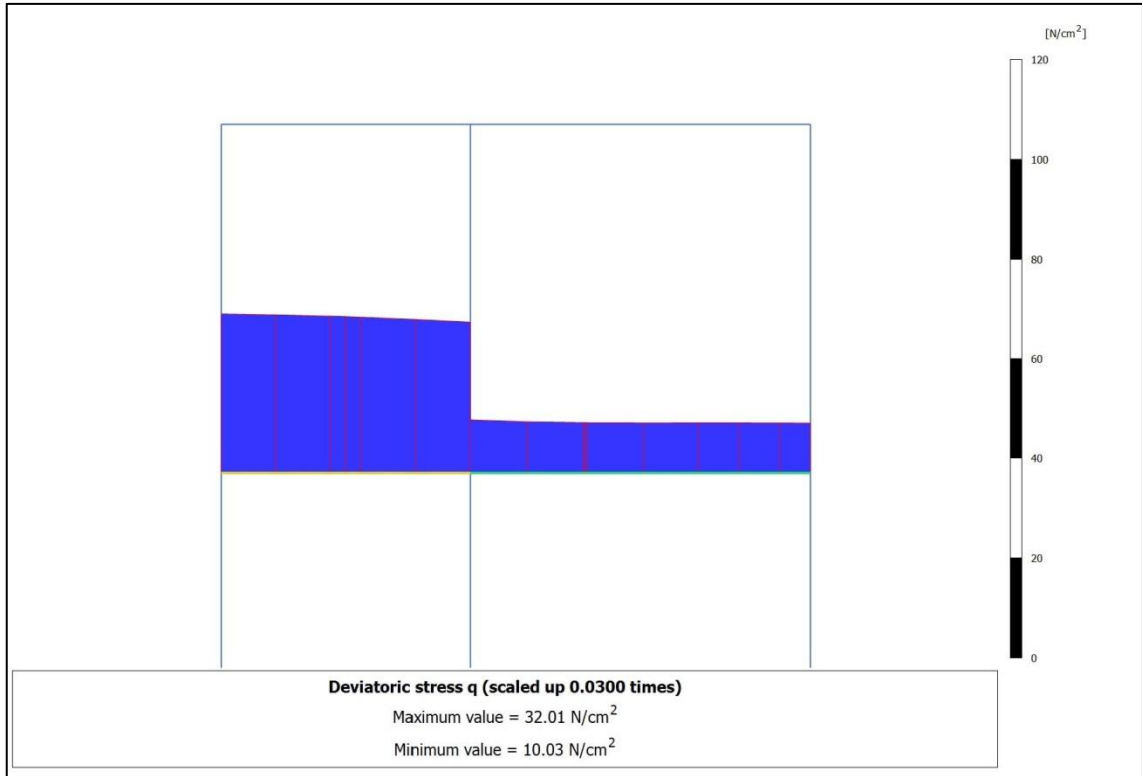


Figure 4.31. Stress distribution along a horizontal axis 3cm below the sample top, in Model M2 (3cm Sand Column, Partial Penetration) at a confining pressure σ_3 of 100 kPa

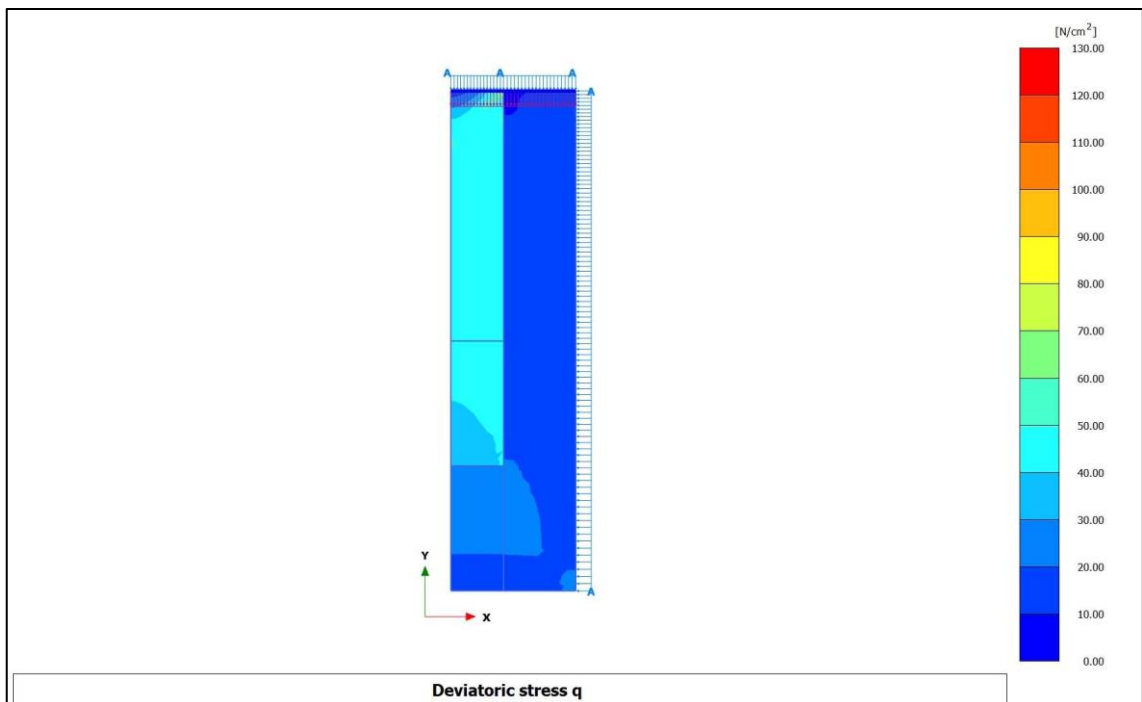


Figure 4.32. Stress distribution in Model M2 (3cm Sand Column, Partial Penetration) at a confining pressure σ_3 of 150 kPa (Global View)

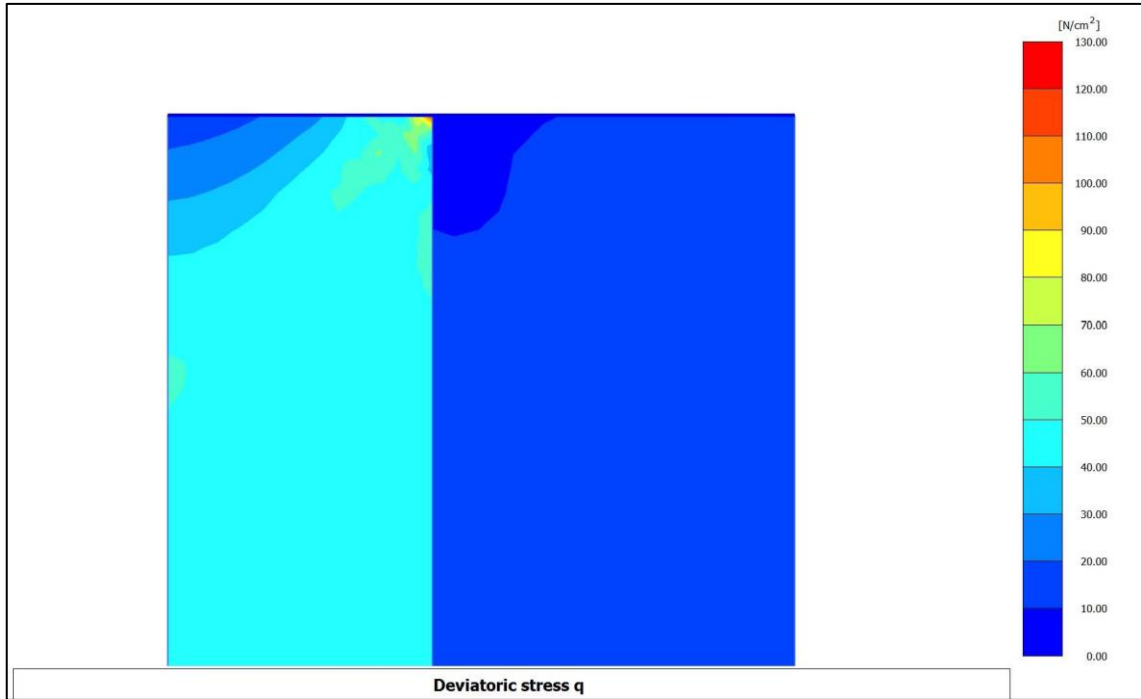


Figure 4.33. Stress distribution in Model M2 (3cm Sand Column, Partial Penetration) at a confining pressure σ_3 of 150 kPa (Zoomed View)

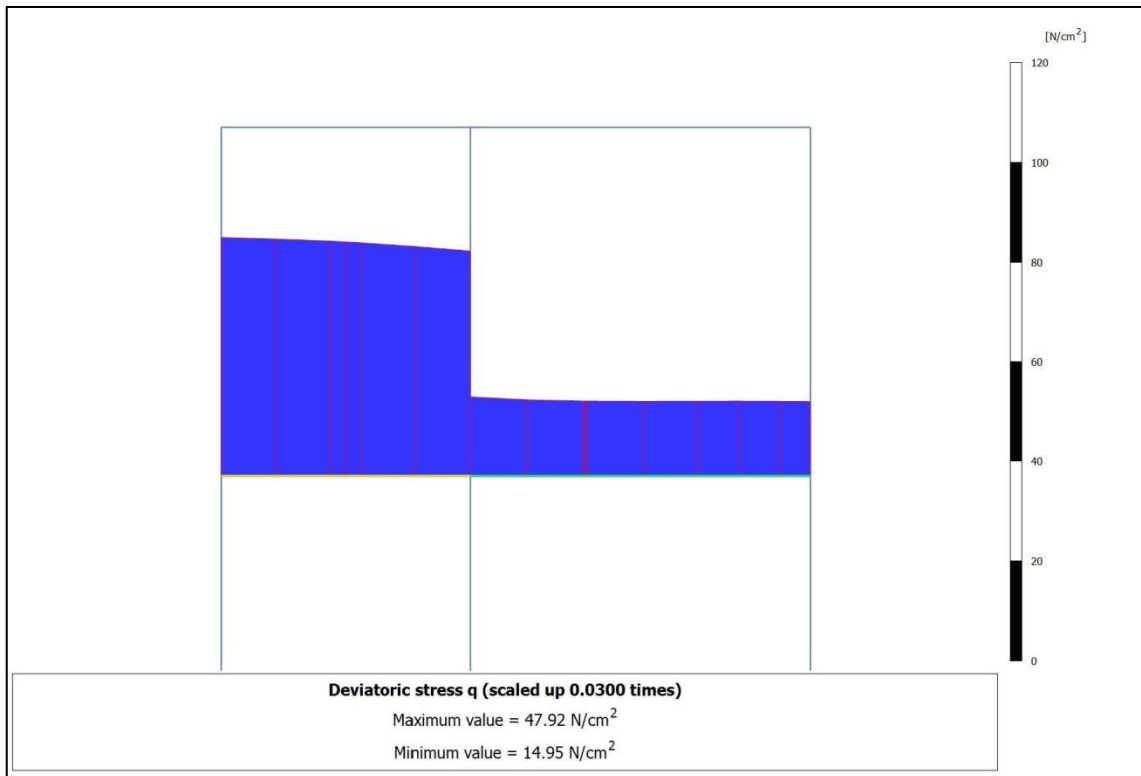


Figure 4.34. Stress distribution along a horizontal axis 3cm below the sample top, in Model M2 (3cm Sand Column, Partial Penetration) at a confining pressure σ_3 of 150 kPa

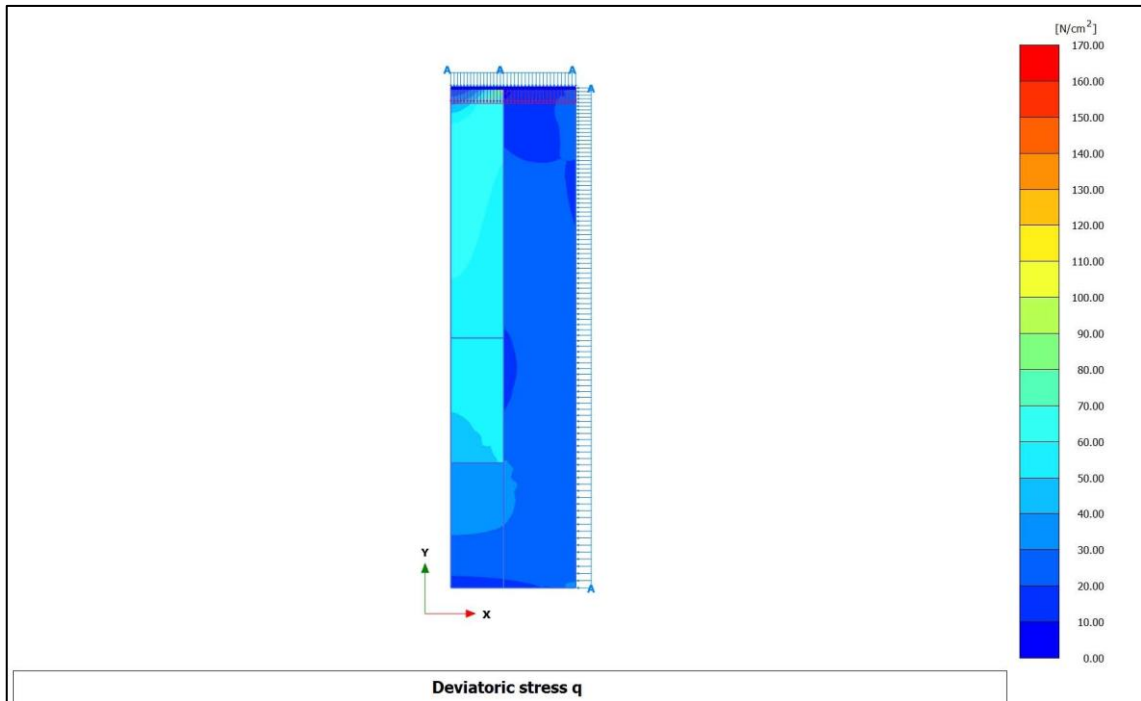


Figure 4.35. Stress distribution in Model M2 (3cm Sand Column, Partial Penetration) at a confining pressure σ_3 of 200 kPa (Global View)

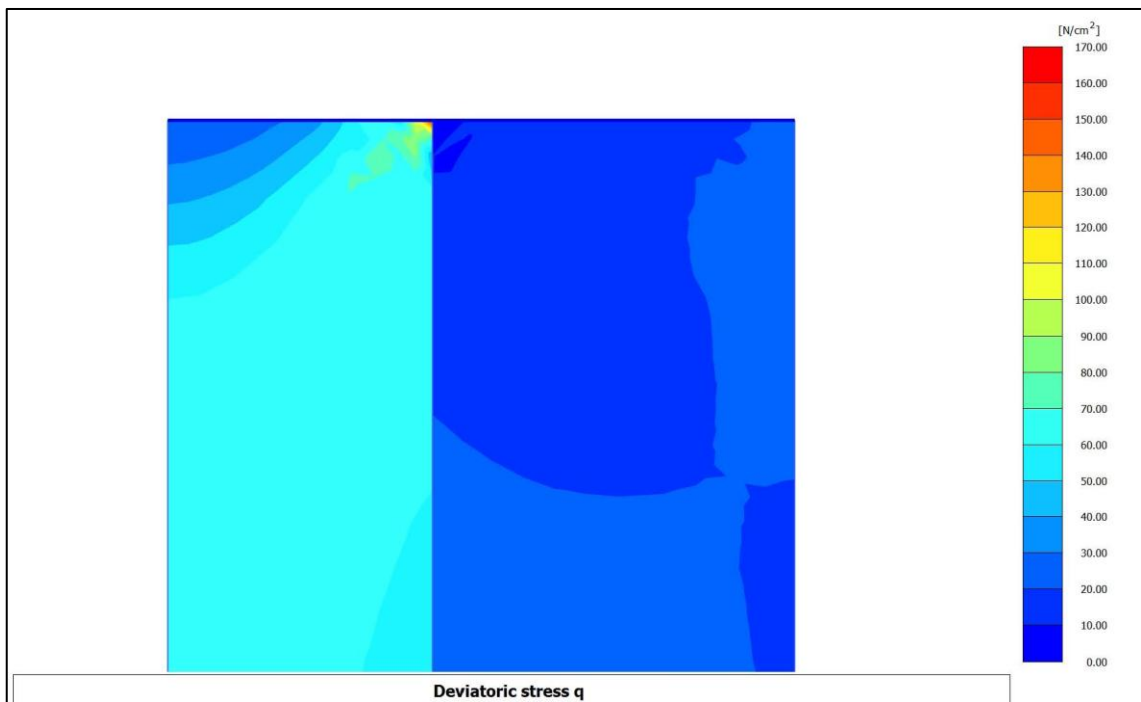


Figure 4.36. Stress distribution in Model M2 (3cm Sand Column, Partial Penetration) at a confining pressure σ_3 of 200 kPa (Zoomed View)

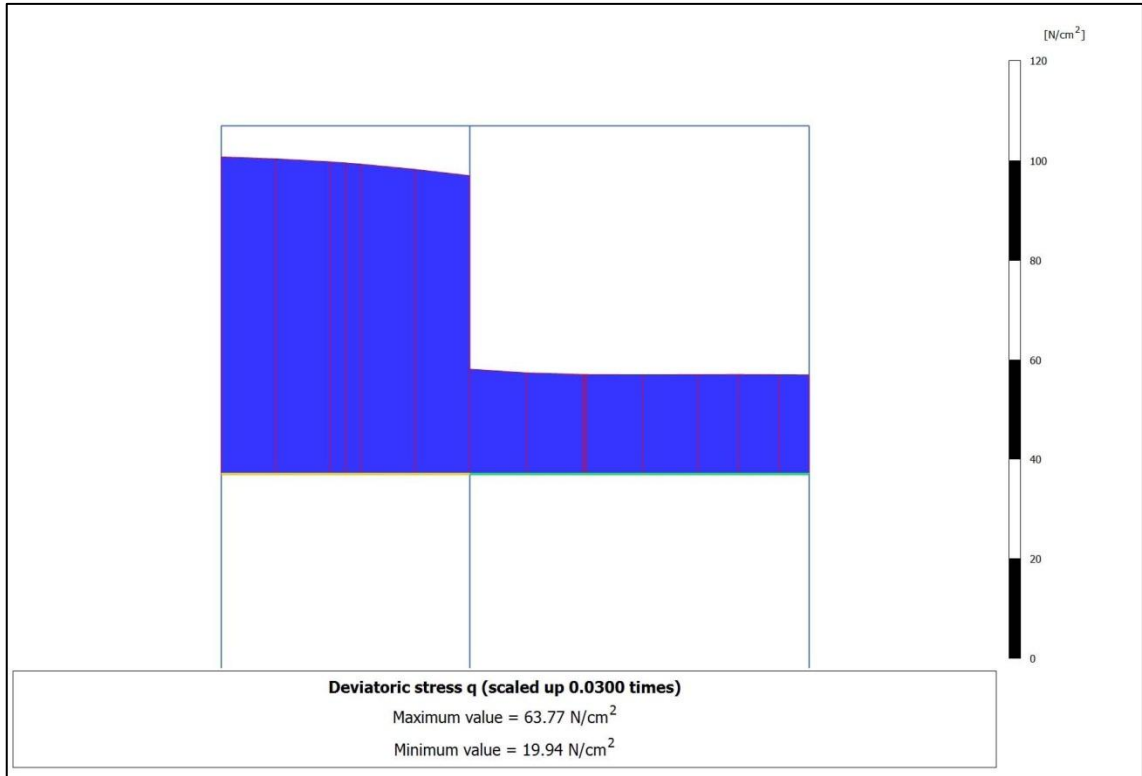


Figure 4.37. Stress distribution along a horizontal axis 3cm below the sample top, in Model M2 (3cm Sand Column, Partial Penetration) at a confining pressure σ_3 of 200 kPa

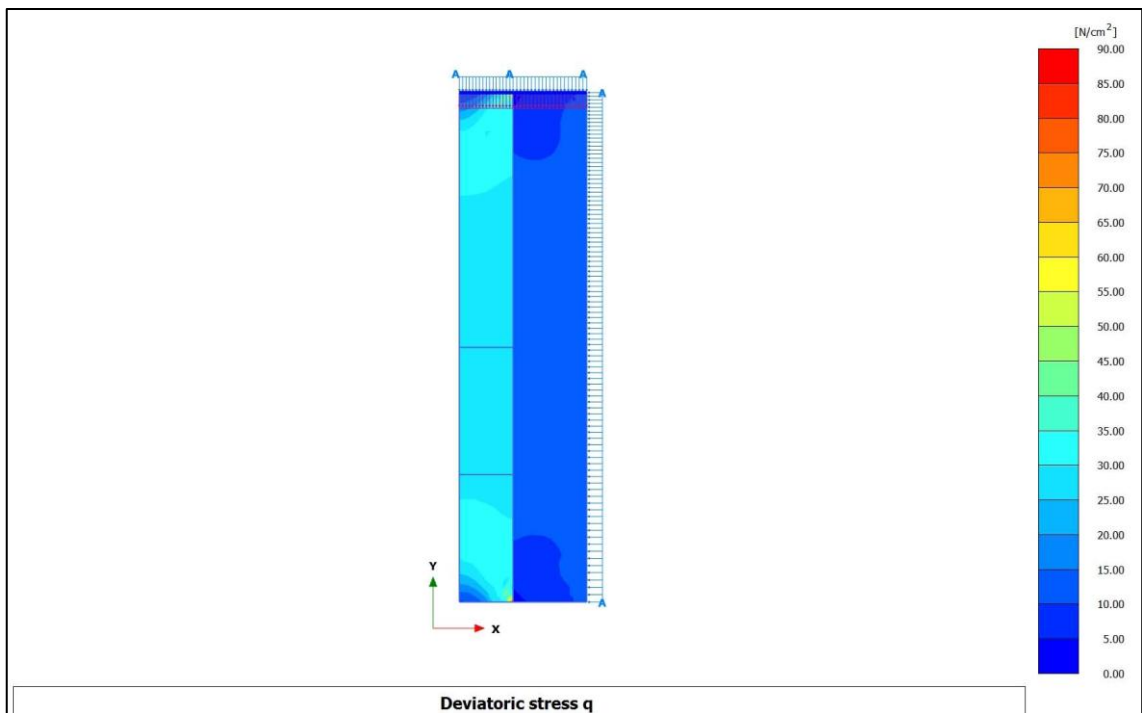


Figure 4.38. Stress distribution in Model M4 (3cm Sand Column, Full Penetration) at a confining pressure σ_3 of 100 kPa (Global View)

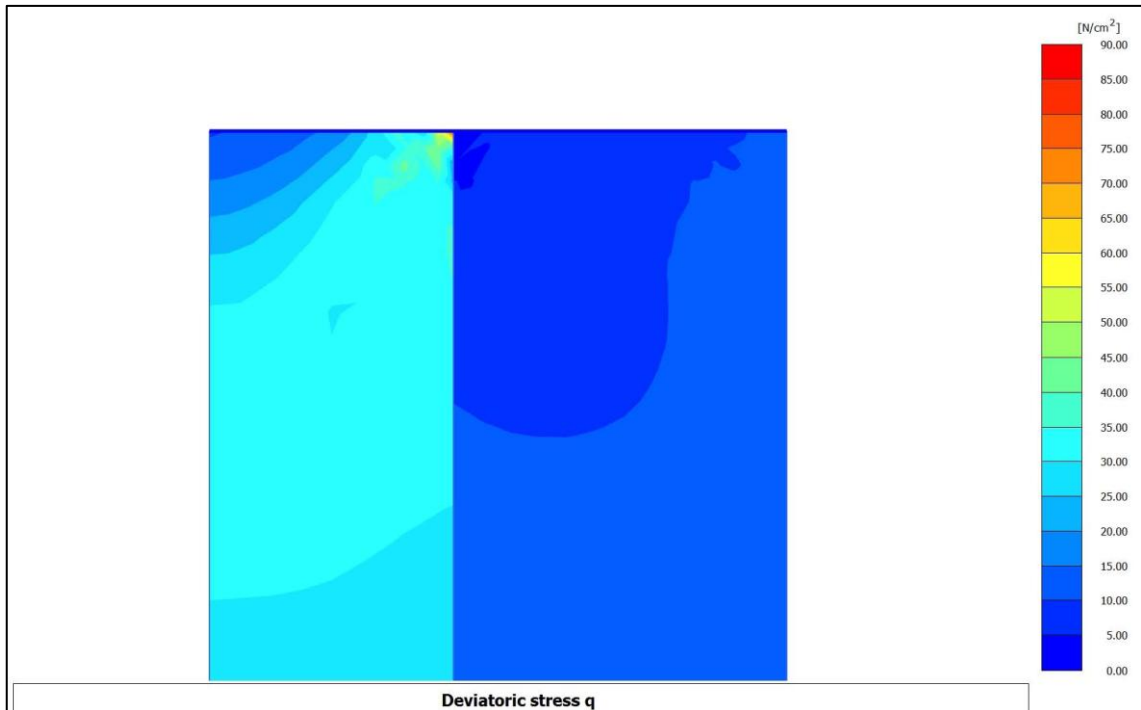


Figure 4.39. Stress distribution in Model M4 (3cm Sand Column, Full Penetration) at a confining pressure σ_3 of 100 kPa (Zoomed View)

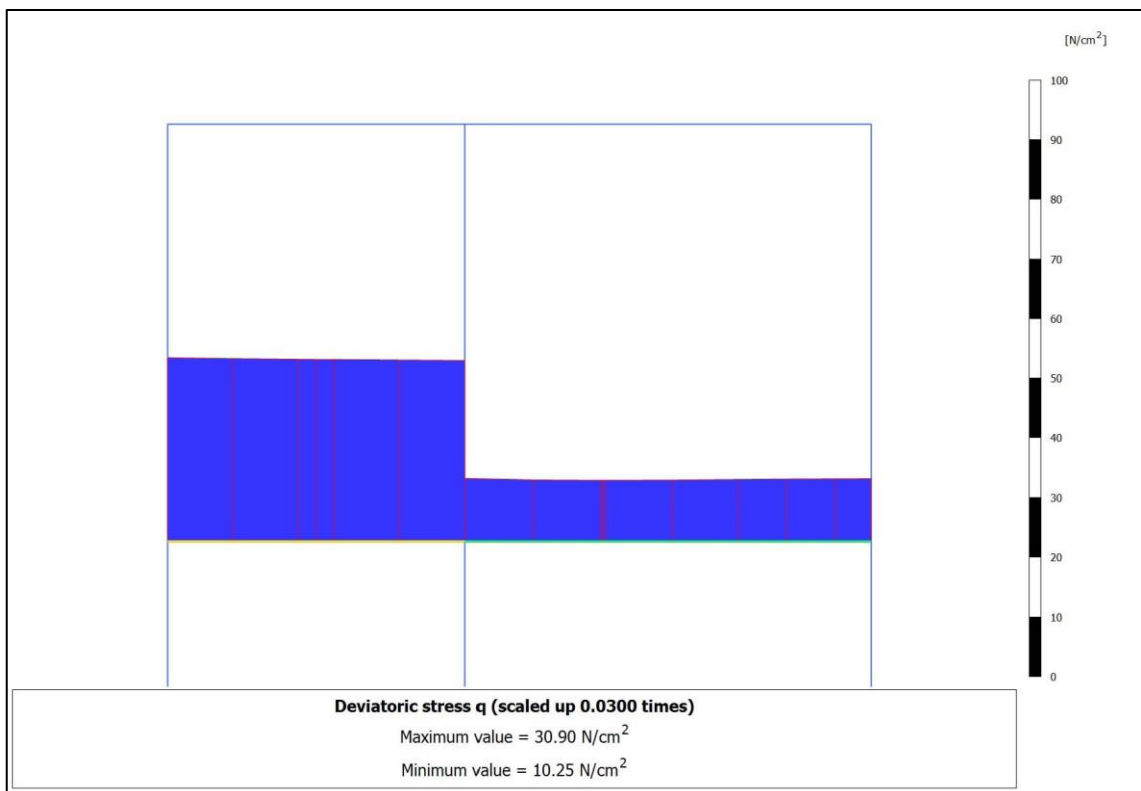


Figure 4.40. Stress distribution along a horizontal axis 3cm below the sample top, in Model M4 (3cm Sand Column, Full Penetration) at a confining pressure σ_3 of 100 kPa

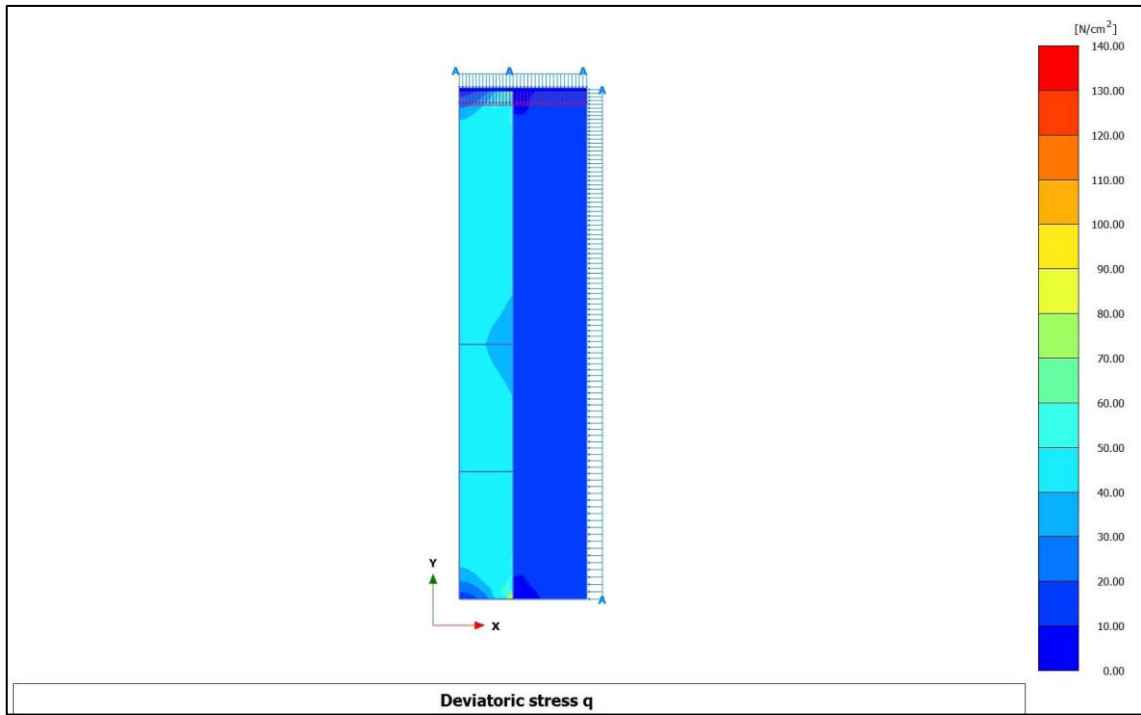


Figure 4.41. Stress distribution in Model M4 (3cm Sand Column, Full Penetration) at a confining pressure σ_3 of 150 kPa (Global View)

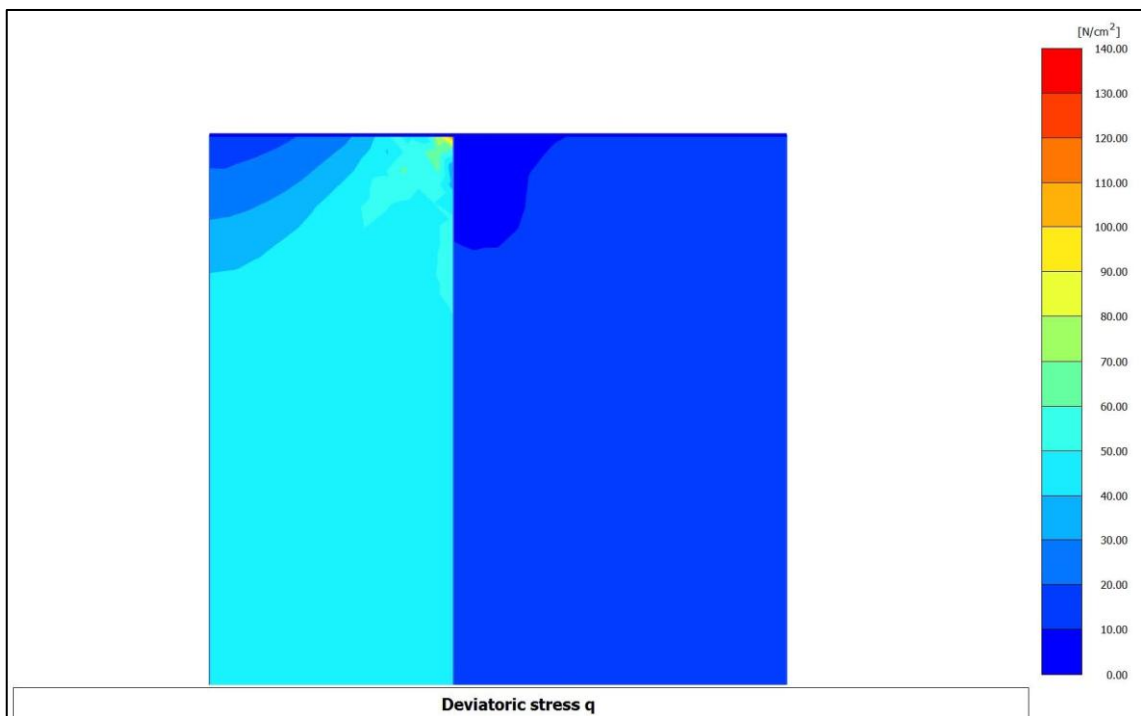


Figure 4.42. Stress distribution in Model M4 (3cm Sand Column, Full Penetration) at a confining pressure σ_3 of 150 kPa (Zoomed View)

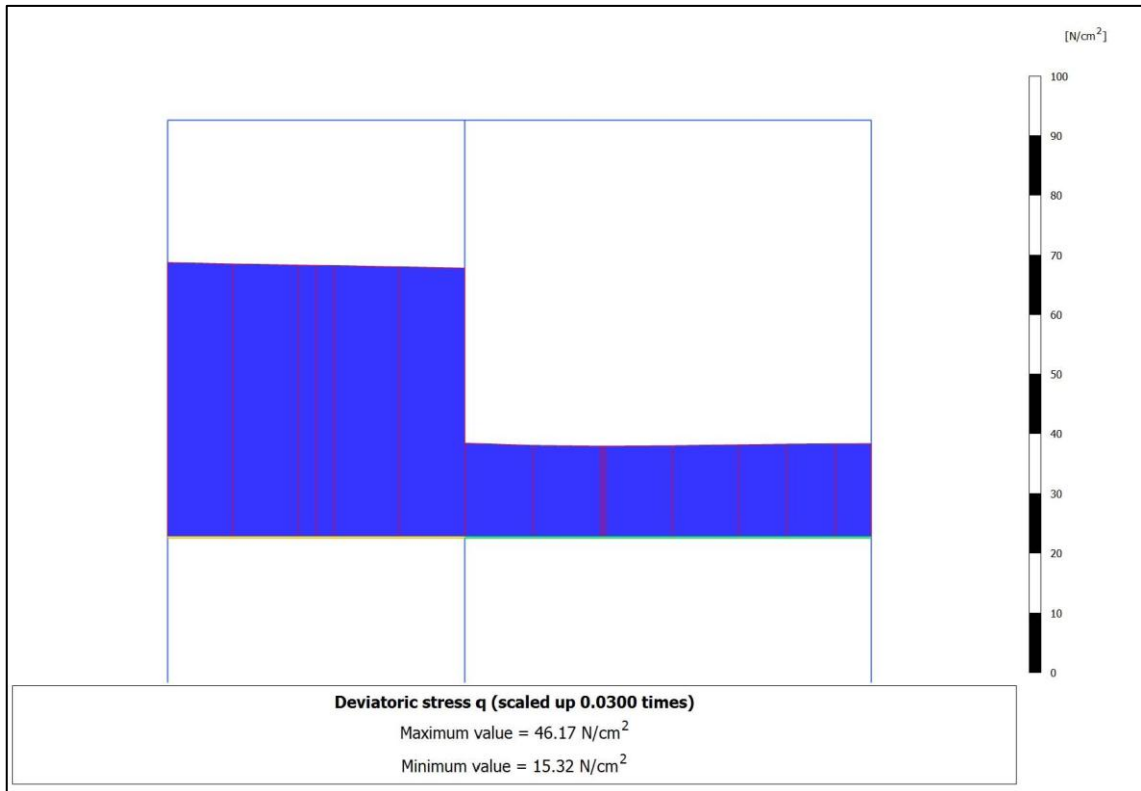


Figure 4.43. Stress distribution along a horizontal axis 3cm below the sample top, in Model M4 (3cm Sand Column, Full Penetration) at a confining pressure σ_3 of 150 kPa

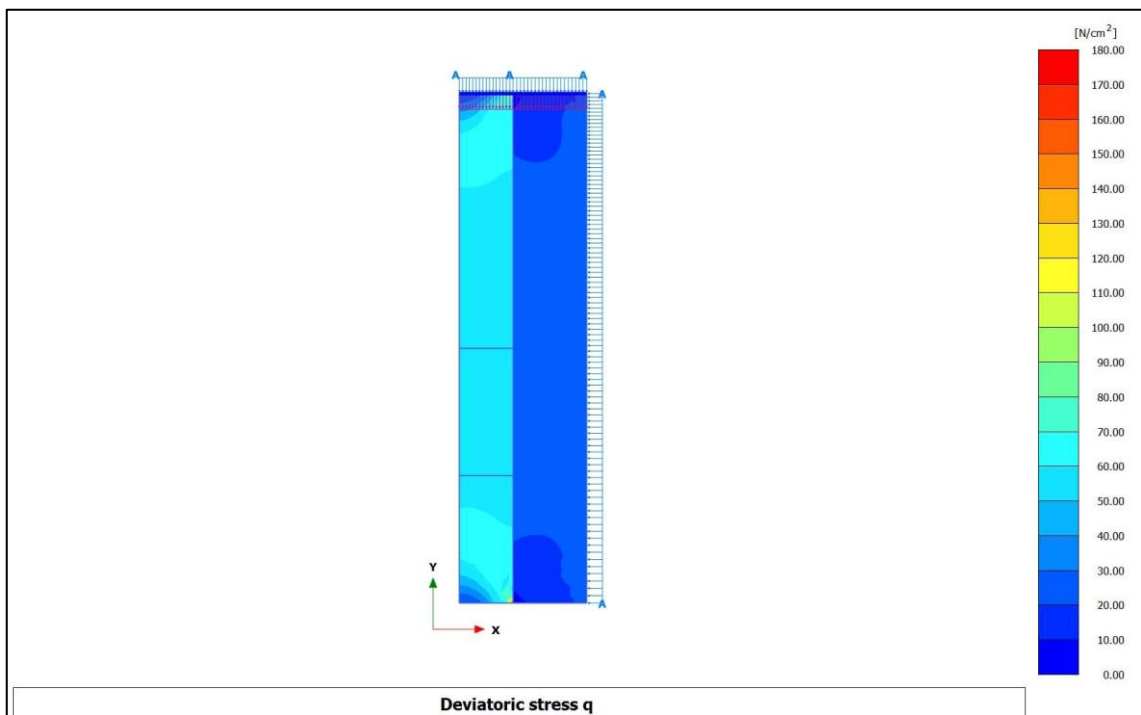


Figure 4.44. Stress distribution in Model M4 (3cm Sand Column, Full Penetration) at a confining pressure σ_3 of 200 kPa (Global View)

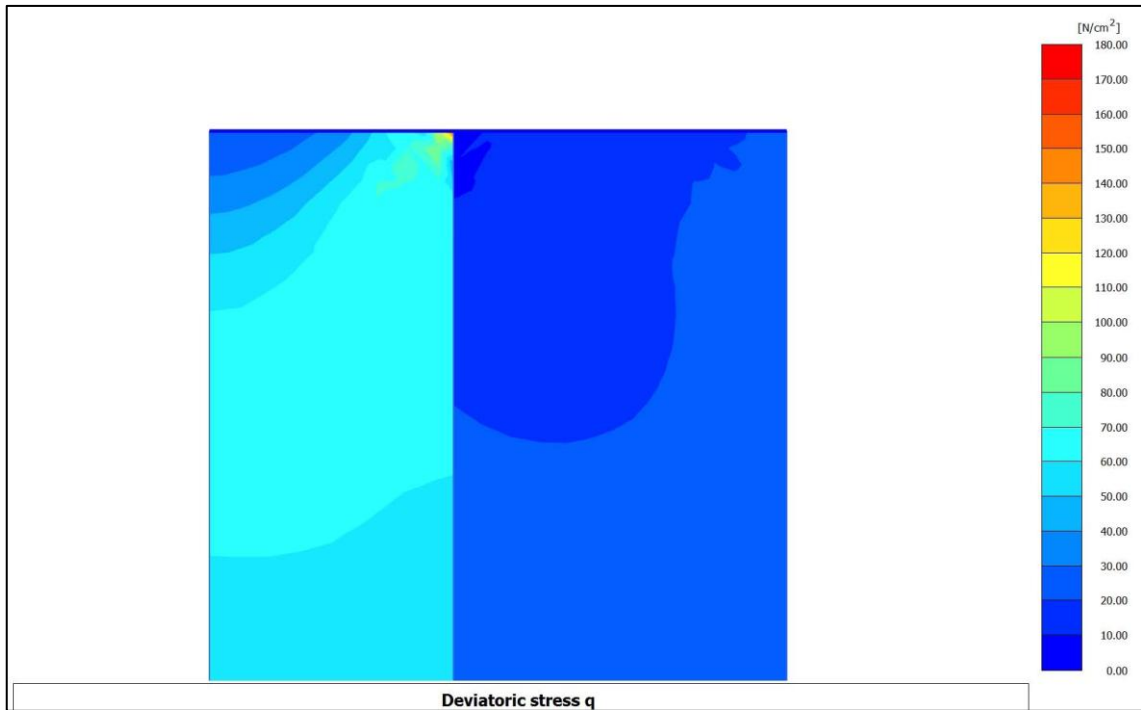


Figure 4.45. Stress distribution in Model M4 (3cm Sand Column, Full Penetration) at a confining pressure σ_3 of 200 kPa (Zoomed View)

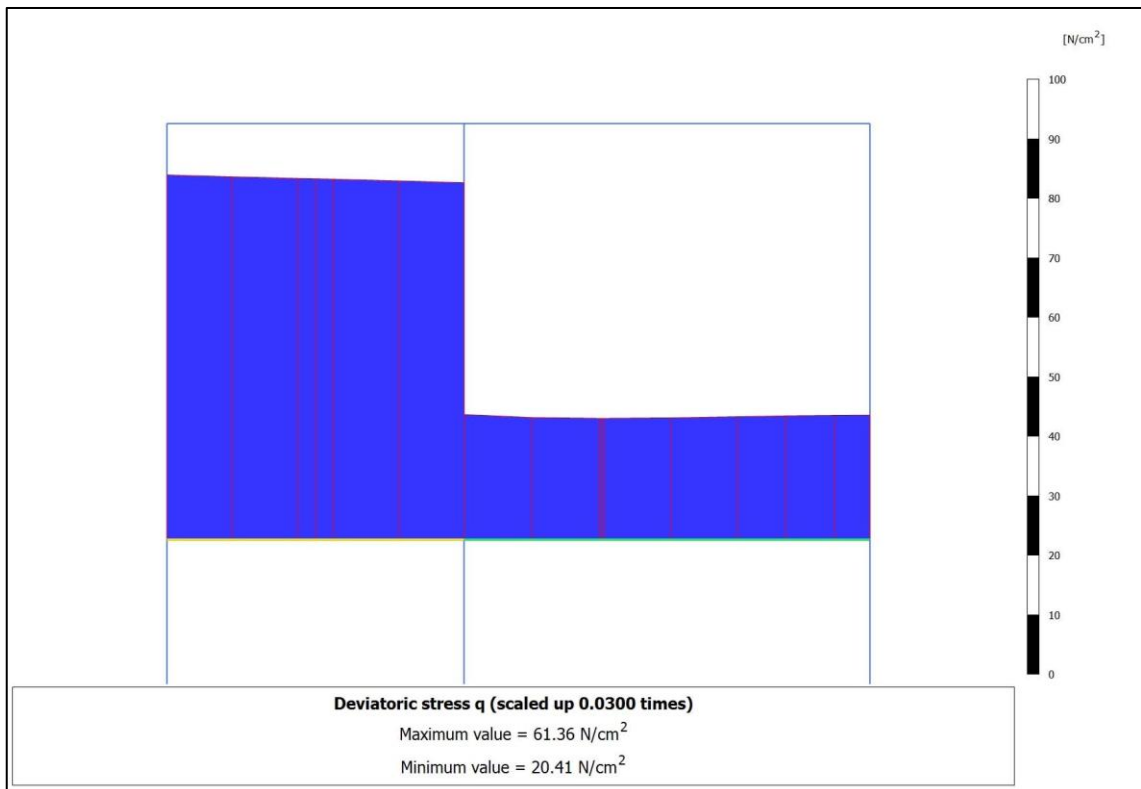


Figure 4.46. Stress distribution along a horizontal axis 3cm below the sample top, in Model M4 (3cm Sand Column, Full Penetration) at a confining pressure σ_3 of 200 kPa

Table 4.3. Average deviatoric stress distribution and SR

Model No.	Test No.	Confining pressure σ_3 (kPa)	Diameter of sand column (mm)	Area replacement ratio: A_c/A_s (%)	Column Penetration Ratio: H_c/H_s	Average Deviatoric Stress in Sand Column* (kPa)	Average Deviatoric Stress in Clay* (kPa)	Stress Ratio (Sand/Clay)* SR
Model 1	M1-100	100	20	7.9	0.75	315	110	2.9
	M1-150	150	20	7.9	0.75	468	164	2.9
	M1-200	200	20	7.9	0.75	621	218	2.8
Model 2	M2-100	100	30	17.8	0.75	315	110	2.9
	M2-150	150	30	17.8	0.75	467	166	2.8
	M2-200	200	30	17.8	0.75	620	220	2.8
Model 3	M3-100	100	20	7.9	1	315	100	3.2
	M3-150	150	20	7.9	1	471	150	3.1
	M3-200	200	20	7.9	1	626	200	3.1
Model 4	M4-100	100	30	17.8	1	306	103	3.0
	M4-150	150	30	17.8	1	457	153	3.0
	M4-200	200	30	17.8	1	607	205	3.0
<i>* Obtained at Axial strains at about 12% - 13%</i>							Average	2.9

The average stress ratio (SR), tabulated in Table 4.3, was ranging between 2.8 and 3.1 with an average of 2.9. The SR for each Model was plotted versus the 3 confining pressures (σ_3) of 100kPa, 150 kPa and 200 kPa in Figure 4.47, and it was clearly reflected that the stress concentration in the sand columns were higher in the full penetration columns compared to the partial penetration columns of the same diameter. The SR increases as the confining pressure decreases, meaning that the more confined the sample is the less portion of stress is being sustained by the sand column.

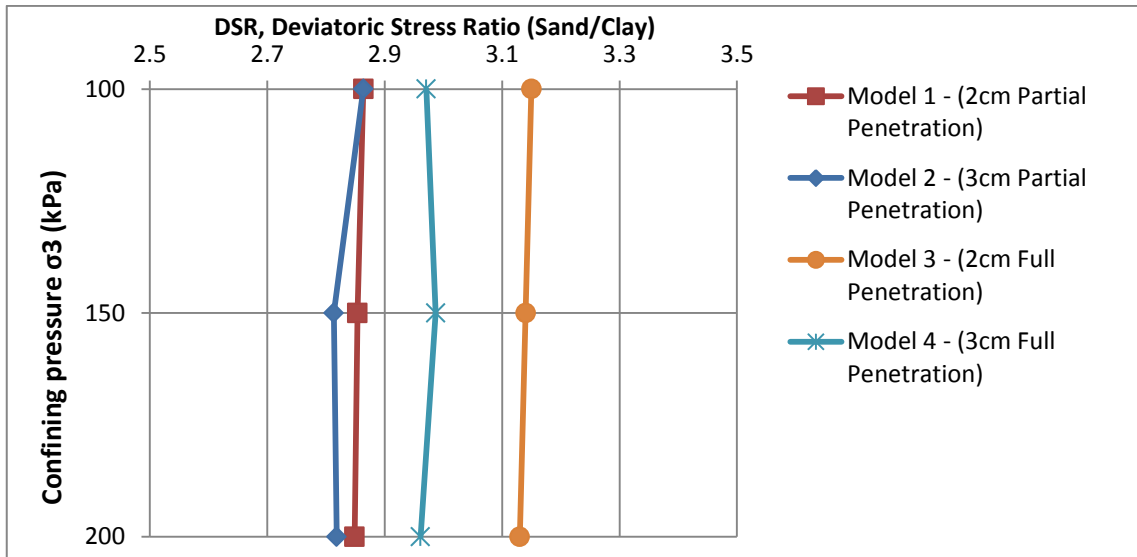


Figure 4.47. Stress Ratio (SR) plotted vs confining pressures, σ_3 of 100kPa, 150 kPa and 200 kPa

To have a better understanding of the change in stress concentration relative to the axial strain, we have considered Model 2 (3cm diameter, partial penetration) and Model 4 (3cm diameter, full penetration) for a more detailed FEM analyses. Two stress points located at about 2cm below the sample top (Figure 4.48) were used to generate in Plaxis 3D's curves application, deviatoric stresses at the whole axial strain range (0% to 12%). The obtained stresses in the sand column were divided by the corresponding stresses in the surrounding clay and plotted versus the vertical axial strain (Figure 4.49 and Figure 4.50).

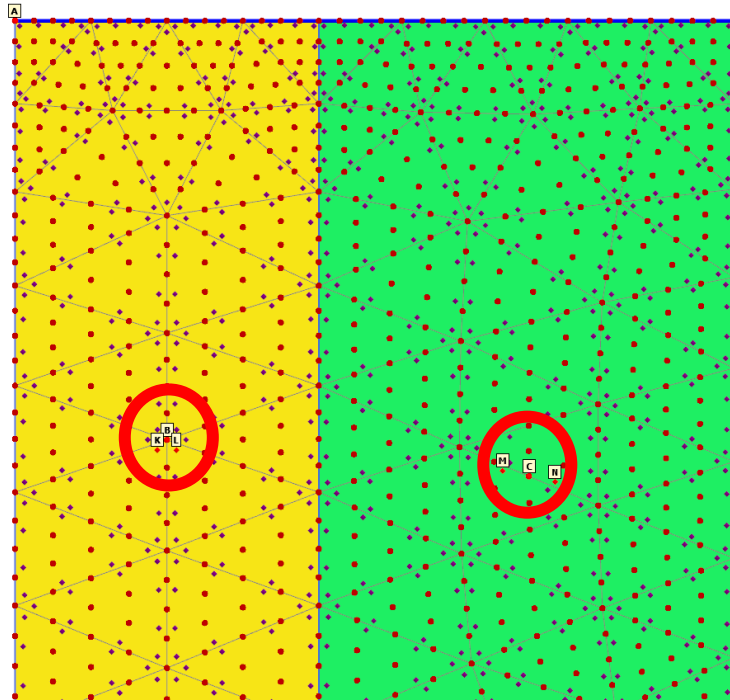


Figure 4.48. Deviatoric Stresses were read from the above indicated stress points locations, one located in the sand column and one in the surrounding clay

For the partially penetrating sand column, the SR is almost the same and the curves in (Figure 4.49) overlaps for the axial strain ranges of 0% - 0.64% and 6% - 12%. Between 0.64% -6% axial strain, the SR of lower confining pressures (i.e. $\sigma_3 = 100\text{kPa}$) is always larger than the SR at higher confining pressures (i.e. $\sigma_3 = 200\text{kPa}$), showing that the lower the confinement pressure (σ_3) the higher the SR in that range of axial strains (0.64%-6%), thus the more of the total deviatoric stresses are concentrated on the sand column.

For the partially penetrating sand column, the SR start from 3.6-3.7 at 0% axial strain and increases steeply to reach the following peak values: 10.4, 10.2 and 9.9 for confinement pressures (σ_3) of 100kPa, 150kPa and 200 kPa respectively, all at about 0.85% axial strain. Then the SR drops to about 3.3 at 12% axial strain for all the confinement pressures.

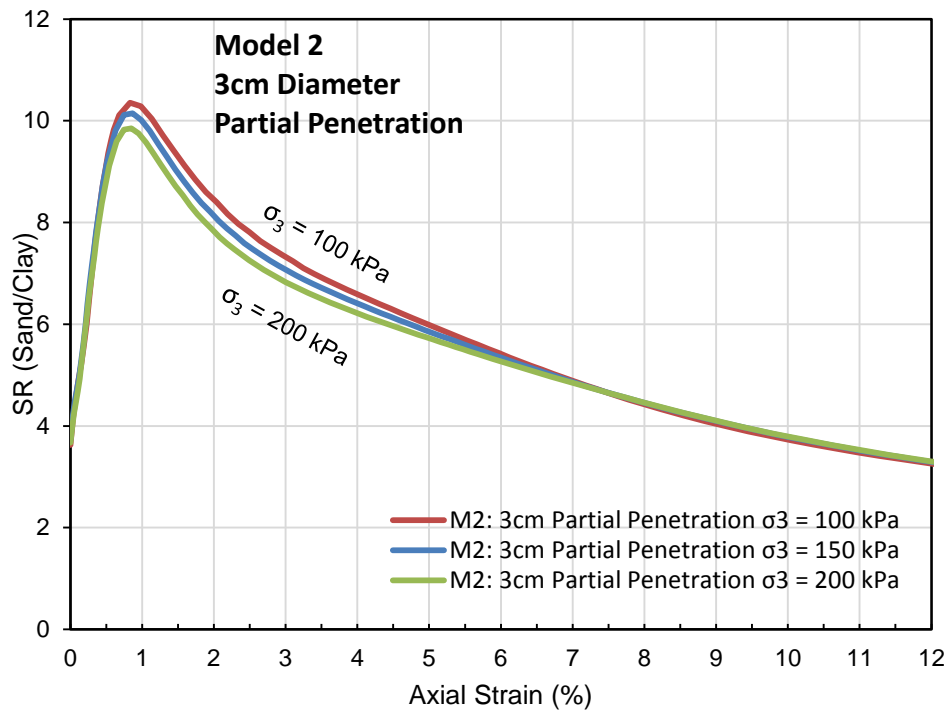


Figure 4.49. Stress Ratio (SR) plotted vs axial strain for σ_3 of 100kPa, 150 kPa and 200 kPa, relative to Model 2: 3cm Diameter sand column / Partial Penetration

For the full penetrating sand column, the SR is almost the same and the curves in (Figure 4.50) overlaps for the axial strain ranges of 0% - 0.32% and 3% - 12%. Between 0.32% -3% axial strain, the SR of lower confining pressures (i.e. $\sigma_3 = 100\text{kPa}$) is always larger than the SR at higher confining pressures (i.e. $\sigma_3 = 200\text{kPa}$), showing that the lower the confinement pressure (σ_3) the higher the SR in that range of axial strains (0.32%-3%), thus the more of the total deviatoric stresses are concentrated on the sand column.

For the full penetrating sand column, the SR start from 3.7 at 0% axial strain and increases steeply to reach the following peak values: 10.6, 10.2 and 10.0 for confinement pressures (σ_3) of 100kPa, 150kPa and 200 kPa respectively, all at about 0.42% axial strain. Then the SR drops to about 2.9 at 12% axial strain for all the confinement pressures.

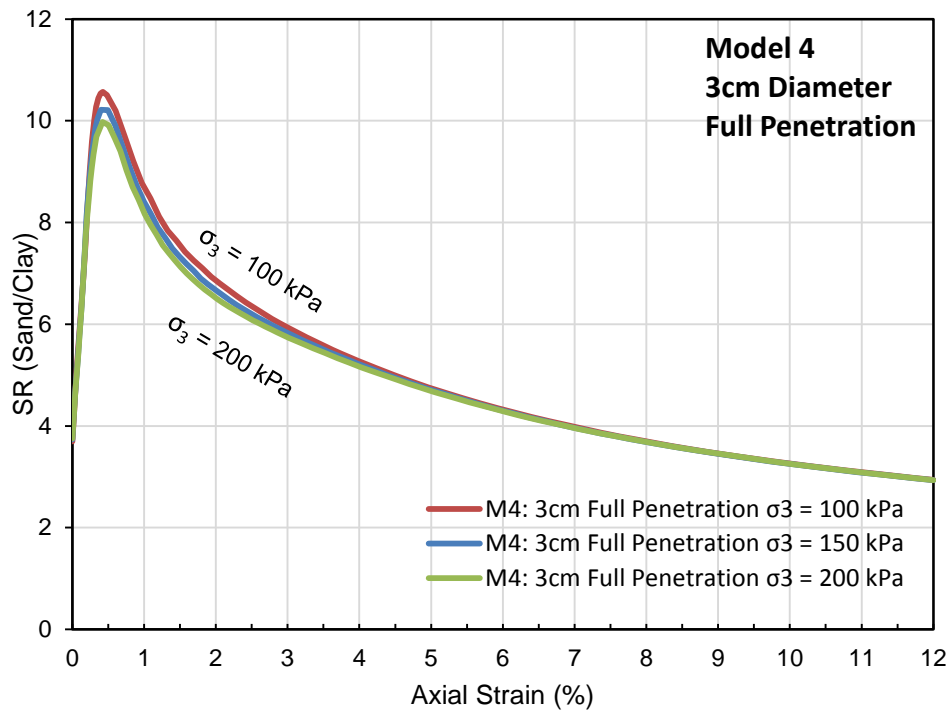


Figure 4.50. Stress Ratio (SR) plotted vs axial strain for σ_3 of 100kPa, 150 kPa and 200 kPa, relative to Model 4: 3cm Diameter sand column / Full Penetration

Both the results for the full and partial penetration (3cm Diameter) sand column were combined in Figure 4.51 to show the penetration rate effect. Both full penetration and partial penetration reached similar SR peaks and lows, however the full penetration column have reached these peaks at almost half the axial strains compared to the partial penetration column.

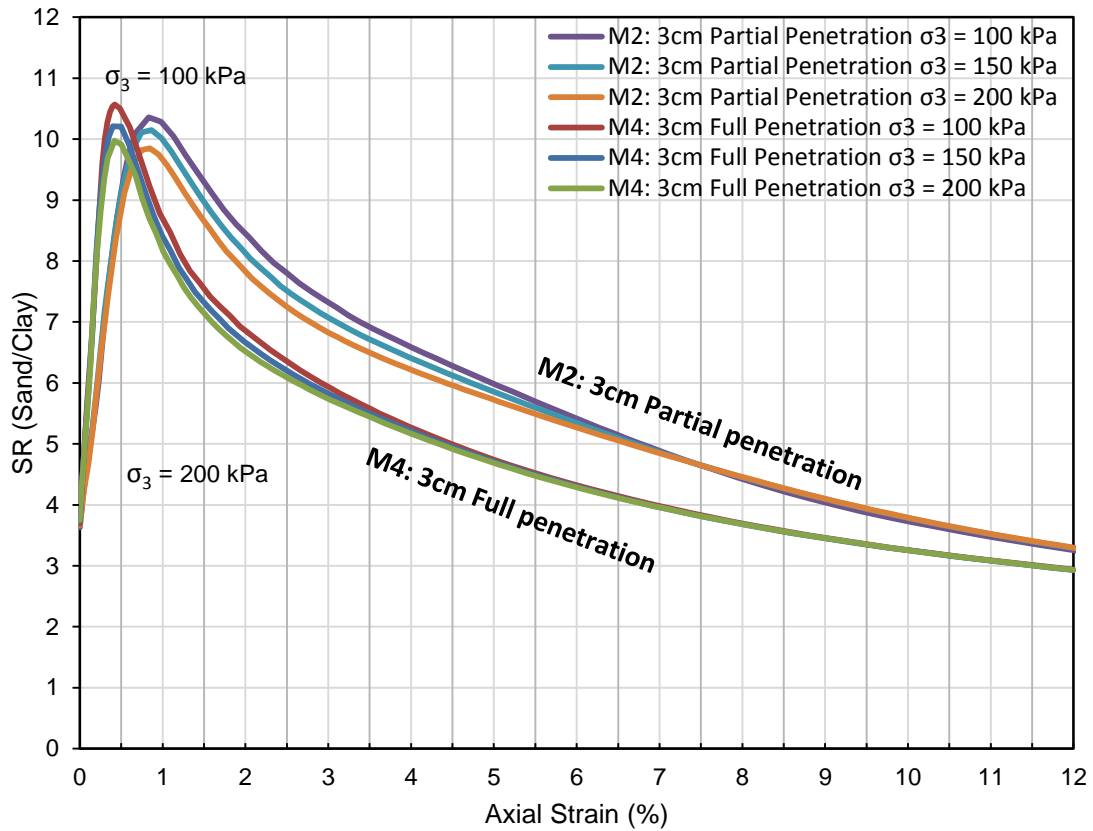


Figure 4.51. Stress Ratio (SR) plotted vs axial strain for σ_3 of 100kPa, 150 kPa and 200 kPa, for both Model 2 and Model 4

4.5. Comparing Hypoplasticity with Other Soil Models

Although Hypoplasticity was selected as the main model for the work of this thesis for several reasons discussed in the previous chapters, a cross check with other models is important to be carried out. Accordingly, the Ottawa sand was modeled as both Mohr Coulomb and Hardening soil (Figure 4.52). The Kaolin Clay was modeled as Hardening Soil (Figure 4.53).

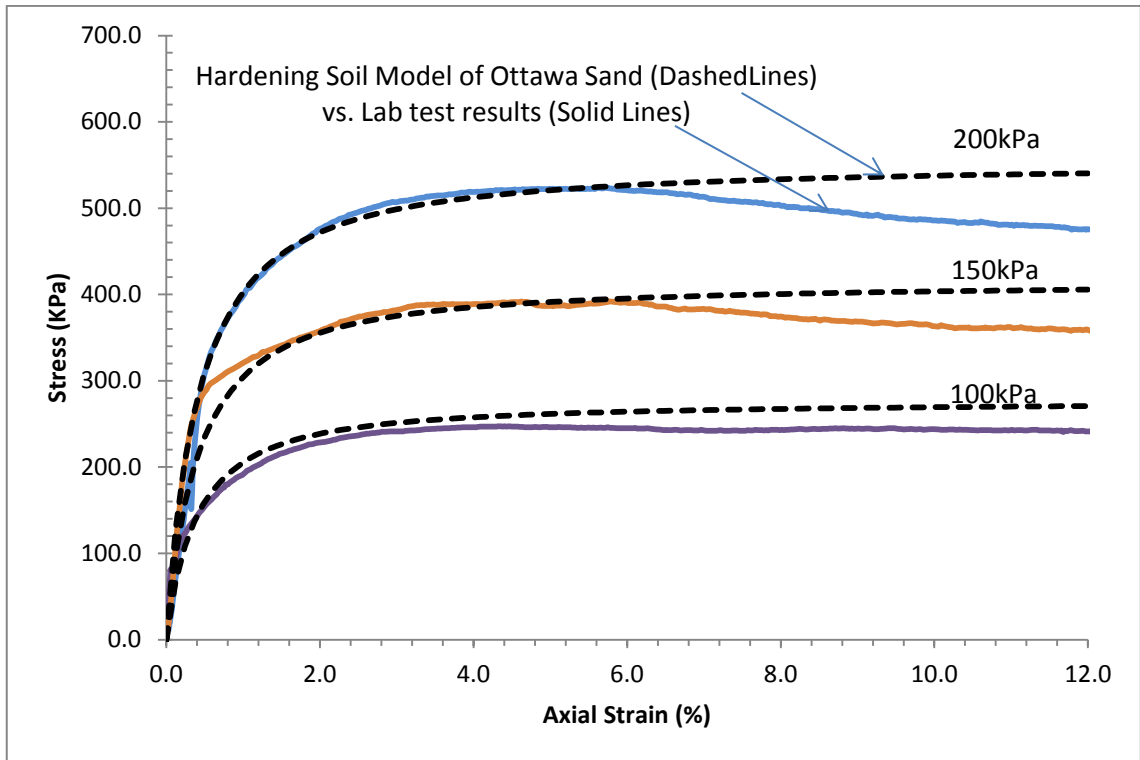


Figure 4.52. Hardening Soil (HS) Model of the Ottawa Sand vs Experimental

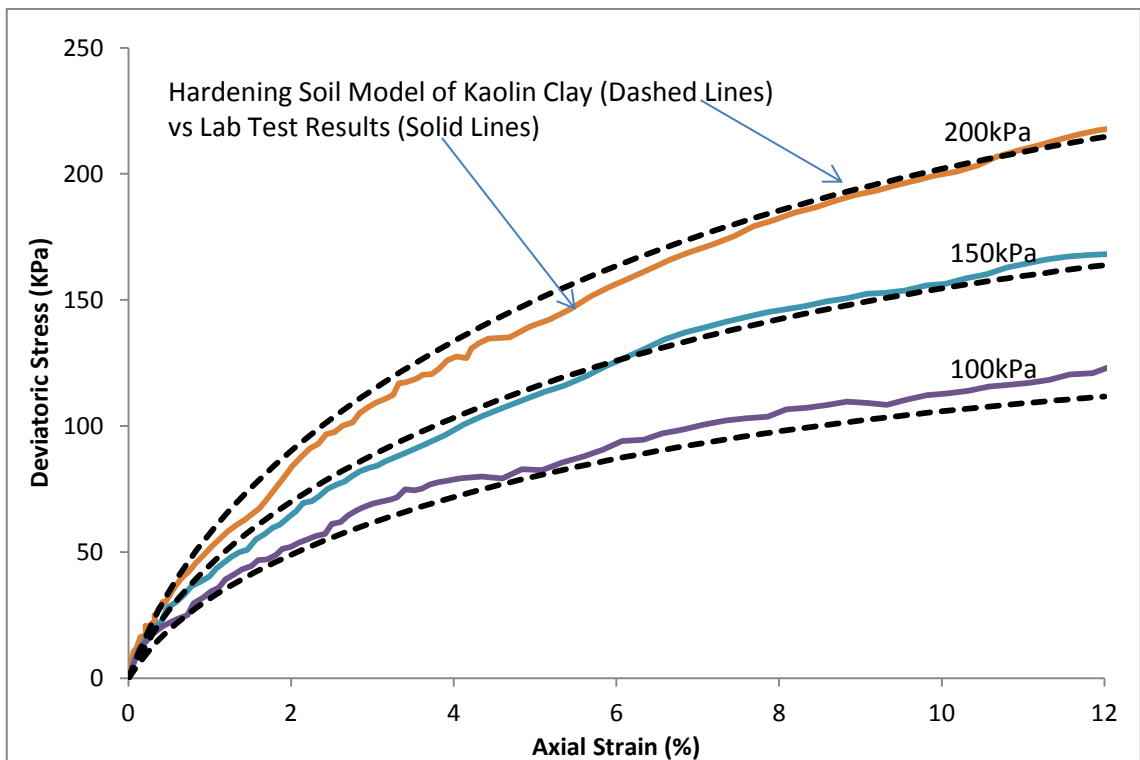


Figure 4.53. Hardening Soil (HS) Model of the Kaolin Clay vs Experimental

After building each soil model, Model M2 which is the 3cm partial penetrating column and Model M4 which is the 3cm full penetration column were modeled using the Mohr Coulomb (MC) and Hardening Soil (HS) Models. All of the HP, HS and MC models showed similar results (Figure 4.54 and Figure 4.55). The only big advantage of the HP model over the other two models is that it is global and applicable for any void ratio, while the others need to be recalibrated / built each time a different void ratio is being used. This crucial property makes Hypoplasticity out stands the other models.

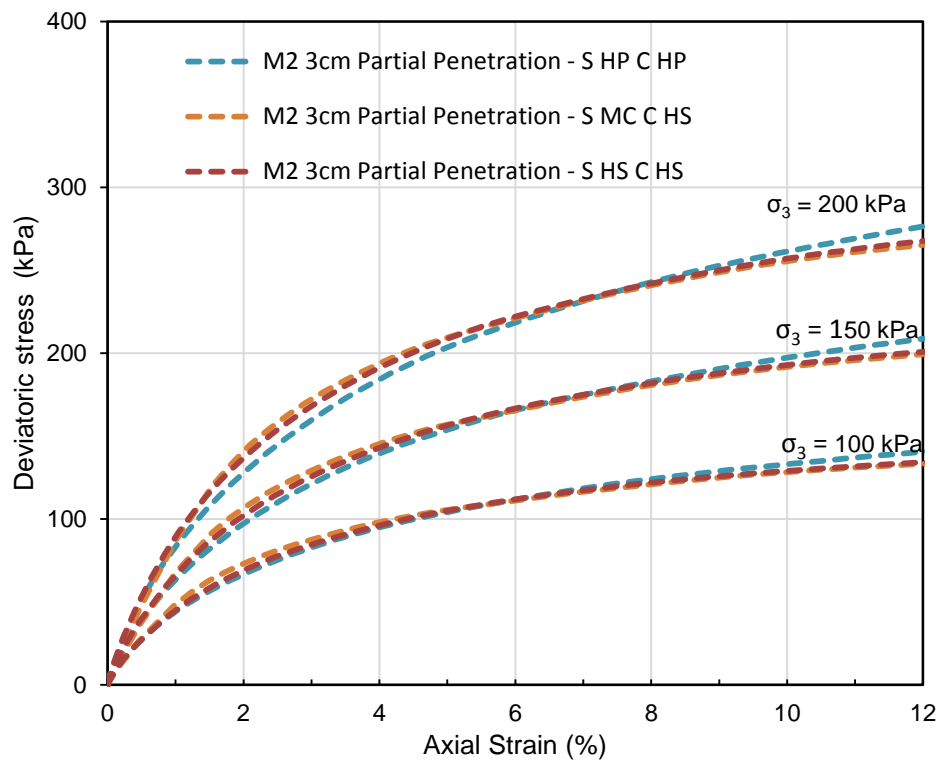


Figure 4.54. Model M2 output of the three soil models

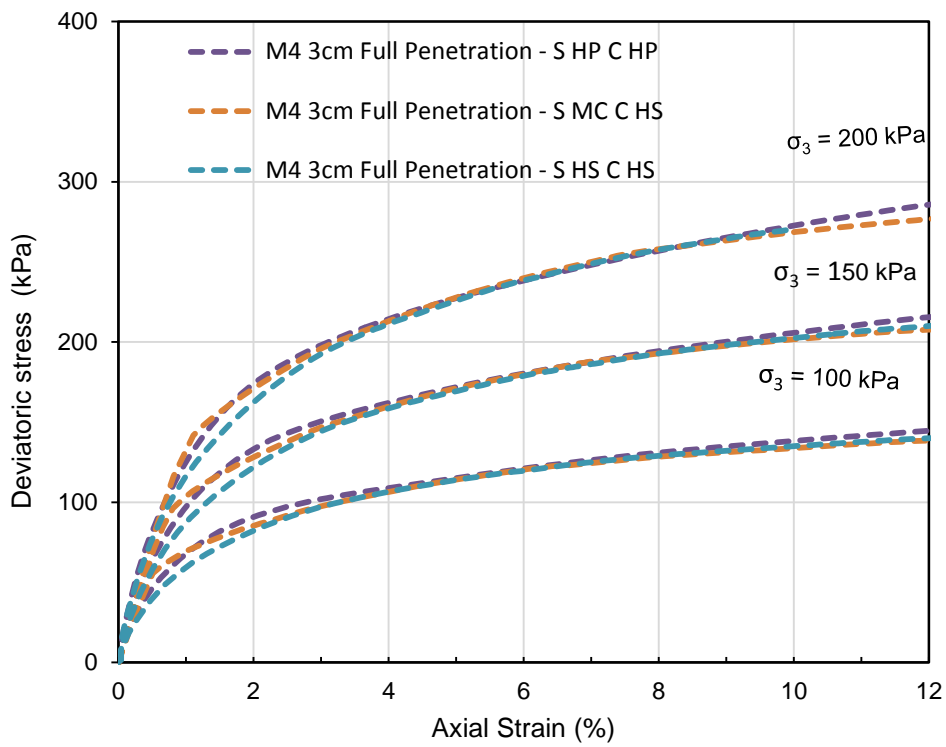


Figure 4.55. Model M4 output of the three soil models

4.6. Comparison of FEM and Experimental results

To compare the FEM with the experimental, both stress-strain curves were combined in Figure 4.56, Figure 4.57 and Figure 4.58 below.

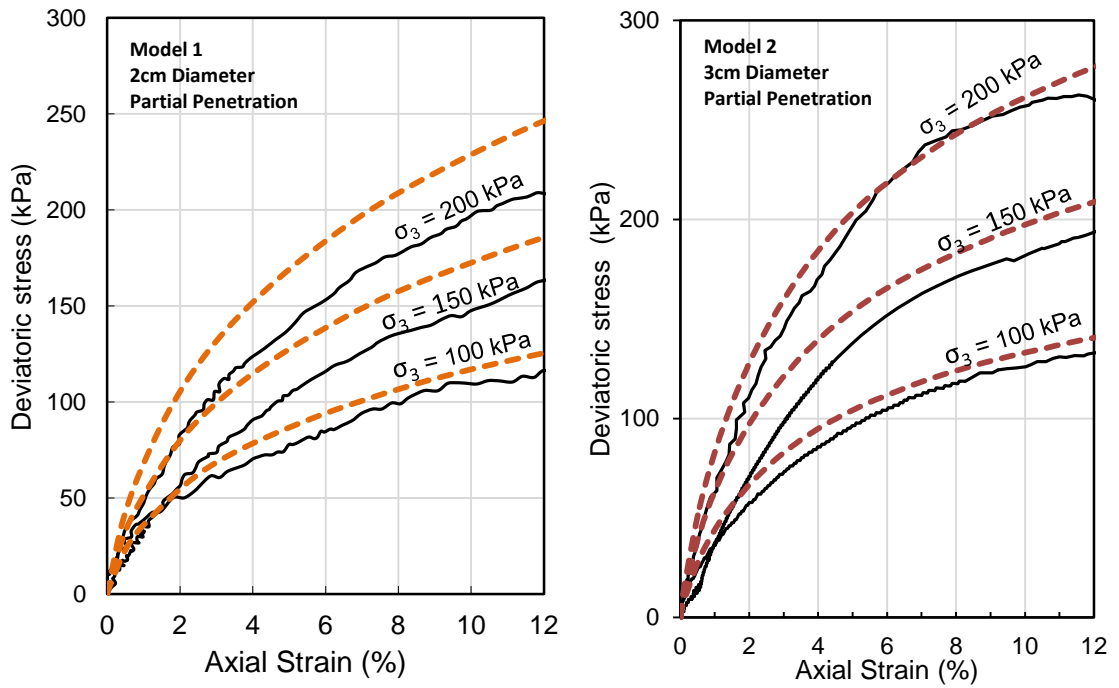


Figure 4.56. Stress Strain curves of Model vs Experimental results for partial penetration M1 and M2

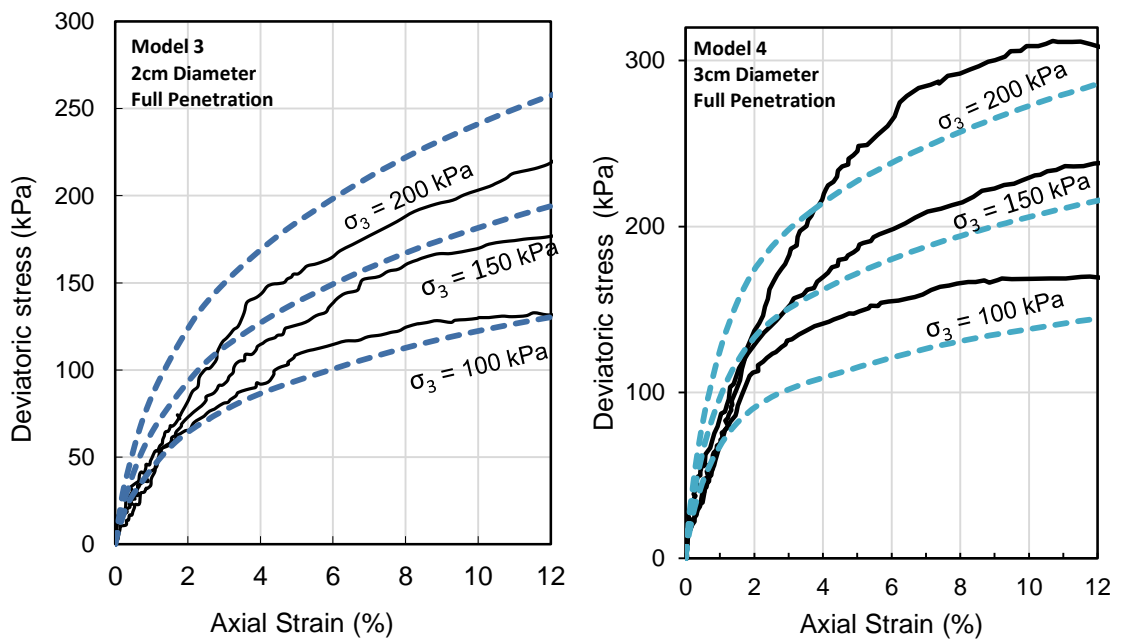


Figure 4.57. Stress Strain curves of Model vs Experimental results for full penetration M3 and M4

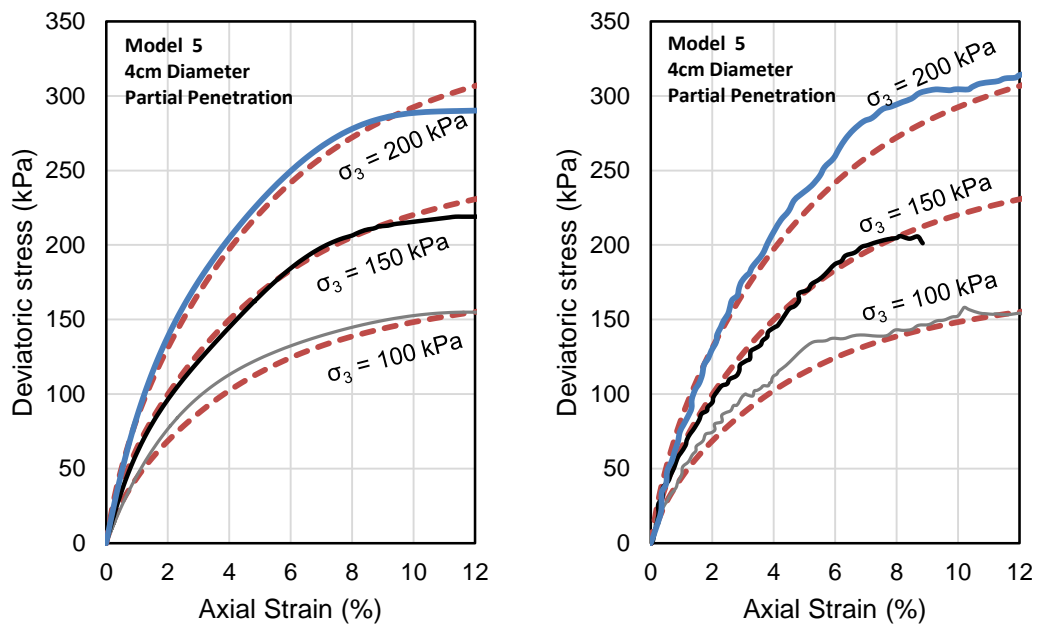


Figure 4.58. Stress Strain curves of Model vs Experimental results for partial penetration M5 (on the left the lab test curve was smoothed, on the right is unprocessed curve)

The partial penetration columns of 3cm and 4cm diameters (Models M2 and M5) showed a good match between the FEM and experimental results. While for the 2cm diameter, only the 100kPa curve showed a good match, while the 150 kPa and 200 kPa FEM over predicted the experimental results. In general, the FEM can be considered as well matching with the experimental results for partially penetrating sand columns.

The full penetration columns of 2cm and 3cm diameters (Models M3 and M4) didn't show a good and reliable match between the FEM and experimental results. Although the 2cm sand column curve of 100 kPa showed a good match, and the 150 kPa curve showed a good match at axial strains exceeding 4%, the FEM cannot be considered as well matching with the experimental results for fully penetrating sand columns. In general, the FEM under predicted the experimental results for fully penetrating sand columns.

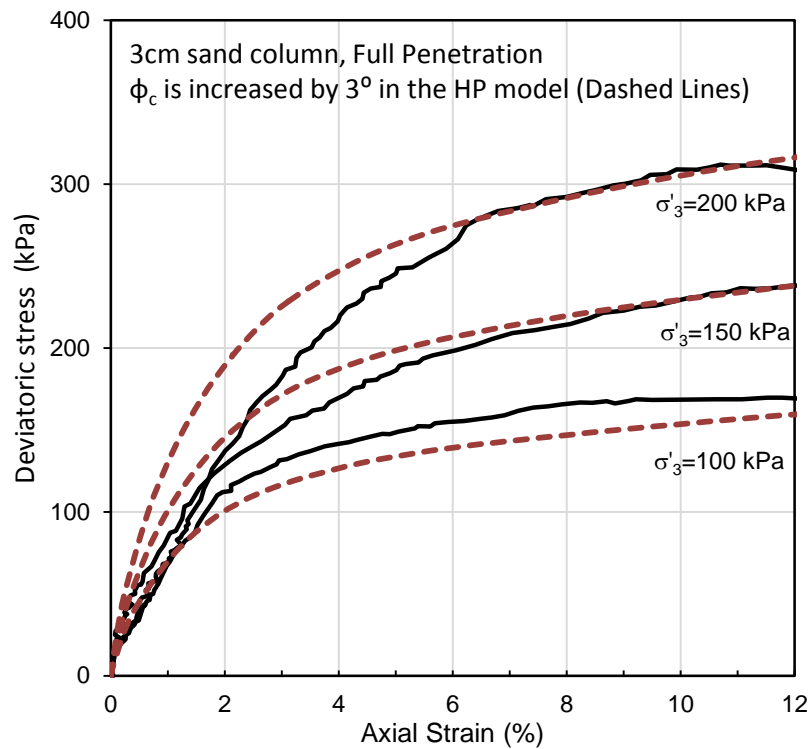


Figure 4.59. A good match between Lab and FEM in the stress strain curve for 3cm full penetration sand column when increasing the critical angle of friction by 3 degrees

A back analysis was carried out to match the lab test results for the full penetration columns and it showed that if we increased the critical angle of friction in the hypoplastic model by 3 degrees we get an almost exact match to the lab test results (Figure 4.59). This will be considered further in the next chapter.

In general, the FEM well matched the experimental results for the partially penetrating sand columns, while under predicted the experimental results for fully penetrating sand columns.

CHAPTER 5

COLUMN PENETRATION RATIO

5.1. Introduction

This chapter investigates the effect of the column penetration ratio on the behavior of the composite specimen under CD triaxial tests. The Finite Element software Plaxis 2D was used to simulate 120 additional triaxial tests models to account for a wider range of sand column penetration ratios.

The results were presented as deviatoric stress and improvement ratio vs penetration ratios, at two selected axial strain values of 2% and 12%. The results were also compared with the experimental results that were discussed in the previous chapter.

5.2. Modeling Various Penetration Ratios

To model the effect of column penetration ratio, four sand column diameters were considered (20mm, 30mm, 35mm and 40mm), three confining pressures (100kPa, 150kPa and 200kPa) and ten column penetration ratios (0.1, 0.2, 0.3, 0.4, 0.5, 0.6, 0.7, 0.8, 0.9 and 1.0). As a result of all these considerations, the 120 triaxial tests listed in Table 5.1 were modeled in Plaxis 2D.

Table 5.1. Modeled triaxial tests representing various penetration ratios.

S/N	Model Code	Confining pressure σ_3 , (kPa)	Dia. of sand column (mm)	Area repl. ratio: A_c/A_s (%)	Column Pen. Ratio: H_c/H_s	Height of Sand Column H_s (cm)
1	20mm-100kPa-0.1Penetration	100	20	7.93	0.1	1.42
2	20mm-150kPa-0.1Penetration	150	20	7.93	0.1	1.42
3	20mm-200kPa-0.1Penetration	200	20	7.93	0.1	1.42
4	20mm-100kPa-0.2Penetration	100	20	7.93	0.2	2.84
5	20mm-150kPa-0.2Penetration	150	20	7.93	0.2	2.84
6	20mm-200kPa-0.2Penetration	200	20	7.93	0.2	2.84
7	20mm-100kPa-0.3Penetration	100	20	7.93	0.3	4.26
8	20mm-150kPa-0.3Penetration	150	20	7.93	0.3	4.26
9	20mm-200kPa-0.3Penetration	200	20	7.93	0.3	4.26
10	20mm-100kPa-0.4Penetration	100	20	7.93	0.4	5.68
11	20mm-150kPa-0.4Penetration	150	20	7.93	0.4	5.68
12	20mm-200kPa-0.4Penetration	200	20	7.93	0.4	5.68
13	20mm-100kPa-0.5Penetration	100	20	7.93	0.5	7.1
14	20mm-150kPa-0.5Penetration	150	20	7.93	0.5	7.1
15	20mm-200kPa-0.5Penetration	200	20	7.93	0.5	7.1
16	20mm-100kPa-0.6Penetration	100	20	7.93	0.6	8.52
17	20mm-150kPa-0.6Penetration	150	20	7.93	0.6	8.52
18	20mm-200kPa-0.6Penetration	200	20	7.93	0.6	8.52
19	20mm-100kPa-0.7Penetration	100	20	7.93	0.7	9.94
20	20mm-150kPa-0.7Penetration	150	20	7.93	0.7	9.94
21	20mm-200kPa-0.7Penetration	200	20	7.93	0.7	9.94
22	20mm-100kPa-0.8Penetration	100	20	7.93	0.8	11.36
23	20mm-150kPa-0.8Penetration	150	20	7.93	0.8	11.36
24	20mm-200kPa-0.8Penetration	200	20	7.93	0.8	11.36
25	20mm-100kPa-0.9Penetration	100	20	7.93	0.9	12.78
26	20mm-150kPa-0.9Penetration	150	20	7.93	0.9	12.78

S/N	Model Code	Confining pressure σ_3 , (kPa)	Dia. of sand column (mm)	Area repl. ratio: Ac/As (%)	Column Pen. Ratio: Hc/Hs	Height of Sand Column Hs (cm)
27	20mm-200kPa-0.9Penetration	200	20	7.93	0.9	12.78
28	20mm-100kPa-1Penetration	100	20	7.93	1	14.2
29	20mm-150kPa-1Penetration	150	20	7.93	1	14.2
30	20mm-200kPa-1Penetration	200	20	7.93	1	14.2
31	30mm-100kPa-0.1Penetration	100	30	17.85	0.1	1.42
32	30mm-150kPa-0.1Penetration	150	30	17.85	0.1	1.42
33	30mm-200kPa-0.1Penetration	200	30	17.85	0.1	1.42
34	30mm-100kPa-0.2Penetration	100	30	17.85	0.2	2.84
35	30mm-150kPa-0.2Penetration	150	30	17.85	0.2	2.84
36	30mm-200kPa-0.2Penetration	200	30	17.85	0.2	2.84
37	30mm-100kPa-0.3Penetration	100	30	17.85	0.3	4.26
38	30mm-150kPa-0.3Penetration	150	30	17.85	0.3	4.26
39	30mm-200kPa-0.3Penetration	200	30	17.85	0.3	4.26
40	30mm-100kPa-0.4Penetration	100	30	17.85	0.4	5.68
41	30mm-150kPa-0.4Penetration	150	30	17.85	0.4	5.68
42	30mm-200kPa-0.4Penetration	200	30	17.85	0.4	5.68
43	30mm-100kPa-0.5Penetration	100	30	17.85	0.5	7.1
44	30mm-150kPa-0.5Penetration	150	30	17.85	0.5	7.1
45	30mm-200kPa-0.5Penetration	200	30	17.85	0.5	7.1
46	30mm-100kPa-0.6Penetration	100	30	17.85	0.6	8.52
47	30mm-150kPa-0.6Penetration	150	30	17.85	0.6	8.52
48	30mm-200kPa-0.6Penetration	200	30	17.85	0.6	8.52
49	30mm-100kPa-0.7Penetration	100	30	17.85	0.7	9.94
50	30mm-150kPa-0.7Penetration	150	30	17.85	0.7	9.94
51	30mm-200kPa-0.7Penetration	200	30	17.85	0.7	9.94
52	30mm-100kPa-0.8Penetration	100	30	17.85	0.8	11.36
53	30mm-150kPa-0.8Penetration	150	30	17.85	0.8	11.36

S/N	Model Code	Confining pressure σ_3 , (kPa)	Dia. of sand column (mm)	Area repl. ratio: A_c/A_s (%)	Column Pen. Ratio: H_c/H_s	Height of Sand Column H_s (cm)
54	30mm-200kPa-0.8Penetration	200	30	17.85	0.8	11.36
55	30mm-100kPa-0.9Penetration	100	30	17.85	0.9	12.78
56	30mm-150kPa-0.9Penetration	150	30	17.85	0.9	12.78
57	30mm-200kPa-0.9Penetration	200	30	17.85	0.9	12.78
58	30mm-100kPa-1Penetration	100	30	17.85	1	14.2
59	30mm-150kPa-1Penetration	150	30	17.85	1	14.2
60	30mm-200kPa-1Penetration	200	30	17.85	1	14.2
61	35mm-100kPa-0.1Penetration	100	35	24.30	0.1	1.42
62	35mm-150kPa-0.1Penetration	150	35	24.30	0.1	1.42
63	35mm-200kPa-0.1Penetration	200	35	24.30	0.1	1.42
64	35mm-100kPa-0.2Penetration	100	35	24.30	0.2	2.84
65	35mm-150kPa-0.2Penetration	150	35	24.30	0.2	2.84
66	35mm-200kPa-0.2Penetration	200	35	24.30	0.2	2.84
67	35mm-100kPa-0.3Penetration	100	35	24.30	0.3	4.26
68	35mm-150kPa-0.3Penetration	150	35	24.30	0.3	4.26
69	35mm-200kPa-0.3Penetration	200	35	24.30	0.3	4.26
70	35mm-100kPa-0.4Penetration	100	35	24.30	0.4	5.68
71	35mm-150kPa-0.4Penetration	150	35	24.30	0.4	5.68
72	35mm-200kPa-0.4Penetration	200	35	24.30	0.4	5.68
73	35mm-100kPa-0.5Penetration	100	35	24.30	0.5	7.1
74	35mm-150kPa-0.5Penetration	150	35	24.30	0.5	7.1
75	35mm-200kPa-0.5Penetration	200	35	24.30	0.5	7.1
76	35mm-100kPa-0.6Penetration	100	35	24.30	0.6	8.52
77	35mm-150kPa-0.6Penetration	150	35	24.30	0.6	8.52
78	35mm-200kPa-0.6Penetration	200	35	24.30	0.6	8.52
79	35mm-100kPa-0.7Penetration	100	35	24.30	0.7	9.94
80	35mm-150kPa-0.7Penetration	150	35	24.30	0.7	9.94

S/N	Model Code	Confining pressure σ_3 , (kPa)	Dia. of sand column (mm)	Area repl. ratio: Ac/As (%)	Column Pen. Ratio: Hc/Hs	Height of Sand Column Hs (cm)
81	35mm-200kPa-0.7Penetration	200	35	24.30	0.7	9.94
82	35mm-100kPa-0.8Penetration	100	35	24.30	0.8	11.36
83	35mm-150kPa-0.8Penetration	150	35	24.30	0.8	11.36
84	35mm-200kPa-0.8Penetration	200	35	24.30	0.8	11.36
85	35mm-100kPa-0.9Penetration	100	35	24.30	0.9	12.78
86	35mm-150kPa-0.9Penetration	150	35	24.30	0.9	12.78
87	35mm-200kPa-0.9Penetration	200	35	24.30	0.9	12.78
88	35mm-100kPa-1Penetration	100	35	24.30	1	14.2
89	35mm-150kPa-1Penetration	150	35	24.30	1	14.2
90	35mm-200kPa-1Penetration	200	35	24.30	1	14.2
91	40mm-100kPa-0.1Penetration	100	40	31.74	0.1	1.42
92	40mm-150kPa-0.1Penetration	150	40	31.74	0.1	1.42
93	40mm-200kPa-0.1Penetration	200	40	31.74	0.1	1.42
94	40mm-100kPa-0.2Penetration	100	40	31.74	0.2	2.84
95	40mm-150kPa-0.2Penetration	150	40	31.74	0.2	2.84
96	40mm-200kPa-0.2Penetration	200	40	31.74	0.2	2.84
97	40mm-100kPa-0.3Penetration	100	40	31.74	0.3	4.26
98	40mm-150kPa-0.3Penetration	150	40	31.74	0.3	4.26
99	40mm-200kPa-0.3Penetration	200	40	31.74	0.3	4.26
100	40mm-100kPa-0.4Penetration	100	40	31.74	0.4	5.68
101	40mm-150kPa-0.4Penetration	150	40	31.74	0.4	5.68
102	40mm-200kPa-0.4Penetration	200	40	31.74	0.4	5.68
103	40mm-100kPa-0.5Penetration	100	40	31.74	0.5	7.1
104	40mm-150kPa-0.5Penetration	150	40	31.74	0.5	7.1
105	40mm-200kPa-0.5Penetration	200	40	31.74	0.5	7.1
106	40mm-100kPa-0.6Penetration	100	40	31.74	0.6	8.52
107	40mm-150kPa-0.6Penetration	150	40	31.74	0.6	8.52

S/N	Model Code	Confining pressure σ_3 , (kPa)	Dia. of sand column (mm)	Area repl. ratio: Ac/As (%)	Column Pen. Ratio: Hc/Hs	Height of Sand Column Hs (cm)
108	40mm-200kPa-0.6Penetration	200	40	31.74	0.6	8.52
109	40mm-100kPa-0.7Penetration	100	40	31.74	0.7	9.94
110	40mm-150kPa-0.7Penetration	150	40	31.74	0.7	9.94
111	40mm-200kPa-0.7Penetration	200	40	31.74	0.7	9.94
112	40mm-100kPa-0.8Penetration	100	40	31.74	0.8	11.36
113	40mm-150kPa-0.8Penetration	150	40	31.74	0.8	11.36
114	40mm-200kPa-0.8Penetration	200	40	31.74	0.8	11.36
115	40mm-100kPa-0.9Penetration	100	40	31.74	0.9	12.78
116	40mm-150kPa-0.9Penetration	150	40	31.74	0.9	12.78
117	40mm-200kPa-0.9Penetration	200	40	31.74	0.9	12.78
118	40mm-100kPa-1Penetration	100	40	31.74	1	14.2
119	40mm-150kPa-1Penetration	150	40	31.74	1	14.2
120	40mm-200kPa-1Penetration	200	40	31.74	1	14.2

For this purpose, the same axisymmetric analysis that was conducted in Chapter 4 was adopted for the above mentioned models.

5.2.1. Test Results

The FEM analysis can produce a wide range of results relative to stresses and strains. Due to the large number of modeled tests (120) it is not possible to display the specific / individual results, such as stress strain curves, for each test. This will require a lot of space and will not be conclusive. Thus the deviatoric stresses and improvement ratios at specific vertical strains (2% and 12%) were plotted for all the tests in unified graphs.

5.2.2. Stress-Strain Behavior

To study the stress-strain behavior in all the models, the deviatoric axial stress was plotted against the axial strain for all the models. These plots were congested due to the large number of curves and accordingly more refined curves will be present in the coming sections for the sake of better analyses. All the curves indicate that for the same sand column diameter, the higher the penetration columns result in a stiffer composite sample. For each penetration ratio, the larger the sand column diameter, the stiffer is the composite specimen. These are in line with what was observed in Maalouf (2012).

The deviatoric stress at a 2% and 12% vertical strains were plotted for each sand column diameter in the below figures (Figure 5.1, Figure 5.2, Figure 5.3, Figure 5.4, Figure 5.5, Figure 5.6, Figure 5.7 and Figure 5.8).

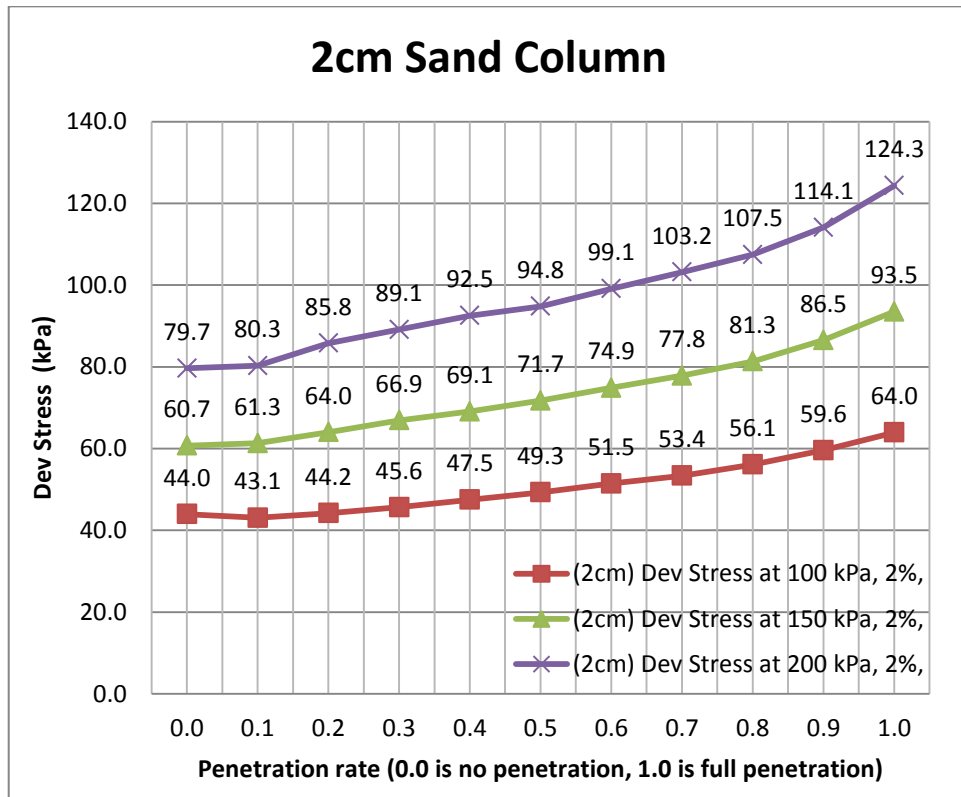


Figure 5.1. Deviatoric stress at a 2% vertical strain for the 2cm diameter column

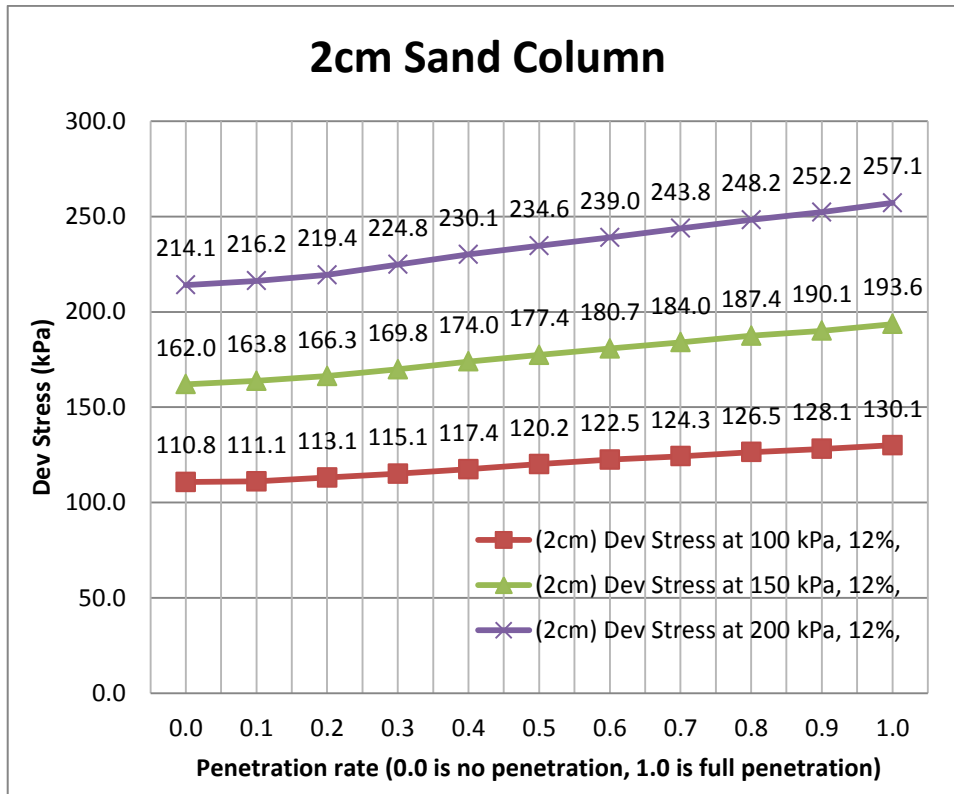


Figure 5.2. Deviatoric stress at a 12% vertical strain for the 2cm diameter column

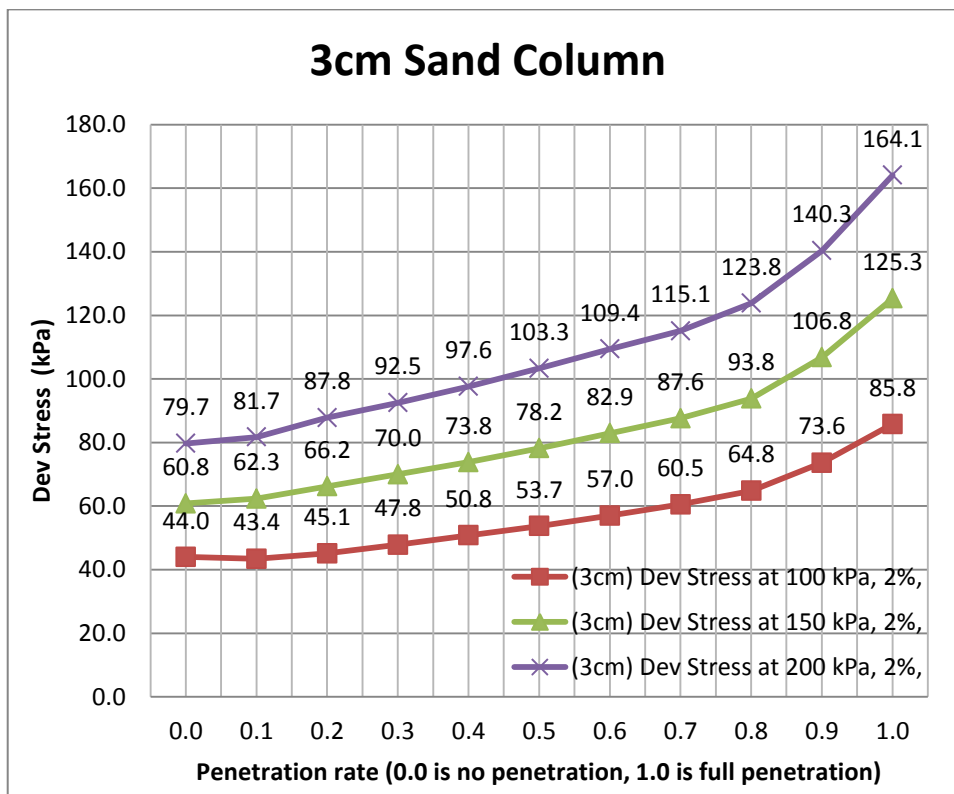


Figure 5.3. Deviatoric stress at a 2% vertical strain for the 3cm diameter column

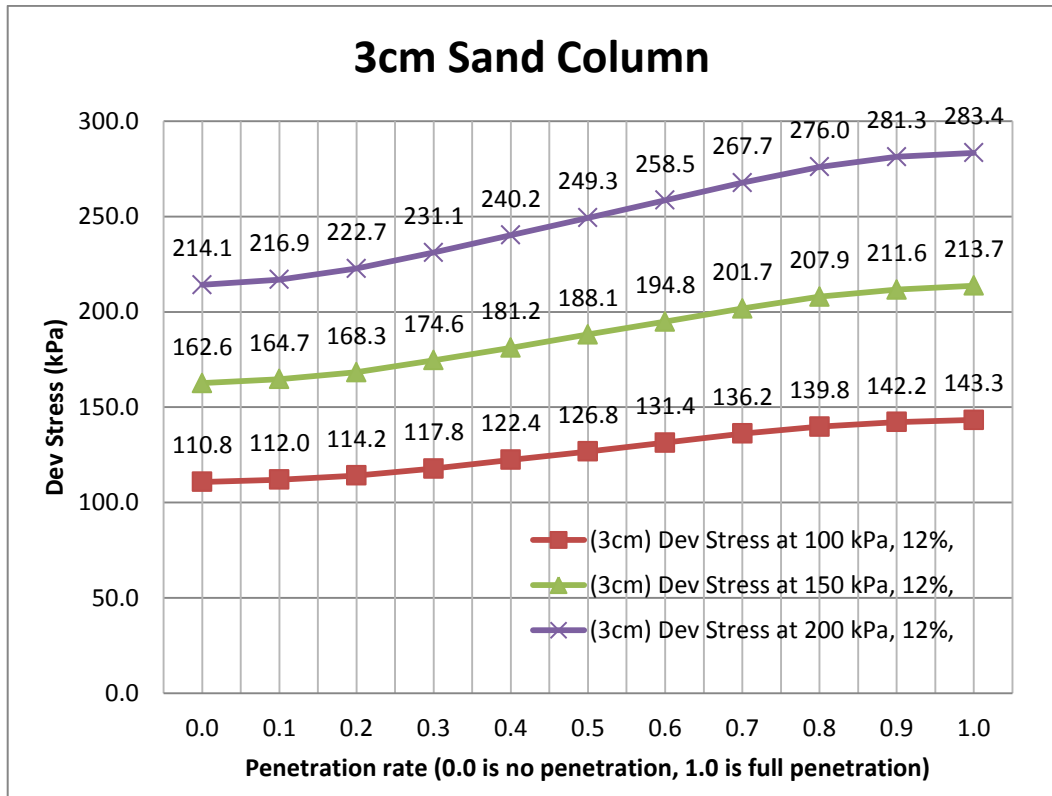


Figure 5.4. Deviatoric stress at a 12% vertical strain for the 3cm diameter column

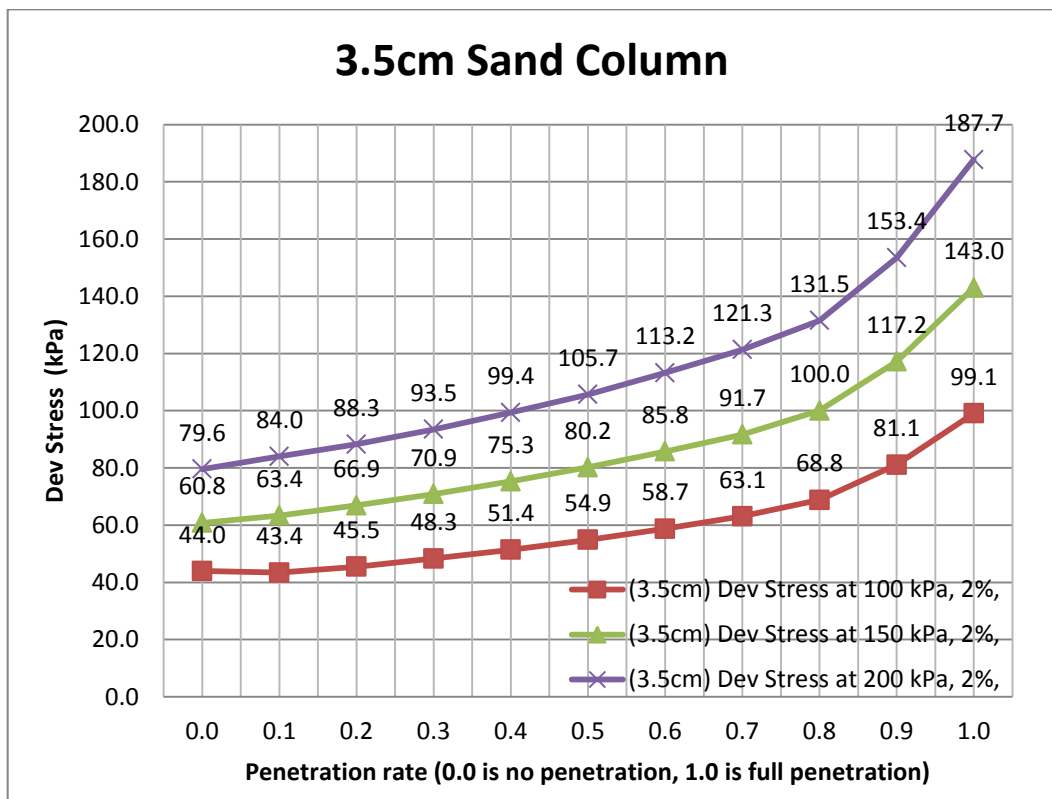


Figure 5.5. Deviatoric stress at a 2% vertical strain for the 3.5cm diameter column

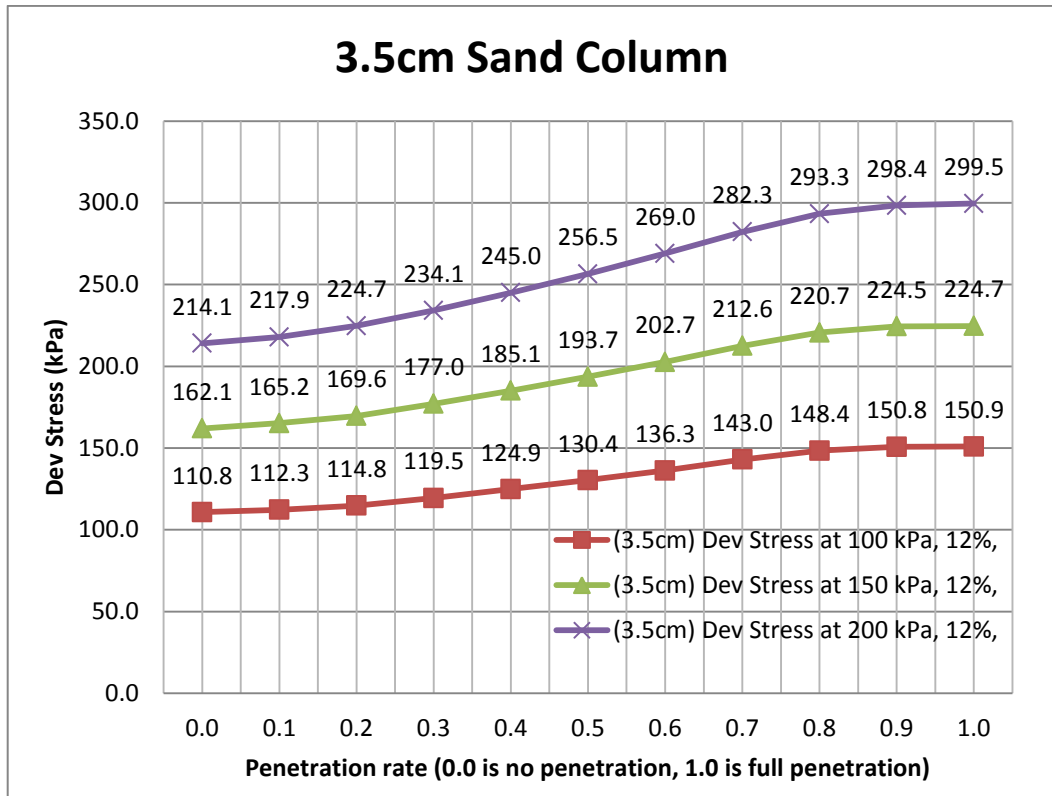


Figure 5.6. Deviatoric stress at a 12% vertical strain for the 3.5cm diameter column

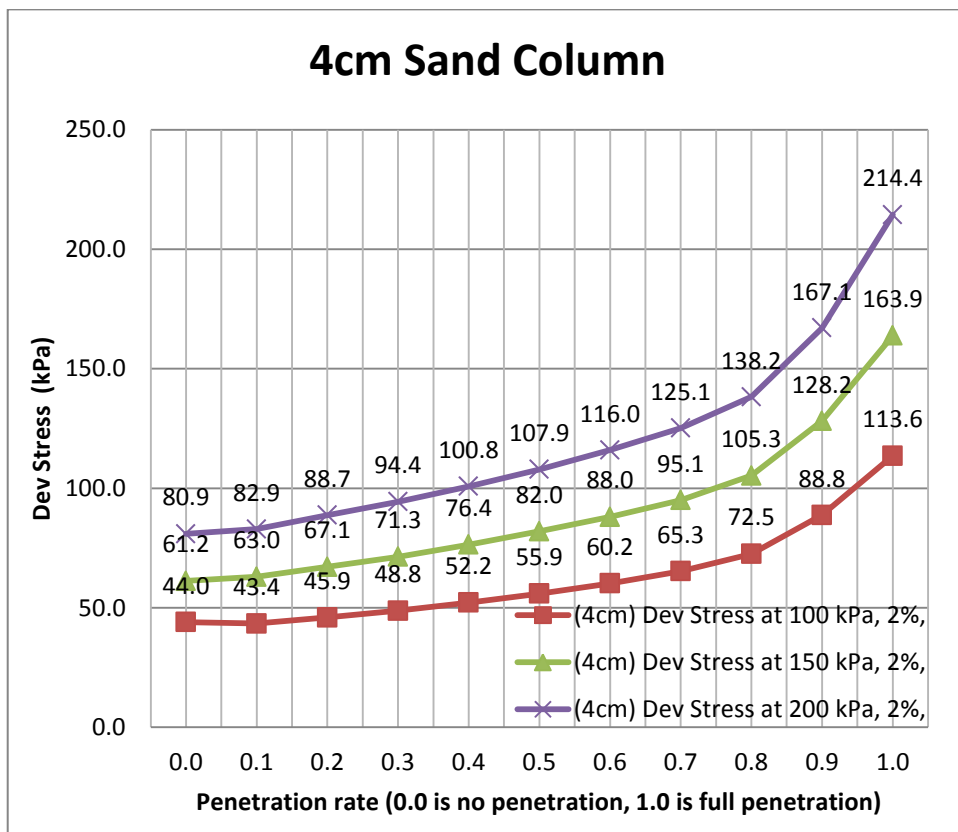


Figure 5.7. Deviatoric stress at a 2% vertical strain for the 4cm diameter column

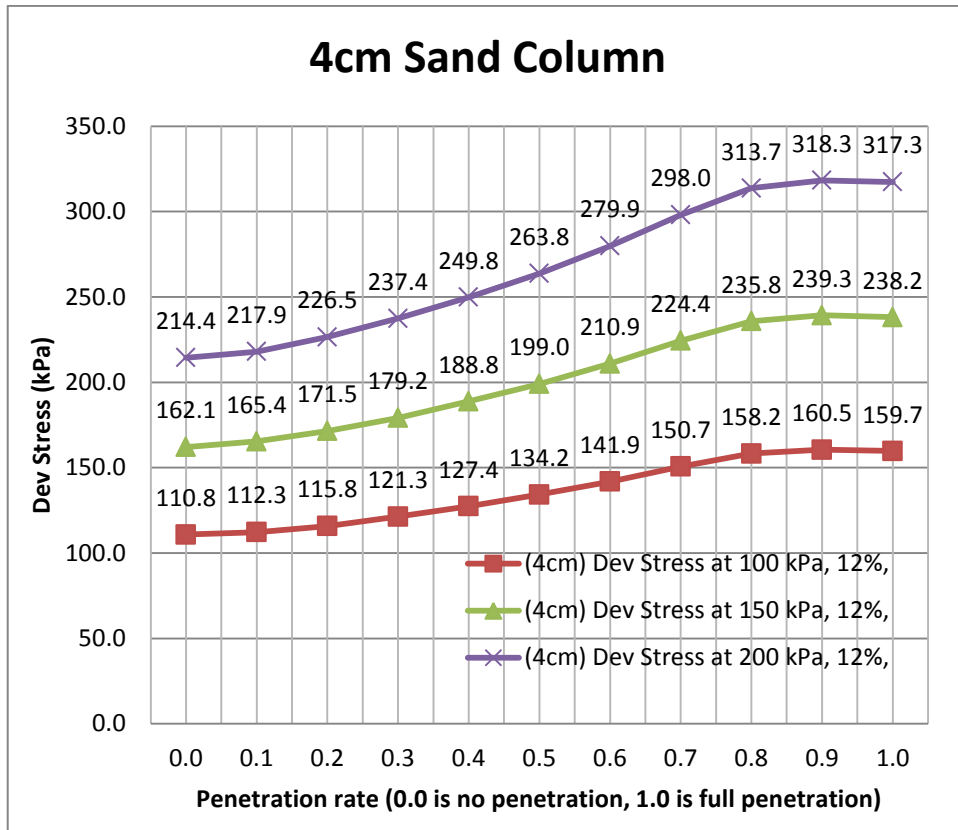


Figure 5.8. Deviatoric stress at a 12% vertical strain for the 4cm diameter column

The improvement ratio is defined as the deviatoric stress of the reinforced specimen at a certain vertical strain value (2% or 12%) divided by the corresponding deviatoric stress of the un reinforced specimen (control Kaolin). The improvement ratio was plotted versus the column penetration ratio for each sand column diameter in the below figures.

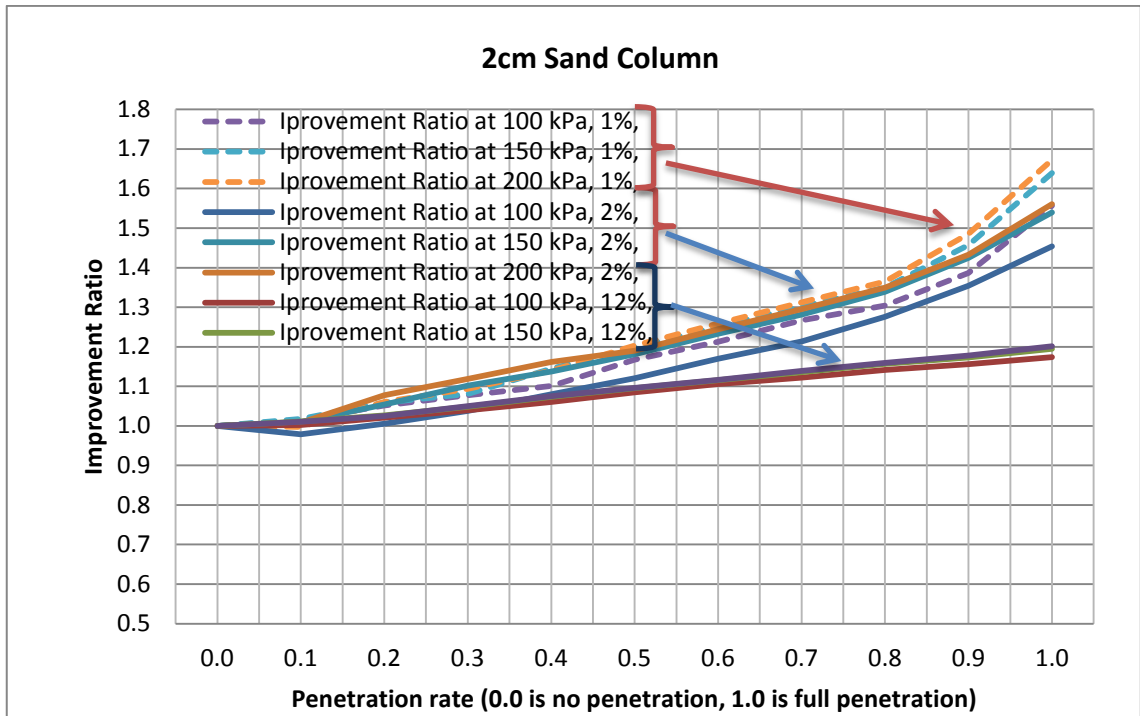


Figure 5.9. Improvement Ratio for the 2cm diameter column

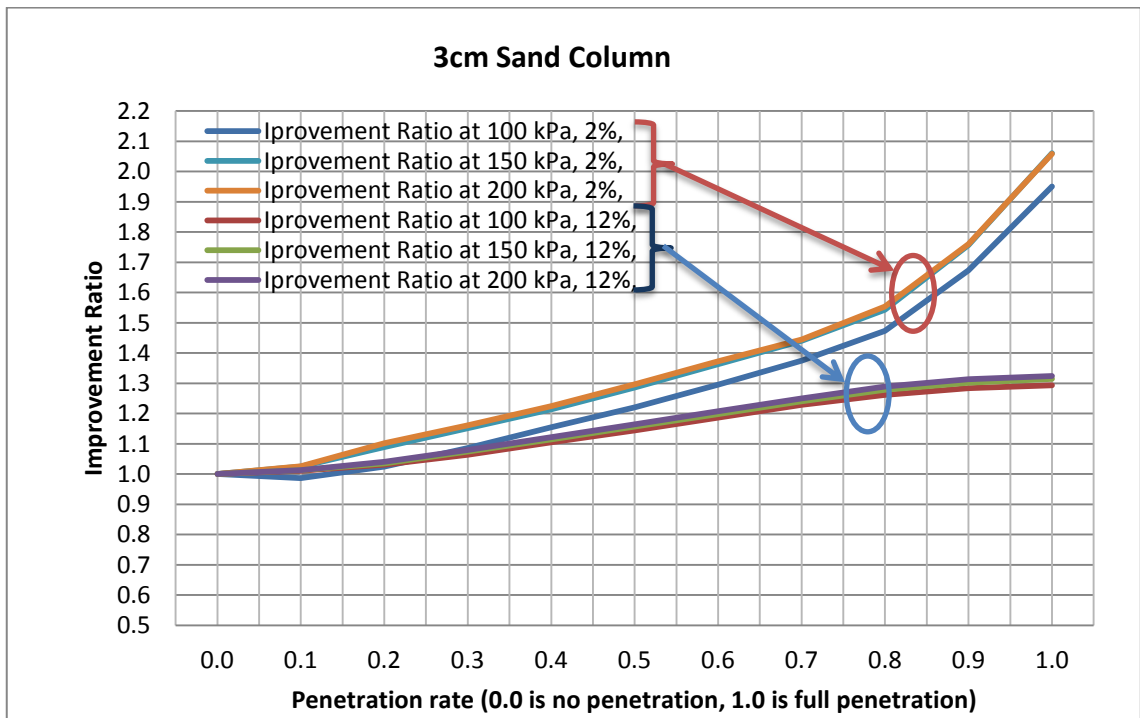


Figure 5.10. Improvement Ratio for the 3cm diameter column

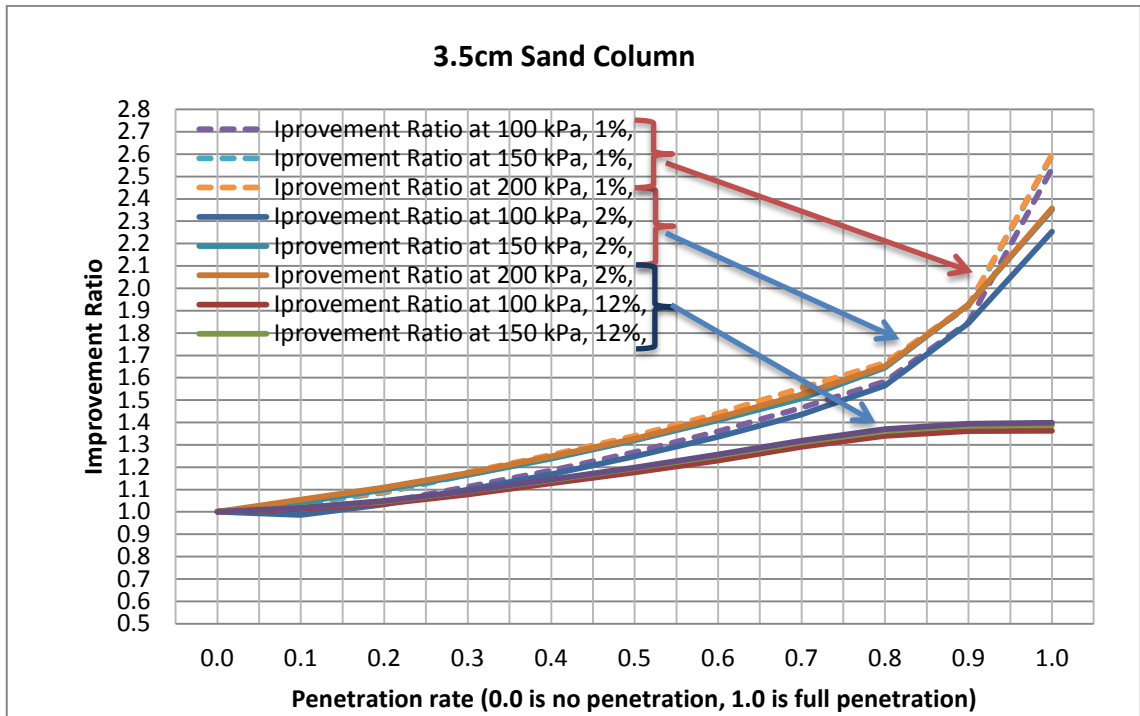


Figure 5.11. Improvement Ratio for the 3.5cm diameter column

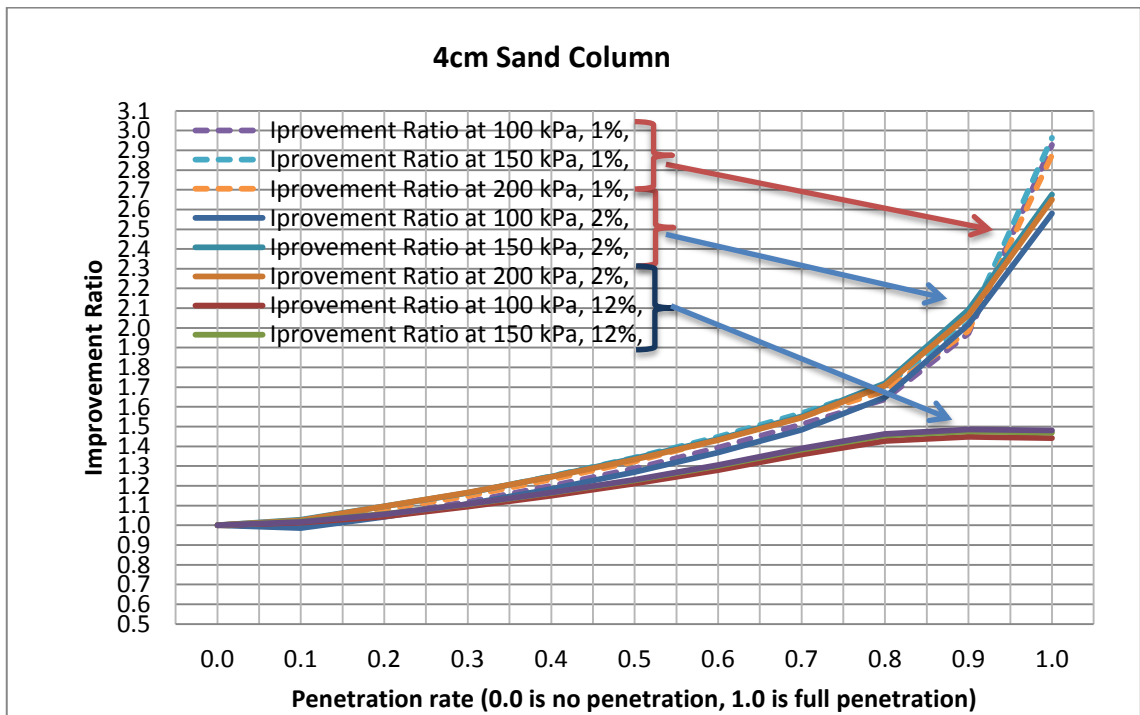


Figure 5.12. Improvement Ratio for the 4cm diameter column

The plots of deviatoric stress at 12% vertical strain for all the modeled tests were combined in Figure 5.13. The plots of deviatoric stress at 2% vertical strain for all the

modeled tests were combined in Figure 5.14. These two plots show the different behavior at different strains. At low strains (i.e. 2%), the improvement increases exponentially with increasing penetration ratio while for high strains (i.e. 12%) the improvement after 0.8 penetration ratio becomes very low and almost flattens out. This latter observation didn't comply with the lab test results for the full penetration sand columns, where much higher improvements were recorded.

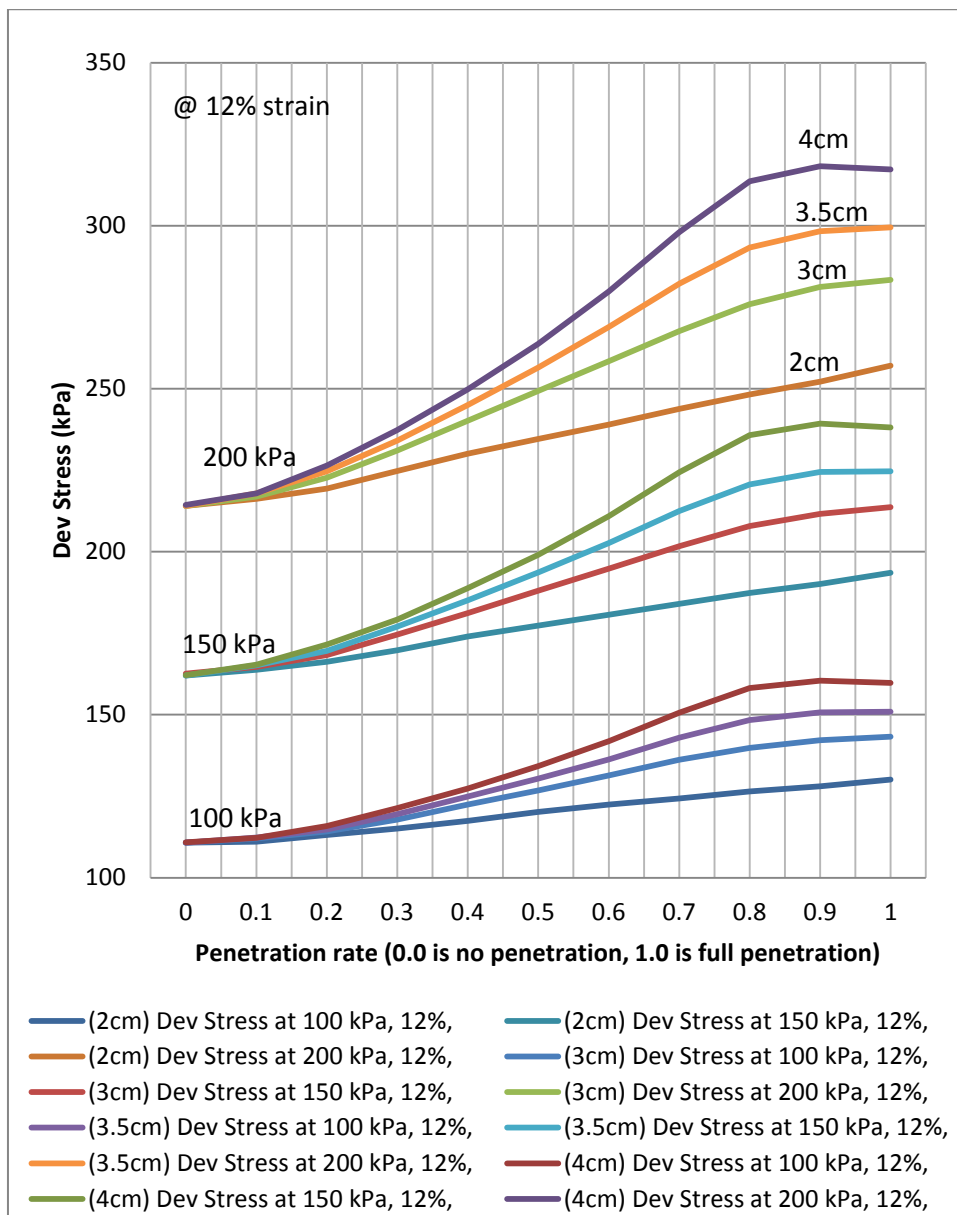


Figure 5.13. Deviatoric stress at 12% vertical strain for all the modeled tests

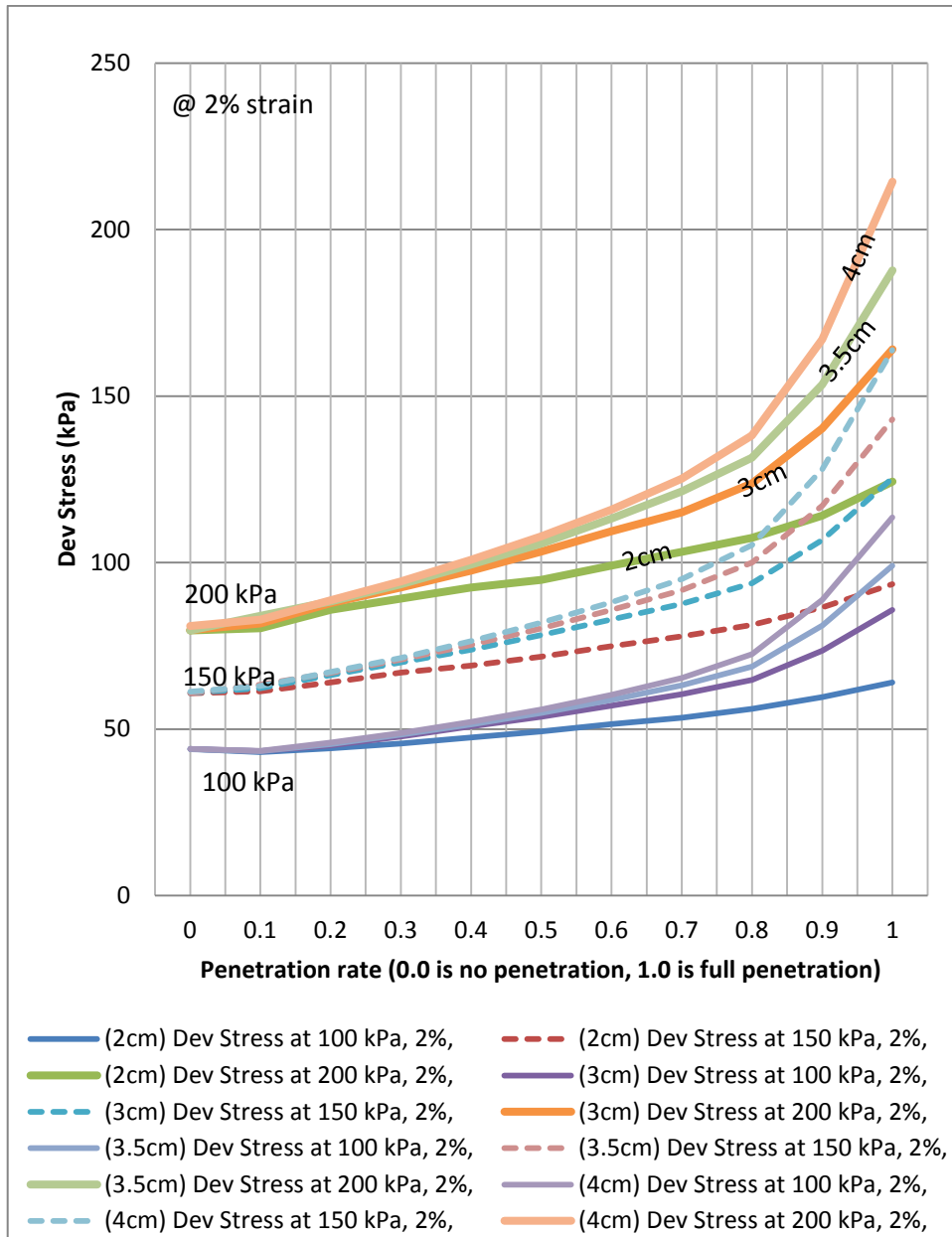


Figure 5.14. Deviatoric stress at 2% vertical strain for all the modeled tests

5.3. FEM vs Experimental

To compare the FEM with the experimental, the deviatoric stress at 12% strain for the 3cm sand column vs penetration ratios were combined in Figure 5.15.

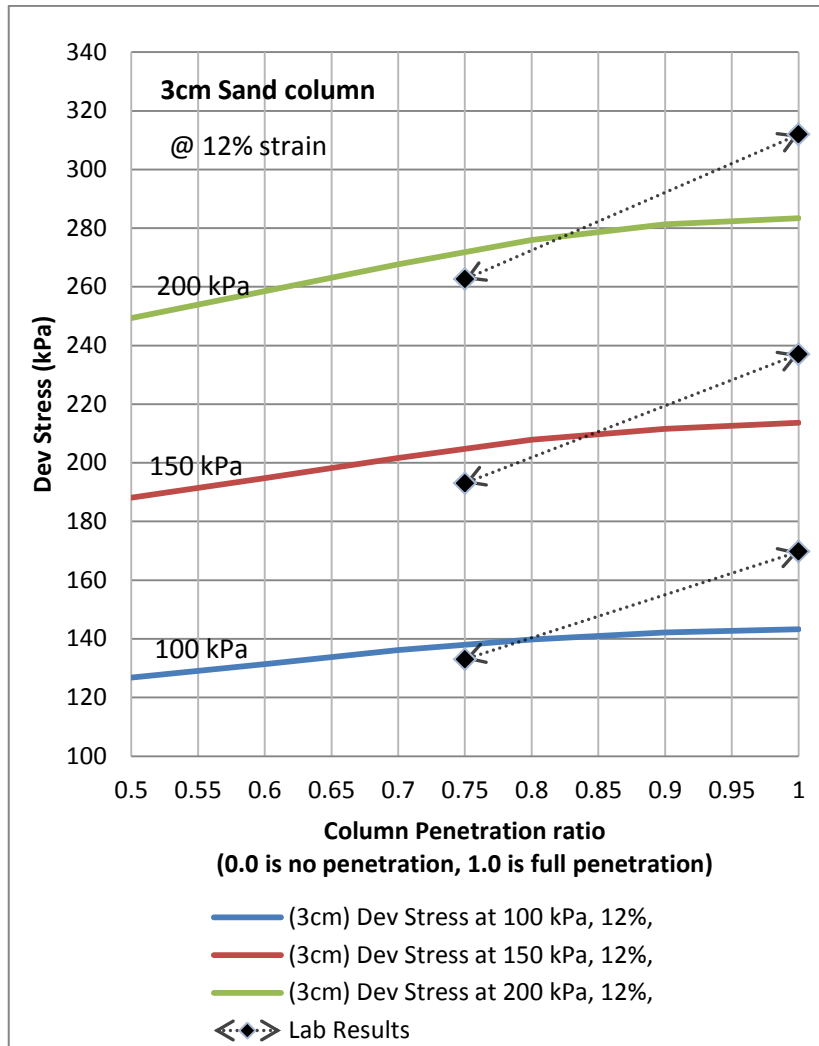


Figure 5.15. Lab vs FEM, the deviatoric stress at 12% strain for the 3cm sand column

The partial penetration columns showed an acceptable match between the FEM and experimental results, and this can be observed in Figure 5.16 for the column penetration ratio of 0.75. In general, the FEM can be considered as well matching with the experimental results for partially penetrating sand columns and realistic.

The full penetration columns didn't show a good and reliable match between the FEM and experimental results. The FEM cannot be considered as well matching with the experimental results for fully penetrating sand columns. In general, the FEM under predicted the experimental results for fully penetrating sand columns. Further research

and analyses is required in this concern, where lab tests are to be carried out at the penetration ratios of 0.8 and 0.9 to check if the deviatoric stress at 1.0 (full penetration) is a specific phenomenon or it is a gradual behavior that occurs after the 0.7 column penetration ratio.

One possible explanation for this jump in the deviatoric stress in the full penetration column is that in the consolidation phase in the triaxial test and when the confinement pressures are applied, the initial vertical stress distribution on the sand column and surrounding clay are not equivalent leading to a non-isotropic loading. Having a non-isotropic loading will result in a different behavior in the composite sample since all the parameters that we use in the hypoplastic, the Mohr Coulomb and Hardening soil models are relative to isotropically loaded samples. The critical angle of friction also correspond to an isotropically loaded soil, and this may explain that when we have increased the critical angle of friction in the hypoplastic model by 3 degrees we got an almost exact match to the lab test results (Figure 5.16). Non isotropic loading conditions are a limitation to all the used models in this research study and this may explain their inability to model such a behavior.

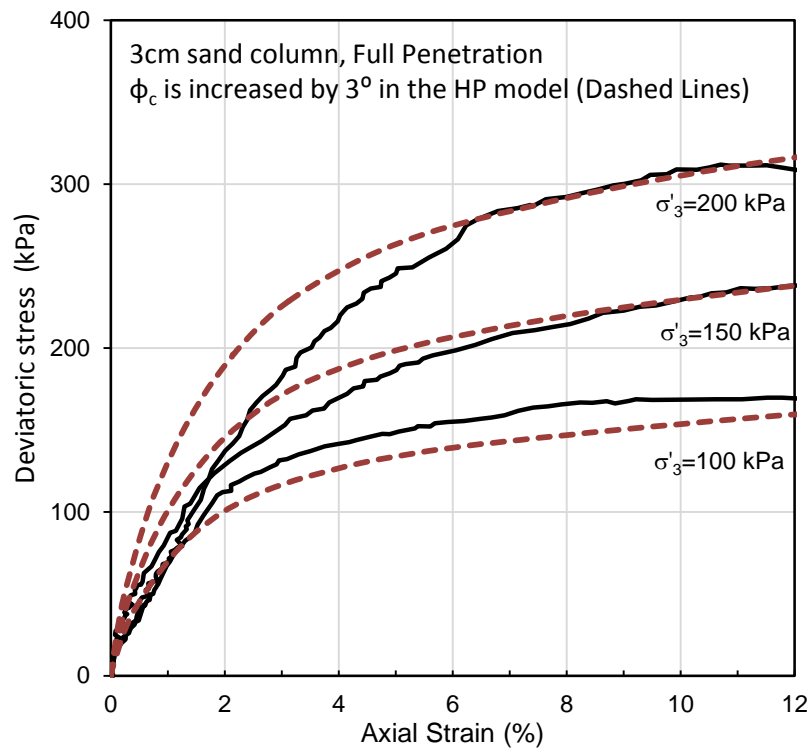


Figure 5.16. A good match between Lab and FEM in the stress strain curve for 3cm full penetration sand column when increasing the critical angle of friction by 3 degrees

Further to the above, the positive side is that non isotropic loading is hard to be present in field applications of sand columns, and thus we can depend on the partial penetration model for further field application studies and keep in mind that even if the full penetration phenomena occurred where we have non isotropic loading conditions, the results will be under predicting reality and thus on the safe side.

CHAPTER 6

MODELING A FIELD-SCALE APPLICATION

6.1. Introduction

Two field-scale applications were considered in this chapter, where they are enumerated as field-scale application 1 and field-scale application 2.

The Finite Element software Plaxis 3D was used to simulate the field-scale application 1, where a 5m x 5m raft foundation is placed over 25 sand columns penetrating 7.5m into the natural clayey ground and loaded uniformly. Another model is also considered for comparison, where the same 5mx5m raft is placed over the unreinforced clayey subsurface. The Mohr Coulomb soil model was used and the sand columns were modeled as circular elements.

To assess the effect of penetration or column length to width ratio (L/D), the Finite Element software Plaxis 3D was also used to simulate another field-scale application (#2), where a 5m x 5m raft foundation is placed over 25 sand columns penetrating 0m, 1m, 2.5m, 5m, 7.5m and 10m into the natural clayey ground and loaded uniformly. Since the Hardening soil model was used, the circular elements were replaced by square elements to allow for considerably less meshing and processing time.

The methodology and results of modeling the field application are presented in this chapter. The results include the deformation patterns and the load - settlement behavior. Then a comparison between the FEM results and the previously discussed triaxial tests was

carried out, followed by another comparison with theory to assess the reliability of the finite element method in such applications.

6.2. The Field-Scale Application – No 1

The raft foundation is assumed to be 100 cm thick and made of reinforced concrete. The natural ground which consists of a 10m thick clay layer overlying bedrock or a relatively incompressible layer / fixed boundary. In the first model, which will be referred to as MODEL 1 (Natural), the raft is directly placed over the natural ground without any soil replacement / sand columns installed beneath it. In the second model, which will be referred to as MODEL 2 (Reinforced), the raft is placed over reinforced ground where the sand columns are 50 cm in diameter and 7.5 m in length, each placed in a 1 m center to center spaced square grid, thus totaling into 25 sand columns (see Figure 6.1 and Figure 6.2). The soil replacement ratio is 19.6% and the penetration ratio is 75%. A summary of both models is in Table 6.1.

Table 6.1. MODEL 1 and MODEL 2

Model No.	Diameter of sand column (m)	Area replacement ratio: A_c/A_s (%)	Column Penetration Ratio: H_c/H_s	Height of Sand Column: H_s (m)
MODEL 1	0	0	0	0
MODEL 2	0.5	19.6	0.75	7.5

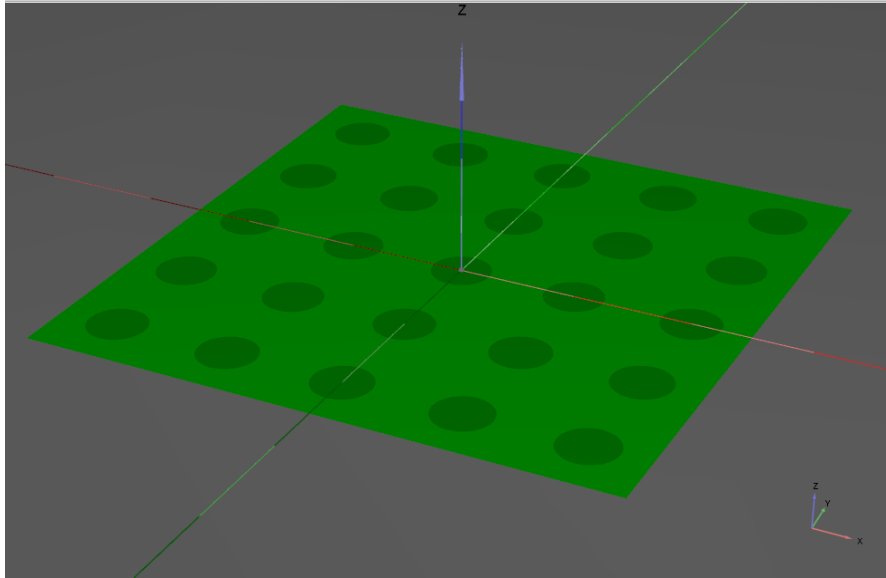


Figure 6.1. Sand columns 0.5m in dia. placed in 1m c-c square grid

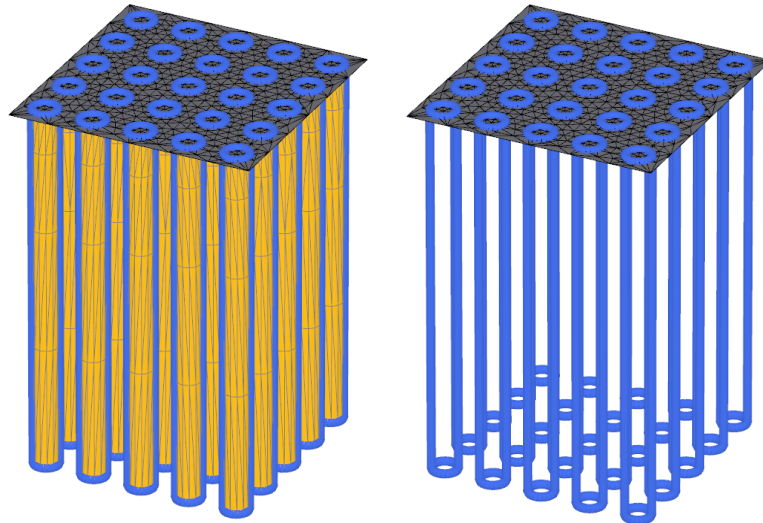


Figure 6.2. The Field Application, a Raft Placed over 25 Sand Columns

In both models, the raft is loaded uniformly until failure. The main output of interest is the load - settlement behavior and the maximum load, which corresponds to the ultimate bearing capacity. Also settlement reduction ratios (SRR) and improvement ratios (IR) will be obtained as part of the comparison between MODEL 1, MODEL 2, the triaxial tests and theory / literature.

6.2.1. The Soil Models

The Mohr Coulomb soil model was used for this field application's 3D modeling, due to the practicality of such model and ease of use. Hypoplasticity, as informed by Plaxis support team, was not tested in Plaxis 3D yet and thus will require a thorough verification before the direct use, which is not part of this study and will be recommended for future and further research and exploration.

The soil parameters for the Mohr Coulomb models of the clay and sand are summarized in Table 6.2. As displayed by Plaxis 3D, the soil properties and the single element analysis results for each soil model (Clay and Sand) are shown in Figure 6.3, Figure 6.4, Figure 6.5, Figure 3.8 and Figure 6.7.

Table 6.2. The MC Soil Models Parameters

Soil	Kaolin Clay	Ottawa Sand
Density γ (KN/m ³)	18	18
Friction Angle ϕ°	21	35
Cohesion, C' (kPa)	0	0
Poisson ratio, ν	0.3	0.3
Youngs Modulus E (kPa)	5,000	50,000
Initial Void Ratio e_0	1.35	0.6
K_0	1	1
Conditions	Drained	Drained



Property	Unit	Value	Value
Material set			
Identification number		1	2
Identification		0 Kaolin Clay - MC	0 Ottawa Sand - MC (36)
Material model		Mohr-Coulomb	Mohr-Coulomb
Drainage type		Drained	Drained
Colour		 RGB 19, 174, 71	 RGB 239, 181, 21
Comments			
General properties			
γ_{unsat}	kN/m ³	18.00	18.00
γ_{sat}	kN/m ³	18.00	18.00
Advanced			
Void ratio			
Dilatancy cut-off		<input type="checkbox"/>	<input type="checkbox"/>
e_{init}		1.350	0.6000
e_{min}		0.000	0.000
e_{max}		999.0	999.0
Damping			
Rayleigh α		0.000	0.000
Rayleigh β		0.000	0.000

Figure 6.3. The MC Soil Parameters-General



Property	Unit	Value	Value
Material set			
Identification number		1	2
Identification		0 Kaolin Clay - MC	0 Ottawa Sand - MC (36)
Material model		Mohr-Coulomb	Mohr-Coulomb
Drainage type		Drained	Drained
Colour		 RGB 19, 174, 71	 RGB 239, 181, 21
Stiffness			
E	kN/m ²	5000	50.00E3
ν (ν_u)		0.3000	0.3000
Alternatives			
G	kN/m ²	1923	19.23E3
E_{oed}	kN/m ²	6731	67.31E3
Strength			
c_{ref}	kN/m ²	1.000	0.000
ϕ (phi)	°	21.00	35.00
ψ (psi)	°	0.000	5.000
Velocities			
V_s	m/s	32.36	102.3
V_p	m/s	60.54	191.4
Advanced			
Set to default values		<input checked="" type="checkbox"/>	<input checked="" type="checkbox"/>
Stiffness			
E_{inc}	kN/m ² /m	0.000	0.000
z_{ref}	m	0.000	0.000
Strength			
c_{inc}	kN/m ² /m	0.000	0.000
z_{ref}	m	0.000	0.000
Tension cut-off		<input checked="" type="checkbox"/>	<input checked="" type="checkbox"/>
Tensile strength	kN/m ²	0.000	0.000

Figure 6.4. The MC Soil Parameters-Strength and Deformation

Property	Unit	Value	Value
Material set			
Identification number		1	2
Identification		0 Kaolin Clay - MC	0 Ottawa Sand - MC (36)
Material model		Mohr-Coulomb	Mohr-Coulomb
Drainage type		Drained	Drained
Colour		RGB 19, 174, 71	RGB 239, 181, 21
K0 settings			
K ₀ determination		Manual	Manual
K _{0,x} = K _{0,y}		<input checked="" type="checkbox"/>	<input checked="" type="checkbox"/>
K _{0,x}		1.000	1.000
K _{0,y}		1.000	1.000

Figure 6.5. The MC Soil Parameters -Initial Conditions

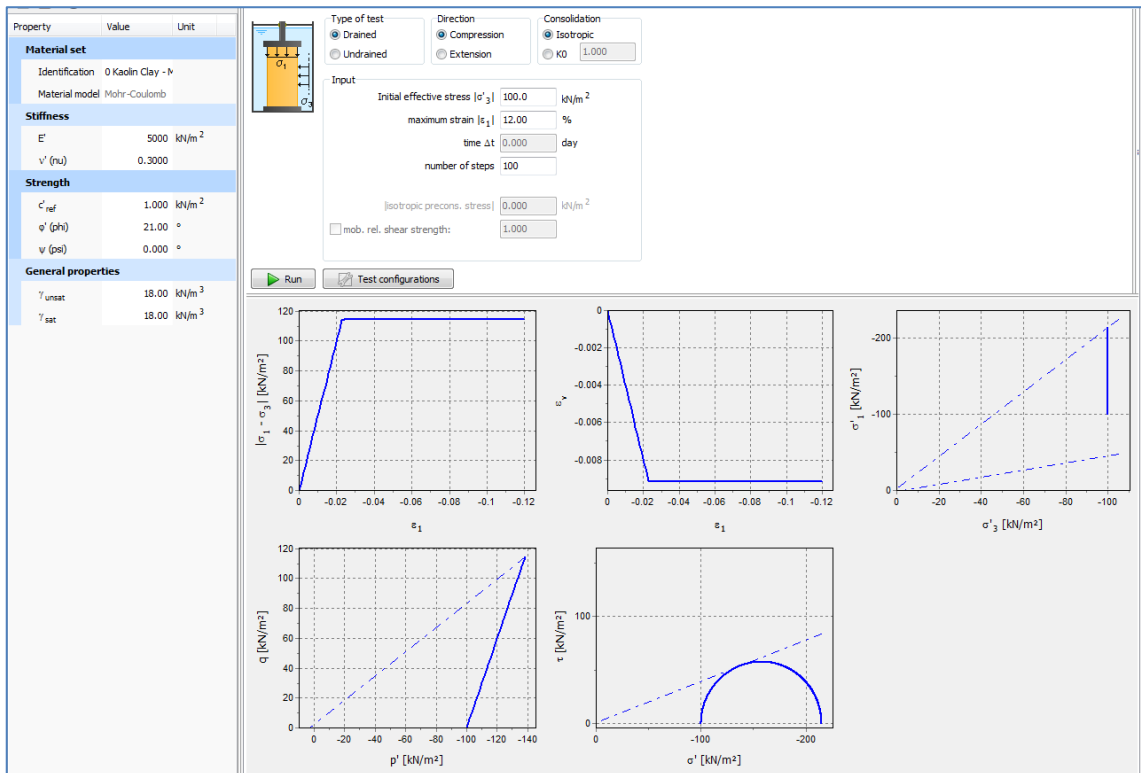


Figure 6.6. Results of the MC single element analysis on the sand under a confining pressure (σ_3) of 100 kPa

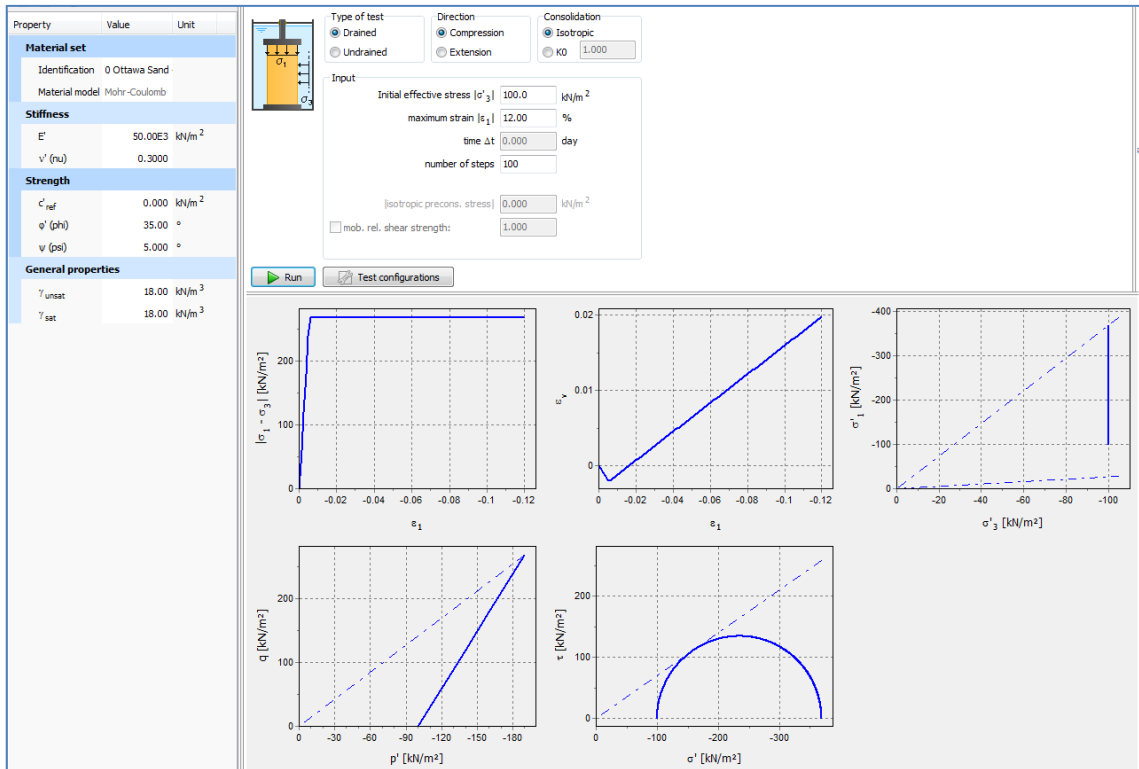


Figure 6.7. Results of the MC-single element analysis on Clay under a confining pressure (σ_3) of 100 kPa

The Raft foundation was modeled as a plate with linear elastic concrete properties. The plate is assumed to be 1 m thick and the concrete is of a modulus of elasticity equal to 30 GPa. A “non realistic” low unit weight was assigned for the concrete (1kN/m³) in order to reduce the own-weight effects in the field application modeling. This was done to facilitate direct comparison with theory and other field tests.

Material set			
Identification number	1		
Identification	Raft		
Comments			
Colour	RGB 101, 101, 108		
Properties			
d	m		1.000
γ	kN/m ³		1.000
Linear		<input checked="" type="checkbox"/>	
Isotropic		<input checked="" type="checkbox"/>	
E ₁	kN/m ²		30.00E6
E ₂	kN/m ²		30.00E6
ν_{12}			0.1500
G ₁₂	kN/m ²		13.04E6
G ₁₃	kN/m ²		13.04E6
G ₂₃	kN/m ²		13.04E6
Rayleigh α			0.2320
Rayleigh β			8.000E-3

Figure 6.8. The Linear Elastic Concrete Raft Parameters

6.2.2. The 3D Model

6.2.2.1. Geometry and Mesh

The numerical model adopted for the field-scale application was built in Plaxis 3D using 10-Noded mesh elements. The pre-defined “Fine” mesh elements distribution in Plaxis 3D were used. The ground profile was setup in a borehole where the 10 m thick clay layer was divided into 4 sub layers (2.5 m each) for the ease of meshing (see Figure 6.9 and Figure 6.10).

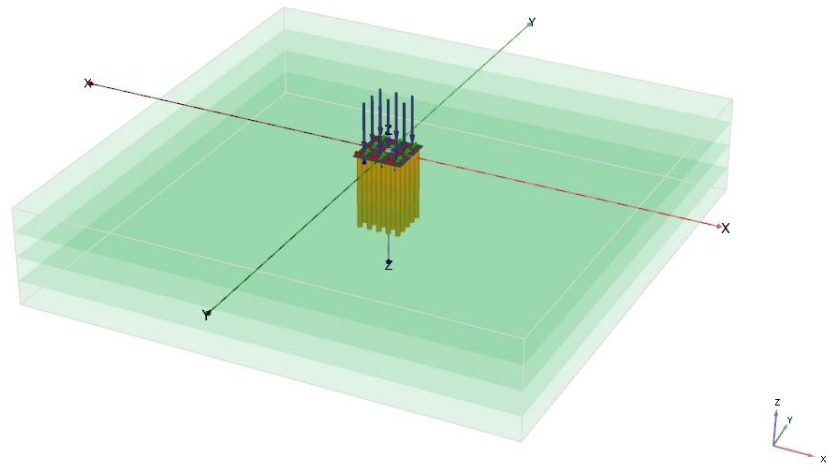


Figure 6.9. The 10 m thick clay layer was divided into 4 sub layers (2.5 m each)

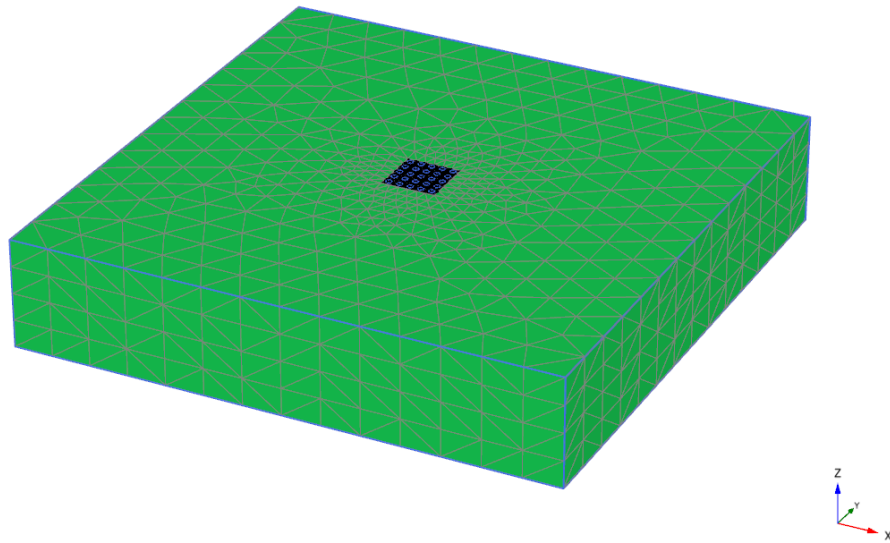


Figure 6.10. The Mesh generated

The mesh was complex due to the presence of curved elements in the model (circular columns). Figure 6.11, Figure 6.12, Figure 6.13 and Figure 6.14 show the built up mesh on each level of the 4 sub layers. Each of the sub layers were hidden from top to bottom to reveal the sand columns' mesh and geometry.

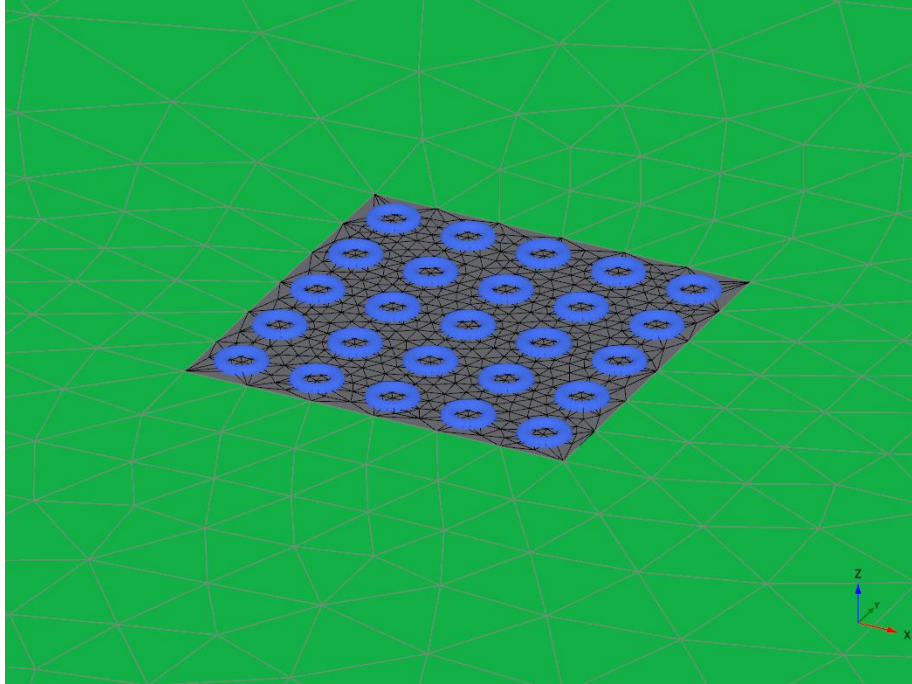


Figure 6.11. The mesh view from the surface

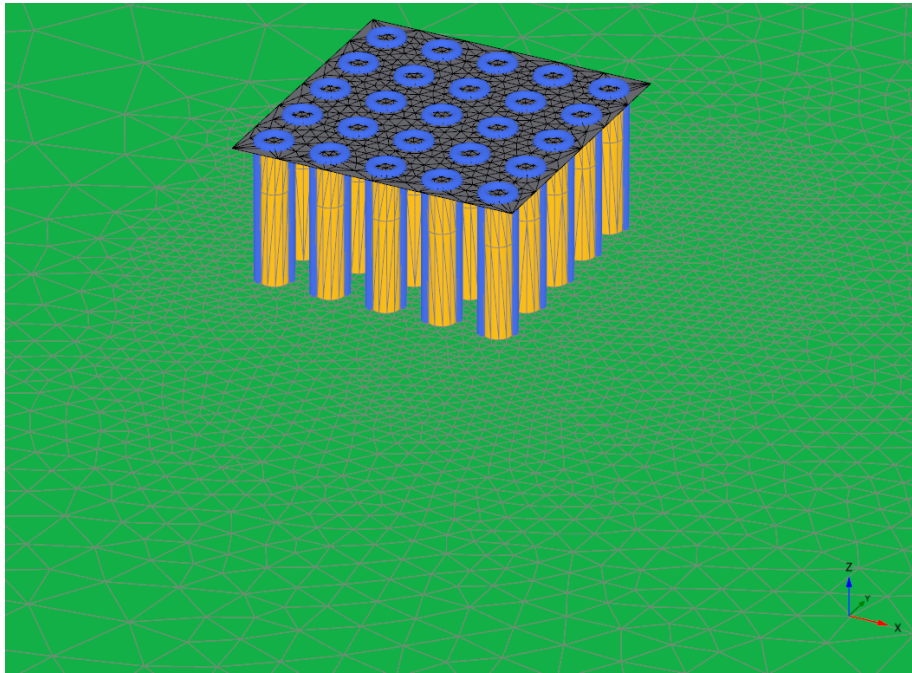


Figure 6.12. The mesh view at 2.5 m below surface

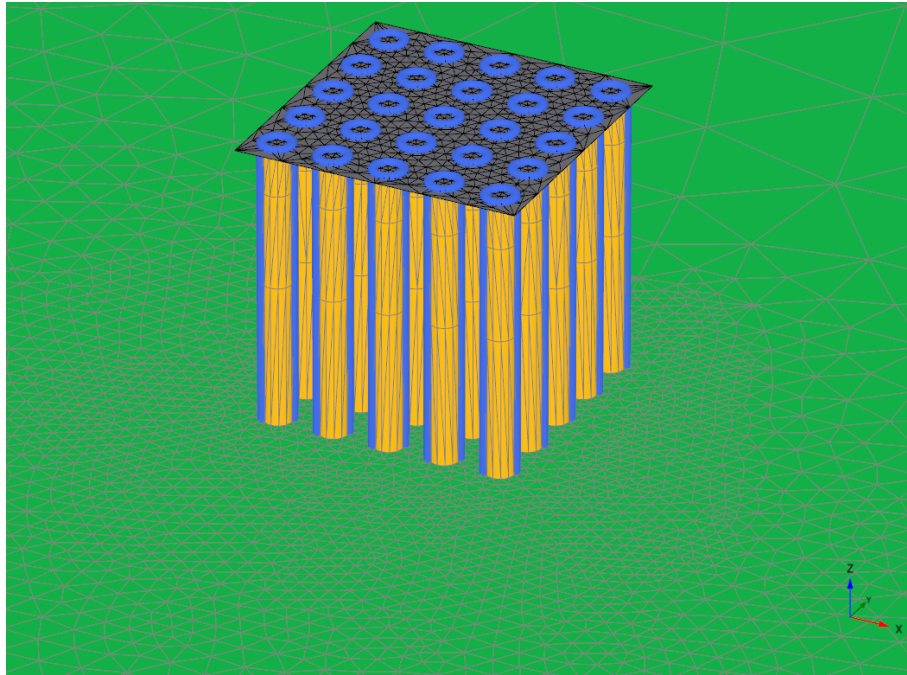


Figure 6.13. The mesh view at 5.0 m below surface

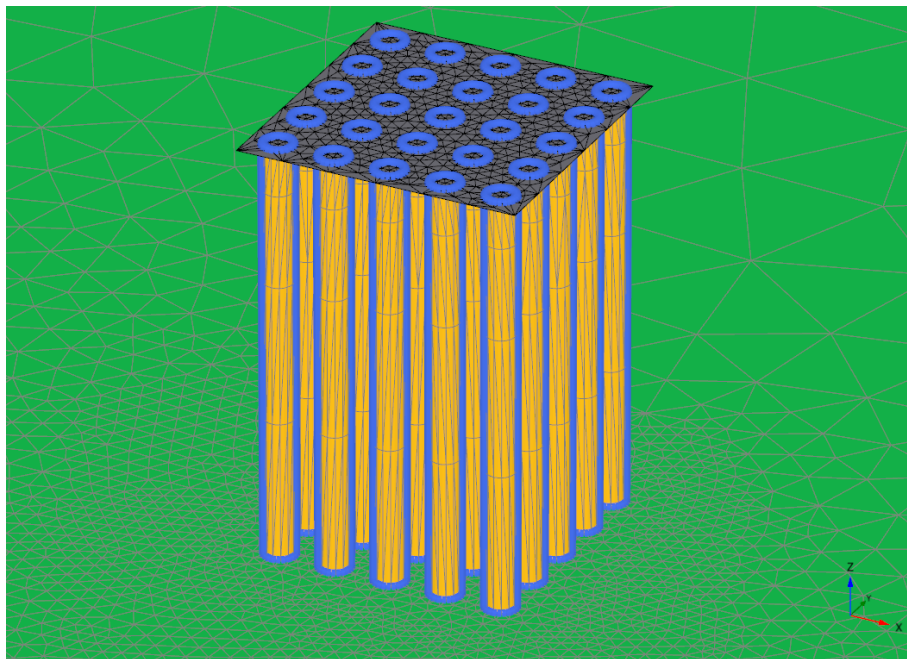


Figure 6.14. The mesh view at 7.5 m below surface

6.2.2.2. Construction Stages and Phases

The field application was simulated in 17 to 19 phases. All the construction stages / phases for MODEL 1 and MODEL 2 are listed below:

- MODEL 1: Natural ground
 - ⇒ Phase 1: Initial phase
 - ⇒ Phase 2: Installing the Raft
 - ⇒ Phase 3: Applying a uniform vertical load of 10 kPa
 - ⇒ Phase 4: Applying a uniform vertical load of 20 kPa
 - ⇒ Phase 5: Applying a uniform vertical load of 30 kPa
 - ⇒ Phase 6: Applying a uniform vertical load of 40 kPa
 - ⇒ Phase 7: Applying a uniform vertical load of 50 kPa
 - ⇒ Phase 8: Applying a uniform vertical load of 60 kPa
 - ⇒ Phase 9: Applying a uniform vertical load of 70 kPa
 - ⇒ Phase 10: Applying a uniform vertical load of 80 kPa
 - ⇒ Phase 11: Applying a uniform vertical load of 90 kPa
 - ⇒ Phase 12: Applying a uniform vertical load of 100 kPa
 - ⇒ Phase 13: Applying a uniform vertical load of 150 kPa
 - ⇒ Phase 14: Applying a uniform vertical load of 175 kPa
 - ⇒ Phase 15: Applying a uniform vertical load of 190 kPa
 - ⇒ Phase 16: Applying a uniform vertical load of 200 kPa
 - ⇒ Phase 17: Applying a uniform vertical load of 210 kPa - Failure Occurred / Calculation stage terminated

- MODEL 2: Reinforced ground with sand columns
 - ⇒ Phase 1: Initial phase
 - ⇒ Phase 2: Installing the Raft
 - ⇒ Phase 3: Applying a uniform vertical load of 10 kPa
 - ⇒ Phase 4: Applying a uniform vertical load of 20 kPa
 - ⇒ Phase 5: Applying a uniform vertical load of 30 kPa
 - ⇒ Phase 6: Applying a uniform vertical load of 40 kPa

- ⇒ Phase 7: Applying a uniform vertical load of 50 kPa
- ⇒ Phase 8: Applying a uniform vertical load of 60 kPa
- ⇒ Phase 9: Applying a uniform vertical load of 70 kPa
- ⇒ Phase 10: Applying a uniform vertical load of 75 kPa
- ⇒ Phase 11: Applying a uniform vertical load of 80 kPa
- ⇒ Phase 12: Applying a uniform vertical load of 100 kPa
- ⇒ Phase 13: Applying a uniform vertical load of 150 kPa
- ⇒ Phase 14: Applying a uniform vertical load of 175 kPa
- ⇒ Phase 15: Applying a uniform vertical load of 190 kPa
- ⇒ Phase 16: Applying a uniform vertical load of 200 kPa
- ⇒ Phase 17: Applying a uniform vertical load of 225 kPa
- ⇒ Phase 18: Applying a uniform vertical load of 250 kPa
- ⇒ Phase 19: Applying a uniform vertical load of 260 kPa - Failure Occurred /
Calculation stage terminated

6.2.3. FEM Results - Plaxis 3D

6.2.3.1. Vertical Deformations and Modes of Failure

The raft settlement under the uniform vertical loads / stress is displayed in the vertical displacement outputs of Figure 6.15 and Figure 6.16. The raft is relatively rigid compared to the ground and thus was settling almost uniformly. The ground failure was propagating to the surface uplifting the ground near the edges of the raft.

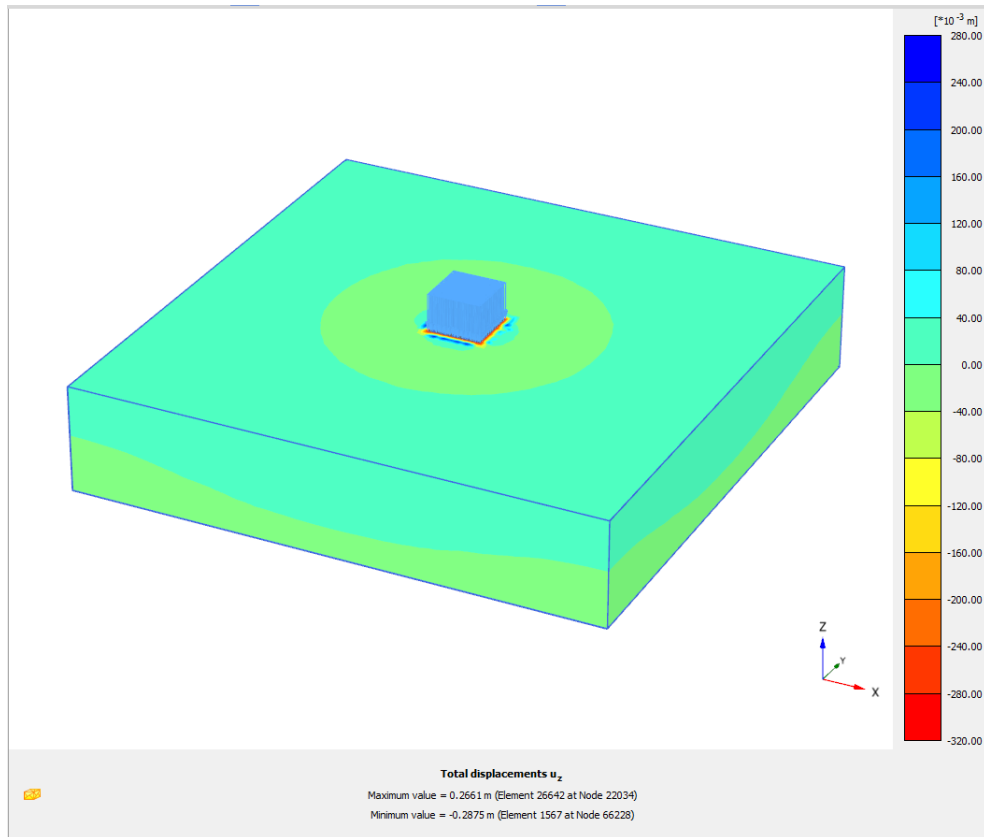


Figure 6.15. The global view of the vertical displacement output

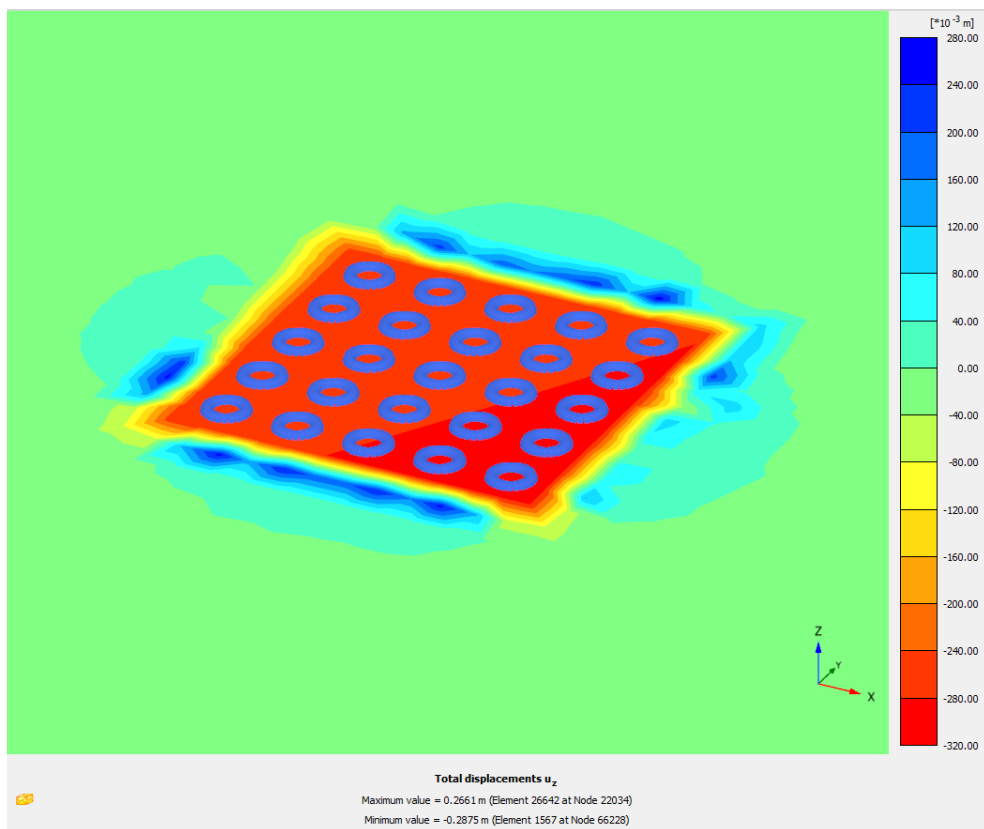


Figure 6.16. The vertical displacement under and around the raft

6.2.3.2. Load-Settlement Behavior

The settlement at the center of the raft foundation, which is also the center of the central sand column (in MODEL 2) is plotted versus the load for both models in Figure 6.17 and also tabulated in Table 6.3, where the corresponding Settlement Reduction Ratio (SRR) is calculated. The settlement was normalized by dividing with the raft width ($B=5\text{m}$) and plotted versus loading stress in Figure 6.18.

Table 6.3. Load vs Settlement at the center of the raft and SRR

Loading Stress (kPa)	Unreinforced Ground Settlement (m)	Reinforced Ground Settlement (m)	Settlement Reduction Ratio (SRR)	Settlement Improvement Ratio (β)
10	0.00601	0.00371	0.62	1.62
20	0.01219	0.00761	0.62	1.60
30	0.01887	0.01190	0.63	1.59
40	0.02606	0.01657	0.64	1.57
50	0.03386	0.02157	0.64	1.57
60	0.04221	0.02695	0.64	1.57
70	0.05106	0.03295	0.65	1.55
80	0.06043	0.03947	0.65	1.53
100	0.08160	0.05366	0.66	1.52
150	0.15016	0.09900	0.66	1.52
175	0.19723	0.12900	0.65	1.53
190	0.23270	0.14953	0.64	1.56
200	0.26085	0.16406	0.63	1.59
<i>Average</i>			<i>0.64</i>	<i>1.56</i>

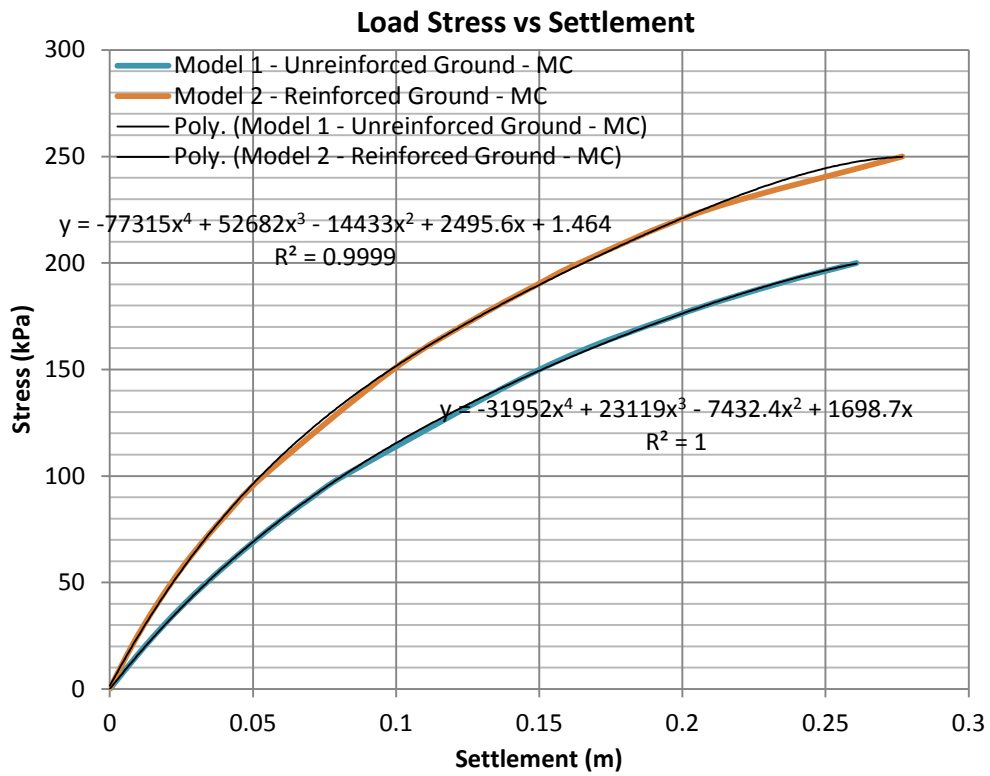


Figure 6.17. Loading Stress vs Settlement at the center of the raft

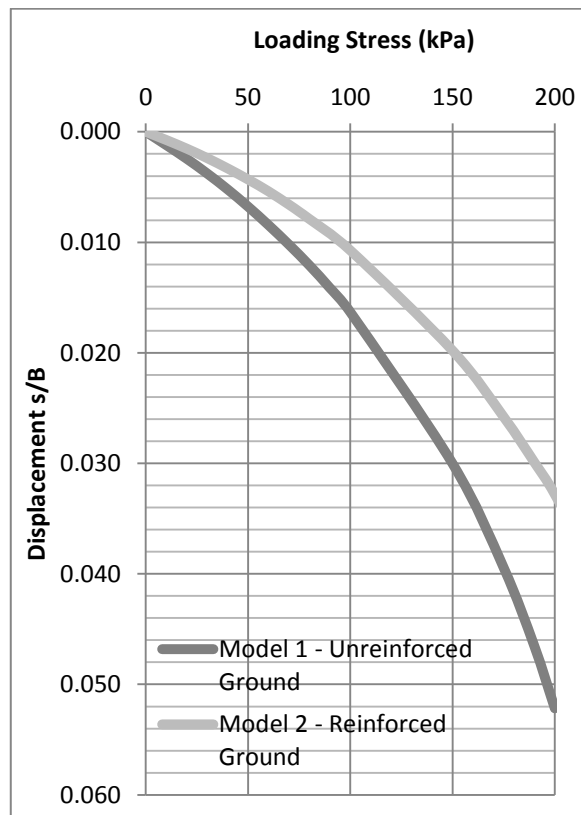


Figure 6.18. Load settlement response of the 5mx5m raft footing

As observed from plotting the Settlement Reduction Ratio (SRR) versus the loading stress in Figure 6.19, the SRR ranges between 0.62 and 0.66 averaging into about 0.64. Also the settlement improvement ratio (β), which is the settlement in the unreinforced ground divided by the settlement in the reinforced ground at a specific load, was calculated and plotted versus loading stress in Figure 6.20. The settlement improvement ratio (β) was ranging between 1.52 and 1.62 averaging into about 1.56.

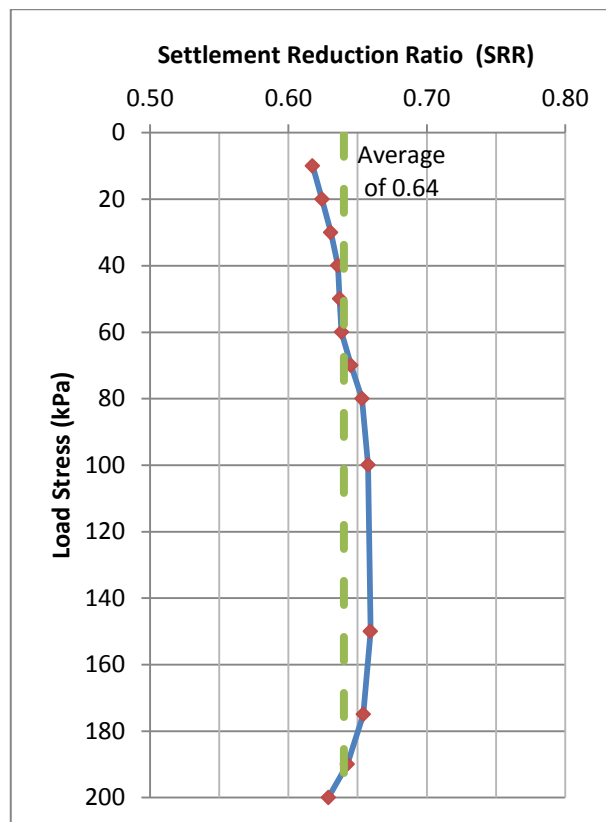


Figure 6.19. Calculated Settlement Reduction Ratio vs loading stress

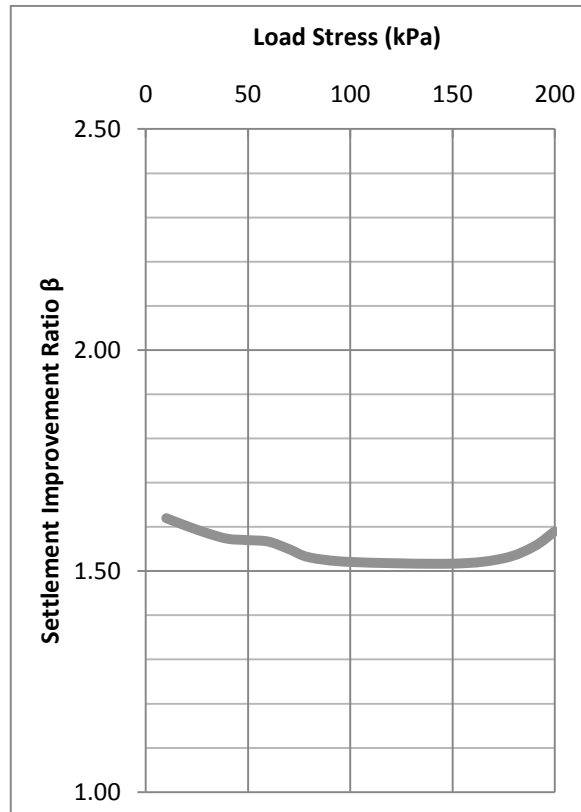


Figure 6.20. Calculated Settlement Improvement Ratio (β) vs loading stress

From the trend lines in Figure 6.17, Table 6.4 was generated where we had the Loading stresses back-calculated for a sequence of settlements, to obtain the corresponding stress Improvement Ratio (IR) versus settlement or axial strain. The axial strain, was assumed as the settlement divided by the 10 m layer thickness, to correlate later with the modeled triaxial lab test results that were discussed in the previous chapters. The stress Improvement Ratio is the ratio of the loading stress on reinforced ground and loading stress on unreinforced ground, corresponding to the same settlement value. Thus, at a specific settlement the IR indicates how much the reinforced ground has improved the load capacity compared to unreinforced ground. The IR was plotted verses the vertical axial strain in Figure 6.21, showing a gradual decrease from 1.5 to 1.3 (at 1% strain), and after that it remains constant at around 1.3.

Table 6.4. Improvement Ratio (IR) due to ground reinforcement

Settlement (m)	Axial Strain (%)	Unreinforced MODEL 1 Stress (kPa)	Reinforced MODEL 2 Stress (kPa)	Stress Improvement Ratio IR
0.00000		0.0	0.0	
0.01000	0.10%	16.5	25.1	1.52
0.02000	0.20%	31.4	46.3	1.47
0.03000	0.30%	45.1	65.0	1.44
0.04000	0.40%	57.6	81.5	1.42
0.05000	0.50%	69.0	96.1	1.39
0.06000	0.60%	79.6	109.1	1.37
0.07000	0.70%	89.4	120.7	1.35
0.08000	0.80%	98.5	131.3	1.33
0.09000	0.90%	107.0	141.1	1.32
0.10000	1.00%	115.0	150.1	1.31
0.11000	1.10%	122.6	158.7	1.29
0.12000	1.20%	129.9	166.8	1.28
0.13000	1.30%	136.8	174.7	1.28
0.14000	1.40%	143.5	182.3	1.27
0.15000	1.50%	149.9	189.8	1.27
0.16000	1.60%	156.1	197.2	1.26
0.17000	1.70%	162.1	204.5	1.26
0.18000	1.80%	167.8	211.6	1.26
0.19000	1.90%	173.2	218.5	1.26
0.20000	2.00%	178.4	225.1	1.26
0.21000	2.10%	183.2	231.3	1.26
0.22000	2.20%	187.6	237.0	1.26
0.23000	2.30%	191.6	242.0	1.26
0.24000	2.40%	195.0	246.1	1.26
0.25000	2.50%	197.8	249.1	1.26

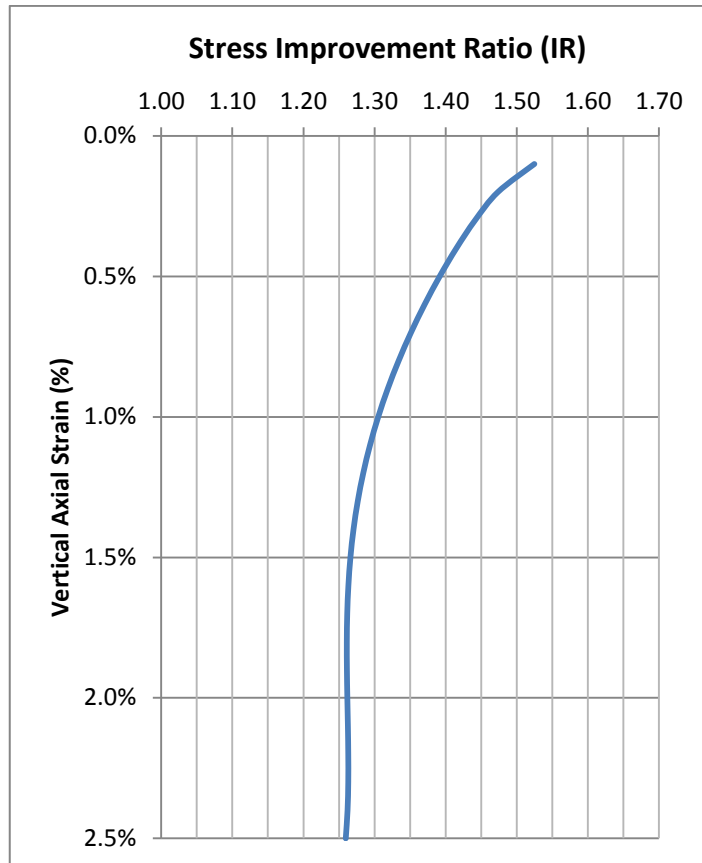


Figure 6.21. Calculated Stress Improvement Ratio vs axial strain

6.2.4. Comparison with the Single column Triaxial Lab tests

The Plaxis 3D FEM was compared to what we had in the simulated lab tests results, for the 1% - 2% strain range in terms of improvement ratio. The improvement ratio for the group of columns (19.6% Replacement Ratio, MODEL 2 - Plaxis 3D) for stresses up to 100 kPa (about 1% axial strain) was around 1.5 – 1.3, the improvement ratio remains constant at around 1.3 as the stress increases. In previous single column analyses (triaxial tests - Plaxis 2D), 0.75 penetration ratio, 3cm Diameter sand column (17.9% Replacement Ratio) had an improvement ratio of about 1.4 to 1.5 while the 3.5 cm sand column (24.3% Replacement Ratio) had an improvement ratio of 1.5 to 1.6. More lab testing is suggested for further research and future work, where triaxial tests

are carried out on a group of columns, and thus can be compared to the findings of this chapter.

6.2.5. Comparison of FEM and Theory / literature

To compare the FEM with theory / literature, we have compared the results to the work done by Zahmatkesh and Choobbasti (2010) and Kirsch (2006).

In Zahmatkesh and Choobbasti (2010) the performance of sand columns was investigated using FEM (2D) and compared to the results of relative theories in literature such as Priebe (1976), Priebe (1995) and Poorooshasb et al (1996).

Zahmatkesh and Choobbasti (2010) conducted finite element analyses using Plaxis 2D to investigate the performance of stone columns in soft clay. The FEM was conducted using the Mohr-Coulomb criterion for the soft clay and the sand/stone columns under drained conditions, where a rigid raft was placed on top of the reinforced ground. The single column models used axisymmetric conditions while the group columns models used an idealized plane strain conditions (See Figure 6.22). From the FEM analyses the authors estimated the settlement reduction ratio (SRR) of the soil. The results were compared to those obtained from standard analytical design methods (see Figure 6.23).

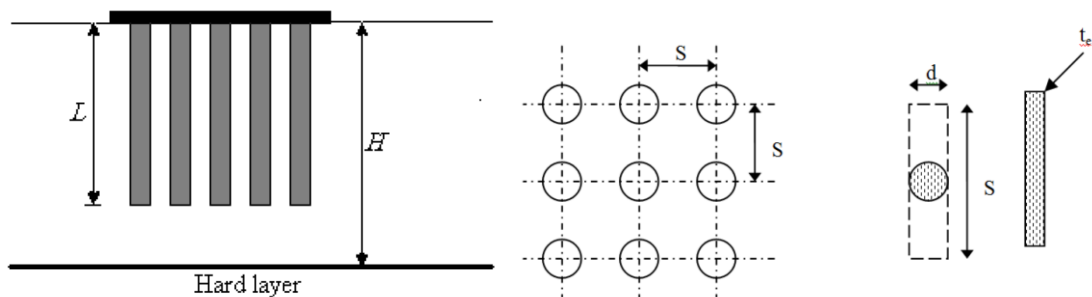


Figure 6.22. Zahmatkesh and Choobbasti (2010),

ρ	Present work			Priebe(1976)	Priebe(1995)	Poorooshab et al(1996)(H/L=1)
	H/L=1	H/L=1.5	H/L=2	(H/L=1)	H/L=1	
10	0.77	0.83	0.86	0.61	0.62	0.65
15	0.67	0.76	0.83	0.50	0.52	0.52
20	0.60	0.71	0.76	0.42	0.44	0.43
25	0.50	0.63	0.69	0.35	0.38	0.35
30	0.41	0.59	0.68	0.29	0.33	0.28

Figure 6.23. Zahmatkesh and Choobbasti (2010), comparison of SRR with existing theories

The average SRR that was obtained from our FEM (Plaxis 3D) was 0.64, which is similar to what was obtained by Zahmatkesh and Choobbasti (2010), estimated as 0.65. However, what was theoretically calculated by Priebe (1976), Priebe (1995) and Poorooshab et al (1996) of which their values were 0.42, 0.44 and 0.43 respectively, were lower than the FEM prediction done in this study and also by Zahmatkesh and Choobbasti (2010). This is because in both FEM works, the authors didn't consider the installation effects that result from vibro-replacement installation procedure. Assuming that the sand columns were installed in the field in a similar way to what was done in the lab in this study, where the installation effects were kept minimal by auguring and filling with previously densified sand columns, then the FEM results are more realistic and thus following the theoretical approach will be unsafe. But in practice, vibro replacement is widely used and thus it should be considered, as Krish (2006) did.

Krish (2006), have carried out field measurements of the change in stresses and stiffens of the ground induced by the vibro stone column installation. Also load tests were carried out on groups of stone columns, with extensive instrumentation. All of this was used to calibrate a 3D numerical model, which was further developed to accommodate different scenarios and settings. Also more detailed results were found in the thesis of Krish (2004).

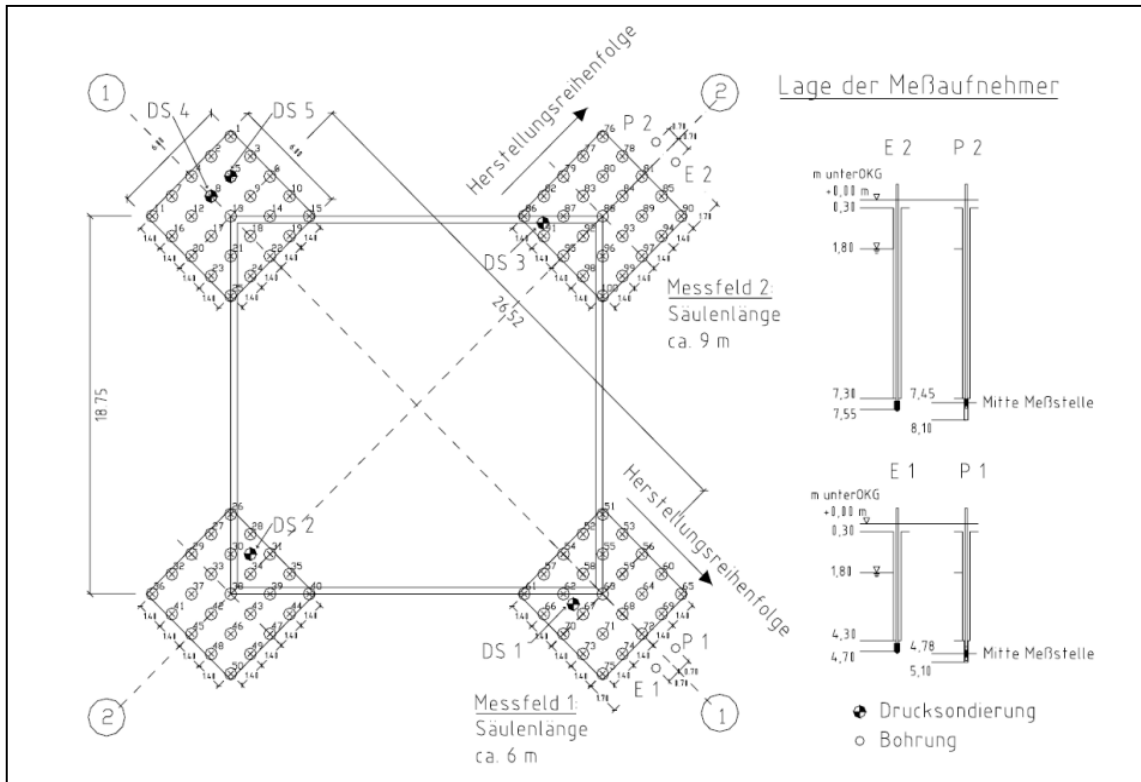


Figure 6.24. The 7.2m wide square footings used for the field tests in Krish (2004), 0.8m diameter stone columns placed in 1.4 m c-c spacing square grid.

To measure the installation effects a field test composed of 7.5m wide square footing placed over 25 stone columns (0.8m diameter each, by vibro replacement) in a square grid of c-c spacing of 1.4m, and the column lengths were 6m to 9m. The raft was loaded up to 180 kPa, during the test.

Another field test was carried out in Krish (2004) to investigate the behavior of stone columns was carried out, with extensive instrumentation. The group load test was carried out on a 3mx3m footing placed over 5 stone columns (0.8m diameter each). The columns lengths were 9m into a soft alluvial deposit. The setup is illustrated in Figure 6.25 and Figure 6.26.

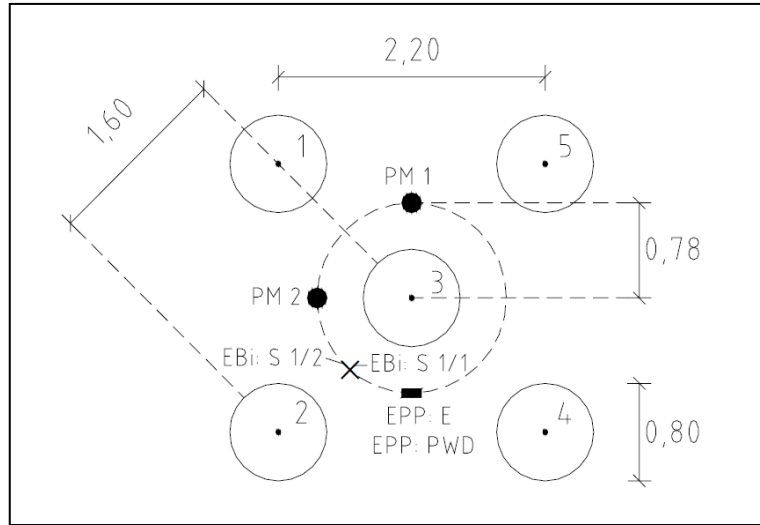


Figure 6.25. The stone column configuration under the 3m wide square footing used for the field tests in Krish (2004).

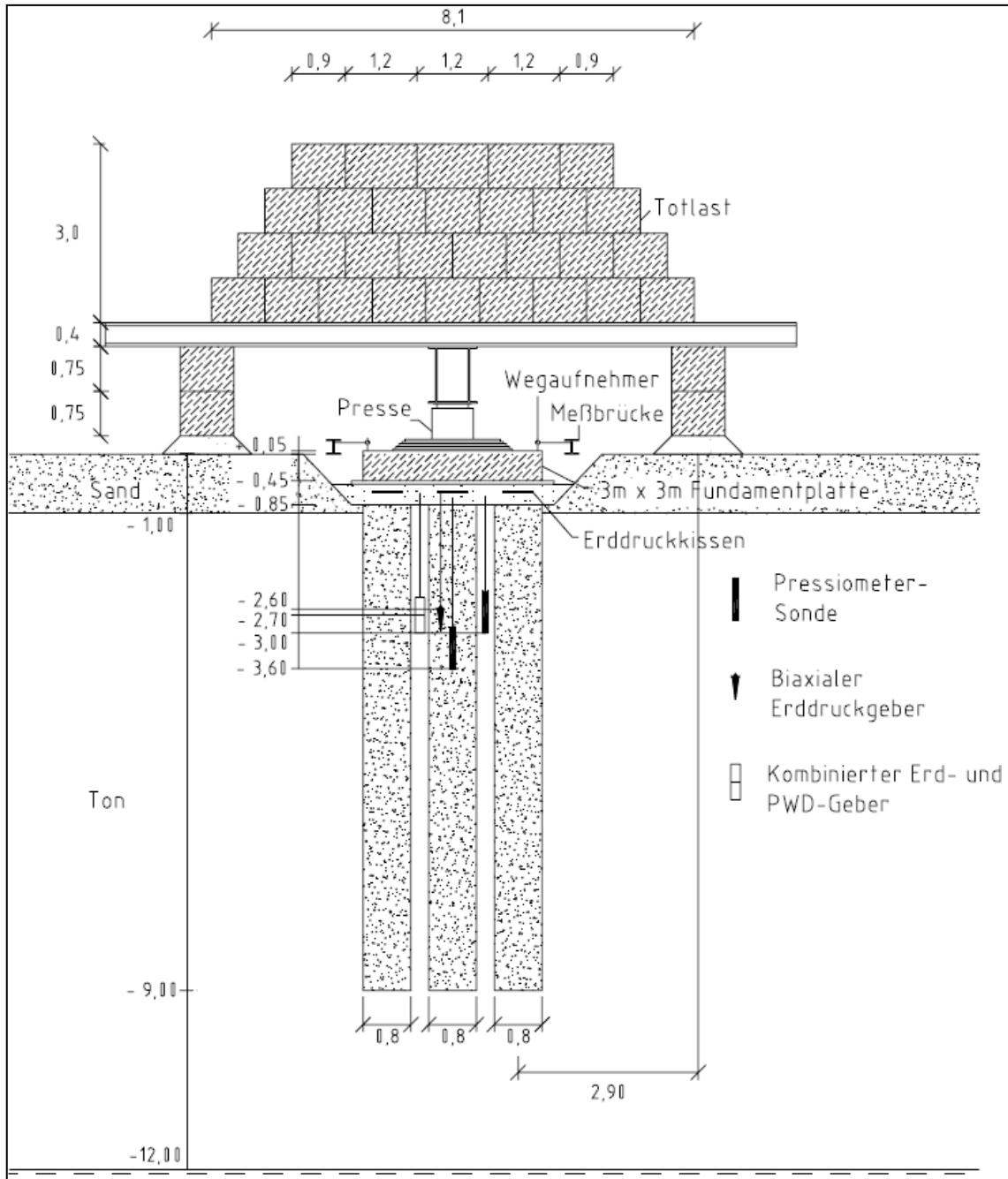


Figure 6.26. The field test setup of the 3m wide square footing in Krish (2004).

The results of our study were complying with the findings of Krish (2006) and Krish (2004), where load settlement response of both studies were compared and showed a relatively complying match in Figure 6.27.

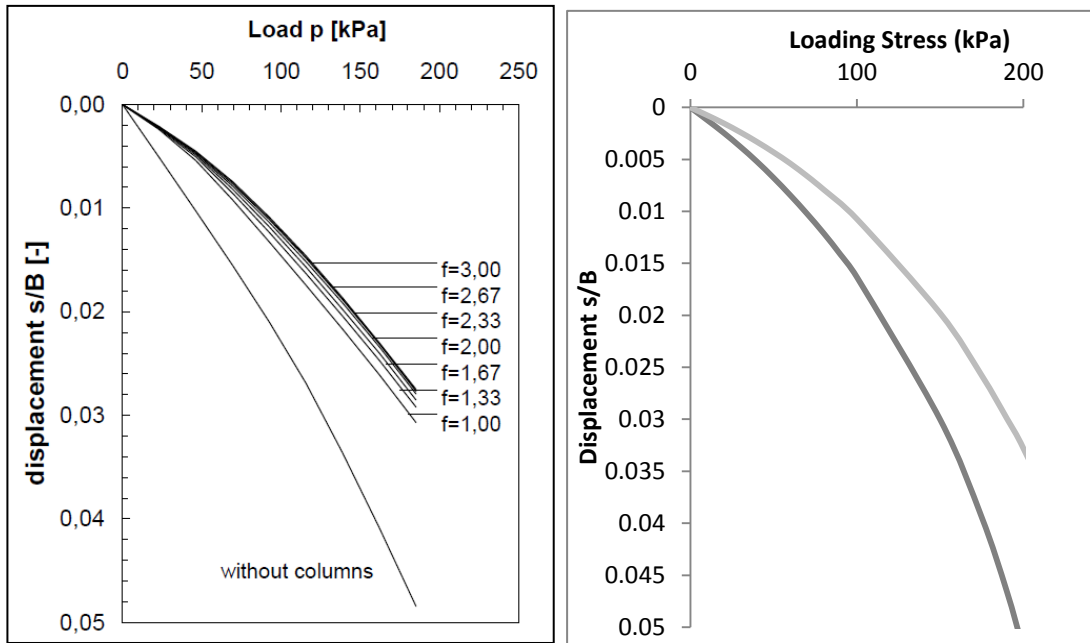


Figure 6.27. Load settlement response of the 7.2m wide square footing in Krish (2006) (Left), and the Load settlement response of the 5mx5m raft done in this research study (right)

The improvement ratio (β) when plotted versus load stress didn't have the same result as of the simulated field test of the 7.2m square footing. This was expected since the stiffness ratio (column / ground) in the 7.2m square footing field test was 100 times while in our field test simulation it is 10 times. Both results comply with what was obtained by Krish (2004), where the variation of the improvement factor (β) is plotted versus loading stress for various stiffness ratios (column / ground), as shown in Figure 6.29.

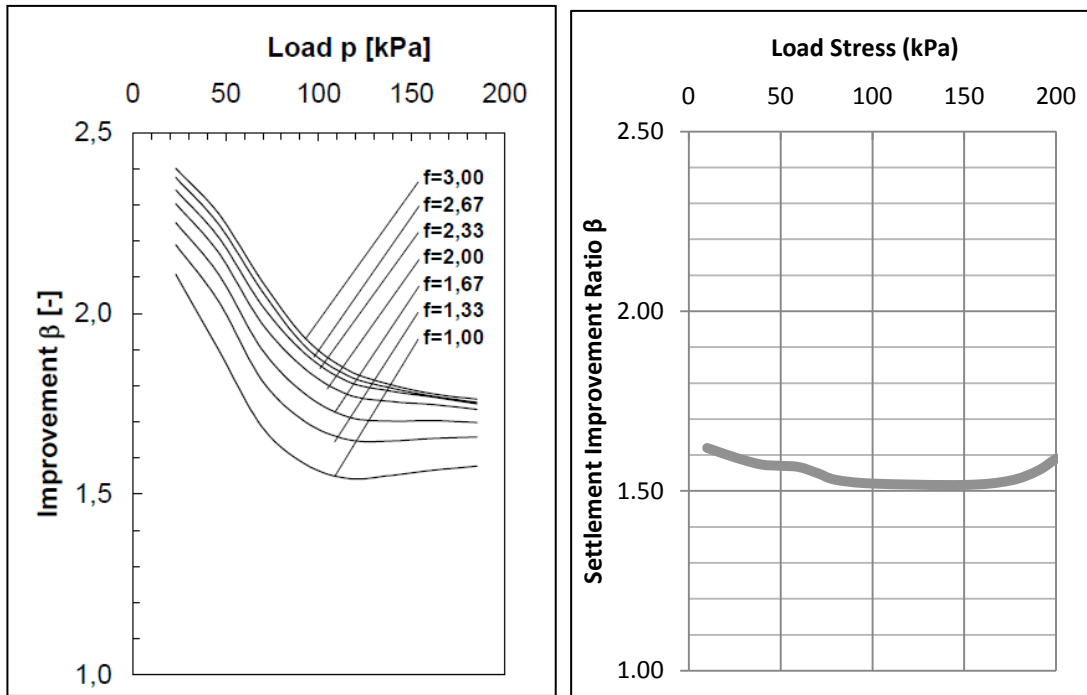


Figure 6.28. Improvement factor (β) for the 7.2m wide square footing in Krish (2006) (Left), and the Improvement factor (β) for the 5mx5m raft done in this research study (right).

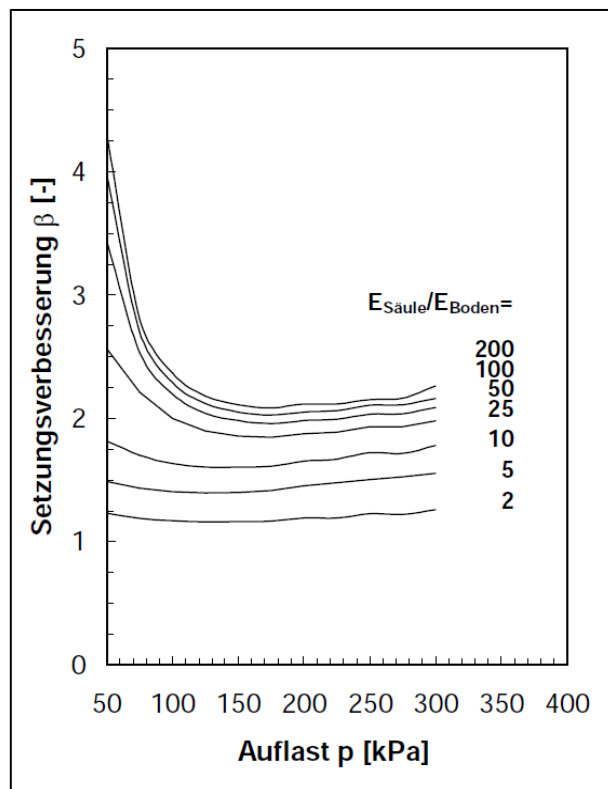


Figure 6.29. Improvement factor (β) vs loadind stress for various column to ground stiffness values, Krish (2004).

Krish (2006) had similar results as what we got previously (Figure 6.30), and gave a clear explanation to the difference between the FEM and analytical results (i.e. Priebe method) that were observed in this research study and also in Zahmatkesh and Choobbasti (2010). The difference was due to the fact that the analytical method of Priebe took into account all the installation improvements due to vibro-replacement, where we have ignored such an improvement in our FEM simulation.

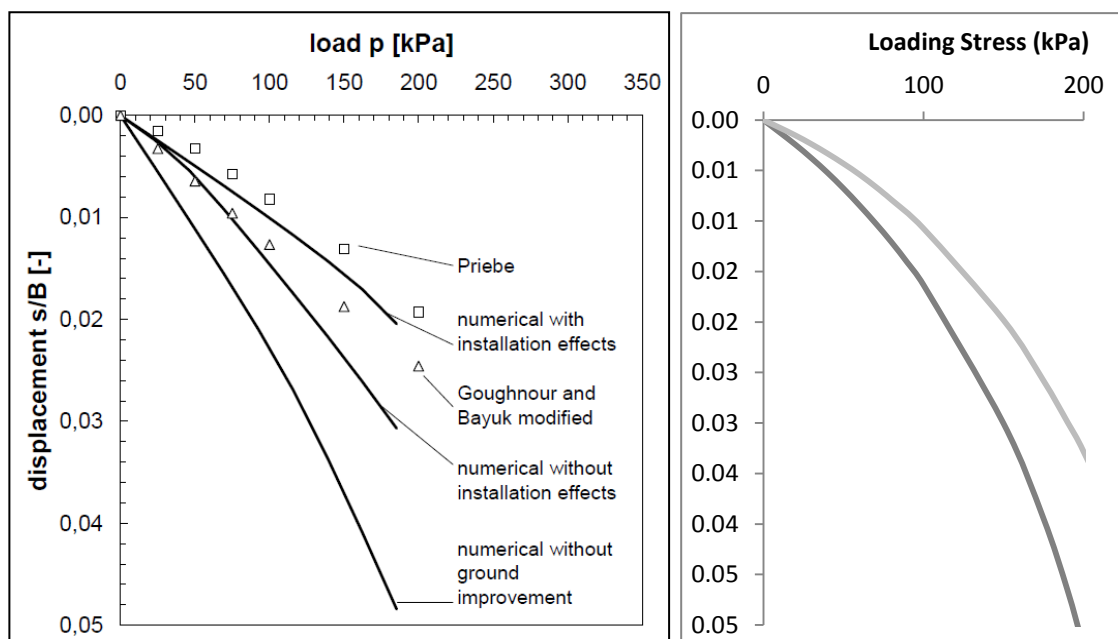


Figure 6.30. Load settlement response of the 7.2m wide square footing in Krish (2006) (Left), and the Load settlement response of the 5m x 5m raft done in this research study (right)

The exercise that we have done in this chapter can be used to design sand columns and predict their behavior in the field. If specific installation methods were used (such as vibro-replacement), that improve the existing soft ground due to vibrations or cavity expansion phenomenon, then these should be accounted for and used to optimize the design.

In all cases, field load tests are important to be carried out as part any design process and verification, so that to calibrate and optimize the FEM model.

6.3. The Field-Scale Application – No 2

Another 3D model was developed for the sake of analyzing the effect of the sand column lengths on the settlement improvement ratio (β). The Soil Hardening model was used for this exercise; however the sand columns were modeled as squares instead of circles and the ground water level was considered at 1m below surface, everything else was kept the same (i.e. spacing, raft dimensions, etc...). This is to cut on the Plaxis 3D runs where the circular elements required a couple of days to be complete, i.e. 10 times that of the square elements.

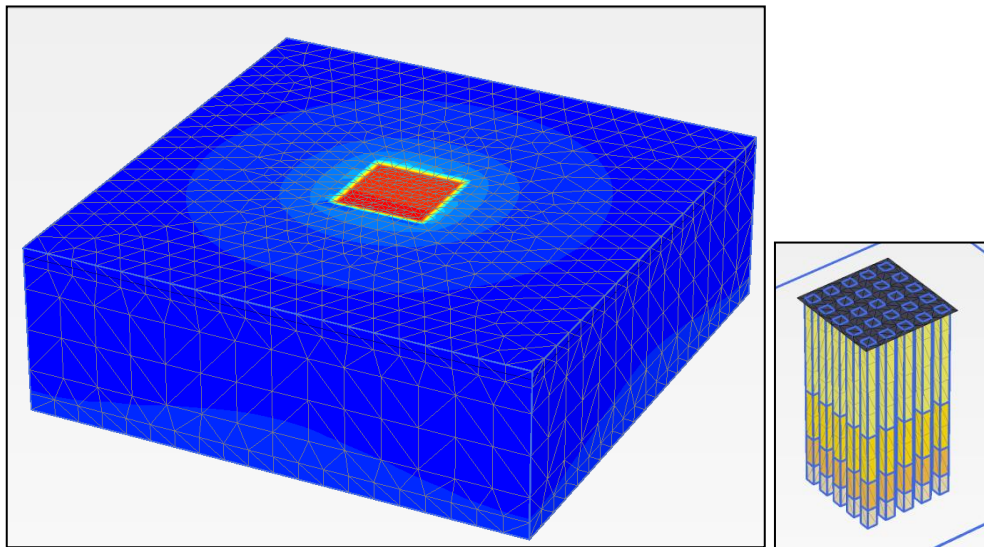


Figure 6.31. The field-scale application No 2

The soil parameters for the Hardening Soil models of the clay and sand are summarized in Table 6.5.

Table 6.5. The Hardening Soil Models Parameters

Soil	Kaolin Clay	Ottawa Sand
Density γ (dry / Sat) (KN/m ³)	18 / 19	17 / 18
Friction Angle ϕ^0	21	35
Cohesion, C' (kPa)	0	10
Poisson ratio, ν'_{ur}	0.2	0.2
E_{50}^{ref} (kPa)	2500	35000
E_{oed}^{ref} (kPa)	2500	40000
E_{ur}^{ref} (kPa)	15000	120000
Power (m)	0.7	0.8
OCR	1.6	3
Initial Void Ratio e_0	1.45	0.5
K_0	0.9	1.5
Conditions	Drained	Drained

The penetration ratio of the sand columns was varied from 0.0 (no reinforcement, $L/D = 0$) to 1.0 (10m length full sand columns, $L/D= 20$). All the models are tabulated below:

Table 6.6. MODEL S1 to MODEL S6

Model No.	Side length of the square sand column (m)	Area replacement ratio: A_c/A_s (%)	Column Penetration Ratio: H_c/H_s	L/D or H_c/D Ratio	Height of Sand Column: H_s (m)
MODEL S1	0	0	0	0	0.0
MODEL S2	0.5	0.25	0.1	2	1.0
MODEL S3	0.5	0.25	0.25	5	2.5
MODEL S4	0.5	0.25	0.5	10	5.0
MODEL S5	0.5	0.25	0.75	15	7.5
MODEL S6	0.5	0.25	1.0	20	10.0

6.3.1. Load-Settlement Behavior

The maximum settlement under the raft foundation is plotted versus the load for all the models in Figure 6.32. The settlement was normalized by dividing with the raft width ($B=5\text{m}$) and plotted versus loading stress in Figure 6.33. The curves for L/D of 15 and 20 almost overlapped, showing that they fall within the low improvement range. This was investigated more in the coming plots.

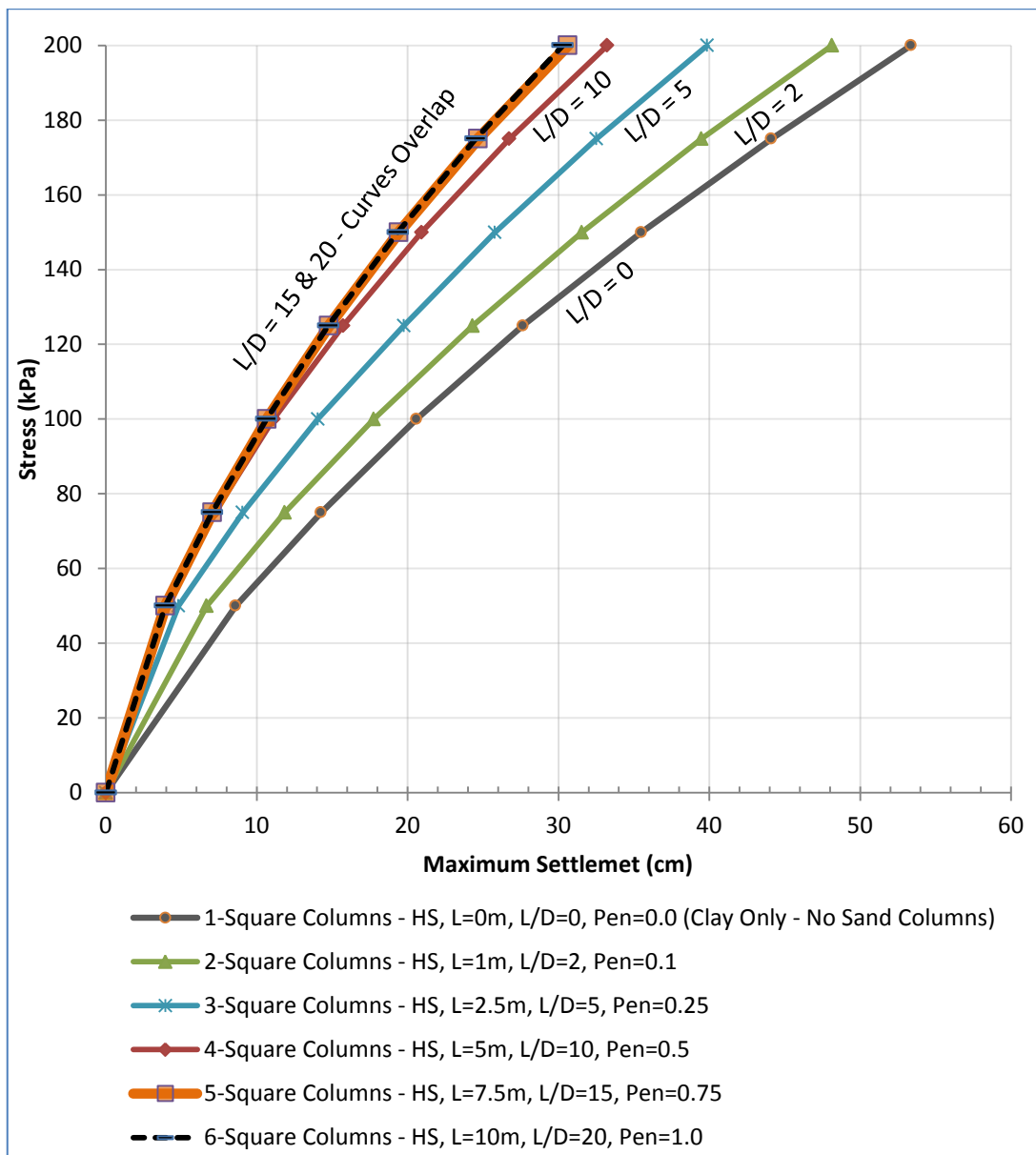


Figure 6.32. Loading Stress vs Settlement at the center of the raft

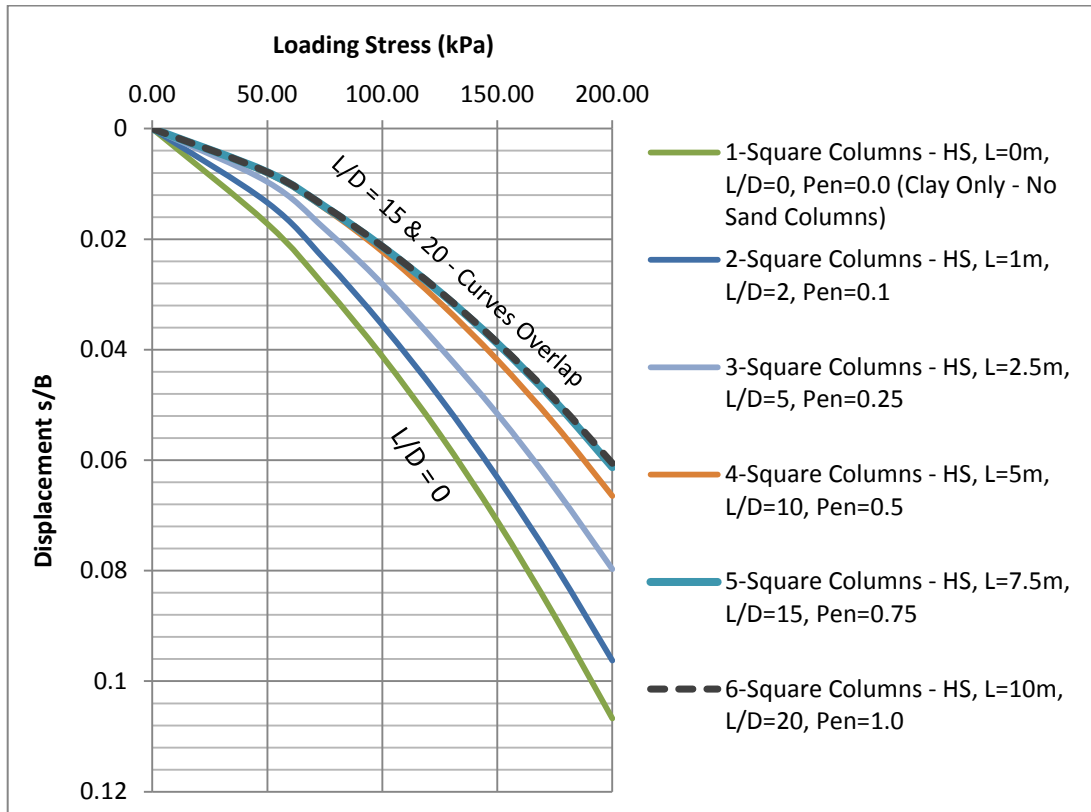


Figure 6.33. Load settlement response of the 5mx5m raft footing, with varied L/D ratios

The settlement improvement ratio (β), which is the settlement in the unreinforced ground divided by the settlement in the reinforced ground at a specific load, was calculated and plotted versus the loading stress and the L/D ratio in Figure 6.34 and Figure 6.35, respectively. The settlement improvement ratio (β) was ranging between 1 and 2.2, where it clearly showed that after an L/D of 10 almost no improvement is gained.

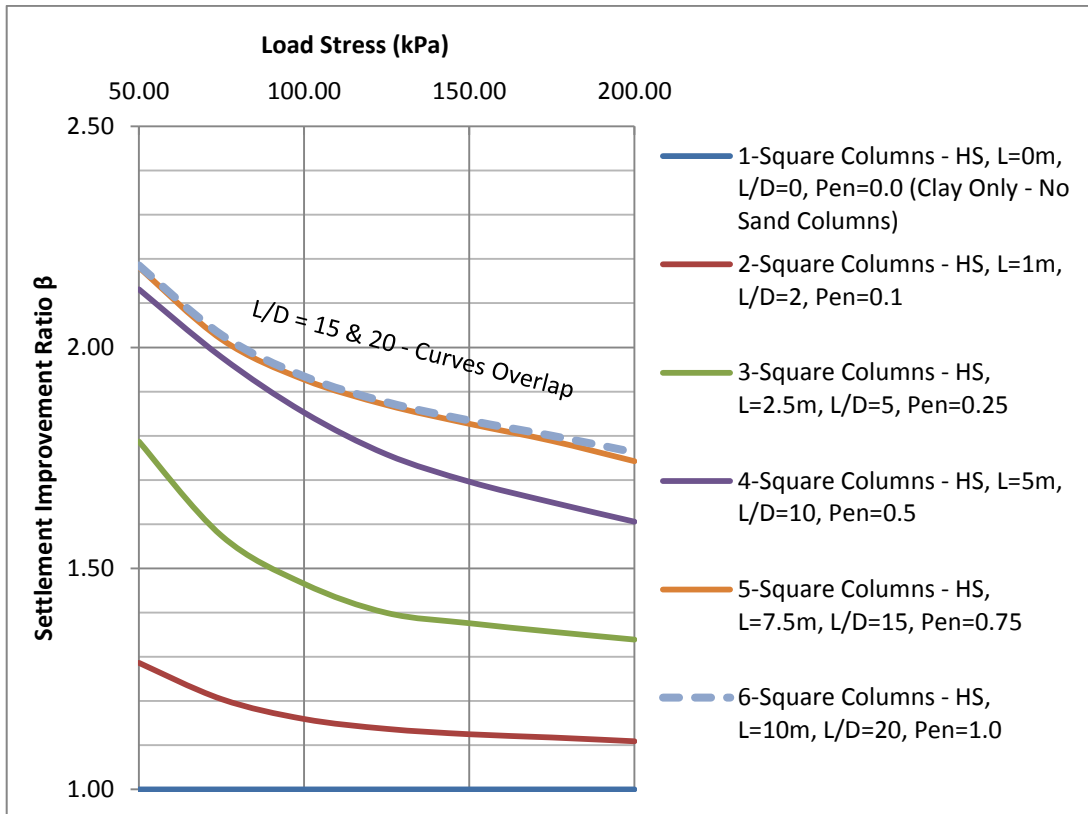


Figure 6.34. Calculated Settlement Improvement Ratio (β) vs Loading Stress

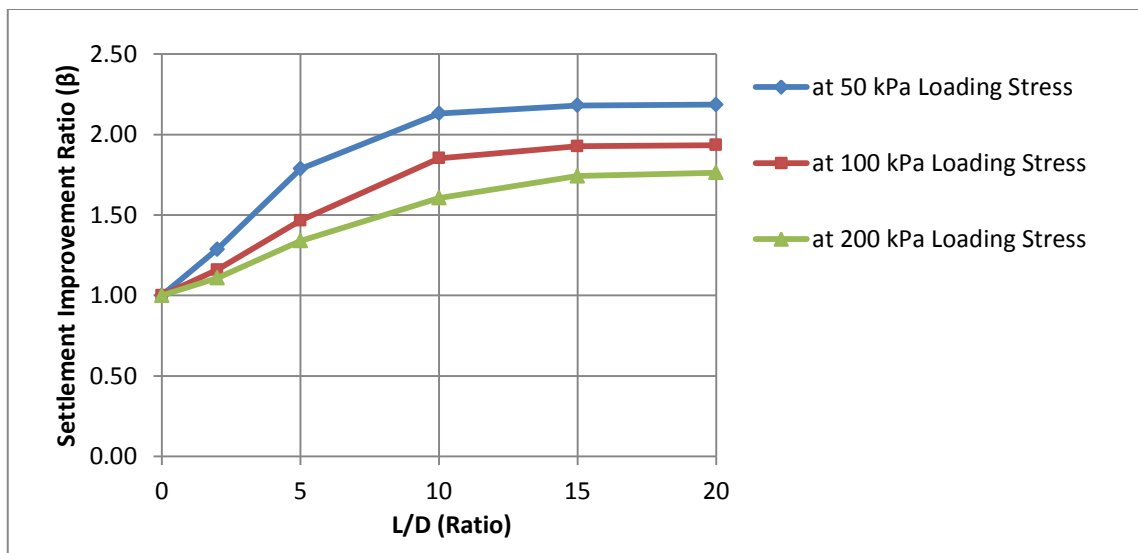


Figure 6.35. Calculated Settlement Improvement Ratio (β) vs L/D

The results comply with what was obtained by Krish (2004), where the variation of the improvement factor (β) is plotted versus loading stress for various stiffness ratios

(column / ground), as shown in Figure 6.36. The stiffness ratio (column / ground) in the 7.2m square footing field test was 100 times (Krish 2006), while in this field test simulation it is about 20 times. The shape and value are relatively similar.

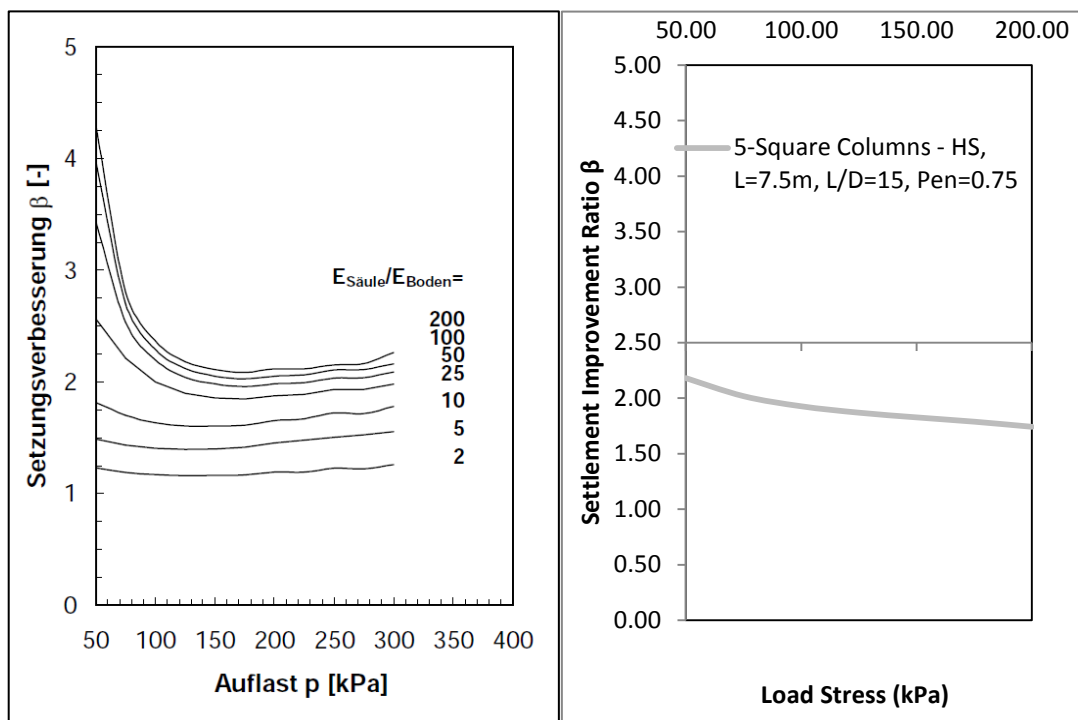


Figure 6.36. Improvement factor (β) vs load stress for various column to ground stiffness values, Krish (2004).

CHAPTER 6

CONCLUSIONS

7.1. Introduction

This chapter includes the main concluding remarks, observations and recommendations resulting from this research study, which aimed at using numerical models within an FEM context to capture the response of sand columns in soft clays, complementing the experimental research work that was conducted by Maalouf (2012).

Maalouf (2012) have carried out an experimental laboratory testing program using “fully drained” triaxial tests on normally consolidated Kaolin specimens, reinforced with partially or fully penetrating single sand columns.

From the mechanical and physical properties of the tested materials (Ottawa Sand and Kaolin Clay) hypoplastic soil models were built (Table 7.1). The single element analysis was carried out to calibrate and verify these soil models and the results were converging.

Table 7.1. Hypoplastic parameters for Ottawa sand and Kaolin

Hypoplastic parameters Ottawa sand	Hypoplastic parameters Kaolin Clay
$e_{d0} = 0.49$ $e_{c0} = 0.76$ $e_{i0} = 0.88$ $\varphi_c = 30^\circ$ $h_s = 4900 \text{ MPa}$ $n = 0.29$ $\alpha = 0.12$ $\beta = 1.0$	$\varphi_c = 27.5^\circ$ $N = 0.113$ $\lambda^* = 0.01$ $K^* = 1.32$ $R = 0.1$

The consolidated drained triaxial tests that were conducted on the reinforced Kaolin specimens in Maalouf (2012) were modeled using the Hypoplastic soil models. The deformation patterns and the stress strain behavior were analyzed. The hypoplastic model was also cross checked and compared to the Mohr Coulomb model and Hardening Soil Models. A comparison between the FEM and Experimental lab test results of Maalouf (2012) was carried out to assess the reliability of the finite element method in such application.

Based on the results of the comparison between FEM and experimental results, more variations were introduced in the FEM analysis to predict the performance of clays that are reinforced with sand columns at different area replacement ratios and sand column penetration depths. Accordingly, clay specimens reinforced with sand columns of 2cm, 3cm, 3.5cm and 4cm diameters were modeled for a range of column penetration ratios (0.1, 0.2, 0.3, 0.4, 0.5, 0.6, 0.7, 0.8, 0.9 and 1.0) under the three confinement pressures of 100kPa, 150kPa and 200 kPa. The Finite Element software Plaxis 2D was used to simulate the 120 additional triaxial tests. The results were presented as deviatoric stresses and improvement ratios versus columns penetration ratios, at two selected axial strain values of 2% and 12%. The results were also compared to the experimental results of Maalouf (2012).

The goal of the whole study was to build representative soil models that can predict the results of additional experimental tests that could be conducted in the future for the same clay and sand material. From the finding of this study, the researchers can use the same obtained models in case the same soils (which are available at AUB) were used.

Also an exercise was carried out to simulate two field-scale applications, where a 5m x 5m raft foundation is placed over 25 sand columns penetrating 7.5m into the natural clayey ground and loaded uniformly. The methodology and results of modeling the field applications were compared with similar previous studies done by others and theory to assess the reliability of the finite element method in such applications and also to evaluate its usefulness in designing sand columns.

7.2. Comments and recommendations

As a result of this research study, the following conclusive comments and recommendations are summarized.

7.2.1. Hypoplasticity, Mohr Coulomb and Hardening Soil

- 1- This research study explored the hypoplastic model for the first time in applications involving sand columns in clay. Hypoplasticity is the basis of a relatively recent constitutive model that is capable of modelling the strain softening behaviour in sands. The generally used models ignore the strain softening that occurs in sand and assume that the load carrying capacity of the sand column increases with strain (strain hardening models) or remains constant beyond the peak strength.
- 2- The hypoplastic model in such an application was compared to the Mohr Coulomb and Hardening Soil models, where from a performance aspect all models resulted in the same behavior of soil, however from usability aspect the hypoplasticity outstands the other models by being more global. Beside the inability to model the post peak soil softening, the Mohr Coulomb and

Hardening Soil models are incapable of accommodating different void ratios of the same material. For each void ratio a new soil model is needed since the angle of friction and cohesion changes accordingly. This is not the case for Hypoplasticity, where one model accommodates all void ratios. Thus, the Hypoplasticity is more global.

- 3- For the sake of comparison, the Ottawa sand was modeled as both Mohr Coulomb and Hardening soil while the Kaolin Clay was modeled as Hardening Soil. After building each soil model, the 3cm partial penetration column and the 3cm full penetration column were modeled using the Mohr Coulomb (MC) and Hardening Soil (HS) Models. All of the HP, HS and MC models showed similar results.
- 4- The only big advantage of the Hypoplastic model over the other two models (Mohr Coulomb and Hardening Soil) is that it is global and applicable for any void ratio, while the others need to be recalibrated / built each time a different void ratio is being used. This crucial property makes Hypoplasticity out stands the other models.

7.2.2. Comparison of Deformations - FEM vs. Experimental

- 5- The sample deformation under the axial stress was illustrated in the two types of output: deformed mesh and the horizontal deformation arrows. For the partially penetrated columns, bulging was observed at the lower third of the specimen. For the fully penetrating columns, bulging was observed at the middle of the specimen.

- 6- The modelled sample deformations under axial stresses are in line with what was visually observed in Maalouf (2012).

7.2.3. Comparison of Stress Strain Behavior - FEM vs. Experimental

- 7- The stress-strain behavior was illustrated in plotting the deviatoric axial stress against the axial strain. All the curves indicate that for the same sand column diameter, the full penetration columns result in a stiffer composite sample compared to the partial penetration columns. For each penetration category (full or partial), the larger the sand column diameter, the stiffer is the composite specimen.
- 8- The partial penetration columns of 3cm and 4cm diameters showed a good match between the FEM and experimental results. While for the 2cm diameter, only the 100kPa curve showed a good match, while the 150 kPa and 200 kPa FEM over predicted the experimental results.
- 9- In general, the FEM can be considered as well matching with the experimental results for partially penetrating sand columns.
- 10- The full penetration columns of 2cm and 3cm diameters didn't show a good and reliable match between the FEM and experimental results. Although the 2cm sand column curve of 100 kPa showed a good match, and the 150 kPa curve showed a good match at axial strains exceeding 4%, the FEM cannot be considered as well matching with the experimental results for fully penetrating sand columns.
- 11- In general, the FEM under predicted the experimental results for fully penetrating sand columns.

7.2.4. Effect on Stress Strain Behavior – Column Penetration Ratios

12- The deviatoric axial stress was plotted against the axial strain for all the 120 models. All the curves indicate that for the same sand column diameter, the higher the penetration columns result in a stiffer composite sample. For each penetration ratio, the larger the sand column diameter, the stiffer is the composite specimen. These are in line with what was observed in Maalouf (2012).

13- The improvement ratio is defined as the deviatoric stress of the reinforced specimen at a certain vertical strain value (2% or 12%) divided by the corresponding deviatoric stress of the un reinforced specimen (control Kaolin). The improvement ratio and deviatoric stress at a 2% and 12% vertical strains were plotted versus the column penetration ratio for each sand column diameter. These plots revealed the different behavior at different strains. At low strains (i.e. 2%), the improvement increases exponentially with increasing penetration ratio while for high strains (i.e. 12%) the improvement after 0.8 penetration ratio becomes very low and almost flattens out. This latter observation didn't comply with the lab test results for the full penetration sand columns, where much higher improvements were recorded.

7.2.5. FEM vs Experimental results – Column Penetration Ratios

14- The partial penetration columns showed an acceptable match between the FEM and experimental results of 0.75. In general, the FEM can be

considered as well matching with the experimental results for partially penetrating sand columns and realistic.

15- The full penetration columns didn't show a good and reliable match between the FEM and experimental results. The FEM cannot be considered as well matching with the experimental results for fully penetrating sand columns.

7.2.6. FEM under prediction for the Full penetration Columns

16- In general, the FEM under predicted the experimental results for fully penetrating sand columns. Further research and analyses is required in this concern, where lab tests are to be carried out at the penetration ratios of 0.8 and 0.9 to check if the deviatoric stress at 1.0 (full penetration) is a specific phenomenon or it is a gradual behaviour that occurs after the 0.7 column penetration ratio.

17- One possible explanation for the jump in the deviatoric stress in the full penetration column is that in the consolidation phase in the triaxial test and when the confinement pressures are applied, the initial vertical stress distribution on the sand column and surrounding clay are not equivalent leading to a non-isotropic loading. Having a non-isotropic loading will result in a different behaviour in the composite sample since all the parameters that we use in the hypoplastic, the Mohr Coulomb and Hardening soil models are relative to isotropically loaded samples. The critical angle of friction also correspond to an isotropically loaded soil, and this may explain that when we have increased the critical angle of friction in the hypoplastic model by 3 degrees we got an almost exact match to the lab test results. Non

isotropic loading conditions are a limitation to all the used models in this research study and this may explain their inability to model such behaviour.

18- Further to the above, the positive side is that non isotropic loading is hard to be present in field applications of sand columns, and thus we can depend on the partial penetration model for further field application studies and keep in mind that even if the full penetration phenomena occurred where we have non isotropic loading conditions, the FEM results will be under predicting reality and thus on the conservative side.

7.2.7. Modeling a field-scale application

19- The Finite Element software Plaxis 3D was used to simulate two field-scale applications, where a 5m x 5m raft foundation is placed over 25 sand columns penetrating 7.5m (1st application) and penetrating 0m, 1m, 2.5m, 5m, 7.5m and 10m (2nd application) into the natural clayey ground and loaded uniformly.

20- The methodology and results of modelling the field application was in line with what was done by others and reflected the reliability and usefulness of the finite element method in such applications, given that all the limitations are well understood and adequately considered.

7.3. Significance of this Research

Published finite element modeling work that was done to analyze the effect of sand columns reinforcement in soft clays was limited to conventional constitutive soil models such as the elastic-perfectly plastic Mohr Coulomb model and hyperbolic models. These models do not capture the strain softening behavior of sand that occurs beyond the peak strength. However, this strain softening behavior can be modeled by advanced constitutive models such as hypoplasticity which was implemented in this research study. The use of hypoplasticity for the first time in such an application didn't reflect an enhancement in prediction, compared to the conventional models. However, it had one big advantage which is the need to be built once since it accommodates different initial void ratios, while other models need to be recalibrated or rebuilt. The FEM approach will minimize the repetitive experimental work in the future.

It is expected that this research study will open the door to more advanced FEM analysis methodologies in assessing the behavior of sand columns in soft clays and will lead to better correlation between the FEM and experimental or field results.

BIBLIOGRAPHY

- Alamgir, M, Zaher, SM. (2001), “Field investigation on a soft ground of Bangladesh reinforced by granular piles”. *Journal of Geotechnical and Geoenvironmental Engineering*, ASCE, vol.133, No.4: pp 51-415 (2007)
- Alamgir, M., Miura, N., Poorooshasb, H. B., and Madhav. M. R. (1996). “Deformation analysis of soft ground reinforced by columnar inclusions.” *Computers & Geotechnics*, 18(4), 267-290.
- Al-Tabba, A. (1987). “Permeability and Stress-Strain Response of Speswhite Kaolin.” PhD thesis, University of Cambridge.
- Ambily, A.P., Gandhi, R. Shailesh (April 2007), “Behavior of stone columns based on experimental and FEM analysis”. *Journal of Geotechnical and Geoenvironmental Engineering*, ASCE, vol.133, No.4: pp 405-415 (2007)
- Ayadat, T. and Hanna, A. M. (2005). “Encapsulated stone columns as a soil improvement technique for collapsible soil.” *Ground Improvement*, 9(4), 137-147.
- Bauman, V. and Bauer, G. E. A. (1974). “The performance of foundations on various soils stabilized by the vibro-compaction method.” *Canadian Geotechnical Journal*, 11(4), 509-530.
- Black, J., Sivakumar, V., Madhav, M. R., and McCabe, B. (2006). “An improved experimental set-up to study the performance of granular columns.” *Geotechnical Testing Journal*, ASTM, 29(3), 193-199.
- Black, J. V., Sivakumar, V., and McKinley, J. D. (2007). “Performance of clay samples reinforced with vertical granular columns.” *Canadian Geotechnical Journal*, 44, 89-95.
- Castro, J. and Sagaseta, C. (2011), “Deformation and consolidation around encased stone columns,” *Geotextiles and Geomembranes*, Vol. 29, pp. 268–276.
- Casagrande, A. (1936). “Determination of the preconsolidation load and its practical significance.” *Proceedings, 1st International Conference on Soil Mechanics and Foundation Engineering*, Cambridge, Mass., 3, 60-64.
- Chen, J. F., Han, J., Oztoprak S., and Yang, X. M. (2009), “Behavior of single rammed aggregate piers considering installation effects,” *Computers and Geotechnics*, Vol. 36, pp. 1191-1199.

- Elshazly, H. A., Elhafez, D. H., and Mossaad, M. E. (2008), "Reliability of Conventional Settlement Evaluation for Circular Foundations on Stone Columns," *Geotechnical and Geological Engineering Journal*, Vol. 26, pp. 323-334.
- Elshazly, H. A., Elkasabjy, M., and Elleboudy, A. (2007), "Effect of Inter-Column Spacing on Soil Stresses due to Vibro-Installed Stone Columns: Interesting Findings," *Geotechnical and Geological Engineering Journal*, Vol. 26, pp. 225-236.
- Greenwood, D. A. (1970). "Mechanical improvement of soils below ground surface." *Ground Engineering Proceedings Conference*, London, 11-22.
- Guétif, Z., Bouassida, M., and Debats J.M (January 2007), "Improved soft clay characteristics due to stone column installation" *Computers and Geotechniques*, vol. 34, pp.104-111 (2007)
- Hughes, J. M. O. and Withers, N. J. (1974). "Reinforcing of soft cohesive soils with stone columns." *Ground Engineering*, 7(3), 42-49.
- Hughes, J. M. O., Withers, N. J., and Greenwood, D. A. (1975). "A field trial of the reinforcing effect of a stone column in soil." *Geotechnique*, 25(1), 31-44.
- Juran, I. and Guermazi, A. (1987). "Settlement response of soft soils reinforced by compacted sand columns." *Journal of Geotechnical Engineering*, ASCE, 114(8), 930-943.
- Krish, F. (2006). "Vibro Stone Column Installation and its Effect on the Ground Improvement." *Int. Conf. on Numerical Simulation of Construction Processes in Geotechnical Engineering for Urban Environment*, Bochum, 115-124.
- Krish, F. (2004). "Experimentelle und numerische Untersuchungen zum Tragverhalten von Rüttelstopfsalengruppen." *Disertation*, TU Braunschweig.
- Lin, H. and Penumadu, D. (2005). "Experimental investigation on principal stress rotation in kaolin clay." *J. of Geotechnical and Geoenvironmental Engineering*, ASCE, 131(5),633-642.
- Lo, S. R., Zhang, R., and Mak, J. (2010), "Geosynthetic-encased stone columns in soft clay: A numerical study," *Geotextiles and Geomembranes*, Vol. 28, pp. 292–302.
- Maakaroun, T., Najjar, S.S. and Sadek, S. (2009). "Effect of sand columns on the load response of soft clay." *Contemporary Topics in Ground Modification*, *Geotechnical Special Publication No. 187*, ASCE, Orlando, Florida, 217-224.

- Malarvizhi, S. N. and Ilamparuthi, K. (2004). "Load versus settlement of claybed stabilized with stone and reinforced stone columns." *Proceedings of Geo-Asia-2004*, Seoul, Korea, 322-329.
- McKelvey, D., Sivakumar, V., Bell, A., and Graham, J. (2004). "Modeling vibrated stone columns in soft clay." *Proceedings of the Institute of Civil Engineers Geotechnical Engineering*, 157(3), 137-149.
- Muir Wood, D., Hu, W., and Nash, D. F. T. (2000). "Group effects in stone column foundations: model tests." *Geotechnique*, 50(6), 689-698.
- Murugesan, S. and Rajagopal, K. (2006). "Geosynthetic-encased stone columns: numerical evaluation." *Geotextiles and Geomembranes*, 24, 349-358.
- Najjar, S.S., Sadek, S., and Maakaroun, T. (2010). "Effect of sand columns on the undrained load response of soft clays." *J. Geotechnical and Geoenvironmental Engrg.* in press (September 2010).
- Najjar, S.S., Sadek, S., Zakharia, M., and Khalaf, T. (2012). "Effect of Sand Column Inclusions on the Drained Response of Soft Clays." *GeoCongress 2012: State of the Art and Practice in Geotechnical Engineering*, pp. 4079-4088.
- NarasimhaRao, S., Prasad, Y. V. S. N, and HanumantaRao, V. (1992). "Use of stone columns in soft marine clays." *Proceedings of the 45th Canadian Geotechnical Conference*, Toronto, Canada, 9/1-9/7.
- Prashant, A. and Penumadu, D. (2005). "A laboratory study of normally consolidated kaolin clay." *Canadian Geotechnical Journal*, 42, 27-37.
- Priebe, H. J. (1995). "The design of vibro replacement." *Ground Engineering*, 28(10),31-37.
- Raithel, M. and Kempfert, H. G. (2000), "Calculation models for dam foundations with geotextile coated sand columns," *Proceedings of the International Conference on Geotechnical*
- Shahu, J. T., and Reddy, Y. R., (2011), "Clayey soil reinforced with stone column group: model tests and analyses," *Journal of Geotechnical and Geoenvironmental Engineering*, ASCE, Vol. 137, No. 12, pp. 1265-1274.
- Sivakumar, V., McKelvey, D., Graham, J., and Hughus, D. (2004). "Triaxial tests on model sand columns in clay." *Canadian Geotechnical Journal*, 41, 299-312.

- Tan, S. A., Tjahyono, S., and Oo, K. K. (2008), "Simplified plane strain modeling of stone-column reinforced ground," *J. of Geot. and Geoenviron. Engineering, ASCE*, Vol. 134, No. 2, pp. 185-194.
- Watts, K. S., Johnson, D., Wood, L. A., and Saadi, A. (2000). "Instrumental trial of vibro ground treatment supporting strip foundations in a variable fill." *Geotechnique*, 50(6), 699-709.
- Zahmatkesh, A. and Choobbasti, A. J. (2012). "Settlement evaluation of soft clay reinforced by stone columns, considering the effect of soil compaction", *International Journal of Research and Reviews in Applied Sciences*, Volume 3, Issue 2, 159-166.
- Gudehus, G. (1996), "A comprehensive constitutive equation for granular materials." *Soils and Foundations*, 36(1):1-12, 1996.
- Herle, I. and Kolymbas, D. (2004), "Hypoplasticity for soils with low friction angles." *Computers and Geotechnics*, 31(5):365-373.
- Kolymbas, D. (1991), "Computer-aided design of constitutive laws." *International Journal for numerical and Analytical Methods in Geomechanics*, 15:593-604
- Masin, D. (2005), "A hypoplastic constitutive model for clays." *International Journal for Numerical and Analytical Methods in Geomechanics*, 29(4):311-336
- Masin, D. (2005), "A hypoplastic constitutive model for clays with meta-stable structure." *Canadian Geotechnical Journal*, 44(3):363-375
- Niemunis, A. (2002), "Extended Hypoplastic Models for Soils." Habilitation thesis, Ruhr University, Bochum
- Niemunis, A. and Herle, I. (1997), "Hypoplastic model for cohesionless soils with elastic strain range." *Mechanics of Cohesive-Frictional Materials*, 2:279-299
- Von Wolffersdorff, P. A. (1996), "A hypoplastic relation for granular materials with a predefined limit state surface." *Mechanics of Cohesive-Frictional Materials*, 1:251-271